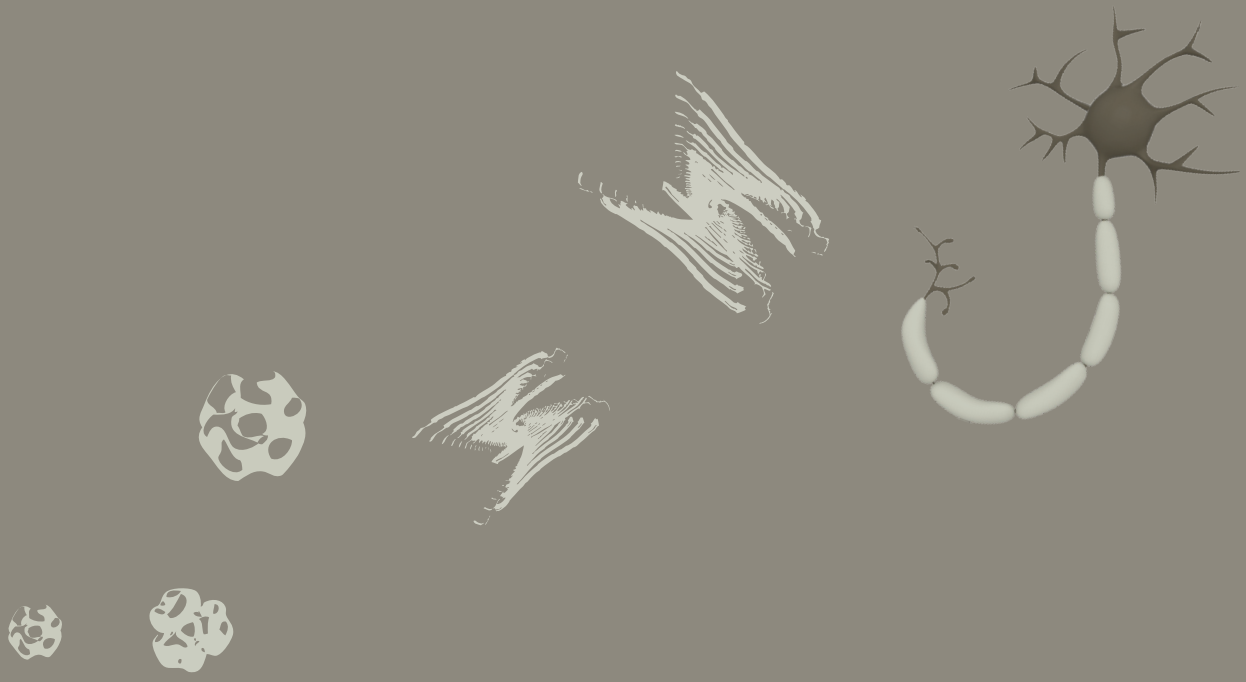

Aggregation and toxicity of amyloid-β peptide in relation to peptide sequence variation

Annelies Vandersteen

Aggregation and toxicity of amyloid-beta peptide in relation to peptide sequence variation

Annelies Vandersteen

Graduation committee members:

Prof. dr.	G. van der Steenhoven	Universiteit Twente	(chairman and secretary)
Prof. dr.	V. Subramaniam	Universiteit Twente	(promotor)
Prof. dr. ir.	F. Rousseau	K.U.Leuven	(promotor)
Prof. dr.	H. Remaut	Vrije Universiteit Brussel	(promotor)
Prof. dr.	K. Broersen	University of Twente	(assistant promotor)
Prof. dr.	L. Van Den Bosch	K.U.Leuven	
Prof. dr.	N. van Nuland	Vrije Universiteit Brussel	
Prof. dr. ir.	M. van Putten	Universiteit Twente	
Prof. dr.	T. Jovin	Max-Planck Institut fur biophysikalische Chemie	
Prof. dr.	F. Conejero-Lara	Universidad de Granada	
Prof. dr.	V. Baekelandt	K.U.Leuven	
Prof. dr.	S. Ballet	Vrije Universiteit Brussel	

The work described in this thesis was performed at:

VIB Switch laboratory
formerly SWIT, Department of Bioengineering Sciences, Vrije Universiteit Brussel,
now at the Department of Cellular and Molecular Medicine, K.U.Leuven.

Nanobiophysics group
MESA+ institute for nanotechnology and MIRA institute for biotechnology and technical medicine, Universiteit Twente.

This research was financially supported by a PhD grant of the Agency for Innovation by Science and Technology (IWT), a Boehringer Ingelheim Fonds travel grant, and an EMBO Short Term Fellowship.

This thesis was printed by DATA PRINT NV - Herdebeekstraat 2a, 1701 Itterbeek

ISBN 978-90-365-3481-9
DOI 10.3990/1.9789036534819

Aggregation and toxicity of amyloid-beta peptide in relation to peptide sequence variation

DISSERTATION

to obtain
the degree of doctor at the University of Twente,
on the authority of the rector magnificus,
prof. dr. H. Brinksma,
on account of the decision of the graduation committee
to be publicly defended
on Wednesday the 12th of December 2012 at 16:45

by
Annelies Vandersteen

born on the 29th of May, 1985
in Jette, Belgium

This dissertation has been approved by:

Prof. dr. ir.	Frederic Rousseau	(promotor)
Prof. dr.	Vinod Subramaniam	(promotor)
Prof. dr.	Han Remaut	(promotor)
Prof. dr.	Kerensa Broersen	(assistant-promotor)
Prof. dr. ir.	Joost Schymkowitz	(assistant-promotor)

Il y a plus de courage que de talent dans la plupart des réussites
F. Leclerc

Contents

Abbreviations

Aβ	amyloid-β
ADAM	a disintegrin and metalloproteinase
ADDL	Aβ-derived diffusible ligand
AFM	atomic force microscopy
AICD	APP intracellular domain
ALS	amyotrophic lateral sclerosis
AP	action potential
APH1	anterior pharynx-defective 1
APP	amyloid precursor protein
APPs	amyloid precursor protein extracellular soluble fragment
ASID	a substrate inhibitory domain
ATR-FTIR	attenuated total reflectance FTIR
BACE	β-site APP cleaving enzyme
CD	circular dichroism
CI	confidence interval
COX	cyclo-oxygenase
CSF	cerebrospinal fluid
CT	computed tomography
CTF	C-terminal fragment
DMEM	Dulbecco's modified eagle medium
DMSO	dimethyl sulfoxide
DSM	diagnostic and statistical manual
DSSP	definition of secondary structure of proteins
ECL	electrochemiluminescence
ELISA	enzyme-linked immunosorbent assay

EM	electron microscopy
EPSP	excitatory post-synaptic potential
ER	endoplasmic reticulum
ERAD	ER-associated degradation
ESI-MS	electrospray ionisation mass spectrometry
FAD	familial Alzheimer disease
FBS	foetal bovine serum
FTIR	Fourier-transform infrared spectroscopy
GSA	γ-secretase activator
GSI	γ-secretase inhibitor
GSM	γ-secretase modulator
HDX	hydrogen-deuterium exchange
HFIP	hexafluoro-isopropanol
HSQC	heteronuclear single quantum coherence
IDP	intrinsically disordered protein
IPOD	insoluble protein deposit
JUNQ	juxta nuclear quality control compartment
LC-MS	iquid chromatography - mass spectrometry
LPP	lambda protein phosphatase
MALDI	matrix assisted laser desorption/ionisation
MCI	mild cognitive impairment
MD	molecular dynamics
MEA	micro-electrode array
MEF	mouse embryonic fibroblast
MMSE	mini-mental state examination
MRI	magnetic resonance imaging
MS	mass spectrometry
NICD	Notch intracellular domain
NMR	nuclear magnetic resonance
NSAID	non-steroidal anti-inflammatory drug
PAGE	poly-acryl gel electrophoresis
PBS	phosphate-buffered saline
PEN2	presenilin enhancer protein 2
PET	positron emission tomography
PI	propidium iodide
Prp	prion protein
PS	presenilin
SAD	sporadic Alzheimer disease
SD	standard deviation
SDS	sodium dodecyl sulfate
SEM	standard error of mean
SFV	Semliki Forest virus
SPR	surface plasmon resonance
TEM	transmission electron microscopy
thioT	thioflavin T
TOF	time-of-flight
UPR	unfolded protein response

1

An introduction to protein aggregation, the Aβ peptide and Alzheimer disease.

DNA is considered the basis of life; it contains all the necessary information for the development of a new organism. When thinking of DNA as the cellular information storage, proteins are the true labourers of the cell. Almost every cellular process is carried out by proteins, whether it is providing structure, controlling reactions, or facilitating them [1]. To be able to take part in that many various reactions with high selectivity and specificity, proteins are amongst the most diverse and versatile macromolecules [2]. All proteins are generated starting from only 20 basic building blocks - called amino acids - to adopt a unique structure relating to their specific function. The slightest structural error can hamper biological functioning and cause disease [1]. This chapter first describes how architecture of proteins is achieved and maintained. Then this chapter focusses on how a small protein engaging aberrant interactions is involved in Alzheimer disease.

1.1 On protein molecules

1.1.1 The protein architecture

Within the cellular nucleus the DNA code is transcribed into messenger RNA (mRNA). This mRNA is transported to the cytoplasm where it is translated by the ribosomal machinery. Many of the produced proteins adopt a specific three-dimensional organization that allows them to carry out their specific cellular actions. Generally this protein structure is organized from primary to quaternary level (Figure 1.1) [1]. Proteins are synthesized as a linear chain of amino acids. The unique combination of number, kind and order of these amino acids is called the primary structure of a protein [2] and contains all necessary information to adopt the final three dimensional structure (active conformation) of the protein [3]. Hydrogen bonding between the amide and carbonyl groups of the protein backbone results in the formation of secondary structures. These are regular local folds such as α-helices and β-strands. Further compacting of the secondary structures into the global conformation of the polypeptide chain forms the tertiary structure which sometimes is stabilized by disulfide bonds. For most proteins, the tertiary structure is the final active conformation. Some active conformations however consist of homogenous or heterogenous protein complexes. These are formed when the tertiary structures of the proteins making up the complex associate through non-covalent interactions into the quaternary protein structure [2].

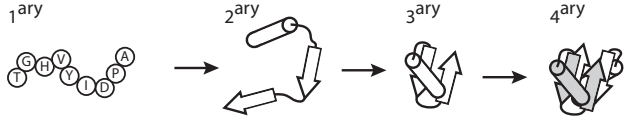

Figure 1.1 Levels of protein structure.
The primary amino acid sequence interacts to adopt secondary local structures. Compacting of these structures yields the global tertiary structure. Some proteins are active as quaternary complexes in which multiple polypeptide chains have associated. Figure is not to scale, adapted from [1].

1.1.2 How proteins fold

Anfinsen's experiments showed that the information required to adopt the final protein conformation is embedded in the primary amino acid sequence (Anfinsen's dogma) [3]. While proteins typically fold within seconds, Levinthal noted that sampling all possible folds to obtain the correct conformation would take longer than the age of the universe (Levinthal's paradox) [4] even when considering the steric hindrance posed by amino acid side chains. To solve this paradox he suggested that folding occurs along a well-defined pathway of intermediates and transition states [5]. Various models for protein folding have been proposed throughout the years [6-12]. The most recent concept is the 'protein energy landscape' that considers macromolecular states as 'ensembles' - distributions of conformations. The landscape starts with numerous unfolded conformations and whilst going through the narrowing funnel the number of conformational possibilities reduces. The idea of parallel transitions leads away from the sequential pathway [13,14] and the roughness of the landscape accounts for the presence of transient intermediates in local minima, and kinetically trapped 'misfolded' intermediates.

1.1.3 Some proteins do not (completely) fold

Proteins are considered to fold during synthesis or immediately thereafter and their function is assumed to be very closely related to their conformation (structure-function paradigm). The structural characterization of the protein database is considered key in understanding the biological role of these sequences. Many protein domains or even whole proteins are found to be unfolded or to adopt a non-globular conformation under physiological conditions [15]. As more and more of these unstructured proteins are discovered, they are classified as 'intrinsically disordered proteins' (IDPs) [16].

IDPs are often located in the cell nucleus where they perform key regulatory functions. These include DNA and RNA binding, signaling, cell cycle control and regulation of transcription [16,17]. The rapid turn-over of IDPs provides an extra advantage for these processes as it allows for quick responses to changing cellular needs. The lack of order in IDPs moreover creates functional advantages. When retaining their loose fold upon binding, IDPs display a larger intermolecular interface allowing for more contact points than a globular protein of similar size [18]. On the other hand their induced folding upon interaction allows for transient binding to multiple ligands [19] as opposed to specific and strong binding to one or two ligands for folded proteins. Many IDPs are reported to 'moonlight', that is exerting different (even opposing) functions on (different) molecules [20]. The induced folding of IDPs seemed to follow the classical structure-function paradigm, but a more detailed characterization of IDPs bound to a partner molecule revealed that large portions of the sequence remained disordered. These observations led to the idea that the classical structure-function paradigm needs to be re-considered [16].

Dunker and colleagues compared a comprehensive set of ordered and disordered domains and trained a neural network to predict disorder from amino acid sequences. Their results indicated that regions with a high tendency to disorder are enriched in preferentially exposed R, S, P, E and K and significantly depleted of W, C, I, Y and V which are mostly buried. This sequence preference allows for identification or prediction of disordered regions [21]. Analysis of the Swiss Protein database using a predictor for disorder revealed many disordered domains and proteins indicating that IDPs are very common within the protein kingdom [22]. Combined with the key functional role of IDPs, it can be argued that specific features of IDPs are maintained throughout evolution. IDPs are now generally accepted as a distinct class of proteins and the "database of protein disorder" (DisProt) gathers and collects structural and functional information on IDPs [23].

1.1.4 Protein quality is monitored and maintained

To monitor and maintain the balance of the protein network, described as proteostasis, the cell has developed an elaborate machinery controlling the synthesis, folding, trafficking and clearance of proteins. Protein folding *in vivo* is considerably challenging due to the crowded environment with protein concentrations in the range of hundreds of mg ml^{-1} [24]. In such conditions non-functional interactions of non-native polypeptide chains, i.e. newly synthesized, denatured, misfolded or damaged, are a likely scenario. To avoid, or resolve, these interactions an extensive network of molecular chaperones has evolved to ensure that proteins adopt and maintain their functional fold [25]. Molecular chaperones are defined as any protein that interacts

with, stabilizes or helps another protein to acquire its functionally active conformation, without being present in its final structure [26]. Molecular chaperones bind nascent polypeptide chains when released from the ribosome. They aid *de novo* protein folding by protecting the uncompleted sequence from hydrophobic interactions with other newly synthesized polypeptides [27]. Further, incorrectly folded proteins are recognized by specific chaperones that sequentially unfold and rescue them by providing a second chance to fold correctly [28] or deliver them to the correct quality control compartment [29]. When chaperones cannot aid or rescue a non-native polypeptide chain to adopt its correct conformation they can assign the sequence for degradation [30].

Several regulating mechanisms have evolved to ensure proteostasis. When the influx of nascent polypeptide chains directed to the secretory pathway exceeds the protein folding capacities of the endoplasmic reticulum (ER), the unfolded protein response (UPR) is activated to return the ER to its normal state. The UPR is threefold: (i) decreasing demand by downregulation of transcription and translation of secretory proteins, (ii) increasing clearance of misfolded proteins through ER-associated degradation (ERAD) or through autophagy (encapsulation of cytoplasmic components into the autophagosome and subsequent fusion with lysosome for degradation), and (iii) increasing synthesis of ER localized chaperones [31]. On the other hand, environmental stresses like temperature increase, tissue injury, or presence of heavy metals as well as metabolic stresses such as increased production of reactive oxygen species or nutrient imbalance can enhance the incorrect folding of proteins. To counter-act the possible detrimental consequences of these external conditions, the negative regulation on the transcription of chaperones is removed, and chaperones accumulate [32].

The question arises how IDPs fit in the cellular quality control. Primarily, some IDPs are part of the quality control system acting as chaperones [33] or serving as a signal for degradation [34]. Concerning the quality control of IDPs, the depletion of preferentially buried amino acids from their sequence minimizes aberrant hydrophobic interactions [35] and thus the need for chaperone assistance. Further, IDPs are reported to have short half-life, and are very sensitive for degradation *in vitro* [34]. This might indicate that non-interacting IDPs are rapidly degraded while they are rescued from degradation by their binding partner. Analysis of high-throughput studies indicates that chaperones mainly interact with globular proteins and not with IDPs [36] suggesting a fundamental difference between IDPs and non-native globular proteins. However IDPs might need chaperone assistance during the assembly of protein complexes or when their concentration is high and they are at risk of making aberrant hydrophobic interactions [37].

1.1.5 When proteostasis is disturbed

Proteostasis can be disturbed by several mechanisms. Viral infections and diseases like cancer manipulate the proteostasis machinery to increase protein folding and trafficking capacities for their benefit. On the other hand, upon aging, the capacity of the quality control system declines [38] and genetics can increase misfolding propensity of proteins or reduce proteostasis mechanisms [39,40]. In the latter cases, the proteostasis mechanisms fail, or are overwhelmed by the amount of accumulated chemically modified or misfolded proteins. All variation of the proteins' native conformation that affects the normal protein functioning, is called 'misfolding'. Some of the accumulated non-native proteins expose hydrophobic patches that are

normally buried and which have high tendency to interact with exposed hydrophobic patches of other proteins. These hydrophobic interactions cause the proteins to cluster - a phenomenon called aggregation [41]. Aggregation is thus only a form of misfolding and is determined by many factors as is described in the following section. Although there seems to be a preference for clustering with the same proteins, co-aggregation with other proteins is possible [42,43].

The often toxic aggregates can be located intra- as well as extracellularly. The quality control system attempts to re-solubilize the aggregates through chaperones [44,45]. Re-solubilization is often not successful and then the aggregates remain insoluble. The intracellular insoluble aggregates can be sequestered into inclusions like aggresomes to isolate them from the cytoplasm [46,47] as a protective measure. The juxtanuclear quality control (JUNQ) compartment stores soluble misfolded proteins that are re-directed to the quality control system. Proteins from the JUNQ can either refold or be tagged for degradation. A second compartment, the insoluble protein deposit (IPOD), concentrates proteins that are meant for elimination through autophagy [29,48].

When aggregates cannot be eliminated effectively they can cause toxicity which leads to disease (Table 1.1). As these diseases are caused by the failure of a protein to adopt or maintain its native conformation, these disease are also called 'conformational diseases'. Many of the aggregating proteins underlying these diseases are IDPs [49].

Disease	Protein or peptide
Alzheimer disease	amyloid-β peptide / tau protein
Parkinson disease	α-synuclein
Huntington disease	huntingtin
Spongiform encephalopathies	prion protein
Amyothropic lateral sclerosis (ALS)	superoxide dismutase 1
senile systemic amyloidosis	transthyretin
hemodialysis-related amyloidosis	β_2-microglobulin
lysozyme amyloidosis	lysozyme
medullary carcinoma of the thyroid	calcitonin
injection-localized amyloidosis	insulin
type II diabetes	amylin
cataract	γ-crystallins

Table 1.1 Overview of some of the best known conformational diseases.
These include neurodegenerative diseases as well as nonneuropathic systemic and localized amyloidoses. Table adapted from [49].

Two possible mechanisms can underlie toxicity: 'loss-of-function' and 'gain-of-function'. The 'loss-of-function' disorders are linked to inherited mutations that may lead to excessive degradation. The 'loss-of-function' phenotype is caused by the insufficient number of active protein molecules to maintain functionality [50] as well as through

entrapping other essential proteins in the aggregates [51]. When the aggregates have toxic properties the related disease is considered a 'gain-of-function' disorder [50].

The recent awareness that IDPs are a common class of the protein kingdom and the insights in the formation of aggregates have led to an adaption of the protein folding landscape (Figure 1.2). Upon folding, globular proteins make intramolecular contacts leading to the native conformation. When engaging non-native, intermolecular contacts, globular proteins aggregate into amorphous or fibrillar aggregates or any possible intermediate morpholgy. IDPs populate an energy plateau at the top of the folding funnel. Intermolecular contacts with specific binding partners can induce the folding of IDPs and guide them through the funnel towards the folded complex. On the other hand intermolecular interactions with proteins that are not interaction partners can lead to aggregation [52].

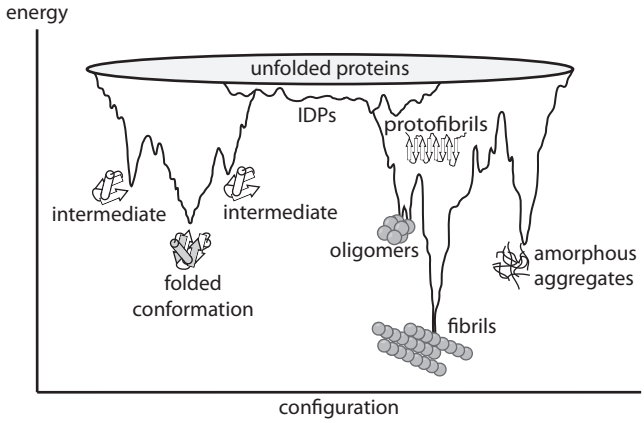

Figure 1.2 The protein folding landscape.
Unfolded proteins are localized at the top of the energy landscape. Under folding conditions the sequence will go down the funnel to adopt the folded conformation. Engaging nonnative interactions leads to a second funnel resulting in aggregation. Figure adapted from [49].

1.2 Fibrillar aggregates

The first observations of insoluble protein deposits in microscopy slices were stained with iodine, a chemical commonly used for the staining of starch ('*amylum*' in Latin), and hence led to the name 'amyloid'. For a while the nature of the deposits was unclear until it was discovered that they were in fact of proteinaceous nature [53]. Nowadays the term amyloid is used to designate fibrillar aggregates adopting a cross-β structure and displaying characteristic tinctorial properties such as green birefringence of Congo Red and enhanced fluorescence of thioflavin T [54-56]. As amyloid deposits were at first observed in conformational diseases (Table 1.1) it was assumed that amyloid formation was a property limited to the small set of proteins related to these diseases. Later, it became clear that aggregation is an intrinsic property of the protein backbone since almost any protein can be induced to form amyloid under conditions that destabilize the native conformation or enhance intermolecular interactions [57]. The generic nature of protein aggregation is also seen in some organisms that exploit this property for a specific purpose. The silk fibers of the spider web [58], the silk moth's eggshell [59] and some bacterial surface structures [60] are composed of amyloidogenic proteins

which are assembled under strict regulation, also termed functional amyloids.

1.2.1 The fibrillar organization

Various proteins without any sequence or conformational homology can form amyloid fibrils with similar characteristics. This suggests that the main interactions within the fibril are made through the common protein backbone and not by the individual amino acid side chain residues [61]. Additional evidence for the intrinsic nature of amyloid formation came from the observation that polythreonine and polylysine sequences could form amyloid [61]. Electron microscopy or atomic force microscopy images showed that amyloid fibrils are long, unbranched and often twisted structures with a diameter of 7-13 nanometer. They consist of a number of aligned or rope-like twisted smaller protofilaments of 2-5 nanometer diameter each [62,63]. X-ray diffraction patterns of fibrils display typical cross-β patterns indicating that the proteins in the protofilaments are structurally organized as β-strands oriented perpendicular to the fibril axis with hydrogen bonds running parallel to the long of the fibril [55]. Individual molecules are stacked every 4.7 Å along the axis; parallel, in register and stabilized by hydrogen bonding. Each protofilament contains two or more β-sheets with an intersheet distance of 10 Å (Figure 1.3) [64,65].

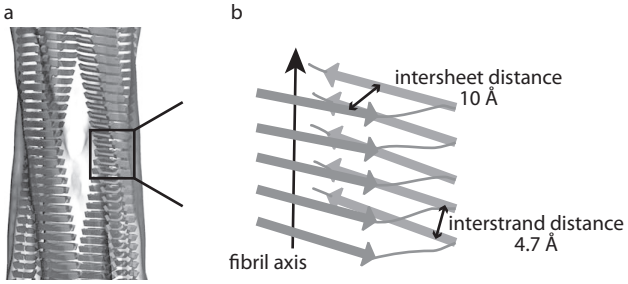

Figure 1.3 Structure of the fibril core.
(a) The fibril consists of various β-sheets running along the fibril axis. (b) The individual sheets are spaced at 10 Å while the β-strands within the sheet are oriented perpendicular to the fibril axis and have an interstrand spacing of 4.7 Å. Figure adapted from [66],[67].

This specific structural organization is recognized by the dyes Congo Red and thioflavin T. When bound to fibrils these compounds display green birefringence and enhanced fluorescence respectively [68]. Aside of these common traits, heterogeneity in fibril structure exists as well. Variation can occur at the level of amino acid side chains as well as in the loops connecting intramolecular β-sheets. Further both length and orientation of the individual β-strands and the number of β-sheets in the fibril can vary. Variation can also be observed between fibrils of the same protein that adopt different internal fibrillar organization due to thermodynamic or kinetic determinants under given conditions [69].

1.2.2 Amyloid characteristics on amino acid level

The observation that co-aggregation is significantly decreased between sequences with a sequence identity lower than 30-40% suggests the presence of amino acid sequence determinants for aggregation [70]. The aggregation rate of a given

sequence correlates with the net charge, hydrophobicity and propensity to adopt β-sheet structure of that sequence [71,72]. In general a low net positive or negative charge allows for the formation of ordered fibrils as a result of these charges allowing a limited number of orientations of the individual amino acids in the fibril structure that maximize the distance between charges of the same sign. Stacking of β-sheets of neutral sequences that have no charge compensations is not limited in orientation and therefore forms amorphous aggregates. Extremely high net charged proteins have too many uncompensated charges that make it energetically unfavorable to aggregate and hence discourage self-assembly [72,73]. Sequence stretches with high hydrophobicity or high propensity to form β-sheet are usually the regions triggering aggregation [71]. Evolutionary pressure developed mechanisms to prevent aggregation *in vivo* such as the incorporation of β-sheet breakers like proline and so-called 'gatekeepers', charged residues flanking aggregation-prone regions. These gatekeeper residues are also the recognizing motifs for chaperone binding in the process of preventing aggregation [74]. Moreover, IDPs are generally significantly more charged than globular proteins, have low β-sheet propensity and thus contain far less aggregation nucleating regions than globular proteins minimizing their risk of aggregation [33,75,76].

The fact that the aggregation of a sequence is partially determined by the physico-chemical properties of the amino acids in that sequence raises the opportunity for prediction of aggregation based on sequence. Over the years several algorithms were developed to identify and score aggregating regions [77-79], as well as a specific predictor of amyloid aggregation [80].

1.2.3 The formation of amyloid

Aggregation of globular proteins can start from unfolded polypeptides, partially folded intermediates or native conformations. The partially folded state generates from both partial unfolding of the globular conformation under de-stabilizing conditions and kinetic trapping of partially folded intermediates during folding (Figure 1.4) [81].

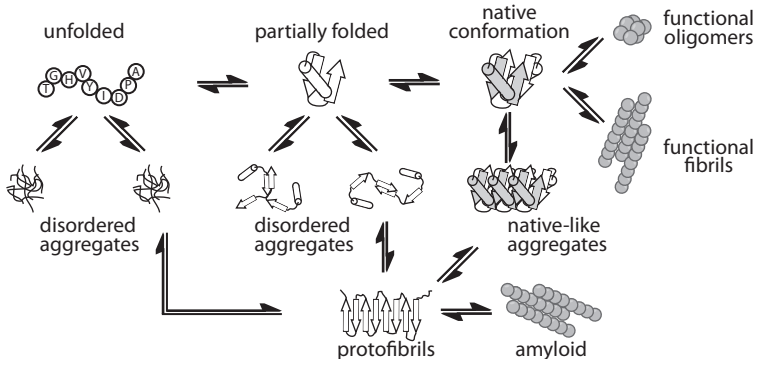

Figure 1.4 Schematic representation of protein folding and misfolding pathways. Protein sequences adopt various conformations and undergo transitions from one conformation to the other. Aggregation might start from any of these conformations. Figure adapted from [49].

The unfolded and partially folded states initially form disordered aggregates that can reorganize into oligomers and further assemble to form amyloid [49]. The native

conformation of some proteins associates to form fibrils which may be functional as described under section 1.2. Other proteins assemble into fibrils with characteristic tinctorial properties but maintaining their native structure, and activity as is the case for actin, Pmel17 and glutamate dehydrogenase [82-84]. For IDPs the scheme as depicted in Figure 1.4 is sligthtly different as IDPs do not need to partially unfold to make intermolecular contacts and aggregate. IDPs might interact in their native, unfolded conformation and aggregate further. On the other hand, analogous to partial (un)folding, IDPs first may have to undergo a transition from a predominant cellular form to an abnormal form - like the prion protein - before aggregation occurs [52].

The association of proteins during aggregation may result in amorphous aggregates or fibrillar amyloid or an intermediate thereof (Figure 1.5). The processes leading to these structures are highly sensitive to environmental conditions and protein concentration. Variation of pH, temperature or the presence of salts affects the possible interactions between polypeptides and hence determines whether amyloid rather than amorphous aggregates are formed [73]. Although typical amyloid fibrils have been primarily defined by cross-β structure, amorphous aggregates are now recognized to not just consist of random clumps of sticky protein without dominant structure characteristics but often also consist of cross-β structure [85].

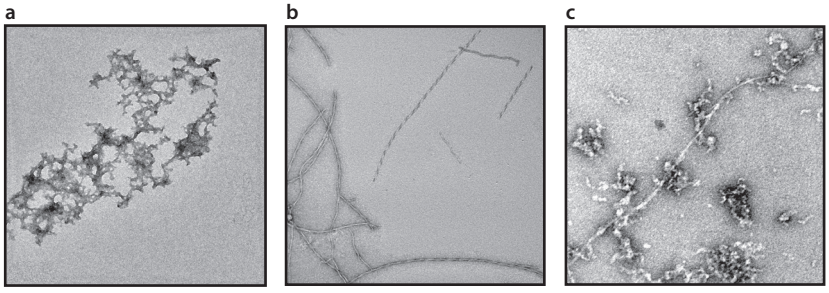

Figure 1.5 The macromolecular morphology of aggregates.
Aggregates as observed using transmission electron microscopy can appear either (a) amorphous, (b) fibrillar or (c) as a mixture of these.

The aggregation processes of some proteins including actin, glutamate dehydrogenase, tubulin, amyloid-β and calcitonin have been studied in detail [86]. The unravelling of the aggregation mechanism involves detailed characterization of key intermediates as well as determination of the thermodynamic and kinetic properties of the conversions of these intermediates. It has been recently suggested that the association mechanisms of all the various amyloidogenic proteins share some key determinants [87]. A number of models have been developed to describe these general association mechanisms. The first model described aggregation as a monomer-addition reaction [88] where aggregation only occurred above a critical protein concentration. While applying this model to the kinetics of sickle-cell hemoglobin gelation, nucleation and polymerization were distinguished, introducing the 'nucleation and polymerization' model [89]. This concept described the thermodynamically unfavorable addition of monomers until a nucleus was formed. Further thermodynamically favorable addition led to polymerization. Later, Benedek and colleagues described the formation of a micelle at concentrations above the critical micelle concentration [90] reminiscent to the

process of lipid association at concentrations above the critical micelle concentration. Nucleation occurs within the micelle followed by elongation. Detailed characterization of glutamate dehydrogenase raised the idea of random association in which two units - monomeric or oligomeric - could associate to form the polymer [91]. The aggregation of the prion protein in which the cellular form, PrP^{C}, converts to the prion form, PrP^{SC}, before aggregation occurs has been described by the nucleation-dependent polymerization mechanism [92]. This model has been used later to describe the aggregation mechanisms of other amyloidogenic proteins [93]. Recently, the two-step model originally describing the formation of transition-metal nanoclusters [94] has been shown to apply to the aggregation of various proteins [95], although being very simplistic and having some limitations [86]. Elongation of fibrils has been shown to occur through monomeric peptide binding [96]. Two models are formulated to describe fibril elongation: a 'dock-and-lock' model and a 'fast deposition' model. The 'dock-and-lock' model is a two-step mechanism in which the monomer attaches to the fibril end through diffusion. The monomer/fibril complex then reorganizes, possibly undergoing conformational change, to lock the monomer in an aggregated state [97]. The 'fast deposition' model on the other hand is a one-step mechanism. The conformation of the monomeric peptide fluctuates and adopts an aggregation-prone state. As this state, while diffusing, encounters a fibril end it will deposit [98]. Increased computational power and available simulations are nowadays used to understand the thermodynamics and kinetics of protein aggregation [87].

As previously mentioned, aggregation is a very complex reaction and consists of many intermediates such as oligomers, critical nuclei, and protofilaments. The general model describing aggregation (Figure 1.6) is based on the nucleation-dependent polymerization [92]. In this model no aggregation is observed at concentrations below a critical concentration. When concentrations are above the critical concentration a lag phase is observed during which monomers associate into an ordered nucleus (rate-limiting step), although in some cases nucleation is very rapid so that no lag phase is observed. The nuclei then rapidly elongate through monomer or oligomer addition during an exponential growth phase to reach an equilibrium between monomers and ordered aggregates.

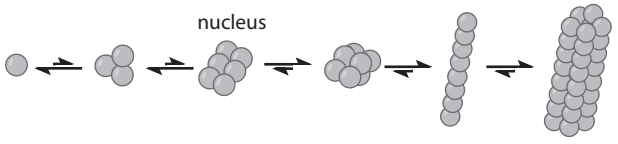

Figure 1.6 Schematic representation of the aggregation mechanism.
Monomers associate into oligomers and form a critical nucleus. The critical nucleus is the starting point for further polymerization. Figure adapted from [86].

Detailed understanding of the *in vitro* behavior of amyloidogenic proteins, and the mechanisms leading to amyloid formation has contributed significantly to the current insights in the various conformational diseases. Currently, interest has shifted away from the fibrillar structures towards the smaller, soluble species of the aggregation pathway. Oligomers are nowadays considered the true harmfull species exerting toxic effects [99-104], although this hypothesis remains to be unequivocally proven. Biophysical understanding and characterization of the oligomers is combined with cell culture set-ups and *in vivo* models to unravel the mechanisms and pathways leading

to toxicity. Better understanding of these mechanisms is a new opportunity to identify drug targets and therapeutic approaches.

1.3 Alzheimer disease

In 2010 about 35 million people worldwide were estimated to suffer from dementia. Estimates are that the number of patients will be tripled by 2050 [105]. Currently, the total cost related to the medical and social care are rated to exceed 600 billion US dollar [106]. The increasing number of patients will challenge society on social, medical and economical level. About 50-75% of above mentioned patients with dementia suffer from Alzheimer disease, the most well-known form of dementia [105]. Currently no cure or treatment to halt or reverse disease progress is available for Alzheimer disease. Better insight into the mechanisms leading to Alzheimer disease can improve diagnosis, treatment and patient care.

1.3.1 Disease course

The course of Alzheimer disease progress is divided into three stages: mild, moderate and severe (Table 1.2) [107]. Early on when symptoms of dementia become noticeable but do not interfere with normal functioning, the term 'mild cognitive impairment' (MCI) is used. MCI can be related to normal aging, or can be the earliest sign of Alzheimer disease [108].The illness then progresses to a stage where symptoms compromise daily living. The mild phase is characterized by a 'simple' loss of memory, manifested by having trouble finding the right word and misplacing objects. These early symptoms evolve into more advanced memory loss, having problems recognizing family and friends and inability to learn new tasks. At this stage accomplishing basic daily tasks becomes challenging or even impossible. During the last, severe stage patients lose control of many normal physiological functions, are no longer able to speak coherently and suffer from weight loss and infections [107].

MILD	MODERATE	SEVERE
getting lost	confusion	weight loss
poor judgement	difficulties with multistep tasks	loss of communication
trouble handling money	paranoia	difficulty swallowing
repeating questions	personality changes	increased sleeping
mood & personality changes	impulsive behavior	skin and lung infections
vocabulary problems	not recognizing family - friends	
misplacing & losing objects	not learning new tasks	
anxiety	language & number problems	
aggression	shortened attention span	
	loss of logic thinking	

Table 1.2 Overview of the most common symptoms related to Alzheimer disease. Symptoms of Alzheimer disease are grouped in stages of disease progress [107].

1.3.2 Diagnosis

Currently, Alzheimer disease cannot be diagnosed with 100% accuracy. As there is no specific test to identify Alzheimer disease in the living patient several tests are used, mainly to rule out all other possible causes for the symptoms. As a consequence diagnosis is either possible or probable. Diagnosis can only be confirmed by postmortem examination of brain tissue [109]. Diagnosis of Alzheimer disease follows the criteria stated in the Diagnostic and Statistical Manual (DSM IV) [110]. A first indication for Alzheimer disease comes from medical and family history and is followed by neurological and physical examination to make a diagnosis and determine the stage of the disease. A first test is the 'mini-mental state examination' (MMSE) [111] examining global cognitive functions. Further, memory function and attention span are assessed using word recall or pictures naming tests [112] and the Wisconsin card sorting test [113], respectively. Psychological examination of patients can indicate the presence of apathy, depression, anxiety or hallucinations, all symptoms of Alzheimer disease. Blood tests and cerebrospinal fluid (CSF) analysis for biomarkers such as total tau and phospho-tau provide additional indications as well as the use of imaging techniques such as computed tomography (CT), magnetic resonance imaging (MRI) and positron emission tomography (PET). The presence of other disorders such as infections, anorexia and cardiovascular disease can worsen the state of the patient and thus need to be examined and treated [114].

1.3.3 Pathology

Alzheimer disease is a progressive neurodegenerative disease characterized by pathological neuronal cell death and corresponding loss of neuronal function and synaptic connections. Neuronal loss occurs gradually throughout different brain regions and eventually leads to severe shrinkage of the brain (Figure 1.7). The first region affected is the hippocampus, involved in the formation of new memories and recalling recent memories. Neurodegeneration then spreads to the cerebral cortex responsible for *i.a.* thought, attention, language, and reasoning. In the last stage of the disease neurodegeneration is spreaded throughout the brain [107].

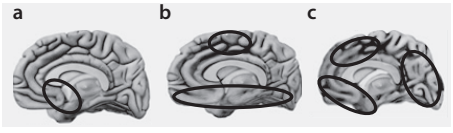

Figure 1.7 Spreading of neuronal brain loss.
(a) Neuronal loss starts in the hippocampus (marked) in mild Alzheimer disease, (b) progresses throughout the brain in moderate disease stages and (c) affects almost all areas of the brain in the severe stage. Figure adapted from [107].

On a molecular level, Alzheimer disease is characterized by the presence of amyloid plaques and neurofibrillary tangles in the brain [115]. Amyloid plaques are extracellular deposits mainly build up from amyloid-β (Aβ) peptides but also containing smaller amounts of many other cellular components [116,117]. Tangles are intracellular helical filaments of hyperphosphorylated tau proteins [118]. The hyperphosphorylated tau proteins no longer associate with microtubules. As a consequence, microtubules dissociate and microtubule-associated transport and cellular shape are no longer

supported [119]. Hardy and Allsop proposed the 'amyloid cascade hypothesis' suggesting that the processing of amyloid precursor protein (APP) to generate Aβ is the key event in developing Alzheimer disease. The subsequent aggregation of Aβ and the formation of neuritic plaques then triggers a cascade of events such as the formation of neurofibrillary tangles leading to neuronal death and dementia [120]. The formulation of this hypothesis led to an exponential increase of experimental study of the Aβ peptide and the amyloid deposits. Accumulating evidence from mutations leading to early-onset familial forms of Alzheimer disease [121], neurotoxicity of the Aβ peptide [99] and the correlation between the amounts of soluble Aβ and the severity of neurodegeneration [102] led to reconsideration of the hypothesis. In its current form, the hypothesis emphasizes the importance of soluble toxic oligomers and Aβ is no longer thought to be the only culprit [122].

1.3.4 Sporadic and familial forms

Both sporadic and hereditary familial forms of Alzheimer disease are known (SAD and FAD respectively). FAD cases, in contrary to SAD, are characterized by early-onset (before the age of 65) of the disease [123]. The familial forms of Alzheimer disease are caused by mutations in either the APP gene [124] or in the genes encoding for presenilin-1 or -2 (PS-1, PS-2), subunits of the APP processing γ-secretase complex (http://www.molgen.ua.ac.be/ADMutations) [125]. Mutations in APP (Table 1.3) are clustered around the secretase cleavage sites suggesting their phenotype is the result of affected secretase activity [126]. Mutations located near the β-secretase cleavage site generally induce an increased Aβ production while mutations close to the γ-secretase cleavage site modulate γ-secretase activity and cause a shift in the spectrum of produced Aβ peptides towards longer forms without necessarily affecting the quantity of Aβ peptides produced [126,127]. Mutations in PS-1 or PS-2 affect the active site of the γ-secretase complex and increase the release of $A\beta_{42}$ [121]. Increased production of APP, located on chromosome 21, as seen in patients with Down syndrome (trisomy 21) also leads to early-onset Alzheimer disease [128].

NAME	MUTATION	NAME	MUTATION
Swedish	K670N / M671L	Austrian	T714I
Tottori	D678N	French	V715M
Flemish	A692G	German	V715A
Dutch	E693Q	Florida	I716V
Arctic	E693G	London	V717I
Italian	E693K	Indiana	V717F
Iowa	D694N	Australian	L723P
Iranian	T714A		

Table 1.3 Selection of the known mutations of APP
The mutations of APP are named after the nationality or location of the first family in which the mutation was demonstrated [129].

1.3.5 Therapeutic approach

Current drugs available for the treatment of Alzheimer disease are cholinesterase inhibitors (donepezil hydrochloride, rivastigmine and galantamine) and an NMDA-receptor antagonist (memantine). The cholinesterase inhibitors prevent the breakdown of acetylcholine. The increased levels of acetylcholine improve communication between neurons and hence temporarily improve or stabilize symptoms of Alzheimer disease. The NMDA-receptor antagonist memantine blocks the effect of glutamate. Glutamate is released by damaged neurons, and causes damage to healthy brain cells. Hence, blocking the action of this molecule protects neurons against damage [130].

The current therapeutic approach thus mainly provides symptomatic relief by mild improvement of cognitive function in the early phases of disease progress, but is not able to reverse or prevent disease progress. The increasing number of patients and the related social and economical burden create an urgent need for development of such therapeutics. Various strategies acting on Aβ, tau or other cellular targets are being investigated and some of these have reached the stage of clinical trials, albeit with little success.

One of the strategies in the fight against Alzheimer disease directly targets the Aβ peptide. The possible different approaches act on (i) the release of Aβ, (ii) prevention of Aβ aggregation, or (iii) reducing deposited protein levels [131].

When trying to reduce or prevent the release of Aβ peptides, the secretases cleaving APP are the main targets. Upregulation of α-secretase activity has been explored with the aim to shift APP processing towards the non-amyloidogenic pathway, producing p3 peptide instead (Figure 1.8). This pathway is considered protective towards Alzheimer disease as it precludes the release of Aβ. However, the p3 peptide released in the non-amyloidogenic pathway is highly hydrophobic and has been reported to be present in amyloid plaques [132]. Moreover, the catalytic site of α-secretase activity is composed of a series of membrane-associated proteases, all members of the ADAM (a disintegrin and metalloproteinase) family [133]. This heterogeneity makes it difficult to specifically target α-secretase activity. Compounds indirectly activating α-secretase activity have been developed and are being tested in clinical trials [134]. A second strategy to reduce Aβ burden is inhibition of β-secretase activity. The β-secretase enzyme (BACE) cleaves multiple transmembrane proteins [135] and thus careful dosage is needed to find an equilibrium between sufficient BACE inhibition and minimal side effects. Compound CTS21166 is currently being evaluated in clinical trials [136]. Although the precise function of Aβ remains elusive, evidence is accumulating that the peptide performs an essential role [137]. Preventing, or reducing the Aβ production might induce side effects. The γ-secretase complex cleaves various transmembrane substrates such as Notch1, essential for cell-cell communication and neuronal function a.o. [138]. The inhibition of γ-secretase activity obstructs the cleavage of these substrates and hence causes important side effects [139]. The high degree of variability of the proteolytic complex however enables the specific inhibition of certain complexes to minimize side effects [140] as could be the case for so-called 'Notch-sparing' γ-secretase inhibitors [141]. Another strategy that received ample attention is to shift the spectrum of produced Aβ peptides towards shorter Aβ as many FAD-related mutations do not affect total Aβ production but specifically increase $A\beta_{42}$ generation. This shift is accomplished by molecules that modulate the cleavage site of γ-secretase to produce less $A\beta_{42}$ and more of the shorter lengths without inducing side-effects [142].

An alternative approach aims at inhibiting the self-assembly of Aβ thereby preventing the formation of soluble toxic species and eventually plaque deposition. One attempt using synthetic glycosaminoglycan 3-amino-1-propaneosulfonic acid (3APS) has been evaluated in clinical trial phase II. Results showed decreased CSF $A\beta_{42}$ levels but no significant cognitive improvement [143]. Another attempt used a zinc and copper binding drug as *in vitro* Aβ aggregation is effectively inhibited by metal chelators. The changes in plasma Aβ levels after administration of the compound were significant in patients with mild disease but not in severe cases [144].

A third strategy directly targeting Aβ focussed on reducing plaque load using immunotherapy. A clinical trial for Aβ vaccination was set-up after promising animal studies but had to be interrupted due to low antibody response and occurrence of meningoencephalitis [145]. Despite significant decrease of plaque load, no cognitive improvements or delay of disease progress was obtained using active immunization [146]. As proteostasis of Aβ is a subtle equilibrium between production and clearance of the peptide, accumulation of the peptide can be the consequence of increased production, or of defective clearance. Various enzymes are reported to degrade Aβ *in vivo* or *in vitro*. Amongst them insulin degrading enzyme, angiotensin-converting enzyme, neprilysin and cathepsin D [147]. It has been observed that Aβ clearance is impaired in patients with Alzheimer disease, providing a possible mechanism for disease development [148]. Upregulation of Aβ clearance might therefore be an alternative approach to prevent plaque formation.

Complementary to Aβ targeting, drugs promoting neuroprotection are being explored. Compounds aiming at inhibition or reduction of oxidative stress, neuroinflammation or mitochondrial dysfunction in neurodegeneration could have potential to minimize the neuronal damage and contribute to improved cognitive function [149]. Further, effective therapy against Alzheimer disease has been hypothesized to use combined action against Aβ and tau hyperphosphorylation or tangle formation [131] as the loss of microtubule-associated cellular transport and structure is an important event in neurodegeneration.

1.4 The amyloid-β peptide

The Aβ peptide (sequence details provided in Appendix A) is widely studied in the light of its role in Alzheimer disease. The production of the intrinsically disordered Aβ peptide is a physiologically normal process that occurs in healthy subjects as well as in Alzheimer disease patients. Hence, the generation of the peptide itself is unlikely to represent the primary cause of Alzheimer disease [150]. It remains however elusive what the actual cellular role of Aβ comprises. The last decade several possible functions of Aβ were hypothesized, but none of these have been confirmed. The property to reduce the metal charge state of some metal ions led to the suggestion that Aβ could protect against metal-induced oxidative damage [151] although this mechanism is also reported to induce toxicity [152]. Further Aβ was suggested to have a signaling function in secretase activity [153], to be involved in cholesterol transport [154] or to act intracellular as a transcription factor [155]. An increased production of Aβ as observed in some early-onset FAD cases and patients with Down syndrome, has been shown to be sufficient for development of Alzheimer disease [126,128].

1.4.1 Generation of Aβ

The Aβ peptide is generated from APP by proteolytic cleavage. The proteolysis of APP can occur through two pathways (Figure 1.8). Both pathways release an extracellular soluble fragment (APPs) and a second membrane-spanning C-terminal fragment (CTF) [156]. The non-amyloidogenic pathway is selected when APP is first cleaved by α-secretase, generating $APP_{s\alpha}$ and CTF_{83}. This cleavage precludes the generation of Aβ as the α-secretase cleavage site is located within the Aβ sequence. The amyloidogenic pathway is entered when APP is first cleaved by β-secretase instead of α-secretase. The β-secretase cleaves at the N-terminus of the Aβ sequence, releasing $APP_{s\beta}$ and CTF_{99}. The CTF_{83} and CTF_{99} fragments are subsequently cleaved by γ-secretase and respectively generate the p3 and Aβ peptides as well as an APP intracellular domain (AICD) [156]. The soluble secreted APPs is reported to have a neuroprotective function and is important for neurogenesis [157]. AICD on the other hand impairs generation of new neurons [158], has a signaling function and is a transcription regulator [159]. The p3 peptide is generally accepted as non-amyloidogenic although it has been reported as highly hydrophobic, aggregating and has been found in amyloid plaques [132].

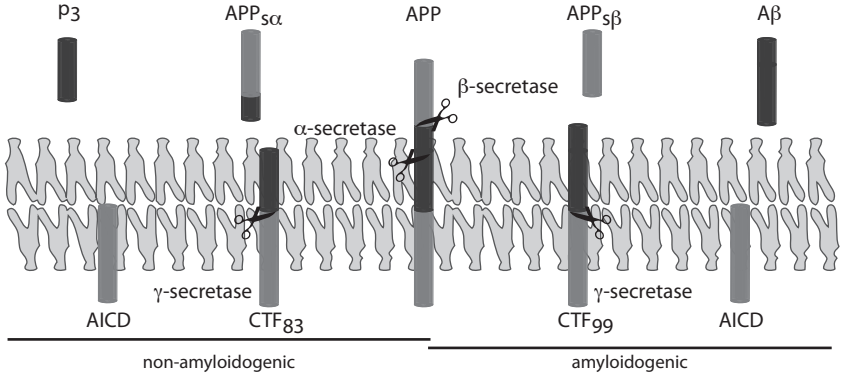

Figure 1.8 Proteolytic processing pathways of APP.
A first cleavage by α-secretase generates p3 peptides while primary cleavage by β-secretase releases Aβ upon subsequent proteolysis by γ-secretase. Figure adapted from [160].

α-Secretase activity is mediated by members of the ADAM membrane-bound protease family while β-secretase, also known as BACE (β-site APP cleaving enzyme), is a transmembrane aspartic protease [161]. However, the recognition that γ-secretase is largely responsible for the generation of Aβ lead to large scale research into its functioning and structure. γ-Secretase is a large proteolytic complex in which the catalytic core is formed by presenilin 1 and 2 (PS-1 and PS-2), complemented by nicastrin, presenilin enhancer protein 2 (PEN2) and anterior pharynx-defective 1 (APH-1) [161]. The γ-secretase complex first cleaves APP at the ε-site producing Aβ peptides of 48 or 49 amino acids long [162]. The γ-secretase complex then proceeds towards the γ-site releasing three to four residues at each step which results into two product lines: $Aβ_{48}$ > $Aβ_{45}$ > $Aβ_{42}$ > $Aβ_{38}$ and $Aβ_{49}$ > $Aβ_{46}$ > $Aβ_{43}$ > $Aβ_{40}$ [162,163]. These two product lines finally result in the generation of about 90% of the 40 amino

acid form with minor amounts of Aβ42 [164]. Besides the two predominant forms Aβ40 and Aβ42 both shorter and longer Aβ peptides have been detected *in vivo* [165,166].

Further heterogeneity of Aβ is introduced at the N-terminus during proteolytic release or afterwards by further modifications such as oxidation, isomerization or racemization [167]. These modifications can alter the hydrophobicity or resistance to proteolytic degradation of the peptides possibly with far-reaching consequences on disease progress [168].

1.4.2 Aggregation of Aβ

The behavior of the predominant Aβ40 and Aβ42 peptides is the subject of scientific research since the early nineties when Aβ peptides were identified as the main constituents of brain plaques [116]. The 42 amino acid isoform is the main component of plaques with smaller amounts of Aβ40 and other molecules [51,167,169,170]. Studies showed that the biophysical and biochemical behavior of both isoforms markedly differ despite a difference of only C-terminal amino acids. The longer Aβ42, being more hydrophobic compared to Aβ40 as a result of an additional C-terminal isoleucine and alanine, rapidly polymerizes into fibrils while Aβ40 is more soluble and displays a lag phase before fibril formation [171]. Differences between these two isoforms are also reflected at the level of early aggregation events and toxicity and indicates that both peptides aggregate through different pathways [172]. When mixing both peptides, Aβ40 reduces the aggregation rate of Aβ42 in a concentration-dependent manner while Aβ42 strongly enhances aggregation of Aβ40. Analogous, toxicity of Aβ42 is moderated by Aβ40 [173,174] which correlates with the finding of increased fractions of elongated Aβ in the brain of Alzheimer disease patients. This effect of Aβ40 on Aβ42 is also observed *in vivo* where increasing amounts of Aβ40 seem to be protective against plaque formation [175].

Recently, focus shifted from the fibrillar forms of Aβ towards the more soluble oligomeric forms. A first indication that fibrillar Aβ was not the main cause of Alzheimer disease came from the low correlation between disease progress and plaque load [100]. The finding that synthetic Aβ peptides had to aggregate to cause neurotoxicity was one of the first clues that aggregated forms of Aβ, and not the monomeric form, were the main culprits in the relation between Aβ and Alzheimer disease [99]. Additionally, studies showing that variable amounts of oligomers found in brain samples correlated well with the severity of dementia, and that memory impairment in transgenic mice occurred before plaque deposition could be observed, confirmed the hypothesis that oligomeric Aβ is the main toxic species [101,102]. Extra evidence came from the observation that conditioned medium containing Aβ oligomers could block long-term potentiation when injected in mice and that anti-Aβ treatment reversed memory deficits in mice, but had no effect on plaque burden [103,104]. Various toxic soluble species have been identified since. Amongst them protofibrils [176], Aβ-derived diffusible ligands (ADDLs) [177], a 56 kDa species - Aβ*56 - [178] and amylospheroids [179]. Characterization of the structural and cytotoxic properties of these various species which all exert significant toxic properties in cell culture and animal studies confirms the importance of soluble oligomers in Alzheimer disease progress. Even though a common building block [180] has been proposed and many intermediates have been identified, a unique toxic species has not been identified so far. The possibility remains thus that toxicity is related to more than one assembly, or to a specific structural feature

that has yet to be defined [181]. Toxic oligomers formed by Aβ, α-synuclein, insulin or prion protein e.g. are all recognized by the same A11 oligomer-specific antibody which indicates a relationship between a structural 'fingerprint' and toxicity [182].

1.4.3 Structure of aggregated Aβ

Fibrils of Aβ adopt, like other amyloid fibrils, a cross-β sheet structure with β-strands oriented perpendicular to the fibril axis [183]. Fibrils of both $A\beta_{40}$ and $A\beta_{42}$ are build out of stacked 'β-strand - turn - β-strand' (β-turn-β) units which are oriented parallel and in-register [184]. The N-terminus does not take part in this β-turn-β motif as it is thought to be unstructured [185,186], although recently stable fibrillar organization involving the first three to four residues of Aβ has been reported [183]. Both isoforms of Aβ adopt the β-turn-β motif in which residues 25 to 29 form the 180° bend [187] and which is stabilized by a salt bridge between residues 23 and 28 [185] (Figure 1.9). Structural differences occur at the level of the sidechain interactions. In $A\beta_{42}$ intermolecular contacts are made between residues 17, 19 and 21 on one sheet and the residues 34, 36 and 40 on the other sheet [185]. $A\beta_{40}$ on the other hand makes intramolecular sidechain interactions and the two β-sheets have shifted to be slightly out-of-register [185,187].

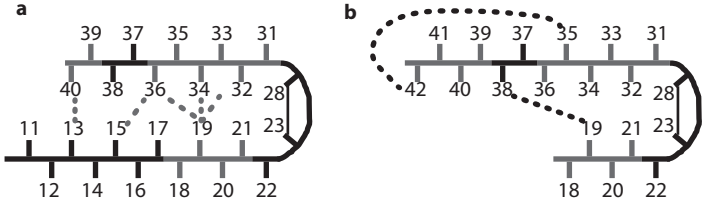

Figure 1.9 Suggested structure of the $A\beta_{40}$ and $A\beta_{42}$ monomer in fibrils.
The turn conformation is stabilized by the interactions of the hydrophobic residues (grey) and a salt bridge is formed between residue 23 and 28 (a) Residues 1-10 of the $A\beta_{40}$ monomer are unstructured. Side chain packing occurs between residues 13-40, 15-36, 19-32/34/36 (dashed grey line). (b) Residues 1-17 are unstructured in the $A\beta_{42}$ monomer. Residue 19 is reported to make molecular contacts with residue 38, residue 35 interacts with residue 42 (dashed black line). Adapted from [188].

1.5 Outline of this thesis

Since the purification of the Aβ peptide from Alzheimer disease brain plaques the peptide has been the subject of numerous studies. Throughout the years it was discovered that Aβ is produced under normal cellular conditions. As the majority of peptide produced is the $A\beta_{40}$ isoform, most studies investigating aggregation behavior of Aβ focussed on the $A\beta_{40}$ peptide. Extensive research on the mutations that are linked to early-onset familial cases of Alzheimer disease revealed that upregulation of total Aβ production, or specifically of the $A\beta_{42}$ isoform leads to disease progress. These findings resulted in an increased interest in the characteristics of this Aβ isoform, and the link to disease. The characterization of the aggregation of the $A\beta_{40}$ and $A\beta_{42}$ peptides in isolation is well reported, as well as the fact that both isoforms can influence the behavior of the other. Although multiple other, both shorter and longer, Aβ peptide lengths have been detected in brain samples, plasma and CSF, information on the

prevalence, aggregation and cytotoxicity of these isoforms remains scarce. The recent findings that the levels of these other Aβ peptide lengths vary upon disease progress suggest that these isoforms contribute to the development of Alzheimer disease. How these peptides could act, however, remains elusive as very little is known about the aggregation behavior and toxic properties of these Aβ peptides.

The aim of this thesis is to report how small variations of the Aβ sequence could relate to Alzheimer disease progress. As the Aβ sequence is very susceptible to variation, only a selection of the known variations are included in this thesis with a focus on peptide length heterogeneity. The various Aβ peptides were investigated using a mainly biophysical approach to characterize the aggregation profile of the peptides in isolation, and in mixtures to investigate the influence of one isoform on the other. In addition cell-culture and mouse studies were used to determine the toxic properties of the peptides. Aside from the detailed *in vitro* study of the peptides, the pathways generating Aβ were explored to understand how C-terminal heterogeneity in the Aβ sequence is generated.

The thesis starts with the description of the protocol used to solubilize the Aβ peptides (Chapter 2). The proposed method generates pure, monomeric solutions of Aβ, virtually free of seeds and contaminants of chemical solvents. Starting from a monomeric solution is of major importance for the characterization of aggregation. Furthermore the absence of traces of solvents makes the Aβ solution compatible for cell culture and mouse studies. Moreover, the presence of minute quantities of solvents would influence the aggregation reaction under study.

Chapter 3 provides a comparative study of the aggregation of a selection of the most common Aβ peptides identified *in vivo*. The oligomerization and aggregation of this extensive set of peptides are compared. The experiments showed that small variation of the Aβ sequence can significantly affect the aggregation properties of the peptide. In the next chapter (Chapter 4) a newly identified mutation of APP, called the 'Leuven mutation' is described. The consequences of this mutation on APP processing and Aβ behavior are evaluated. The novel mutation is found to interact with APP processing while the resulting mutation in Aβ has little effect on the behavior of the peptide. Understanding APP processing and how it is affected by mutations gains novel insights in the generation of Aβ. These insights contribute highly to the unravelling of Alzheimer disease as the aberrant Aβ production might be the primary event in disease onset.

The following part of the thesis focuses on the interaction between $A\beta_{40}$ and $A\beta_{42}$. Chapter 5 describes how the behavior of $A\beta_{42}$:$A\beta_{40}$ mixtures varies with variation of the ratio between these two peptides. A minor increase of the $A\beta_{42}$:$A\beta_{40}$ ratio induces significant changes in aggregation rate and results in stabilized toxic oligomers. In Chapter 6 the $A\beta_{42}$:$A\beta_{40}$ mixtures are further analyzed to understand how both peptides interact and how this interaction affects oligomerization. The data presented suggest that toxic properties of Aβ are the result of a dynamic structure, and are not associated with a specific assembly.

In the last part of the thesis other Aβ peptide lengths which are less abundant *in vivo* are investigated. In Chapter 7 the mechanisms by which FAD mutations affect APP processing are unravelled. The mutations mainly act through shifting the profile of Aβ peptides produced. The observed changes do not only affect the levels of $A\beta_{42}$ but also concern $A\beta_{38}$ and $A\beta_{43}$ levels. Analogous to the study of $A\beta_{42}$:$A\beta_{40}$

mixtures as described in chapter 6, the effects of $A\beta_{38}$ and $A\beta_{43}$ on the behavior of $A\beta_{40}$ and $A\beta_{42}$ are described in Chapter 8. The results show that mixtures of Aβ display complex, unexpected and unpredictable behavior. Moreover $A\beta_{38}$ was shown to induce toxicity of $A\beta_{40}$ while tempering that of $A\beta_{42}$. These data shine new light on current therapeutic strategies aiming to decrease $A\beta_{42}$ levels and at the same time increasing $A\beta_{38}$ levels.

1.6 References

[1] Petsko G & Ringe D (2004). *Protein structure and function*. (1st edition). London: New Age Press.

[2] Berg J, Tymoczko J, Stryer L (2002). *Biochemistry*. (5th edition). New York: W H Freeman.

[3] Anfinsen C, Haber E, Sela M, Withe F Jr (1961). The kinetics of formation of native ribonuclease during oxidation of the reduced polypeptide chain. *Proc. Natl. Acad. Sci. USA*, 47:1309-1314.

[4] Levinthal C (1969). How to fold graciously. *Mossbauer spectroscopy in biological systems: Proceedings of a meeting held at Allerton House, Monticello, Illinois. JTP DeBrunner & E Munck eds., University of Illinois Press*:22-24.

[5] Levinthal C (1968). Are there pathways for protein folding? *J. Chim. Phys.* 65:44-45.

[6] Wetlaufer D (1973). Nucleation, rapid folding, and globular intrachain regions in proteins. *Proc. Natl. Acad. Sci. USA*, 70:697-701.

[7] Karplus M & Weaver D (1979). Diffusion-collision model for protein folding. *Biopolymers*, 18:1421-1437.

[8] Dill K (1985). Theory for the folding and stability of globular proteins. *Biochemistry*, 24:1501-1509.

[9] Ptitsyn O (1973). Stages in the mechanism of self-organization of protein molecules. *Dokl. Akad. Nauk. SSSR*, 210:1213-1215.

[10] Harrison S & Durbin R (1985). Is there a single pathway for the folding of a polypeptide chain? *Proc. Natl. Acad. Sci. USA,* 82:4028-4030.

[11] Creighton T (1988). Toward a better understanding of protein folding pathways. *Proc. Natl. Acad. Sci. USA,* 85:5082-5086.

[12] Ithzaki L, Otzen D, Fersht A (1995). The structure of the transition state for folding of chymotrypsin inhibitor 2 analysed by protein engineering methouds: evidence for a nucleation-condensation mechanism for protein folding. *J. Mol. Biol.*, 254:260-288.

[13] Bryngelson J, Onuchic J, Socci N, Wolynes P (1995). Funnels, pathways, and the energy landscape of protein folding: a synthesis. *Proteins*, 21:167-195.

[14] Dill K & Chan H (1997). From Levinthal to pathways to funnels. *Nat. Struct. Biol.*, 4:10-19.

[15] Huber R (1979). Conformational flexibility and its functional significance in some protein molecules. *Trends Biochem. Sci.*, 4:271-276.

[16] Wright P & Dyson H (1999). Intrinsically unstructured proteins: re-assessing the protein structure-function paradigm. *J. Mol. Biol.*, 293:321-331.

[17] Ward J, Sodhi J, McGuffin L, Buxton B, Jones D (2004). Prediction and functional analysis of native disorder in proteins from the three kingdoms of life. *J. Mol. Biol.*, 337:635-645.

[18] Gunasekaran K, Tsai C, Kumar S, Zanuy D, Nussinov R (2003). Extended disordered proteins: targeting function with less scaffold. *Trends Biochem. Sci.*, 28:81-85.

[19] Daughdrill G, Chadsey M, Karlinsey J, Hughes K, Dahlquist F (1997). The C-terminal half of the anti-sigma factor, FlgM, becomes structured when bound to its target, s^{28}. *Nat. Struct. Biol.*, 4:285-291.

[20] Tompa P, Szász C, Buday L (2005). Structural disorder throws new light on moonlighting. *Trends Biochem. Sci.*, 30:484-489.

[21] Romero P, Obradovic Z, Li X, Garner E, Brown C, Dunk A (2001). Sequence complexity of disordered protein. *Proteins*, 42:38-48.

[22] Romero P, Obradovic Z, Kissinger C, Villafranca J, Garner E, Guilliot S, Dunker A (1998). Thousands of proteins likely to have long disordered proteins. *Pac. Symp. Biocomp.*, 3:437-448.

[23] Sickmeier M, Hamilton J, LeGall T, Vacic V, Cortese M, Tantos A, Szabo B, Tompa P, Chen J, Uversky V, Obradovic Z, Dunker A (2007). DisProt: the database of disordered proteins. *Nucl. Acid. Res.*, 35:D786-793.

[24] Zimmerman S & Trach S (1991). Estimation of macromolecule concentrations and excluded volume effects for the cytoplasm of Escherichia coli. *J. Mol. Biol.*, 222:599-620.

[25] Hartl F, Bracher A, Hayer-Hartl M (2011). Molecular chaperones in protein folding and proteostasis. *Nature*, 475:324-332.

[26] Ellis J (1987). Proteins as molecular chaperones. *Nature*, 328:378-379.

[27] Teter S, Houry W, Ang D, Tradler T, Rockabrand D, Fischer G, Blum P, Georgopoulos C, Hartl F (1999). Polypeptide flux through Hsp70: DnaK cooperates with trigger factor in chaperoning nascent chains. *Cell*, 97:755-765.

[28] Bukau B & Horwich A (1998). The Hsp70 and Hsp60 chaperone machines. *Cell*, 92:351-266.

[29] Kaganovich D, Kopito R, Frydman J (2008). Misfolded proteins partition between two distinct quality control compartments. *Nature*, 454:1088-1095.

[30] Connell P, Ballinger C, Jiang J, Wu Y, Thompson L, Hö (2001). The co-chaperone CHIP regulates protein triage decisions mediated by heat-shock proteins. *Nat. Cell. Biol.*, 3:93-96.

[31] Schröder M & Kaufman R (2005). The mammalian unfolded protein response. *Annu. Rev. Biochem.*,

74:738-789.
[32] Morimoto R (1993). Cells in stress: transcriptional activation of heat shock genes. *Science*, 259:1409-1410.
[33] Bhattacharyya J & Das K (1999). Molecular chaperone-like properties of an unfolded protein, α_S-casein. *J. Biol. Chem.*, 274:15505-15509.
[34] Tompa P, Prilusky J, Silman I, Sussman J (2008). Structural disorder serves as a weak signal for intracellular protein degradation. *Proteins*, 71:903-909.
[35] Uversky V, Gillespie J, Fink A (2000). Why are "natively unfolded" proteins unstructured under physiologic conditions? *Proteins*, 41: 415-427.
[36] Hegyi H & Tompa P (2008). Intrinsically disordered proteins display no preference for chaperone binding in vivo. *PLoS Comput. Biol.*, 4:e1000017.
[37] Vavouri T, Semple J, Garcia-Verdugo R, Lehner B (2009). Intrinsic protein disorder and interaction promiscuity are widely associated with dosage sensitivity. *Cell*, 138:198-208.
[38] Ben-Zvi A, Miller E, Morimoto R (2009). Collapse of proteostasis represents an early molecular event in Caenorhabditis elegans aging. *Proc. Natl. Acad. Sci. USA*, 106:14914-14919.
[39] Conway K, Harper J, Lansbury P (1998). Accelerated in vitro fibril formation by a mutant alpha-synuclein linked to early-onset Parkinson disease. *Nat. med.*, 4:1318-1320.
[40] Drummond D & Wilke C (2008). Mistranslation-induced protein misfolding as a dominant constraint on coding-sequence evolution. *Cell*, 134:341-352.
[41] Fink A (2005). Natively unfolded proteins. *Curr. Opin, Struct. Biol.*, 15:35-41.
[42] Rajan R, Illing M, Bence N, Kopito R (2001). Specificity in intracellular protein aggregation and inclusion body formation. *Proc. Natl. Acad. Sci. USA*, 98:13060-13065.
[43] Xu J, Reumers J, Couceiro J, De Smet F, Gallardo R, Rudyak S, Cornelis A, Rozenski J, Zwolinska A, Marine J Lambrechts D, Suh Y, Rousseau F, Schymkowitz J (2011). Gain of function of mutant p53 by coaggregation with multiple tumor suppressors. *Nat. Chem. Biol.*, 7:285-295.
[44] Parsell D, Kowal A, Singer M, Lindquist S (1994). Protein disaggregation mediated by heat-shock protein Hsp104. *Nature*, 372:475-478.
[45] Wyatt A, Yerbury J, Dabbs R, Wilson M (2012). Roles of extracellular chaperones in amyloidosis. *J. Mol. Biol.*, 421:499-516.
[46] Taylor J, Tanaka F, Robitschek J, Sandoval C, Taye A, Markovic-Plese S, Fischbeck K (2003). Aggresomes protect cells by enhancing the degradation of toxic polyglutamine-containing protein. *Hum. Mol. Genet.*, 12:749-757.
[47] Kopito R (2000). Inclusion bodies and protein aggregation. *Trends Cell Biol.*, 10:524-530.
[48] Chen B, Retzlaff M, Roos T, Frydman J (2011). Cellular strategies of protein quality control. *Cold Spring Harb. Perspect. Biol.*, 3:a004374.
[49] Chiti F & Dobson C (2006). Protein misfolding, functional amyloid, and human disease. *Annu. Rev. Biochem.*, 75:333-366.
[50] Gregersen N, Bross P, Vang S, Christensen J (2006). Protein misfolding and human disease. *Annu. Rev. Genom. Hum. G.*, 7:103-124.
[51] DeWitt D, Silver J, Canning D, Perry G (1993). Chondroitin sulfate proteoglycans are associated with the lesions of Alzheimer's disease. *Exp. Neurol.*, 121:149-152.
[52] Turoverov K, Kuznetsova I, Uversky V (2010). The protein kingdom extended: ordered and intrinsically disordered proteins, their folding, supramolecular complex formation, and aggregation. *Prog. Biophys. Mol. Biol.*, 102:73-84.
[53] Kyle R (2001). Amyloidosis: a convoluted story. *Brit. J. Haematol.*, 114:529-538.
[54] Cohen A & Calkins E (1959). Electron microscopic observations on a fibrous component in amyloid of diverse origins. *Nature*, 183:1202-1203.
[55] Sunde M, Serpell L, Bartlam M, Fraser P, Pepys M, Blake C (1997). Common core structure of amyloid fibrils by synchrotron X-ray diffraction. *J. Mol. Biol.*, 273:729-739.
[56] Groenning M (2009). Binding mode of Thioflavin T and other molecular probes in the context of amyloid fibrils - current status. *J. Chem. Biol.*, 3:1-18.
[57] Chiti F, Webster P, Taddei N, Clark A, Stefani M, Ramponi G, Dobson C (1999). Designing conditions for in vitro formation of amyloid protofilaments and fibrils. *Proc. Natl, Acad. USA*, 96:3590-3594.
[58] Kenney J, Knight D, Wise M, Vollrath F (2002). Amyloidogenic nature of spider silk. *Eur. J. Biochem.*, 269:4159-4163.
[59] Iconomidou V, Vriend G, Hamodrakas S, (2000). Amyloids protect the silkmoth oocyte and embryo. *FEBS Lett.*, 479:141-145.
[60] Claessen D, Rink R, De Jong W, Siebring J, De Vreugd P, Boersma F, Dijkhuizen L, Wösten H (2003). A novel class of secreted hydrophobic proteins is involved in aerial hyphae formation in

Streptomyces coelicolor by forming amyloid-like fibrils. *Genes Dev.*, 17:1714-1726.
[61] Fändrich M & Dobson C (2002). The behavior of polyamino acids reveals an inverse side chain effect in amyloid structure formation. *EMBO J.*, 21:5682-5690.
[62] Bauer H, Aebi U, Häner M, Hermann R, Müller M, Arvinte T, Merkle H (1995). Architecture and polymorphism of fibrillar supramolecular assemblies produced by in vitro aggregation of human calcitonin. *J. Struct. Biol.*, 115:1-15.
[63] Serpell L, Sunde M, Benson M, Tennent G, Pepys M, Fraser P (2000). The protofilament substructure of amyloid fibrils. *J. Mol. Biol.*, 300:1033-1039.
[64] Kirschner D, Abraham C, Selkoe D (1986). X-ray diffraction from intraneuronal paired helical filaments and extraneuronal amyloid fibers in Alzheimer disease indicates cross-b conformation. *Proc. Natl. Acad. Sci. USA*, 83:503-507.
[65] Nelson R, Sawaya M, Balbirnie M, Madsen A, Riekel C Grothe R, Eisenberg D (2005). Structure of the cross-beta spine of amyloid-like fibrils. *Nature*, 435:773-778.
[66] Fowler D, Koulov A, Balch W, Kelly J (2007). Functional amyloid - from bacteria to humans, *Trends Biochem. Sci.*, 32:217-224.
[67] Jahn T & Radford S (2008). Folding versus aggregation: polypeptide conformations on competing pathways. *Arch. Biochem. Biophys.*, 469:100-117.
[68] Westermark P (2005). Amyloidosis and amyloid proteins: brief history and definitions. In: J Sipe ed. (2005). *Amyloid proteins. The beta sheet conformation and disease. volume 1* Wheinheim: WILEY-VCH, ch 1.
[69] Pedersen J, Dikov D, Flink J, Hjuler H, Christiansen G, Otzen D (2006). The changing face of glucagon fibbrillation: structural polymorphism and conformational imprinting. *J. Mol. Biol.*, 355:501-523.
[70] Wright C, Teichmann S, Clarke J, Dobson C (2005). The importance of sequence diversity in aggregation and evolution of proteins. *Nature*, 438:878-881.
[71] Chiti F, Taddei N, Baroni F, Capanni C, Stefani M, Ramponi G, Dobson C (2002). Kinetic partitioning of protein folding and aggregation. *Nat. Struct. Biol.*, 9:137-143.
[72] Chiti F, Calamai N, Taddei N, Stefani M, Ramponi G, Dobson C (2002). Studies of the aggregation of mutant proteins in vitro provide insights into the genetics of amyloid diseases. *Proc. Natl. Acad. Sci. USA*, 99:16419-16426.
[73] Lopez-De La Paz M, Goldie K, Zurdo J, Lacroix E, Dobson C, Hoenger A, Serrano L (2002). De novo designed peptide-based amyloid fibrils. *Proc. Natl. Acad. Sci. USA*, 99:16052-16057.
[74] Rousseau F, Serrano L, Schymkowitz J (2006). How evolutionary pressure against protein aggregation shaped chaperone specificity. *J. Mol. Biol.*, 355:1037-1047.
[75] Williams R, Obradovic Z, Mathura V, Braun W, Garner E, Young J, Takayama S, Brown C, Dunker A (2001). The protein non-folding problem: amino acid determinants of intrinsic order and disorder. *Pac. Symp. Biocomp.*, 6:89-100.
[76] Linding R, Schymkowitz J, Rousseau F, Diella F, Serrano L (2004). A comparative study of the relationship between protein structure and beta-aggregation in globular and intrinsically disordered proteins. *J. Mol. Biol.*, 342:345-353.
[77] Fernandez-Escamilla A, Rousseau F, Schymkowitz J, Serrano L (2004). Prediction of sequence-dependent and mutational effects on the aggregation of peptides and proteins. *Nat. Biotechnol.*, 22:1302-1306.
[78] Tartaglia G, Cavalli A, Pellarin R, Caflisch A (2005). Prediction of aggregation rate and aggregation-prone segments in polypeptide sequences. *Prot. Sci.*, 14:2723-2734.
[79] Trovato A, Seno F, Tosatto S (2007). The PASTA server for protein aggregation prediction. *Prot. Eng. Des. Sel.*, 20:521-523.
[80] Maurer-Stroh S, Debulpaep M, Kuemmerer N, Lopez-de la Paz M, Martins I, Reumers J, Morris K, Copland A, Serpell L, Serrano L, Schymkowitz J, Rousseau F (2010). Exploring the sequence determinants of amyloid structure using position-specific scoring matrices. *Nat. Methods*, 7:237-242.
[81] Kelly J (1998). The alternative conformations of amyloidogenic proteins and their multi-step assembly pathways. *Curr. Opin. Struct. Biol.*, 8:101-106.
[82] Fowler D, Koulov A, Alory-Jost C, Marks M, Balch W, Kelly J (2006). Functional amyloid formation within mammalian tissue. *PLoS Biol.*, 4:e6.
[83] Lodish H, Berk A, Zipursky S, Matsudaira P, Baltimore D, Darnell J (2000). *Molecular Cell Biology.* (4th edition). New York: W H Freeman.
[84] Cohen R, Jedziniak J, Benedek G (1976). The functional relationship between polymerization and catalytic activity of beef liver glutamate dehydrogenase. *J. Mol. Biol.*, 108:179-199.
[85] Rousseau F, Schymkowitz J, Serrano L (2006). Protein aggregation and amyloidosis: confusion of the kinds? *Curr. Opin. Struc. Biol.*, 16:118-126.

[86] Morris A, Watzky M, Finke R (2009). Protein aggregation kinetics, mechanism, and curve-fitting: a review of the literature. *Biochim. Biophys. Acta*, 1794:375-397.
[87] Straub J & Thirumalai D (2011). Toward a molecular theory of early and late events in monomer to amyloid fibril formation. *Annu. Rev. Phys. Chem.*, 62:437-463.
[88] Oosawa F, Asakura S, Hotta K, Imai N, Ooi T (1959). G-F transformation of actin as a fibrous condensation. *J. Polym. Sci.*, 37:323-336.
[89] Hofrichter J, Ross P, Eaton W (1974). Kinetics and mechanism of deoxyhemoglobin S gelation: a new approach to understanding sickle cell disease. *Proc. Natl. Acad. Sci. USA,* 71:4864-4868.
[90] Lomakin A, Chung D, Benedek G, Kirschner D, Teplow D (1996). On the nucleation and growth of amyloid β-protein fibrils: detection of nuclei and quantitation of rate constants. *Proc. Natl. Acad. Sci. USA*, 93:1125-1129.
[91] Thusius D, Dessen P, Jallon J-M (1975). Mechanism of bovine liver glutamate dehydrogenase self-association. I Kinetic evidence for a random association of polymer chains. *J. Mol. Biol.*, 92:413-432.
[92] Harper J & Lansbury P (1997). Models of amyloid seeding in Alzheimer's disease and scrapie: Mechanistic truths and physiological consequences of the time-dependent solubility of amyloid proteins. *Annu. Rev. Biochem.*, 66:385-407.
[93] Wood S, Wypych J, Steavenson S, Louis J-C, Citron M, Biere A (1999). α-Synuclein fibrillogenesis is nucleation-dependent. Implications for the pathogenesis of parkinson's disease. *J. Biol. Chem.*, 274:19509-19512.
[94] Watzky M & Finke R (1997). Transition metal nanocluster formation kinetic and mechanistic studies. A new mechanism when hydrogen is the reductant: slow, continuous nucleation and fast autocatalytic surface growth. *J. Am. Chem. Soc.*, 119:10382-10400.
[95] Kamihira M, Naito A, Tuzi S, Nosaka A, Saito H (2000). Conformational transitions and fibrillation mechanism of human calcitonin as studied by high-resolution solid-state 13C NMR. *Protein Sci.*, 9:867-877.
[96] Esler W, Stimson E, Ghilardi J, Vinters H, Lee J, Mantyh P, Maggio J (1996). In vitro growth of Alzheimer's disease β-amyloid plaques display first-order kinetics. *Biochemistry*, 35:749.757.
[97] Esler W, Stimson E, Jennings J, Vinters H, Ghilardi J, Lee J, Mantyh P, Maggio J (2000). Alzheimer's disease amyloid propagation by a template-dependent dock-lock mechanism. *Biochemistry*, 39:6288-6295.
[98] Massi F & Straub J (2001). Energy landscape theory for Alzheimer's amyloid β-peptide fibril elongation. *Proteins*, 42:217-229.
[99] Pike C, Walencewicz A, Glabe C, Cotman C (1991). In vitro aging of β-amyloid protein causes peptide aggregation and neurotoxicity. *Brain Res.*, 563:311-314.
[100] Terry R, Masliah E, Salmon D, Butters N, DeTeresa R, Hill R, Hansen L, Katzman R (1991). Physical basis of cognitive alterations in Alzheimer's disease: synapse loss is the major correlate of cognitive impairement. *Ann. Neurol.*, 30:572-580.
[101] Chapman P, White G, Jones M, Cooper-Blacketer D, Marshall V, Irizarry M, Younkin L, Good M, Bliss T, Hyman B, Younkin S, Hsiao K (1999). Impaired synaptic plasticity and learning in aged amyloid precursor protein transgenic mice. *Nat. Neurosci.*, 2:271-276.
[102] McLean C, Cherny R, Fraser F, Fuller S, Smith M, Beyreuther K (1999). Soluble pool of Aβ amyloid as a determinant of severity of neurodegeneration in Alzheimer's disease. *Ann. Neurol.*, 46:860-866.
[103] Dodart J, Bales K, Gannon K, Greene S, DeMattos R, Mathis C, DeLong C, Wu S, Holtzman D, Paul S (2002). Immunization reverses memory deficits without reducing brain Aβ burden in Alzheimer's disease model. *Nat. Neurosci.*, 5:452-457.
[104] Walsh D, Klyubin I, Fadeeva J, Cullen W, Anwyl R, Wolfe M, Rowan M, Selkoe D (2002). Naturally secreted oligomers of amyloid-β protein potently inhibit hippocampal long-term potentiation in vivo. *Nature*, 416:535-539.
[105] Prince M & Jackson J (2009). *World Alzheimer Report 2009*. London: Alzheimer's disease International (ADI).
[106] Wimo A & Prince M (2010). *World Alzheimer Report 2010: the global economic impact of dementia*. London: Alzheimer's disease International (ADI).
[107] Alzheimer's disease education and referral (ADEAR) Center (2008). Alzheimer's disease: Unraveling the mystery. NIH Publication No. 08-3782.
[108] Dash P & Villemarette-Pitman N (2005). *Alzheimer's disease*. New York: Demos Medical Publishing.
[109] Trojanowski J *et al.* (1997). Consensus Recommendations for the postmortem diagnosis of Alzheimer's disease. *Neurobiol. Aging*, 18:S1-2.
[110] American Psychiatric Association (2000). *Diagnostic and statistical manual of mental disorders*. (4th edition, text revision). Washington DC: American Psychiatric Association.

[111] Anthony J, LeResche L, Niaz U, von Korff M, Folstain M (1982). Limits of the 'mini-mental state' as a screening test for dementia and delirium among hospital patients. *Psychol. Med.*, 12:397-408.
[112] Antonelli Incalzi R, Capparella O, Gemma A, Marra C, Carbonin P (1995). Effects of aging and of Alzheimer's disease on verbal memory. *J. Clin. Exp. Neuropsyc.*,17:580-589.
[113] Nelson H (1976). A modified card sorting test sensitive to frontal lobe defects. *Cortex*, 12:313-324.
[114] Waldemar G, Dubois B, Emre M, Georges J, McKeith I, Rossor M, Scheltens P, Tariska P, Winblad B (2007). Recommendations for the diagnosis and management of Alzheimer's disease and other disorders associated with dementia: EFNS guideline. *Eur. J. Neurol.*, 14:e1-26.
[115] Braak H, Braak E, Yilmazer D, de Vos R, Jansen E, Bohl J (1996). Pattern of brain destruction in Parkinson's and Alzheimer's disease. *J. Neurol. Transm.*, 103:455-490.
[116] Glenner G & Wong C (1984). Alzheimer's disease: initial report of the purification and characterization of a novel cerebrovascular amyloid protein. *Biochem. Biophys. Res. Commun.*, 120:885-890.
[117] Lovell M, Robertson J, Teesdale W, Campbell J, Markesbery W (1998). Copper, iron and zinc in Alzheimer's disease senile plaques. *J. Neurol. Sci.*, 158:47-52.
[118] Brion J, Passareiro H, Nunez J, Flamant-Durand J (1985). Immunological demonstration of tau protein into neurofibrillary tangles of Alzheimer's disease. *Arch. Biol. (Brux.)*, 95:229-235.
[119] Johnson G & Stoothoff W (2004). Tau phosphorylation in neuronal cell function and dysfunction. *J. Cell Sci.*, 117:5721-5729.
[120] Hardy J & Allsop D (1991). Amyloid deposition as the central event in the aetiology of Alzheimer's disease. *Trends Pharmacol. Sci.*, 12:383-388.
[121] Scheuner D, Eckman C, Jensen M, Song X, Citron M, Suzuki N, Bird T, Hardy J, Hutton M, Kukull W, Larson E, Levy-Lahad E, Viitanen M, Peskind E, Poorkaj P, Schellenberg G, Tanzi R, Wasco W, Lannfelt L, Selkoe D, Younkin S (1996). Secreted amyloid β-protein similar to that in the senile plaques of Alzheimer's disease is increased in vivo by the presenilin 1 and 2 and APP mutations linked to familial Alzheimer's disease. *Nat. med.*, 2:864-870.
[122] Pimplikar S (2009). Reassessing the amyloid cascade hypothesis of Alzheimer's disease. *Int. J. Biochem. Cell. B.*, 41:1261-1268.
[123] Hendriks L, van Duijn C, Cras P, Cruts M, Van Hul W, van Harskamp F, Warren A, McInnis M, Antonarakis S, Martin J-J, Hofman A, Van Broeckhoven C (1992). Presenile dementia and cerebral haemorrhage linked to a mutation at codon 692 of the β-amyloid precursor protein gene. *Nat. Genet.*, 1:218-221.
[124] Mullan M, Crawford F, Axelman K, Houlden H, Lilius L, Winblad B, Lannfelt L (1992). A pathogenic mutation for probable Alzheimer's disease in the APP gene at the N-terminus of β-amyloid. *Nat. Genet.*,1:345-347.
[125] Cruts M & Van Broeckhoven C (1998). Molecular genetics of Alzheimer's disease. *Ann. Med.*, 30:560-565.
[126] Citron M, Oltersdorf T, Haass C, McConlongue L, Hung A, Seubert P, Vigo-Pelfrey C, Lieberburg I, Selkoe D (1992). Mutation of the β-amyloid precursor protein in familial Alzheimer's disease increases β-protein production. *Nature*, 360:672-674.
[127] Suzuki N, Cheung T, Cai X, Odaka A, Otvos L, Eckman C, Golde T, Younkin S (1994). An increased percentage of long amyloid β protein secreted by familial amyloid β protein precursor (β APP717) mutants. *Science*, 264:1336-1340.
[128] Jervis G (1948). Early senile dementia in mongoloid idiocy. *Am. J. Psychiat.*, 105:102-106.
[129] Van Dam D & De Deyn P (2006). Drug discovery in dementia: the role of rodent models. *Nat. Rev. Drug Discov.*, 11:956-970.
[130] Hartman S & Möbius H (2003). Tolerability of memantine in combination with cholinesterase inhibitors in dementia therapy. *Int. Clin. Psychopharm.*, 18:81-85.
[131] Rafii M & Aisen P (2009). Recent developments in Alzheimer's disease therapeutics. *BMC Med.*, 7:7.
[132] Gowing E, Roher A, Woods A, Cotter R, Chaney M, Little S, Ball M (1994). Chemical characterization of Aβ 17-42 peptide, a component of diffuse amyloid deposits of Alzheimer disease. *J. Biol. Chem.*, 269:10987-10990.
[133] Allinson T, Parkin E, Turner A, Hooper N (2003). ADAMs family members as amyloid precursor protein α-secretases. *J. Neurosci. Res.*, 74:342-352.
[134] Vellas B, Sol O, Snyder P, Ousset P, Haddad R, Maurin M, Lemarié J-C, Désiré L, Pando M (2011). EHT0202 in Alzheimer's disease: A 3-month, randomized, placebo-controlled, double-blind study. *Curr. Alz. Res.*, 8:203-212.
[135] Kitazume S, Tachida Y, Oka R, Shirotani K, Saido T, Hashimoto Y (2001). Alzheimer's β-secretase, β-site amyloid precursor protein-cleaving enzyme, is responsible for cleavage secretion of a golgi-resident sialyltransferase. *Proc. Natl. Acad. Sci. USA,* 98:13554-13559.

[136] Hey J, Koelsch G, Bilcer G, Jacobs A, Tolar M, Tang J, Ghosh A, Hsu H (2008). Single dose administration of the β-secretase inhibitor CTS21166 (ASP1702) reduces plasma Aβ40 in human subjects. Presented at the International Conference on Alzheimer's Disease (ICAD) Chicago, IL.
[137] Abramov E, Dolev I, Fogel H, Ciccotosto G, Ruff E, Slutsky I (2009). Amyloid-β as a positive endogenous regulator of release probability at hippocampal synapses. *Nat. Neurosci.*, 12:1567-1576.
[138] Hitoshi S, Alexson T, Tropepe V, Donoviel D, Elia A, Nye J, Conlon R, Mak T, Bernstein A, van der Kooy D (2002). Notch pathway molecules are essential for the maintenance, but not the generation, of mammalian neural stem cells. *Genes Dev.*, 16:846-858.
[139] Milano J, McKay J, Dagenais C, Foster-Brown L, Pognan F, Gadient R, Jacobs R, Zacco A, Greenberg B, Ciaccio P (2004). Modulation of notch processing by γ-secretase inhibitors causes intestinal goblet cell metaplasia and induction of genes known to specify gut secretory lineage differentiation. *Toxicol. Sci.*, 82:341-358.
[140] Serneels L, Van Biervliet J, Craessaerts K, Dejaegere T, Horré K, Van Houtvin T, Esselmann H, Paul S, Schäfer M, Berezovska O, Hyman B, Sprangers B, Sciot R, Moons L, Jucker M, Yang Z, May P, Karran E, Wiltfang J, D'Hooge R, De Strooper B (2009). γ-Secretase heterogeneity in the Aph1 subunit: relevance for Alzheimer's disease. *Science*, 324:639-642.
[141] Mayer S, Kreft A, Harrison B, Abou-Gharbia M, Antane M, Aschmies S, Atchison K, Chlenov M, Cole D, Comery T, Diamantidis G, Ellingboe J, Fan K, Galante R, Gonzales C, Ho D, Hoke M, Hu Y, Huryn D, Jain U, Jin M, Kremer K, Kubrak D, Lin M, Lu P, Magolda R, Martone R, Moore W, Oganesian A, Pangalos M, Porte A, Reinhart P, Resnick L, Riddell D, Sonnenberg-Reines J, Stock J, Sun S-C, Wagner E, Wang T, Woller K, Xu Z, Zaleska M, Zeldis J, Zhang M, Zhou H, Jacobsen J (2008). Discovery of beacestat, a notch-1-sparing γ-secretase inhibitor for the treatment of Alzheimer's disease. *J. Med. Chem.*, 51:7348-7351.
[142] Weggen S, Eriksen J, Das P, Sagi S, Wang R, Pietrzik C, Findlay K, Smith T, Murphy M, Bulter T, Kang D, Marquez-Sterling N, Golde T, Koo E (2001). A subset of NSAIDs lower amyloidogenic Aβ42 independently of cyclooxygenase activity. *Nature*, 414:212-216.
[143] Aisen P, Saumier D, Briand R, Laurin J, Gervais F, Tremblay P, Garceau D (2006). A phase II study targeting amyloid-β with 3APS in mild-to-moderate Alzheimer disease. *Neurology*, 67:1757-1763.
[144] Ritchie C, Bush A, Mackinnon A, Macfarlane S, Mastwyk M, MacGregor L, Kiers L, Cherny R, Li Q, Tammer A, Carrington D, Mavros C, Volitakis I, Xilinas M, Ames D, Davis S, Beyreuther K, Tanzi R, Masters C (2003). Metal-protein attenuation with iodochlorhydroxyquin (clioquinol) targeting Aβ amyloid deposition and toxicity in Alzheimer disease. *Arch. Neurol.*, 60:1685-1691.
[145] Gilman S, Koller M, Black R, Jenkins L, Griffith S, Fox N, Eisner L, Kirby L, Rovira B, Forette F, Orgogozo J-M (2005). Clinical effects of Aβ immunization (AN1792) in patients with AD in an interrupted trial. *Neurology*, 64:1553-1562.
[146] Holmes C, Boche D, Wilkinson D, Yadegarfar G, Hopkins V, Bayer A, Jones R, Bullock R, Love S, Neal J, Zotova E, Nicoll J (2008). Long-term effects of Aβ42 immunisation in Alzheimer's disease: follow-up of a randomised, placebo-controlled phase I trial. *Lancet*, 372:216-223.
[147] Wang D-S, Dickson D, Malter J (2006). β-Amyloid degradation and Alzheimer's disease. *J. Biomed. Biotechnol.*, 2006:58406.
[148] Mawuenyega K, Sigurdson W, Ovod V, Munsell L, Kasten T, Morris J, Yarasheski K, Bateman R (2010). Decreased clearance of CNS β-amyloid in Alzheimer's disease. *Science*, 330:1774.
[149] Longo F & Massa S (2004). Neuroprotective strategies in Alzheimer's disease. *Neurotherapeutics*, 1:117-127.
[150] Haass C, Schlossmacher M, Hung A, Vigo-Pelfrey C, Mellon A, Ostaszewski B, Lieberburg I, Koo E, Schenk D, Teplow D, Selkoe D (1992). Amyloid β-peptide is produced by cultured cells during normal metabolism. *Nature*, 359:322-325.
[151] Baruch-Suchodolsky R & Fischer B (2009). Aβ40, either soluble or aggregated is a remarkably potent antioxidant in cell-free oxidative systems. *Biochemistry*, 48:4354-4370.
[152] Kontusch A (2001). Amyloid-β: an antioxidant that becomes a pro-oxidant and critically contributes to Alzheimer's disease. *Free Radical Bio. Med.*, 31:1120-1131.
[153] Tabaton M, Zhu X, Perry G, Smith M, Giliberto L (2010). Signaling effect of amyloid-β42 on the processing of AβPP. *Exp. Neurol.*, 221:18-25.
[154] Igbavboa U, Sun G, Weisman G, He Y, Wood G (2009). Amyloid β-protein stimulates trafficking of cholesterol and caveolin-1 from the plasma membrane to the golgi complex in mouse primary astrocytes. *Neuroscience*, 18:328-338.
[155] Ohyagi Y, Asahara H, Chui D-H, Tsuruta Y, Sakae N, Miyoshi K, Yamada T, Kikuchi H, Taniwaki T, Murai H, Ikezoe K, Furuya H, Kawarabayashi T, Shoji M, Checler F, Iwaki T, Makifuchi T, Takeda K, Kira J, Tabira T (2005). Intracellular Aβ42 activates p53 promotor: a pathway to neurodegeneration

in Alzheimer's disease. *FASEB J.*, 19:255-257.
[156] Gandy S (2005). The role of cerebral amyloid β accumulation in common forms of Alzheimer disease. *J. Clin. Invest.*, 115:1121-1129.
[157] Zhou Z, Chan C, Ma Q, Xu X, Xiao Z, Tan E (2011). The roles of amyloid precursor protein (APP) in neurogenesis: implications to pathogenesis and therapy of Alzheimer disease. *Cell Adh. Migr.*, 5:280-292.
[158] Ghosal K, Stathopoulos A, Pimplikar S (2010). APP intracellular domain impairs adult neurogenesis in transgenic mice by inducing neuroinflammation. *PLoS one*, 5:e11866.
[159] Raychaudhuri M & Mukhopadhayay D (2011). AICD overexpression in neuro 2A cells regulates expression of PTCH1 and TRPC5. *Int. J. Alz. Dis.*, 2011:239453.
[160] De Strooper B, Vassar R, Golde T (2010). The secretases: enzymes with therapeutic potential in Alzheimer disease. *Nat. Rev. Neurol.*, 6:99-107.
[161] De Strooper B (2003). APH-1, PEN-2, and nicastrin with presenilin generate an active γ-secretase complex. *Neuron*, 38:9-12.
[162] Qi-Takahara Y, Morishima-Kawashima M, Tanimura Y, Dolios G, Hirotani N, Horikoshi Y, Kametani F, Maeda M, Saido T, Wang R, Ihara Y (2005). Longer forms of amyloid β protein: Implications for the mechanism of intramembrane cleavage by γ-secretase. *J. Neurosci.*, 25:436-445.
[163] Takami M, Nagashima Y, Sano Y, Ishihara S, Morishima-Kawashima Y, Funamoto S, Ihara Y (2009). γ-Secretase: successive tripeptide and tetrapeptide release from the transmembrane domain of beta-carboxyl terminal fragment. *J. Neurosci.*, 29:13042-13052.
[164] Vigo-Pelfrey C, Lee D, Keim P, Lieberburg I, Schenk D (1999). Characterization of β-amyloid peptide from human cerebrospinal fluid. *J. Neurochem.*, 61:1965-1968.
[165] Lewczuk P, Esselmann H, Otto M, Maler J, Henkel A, Henkel M, Eikenberg O, Antz C, Krause W-R, Reulbach U, Kornhuber J, Wiltfang J (2004). Neurochemical diagnosis of Alzheimer's dementia by CSF Aβ42, Aβ42/Aβ40 ratio and total tau. *Neurobiol. aging* 25:273-281.
[166] Maddalena A, Papassotiropoulos A, Gonzalez-Agosti C, Signorell A, Hegi T, Pasch T, Nitsch R, Hock C (2004). Cerebrospinal fluid profile of amyloid β peptides in patients with Alzheimer's disease determined by protein biochip technology. *Neurodegener. Dis.*, 1:231-235.
[167] Iwatsubo T, Saido T, Mann D, Lee V, Trojanowski J (1996). Full-length amyloid-β(1-42(43)) and amino-terminally modified and truncated amyloid-β42(43) deposit in diffuse plaques. *Am. J. Pathol.*, 149:1823-1830.
[168] Russo C, Violani E, Salis S, Venezia V, Dolcini V, Damonte G, Benatti U, D'Arrigo C, Patrone E, Carlo P, Schettini G (2002). Pyroglutamate-modified amyloid β-peptides - AβN3(pE) - strongly affect cultured neuron and astrocyte survival. *J. Neurochem.*, 3:1480-1489.
[169] Gravina S, Ho L, Eckman C, Long K, Otvos L, Younkin L, Suzuki N, Younkin S (1995). Amyloid β protein (Aβ) in Alzheimer's disease brain. *J. Biol. Chem.*, 270:7013-7016.
[170] Welander H, Franberg J, Graff C, Sundström E, Winblad B, Tjernberg L (2009). Aβ43 is more frequent than Aβ40 in amyloid plaque cores from Alzheimer disease brains. *J. Neurochem.*, 110:697-706.
[171] Jarrett J, Berger E, Lansbury P (1993). The carboxy terminus of the β amyloid protein is critical for the seeding of amyloid formation: implications for the pathogenesis of Alzheimer's disease. *Biochem.*, 32:4693-4697.
[172] Bitan G, Kirkitadze M, Lomakin A, Vollers S, Benedek G, Teplow D (2003). Amyloid β-protein (Aβ) assembly: Aβ40 and Aβ42 oligomerize through distinct pathways. *Proc. Natl. Acad. Sci. USA,* 100:330-335.
[173] Yoshiike Y, Chui D, Akagi T, Tanaka N, Takashima A (2003). Specific compositions of amyloid-β peptides as the determinant of toxic β-aggregation. *J. Biol. Chem.*, 278:23648-23655.
[174] Jan A, Gokce O, Luthi-Carter R, Lashuel H (2008). The ratio of monomeric to aggregated forms of Aβ40 and Aβ42 is an important determinant of amyloid-β aggregation, fibrillogenesis, and toxicity. *J. Biol. Chem.*, 283:28176-28189.
[175] Kim J, Onstead L, Randle S, Price R, Smithson L, Zwizinski C, Dickson D, Golde T, McGowan E (2007). Aβ40 inhibits amyloid deposition in vivo. *J. Neurosci.*, 27:627-633.
[176] Walsh D, Lomakin A, Benedek G, Condron M, Teplow D (1997). Amyloid β-protein fibrillogenesis. Detection of a protofibrillar intermediate. *J. Biol. Chem.*, 272:22364-22373.
[177] Lambert M, Barlow A, Chromy B, Edwards C, Freed R, Liosatos M, Morgan T, Rozovsky I, Trommer B, Viola K, Wals P, Zhang C, Finch C, Krafft G, Klein W (1998). Diffusible, nonfibrillar ligands derived from Aβ1-42 are potent central nervous system neurotoxins. *Proc. Natl. Acad. Sci. USA,* 95:6448-6453.
[178] Lesné S, Koh M, Kotilinek L, Kayed R, Glabe C, Yang A (2006). A specific amyloid-β protein assembly in the brain impairs memory. *Nature*, 440:352-357.

[179] Hoshi M, Sato M, Matsumoto S, Noguchi A, Yasutake K, Yoshida N, Sato K (2003). Sperical aggregates of β-amyloid (amylosperoid) show high neurotoxicity and activate tau protein kinase I/ glycogen synthase kinase-3β. *Proc. Natl. Acad. Sci. USA,* 100:6370-6375.
[180] Walsh D & Selkoe D (2007). Aβ oligomers - a decade of discovery. *J. Neurochem.*, 101:1172-1184.
[181] Ward R, Jennings K, Jepras R, Neville W, Owen D, Hawkins J, Christie G, Davis J, George A, Karran E, Howlett D (2000). Fractionation and characterization of oligomeric, protofibrillar and fibrillar forms of β-amyloid peptide. *Biochem. J.*, 348:137-144.
[182] Kayed R, Head E, Thompson J, McIntire T, Milton S, Cotman C, Glabe C (2003). Common structure of soluble amyloid oligomers implies common mechanism of pathogenesis. *Science*, 300:486-489.
[183] Kodali R, Williams A, Chemuru S, Wetzel R (2010). Aβ(1-40) forms five distinct amyloid structures whose β-sheet contents and fibril stabilities are correlated. *J. Mol. Biol.*, 401:503-517.
[184] Balbach J, Petkova A, Oyler N, Antzutkin O, Gordon D, Meredith S, Tycko R (2002). Supramolecular structure in full-length Alzheimer's β-amyloid fibrils: evidence for a parallel β-sheet organization from solid-state nuclear magnetic resonance. *Biophys. J.*, 83:1205-1216.
[185] Luhrs T, Ritter C, Adrian M, Riek-Loher D, Bohrmann B, Döbeli H, Schubert D, Riek R (2005). 3D Structure of Alzheimer's amyloid-β(1-42) fibrils. *Proc. Natl. Acad. Sci. USA,* 102:17342-17347.
[186] Petkova A, Yau W, Tycko R (2006). Experimental constraints on quaternary structure in Alzheimer's β-amyloid fibrils. *Biochemistry*, 45:498-512.
[187] Petkova A, Ishii Y, Balbach J, Antzutkin O, Leapman R, Delaglio F, Tycko R (2002). A structural model for Alzheimer's β-amyloid fibrils based on experimental constraints from solid state NMR. *Proc. Natl. Acad. Sci. USA,* 99:16742-16747.
[188] Ahmed M, Davis J, Aucoin D, Sato T, Ahuja S, Aimoto S, Elliot J, Van Nostrand W, Smith S (2010). Structural conversion of neurotoxic amyloid-β1-42 oligomers to fibrils. *Nat. Struct. Mol. Biol.*, 17:561-568.

2

A standardized and biocompatible preparation of aggregate-free Aβ for biophysical and biological studies of Alzheimer disease.

We provide a validated and rapid protocol for the solubilization of Aβ. This procedure involves sequential solubilization using structure-breaking organic solvents hexafluoroisopropanol and dimethyl sulfoxide followed by column purification. The low solubility and tendency of Aβ to aggregate considerably impede the *in vitro* handling and biophysical or biological investigation of Aβ, despite the interest in this peptide because of its implication in Alzheimer disease. The main advantage of the proposed protocol over others is that it results in standardized aggregate-free Aβ peptide samples that are biocompatible for cell culture studies and yield reproducible aggregation kinetics and cytotoxicities. This three-step protocol also enables the co-solubilization of the longer $A\beta_{42}$ variant with $A\beta_{40}$ in ratios relevant to Alzheimer disease.

The results described in this chapter have been published in:
Broersen K, Jonckheere W, Rozenski J, Vandersteen A, Pauwels K, Pastore A, Rousseau F, and Schymkowitz J (2011). *Prot. Eng. Des. Sel.*, 24:743-750.

2.1 Introduction

Among the proteins identified in amyloid plaques, Aβ peptides are special because they constitute what could be considered as the prototype of an intrinsically unstructured sequence with an unusually high amphipathic character. Although the majority of the Aβ pool is composed of $A\beta_{40}$ and $A\beta_{42}$ [1,2], it is now thought that the Aβ variation pattern in the brains of patients with Alzheimer disease is reflected by a general elongation of the Aβ peptides through a modulated γ-secretase activity [3-5]. These longer Aβ peptides appear to be directly involved in plaque formation in the brains of patients with Alzheimer disease [1,2,6]. The extra residues in the elongated Aβ are hydrophobic thus drastically influencing the solubility and amyloidogenicity of the peptide. To effectively study the impact of Aβ on toxicity and to elucidate the structural pathway of aggregation and formation of toxic oligomers, it is crucial to initiate the studies with a well-defined aggregate-free Aβ species. It is, however, difficult to deal with Aβ peptides precisely for the very reason that makes them interesting: they are poorly soluble and aggregation-prone in aqueous solutions. Proteins that are prone to aggregate under physiologically relevant conditions are usually characterized by high hydrophobicity and/or low net charge [7-10]. Apart from their tendency to induce pathological conditions and high aggregation propensity, the low solubility of these peptides also results in inherent difficulties in the experimental handling and investigation by biophysical techniques and in cell culture. Nevertheless, high-resolution characterization of these proteins may provide the information required to tackle key questions aiming at therapeutic targeting. In response to these technical difficulties that significantly hamper the research into neurodegenerative diseases, a variety of protocols to aid the solubilization of Aβ are available in the literature. However, these procedures often involve the use of extremely alkaline [11] or acidic solutions [12] or rely on the presence of organic solvents [13], thus introducing biologically incompatible compounds and/or conditions that are toxic to cell cultures. Filtration of freshly prepared Aβ samples is also frequently used to remove pre-existing aggregates, but often leads to significantly reduced recovery of soluble Aβ material [14]. It is therefore essential to develop a robust and reproducible preparation protocol that allows the solubilization of these peptides under biocompatible buffer conditions.

In this chapter, a new and validated procedure to solubilize the Aβ peptide that circumvents the above-mentioned problems and allows to obtain appreciable quantities of virtually aggregate-free material is described. The method relies on the use of a sequential solubilization procedure with organic solvents, followed by the complete removal of these chemicals to provide a non-toxic environment that is suitable for biophysical characterization. The procedure is validated by demonstrating complete solubilization of the peptide and providing evidence that all chemicals involved are effectively removed from the peptide solution without introducing oxidation of the peptide. By using thioflavin T fluorescence (thioT) assays and cell culture studies, we show that the resulting solutions exert highly reproducible aggregation kinetics and toxicities. We conclude that our procedure provides monomeric Aβ preparations in a cell-biology-compatible environment, and is suitable for biophysical characterization.

2.2 Results and discussion

2.2.1 Overview of the protocol and comparison with other methods

The proposed protocol provides for a method to dissolve Aβ peptide via a rapid three-step procedure. Dissolving recombinant produced $A\beta_{42}$ directly into buffer shows that a thioT curve to follow the kinetic aspects of the aggregation curve lacks the typical sigmoidal shape commonly observed for aggregating peptides and proteins (Figure 2.1a). No lag phase is apparent and also the thioT fluorescence intensity is already increased on starting the assay, both indicative for the presence of pre-formed seeds or aggregates in the solution. Fourier transform infrared spectroscopy (FTIR) is used for a wide range of applications and also has shown its applicability in the field of protein conformation determination [15]. $A\beta_{42}$ that has been prepared using the proposed three-step dissolving procedure is intrinsically unstructured directly after solubilization in aqueous solution, characterized by a broad peak centered around 1654 cm^{-1}, but assumes a β-sheet aggregate fold (peak at 1627 cm^{-1}) on incubation for 24 h. $A\beta_{42}$ that has been directly dissolved in buffer on the other hand exerts a high degree of β-sheet structure (Figure 2.1b), while monomeric dissolved Aβ is an intrinsically disordered peptide. These results underline the necessity to develop an alternative procedure to dissolve Aβ.

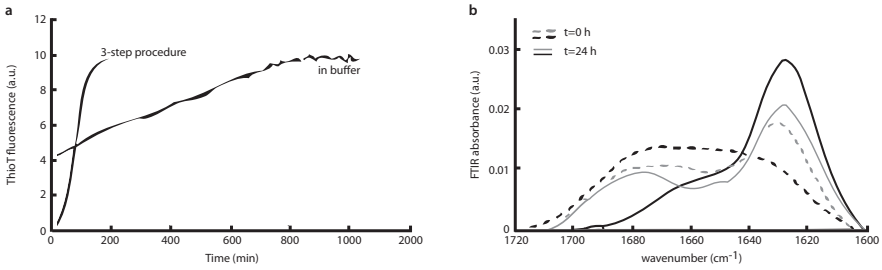

Figure 2.1 Solubilization of $A\beta_{42}$ directly into buffer indicates the presence of pre-formed aggregates.
(a) Comparison of aggregation kinetics probed by thioT fluorescence of Aβ dissolved directly into buffer and the novel proposed three-step procedure. A concentration of 50 μM Aβ was either dissolved directly into buffer or solubilized using the proposed three-step procedure. (b) FTIR spectroscopy of $A\beta_{42}$ dissolved into buffer using the three-step dissolving procedure (black). Directly on elution off the column the broad FTIR spectrum is characteristic for an unstructured peptide while after 24 h incubation at a concentration of 100 μM at 25 °C the intensity at 1627 cm^{-1} increases characteristic for β-sheet amyloid aggregation. FTIR spectroscopy of $A\beta_{42}$ dissolved directly into buffer (grey). Directly on solubilization the spectrum is characteristic for a mixture of unfolded peptide and β-sheet aggregation with a main intensity at 1627 cm^{-1} and a broad shoulder at 1654 cm^{-1}. After 24 h incubation at a concentration of 100 μM at 25 °C the intensity at 1627 cm^{-1} increased slightly and the shoulder at 1654 cm^{-1} is smaller.

We first exploited the structure-promoting properties of hexafluoroisopropanol (HFIP). From a number of tested alcohols, HFIP was shown to most effectively denature the model protein β-lactoglobulin and to induce a non-native α-helix conformation [16]. Dilute solutions of HFIP (1-4%) promote fibril formation of the islet amyloid polypeptide [17] but concentrated HFIP solutions have been shown to actively remove pre-formed

aggregate seeds from solutions
containing amyloidogenic proteins [18-20]. Later studies confirmed similar observations for Aβ [20]. HFIP owes its activity due to its high degree of fluorination and induces helical formation [21,22]. Even though HFIP has been shown to dissociate fibrils, β_2-microglobulin aggregates can resist the application of this solvent [21]. The insufficient ability of HFIP to completely dissociate amyloid fibrils has been ascribed to its non-polar character that weakens hydrophobic interactions but cannot dissolve rigid fibrils [21]. Therefore, in the presented procedure HFIP solubilization is followed by dimethyl sulfoxide (DMSO), as this polar compound has been shown to completely dissociate amyloid fibrils based on its ability to destruct a hydrogen bond network [23]. HFIP can be removed using oxygen-free nitrogen gas or, alternatively, argon gas as methionine-35 of the Aβ peptide is susceptible to oxidation [24]. A molecular dynamics simulation of the effects of DMSO on the structure and function of subtilisin confirmed that DMSO acts as a highly effective hydrogen bond acceptor and, hence, can strip away water from the protein surface [25]. Many published methods to solubilize Aβ suggest preparation of concentrated Aβ stock solutions in DMSO followed by a 10- to 100-fold dilution in buffer to induce aggregation. However, as a result of the effect of DSMO on the hydrogen network of proteins, the kinetics and mechanism of the aggregation of Aβ are adversely affected by the presence of small (± 5%) concentrations of DMSO (Figure 2.2) [26] in a non-physiologically relevant manner. We therefore apply a column-exchange step to remove all traces of DMSO. Other published methods often employ the effects of HCl and NaOH to aid Aβ solubility at a pH far removed from its isoelectric point (± pH5.3). In order to adjust the pH of the solution to approach more physiologically relevant pH values from an acidic pH requires transition through the isoelectric point at which the peptide is most prone to aggregate. Also the addition of these pH-affecting compounds introduces an additional factor that could induce artifacts in the aggregation mechanism of Aβ.

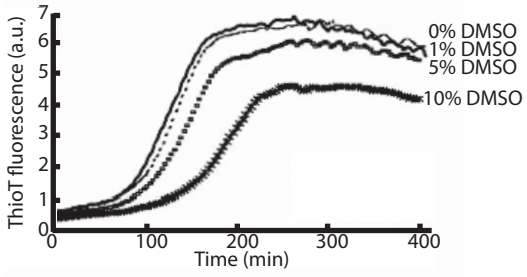

Figure 2.2 Different solubilization procedures affect the aggregation of Aβ.
The presence of traces of DMSO affects the aggregation kinetics of $A\beta_{42}$. Dilution of concentrated Aβ stocks in DMSO into buffer followed by monitoring of the aggregation rate of Aβ by thioT fluorescence. The aggregation of Aβ is linearly inhibited with increasing concentrations of DMSO.

2.2.2 Experimental design

The protocol for Aβ solubilization that provided best results consists of sequential treatment using HFIP and DMSO followed by exchange of DMSO into buffer using a desalting column (Figure 2.3a). The use of a high concentration (± 100%) of HFIP, a fluorinated alcohol, provides a means of interaction with the backbone and removal

of water from the surface. Subsequently, the HFIP is evaporated off by the use of oxygen-free nitrogen gas or argon gas that protects the peptide from oxidative modification. The hydrophobic methyl groups of DMSO have the ability to then interact with hydrophobic side chains of the Aβ peptide while the polar S=O group interacts with water molecules. DMSO is then removed by buffer exchange using a desalting column resulting in Aβ virtually free from aggregating seeds in buffer (Figure 2.3b). The electrophoretic analysis of the elution of Aβ from the column shows that fractions 2 to 5 are enriched with Aβ (150-750 μl). $A\beta_{40}$ elutes as a pure monomeric solution while $A\beta_{42}$ elutes as a primarily monomeric solution containing small quantities of an SDS-resistant species with an apparent molecular weight resembling trimeric Aβ. No higher-molecular-weight aggregates were observed. As the presence of small amounts of HFIP and DMSO can modify the aggregation rates of Aβ [20] (Figure 2.2), it is important to validate their complete removal. We use FTIR that provides characteristic and sensitive fingerprints for the presence of trace amounts of HFIP [27] or DMSO. FTIR spectra of the various elution fractions after column elution show that with increasing elution fraction the concentration of DMSO increases (Figure 2.3c). It is also shown that HFIP has been effectively removed during the procedures supported by the lack of characteristic intensity in the FTIR spectrum between 1300 and 1100 cm^{-1}. A 1% DMSO solution in buffer has two characteristic peaks: at 1011 cm^{-1} and at 951 cm^{-1}. Plotting the intensity at these two wavelengths against the fraction number shows that only from fraction 9 (1350 μl) up the concentration of DMSO starts to increase (Figure 2.3c). In addition, the absence of a detectable signal at 2.5 p.p.m., which is characteristic of DMSO, in the one-dimensional ^1H NMR spectrum of the Aβ preparations, confirms that elution of the first 1 ml of Aβ from the column yields DMSO-free Aβ (Figure 2.3d). The electrospray ionization mass spectrum shows that $A\beta_{42}$, using the protocol, eluted free of contaminants and without apparent modifications (Figure 2.3e), such as dityrosine-formation that is commonly observed for Aβ peptides as a function of oxidation [28].

We tested the reproducibility of the behavior of the prepared Aβ solutions and their performance in a variety of assays related to aggregate formation or cell viability commonly used to study the effects of Aβ. Commonly used assays to study the aggregation of Aβ *in vitro* consist of thioT fluorescence [29], electron microscopy [29] [30,31] and FTIR [30,32] and the effect of Aβ on the toxicity is usually assayed by viability assays on neuroblastoma cells [31,33] or neuronal cultures [29,30,34].

2.2.3 Nuclear magnetic resonance

NMR analysis shows that $A\beta_{40}$ and $A\beta_{42}$ prepared by our procedure are mainly monomeric species as shown by the sharp resonances in 2D HSQC experiments (Figure 2.4). NMR analysis also assures us that the protocol does not induce oxidation of Met35: oxidation of this residue is known to result in a notable chemical shift that affects several crosspeaks in the HSQC [35]. Our spectra of $A\beta_{40}$ and $A\beta_{42}$ are in excellent agreement with literature data reporting NH of Met35 in the reduced state at ± 8.5 p.p.m. for the ^1H-frequency, while the NH of Met35 of the oxidized state appeared upfield at ± 8.8 p.p.m. (Figure 2.4 a,b) [35]. This observation is an important point to note because pre-treatment with HFIP might occasionally promote oxidation of the Aβ peptide [35].

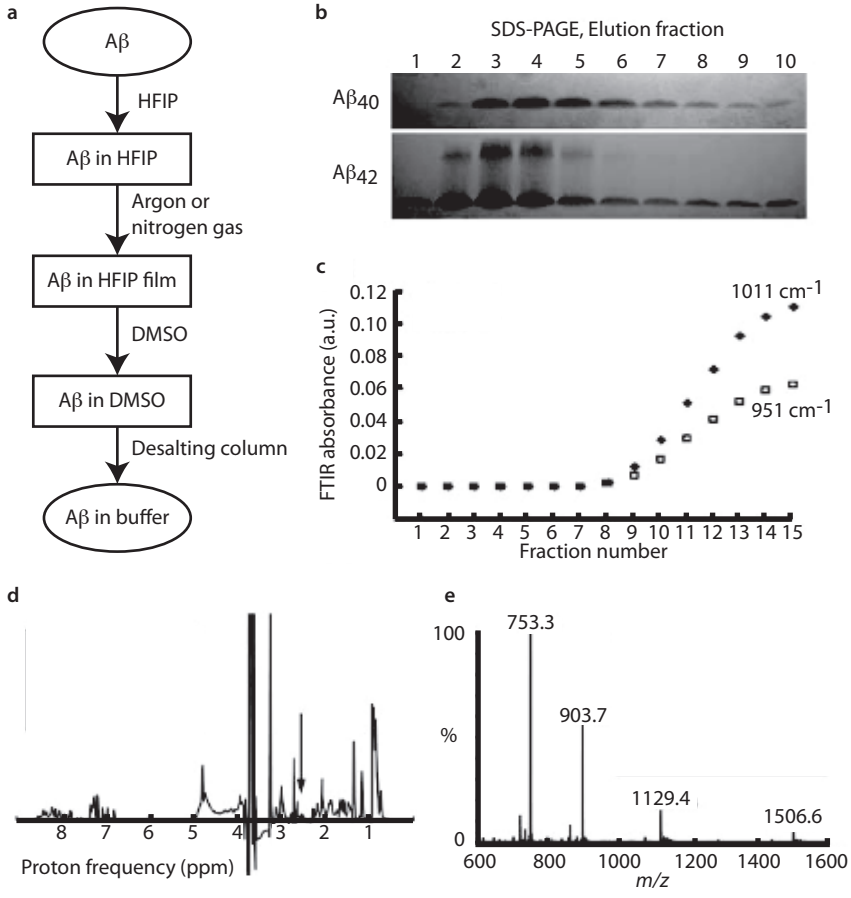

Figure 2.3 Novel solubilization procedure for Aβ leads to primarily monomeric Aβ and absence of contaminating chemicals.
(a) Treatment of the Aβ peptide to dissolve it into buffer involves sequential dilution in HFIP, and DMSO followed by buffer exchange by means of a desalting column. Details of the procedure are described in the text. (b) Non-reducing SDS-PAGE analysis of fractions of 150 μl each eluted off the desalting column shows that fractions 2-5 (300-750 μl) are enriched in Aβ peptide. $A\beta_{40}$ is primarily monomeric on elution while $A\beta_{42}$ is primarily monomeric with a small fraction of apparently trimeric peptide. (c) Up to and including fraction 8 (1200 μl) can be eluted off the desalting column without contamination by DMSO. The intensities of FTIR peaks characteristic for the presence of DMSO (1011 and 951 cm^{-1}) are plotted against eluted fraction number. (d) One-dimensional ^1H NMR spectrum of an $A\beta_{42}$ preparation confirms the complete removal of DMSO because of the absence of characteristic solvent signal at 2.5 p.p.m., as indicated by the arrow. (e) Electrospray mass spectrum of $A\beta_{42}$ in positive mode.

2.2.4 Thioflavin T fluorescence

ThioT fluorescence is a useful probe to assay the aggregation of proteins. The quantum yield for fluorescence of this weakly fluorescent dye increases strongly on complexation with amyloid fibrils [36]. The differences in aggregation rates between the aggregating $A\beta_{42}$ and less aggregation-prone $A\beta_{40}$ can be distinguished using *in situ* thioT fluorescence (Figure 2.5a). Reproducibility of the obtained results is an

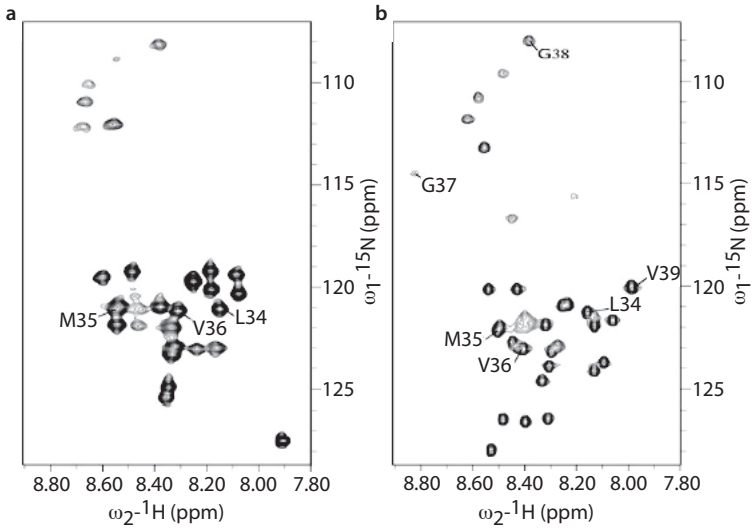

Figure 2.4 NMR ^{15}N-^{1}H HSQC spectra
(a) $A\beta_{40}$ and (b) $A\beta_{42}$ recorded at 600 MHz and 25 and 5 °C, resp. Oxidation of Met35 residue in Aβ is prevented by the novel solubilization procedure. Spectrum assignment is shown only for those crosspeaks that would undergo a chemical shift displacement as a function of the redox state of Met35 (i.e. Leu34-Met35-Val36 in $A\beta_{40}$ and Leu34-Met35-Val36-Gly37-Gly38 in $A\beta_{42}$) [35].

important parameter to evaluate the quality of the developed procedures. Figure 2.5a shows thioT fluorescence curves obtained for three independent experiments. The standard error between the experiments is ± 7-10% and the differences between the aggregation rates of $A\beta_{40}$ and $A\beta_{42}$ are therefore significant.

2.2.5 Transmission electron microscopy

We used transmission electron microscopy (TEM) to characterize fibril morphology of aggregates formed by $A\beta_{40}$ and $A\beta_{42}$ on incubation at a concentration of 100 μM for 24 h at 25 °C. Amyloidogenic $A\beta_{42}$ (Figure 2.5b) forms aggregates characterized by short fibrils which intertwine and appear rigid. $A\beta_{40}$ (Figure 2.5c) on the other hand forms long semi-flexible negatively stained fibrils with a characteristic periodic twist that is regularly found in fibrils of other origin, such as insulin [37].

2.2.6 Toxicity on SH-SY5Y cells

The toxicity of 1.5 h incubated 100 μM $A\beta_{40}$ and $A\beta_{42}$ preparations was tested using neuroblastoma SH-SY5Y cells plated at a cell density of 20 000 cells/well in serum-deprived medium. To this end, Aβ preparations were diluted to various concentrations ranging from 1 to 50 μM in serum-deprived medium and 100 μl was added to each well in 6-fold. After 48 h incubation cells were tested for cell death using Cell Titer-Blue viability assay. Figure 2.5d shows that cell viability is Aβ concentration dependent and that $A\beta_{42}$ aggregates induce cell death at lower concentrations (from 7.5 μM) compared with $A\beta_{40}$ aggregates (from 30 μM). The results in Figure 2.5d are obtained from three independent experiments and the standard error is maximum 12% (for 30 μM $A\beta_{40}$) but in most cases > 5%.

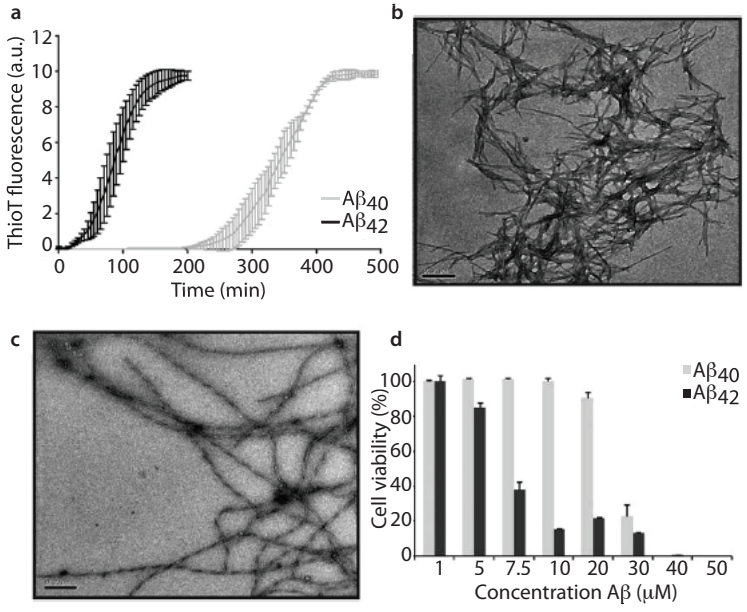

Figure 2.5 Anticipated results for commonly used biophysical and cell biological characterization methods of Aβ dissolved by the HFIP/DMSO/column procedure.
(a) $A\beta_{40}$ (grey) and $A\beta_{42}$ (black) aggregation monitored by thioT fluorescence: the nucleation phase for $A\beta_{40}$ is extended significantly compared with $A\beta_{42}$. The rate of polymerization is faster for $A\beta_{40}$ than for $A\beta_{42}$. Reproducibility of thioT curves shown by error bars of $A\beta_{40}$ and $A\beta_{42}$ prepared at three different occasions from three different batches of Aβ peptide. The limited variability in the obtained results illustrates that differences in aggregation rates between different Aβ peptides are significant. (b) Transmission electron microscopy (TEM) image for $A\beta_{42}$ aggregates matured at 100 μM at 25 °C for 24 h. The fibrils are short and intertwined. (c) Aggregates of $A\beta_{40}$ matured at 100 μM at 25 °C for 24 h and imaged by TEM show long, semi-flexible and twisted fibrils. The length of the segment is 0.2 mm for both micrographs depicted in (b) and (c). (d) Toxicity of Aβ matured for 1.5 h at 100 μM at 25 °C and then added at various final concentrations in medium to SH-SY5Y neuroblastoma cells. Cell viability is measured using Cell Titer Blue (Promega) assay. The cell viability of cells incubated with $A\beta_{42}$ (black bars) is lost between 7.5 and 10 μM while cells incubated with $A\beta_{40}$ (grey bars) only lose cell viability at an Aβ concentration of 30 μM.

2.3 Conclusions

A robust and validated three-step procedure is presented to prepare biocompatible virtually aggregate-free solutions with an efficient recovery of amyloidogenic $A\beta_{42}$ implicated in Alzheimer disease. The procedure involves the sequential use of HFIP, DMSO and a column exchange step. While the use of organic solvents also allows the reliable preparation of biologically relevant quantities of $A\beta_{42}$ and $A\beta_{40}$ and their mixtures, the incorporation of a desalting column in the solubilization procedure makes it possible to obtain the Aβ peptide in any desirably buffer system. The resulting Aβ preparation shows highly reproducible biophysical and cell biological behavior. The use of this protocol may be extended to the solubilization of other highly amphipathic or hydrophobic polypeptides.

2.4 Experimental procedures

2.4.1 Preparation of Aβ peptide solutions

Escherichia coli expressed human recombinant Alzheimer's beta peptide 1-40, Ultra Pure HFIP, 1-42 Ultra Pure HFIP and their uniformly ^{15}N-isotope-labeled variants were purchased from rPeptide. Various ratios of $A\beta_{42}$:$A\beta_{40}$ were prepared starting from material previously stored in a -20 °C freezer. The vials containing 0.5 mg Aβ-HFIP films were allowed to defrost at room temperature (25 °C) for 10 min. A quantity of 0.5 mg $A\beta_{40}$ or $A\beta_{42}$ was dissolved in 500 µl hexafluoroisopropanol (HFIP). The sample was mixed vigorously using a vortex for 1 min and visually inspected for efficient solubilization. To prepare $A\beta_{42}$:$A\beta_{40}$ ratios, a gas tight syringe was used to add together specific volumes of $A\beta_{40}$ in HFIP and $A\beta_{42}$ in HFIP to obtain a defined ratio of $A\beta_{42}$:$A\beta_{40}$ followed by mixing using a vortex for 1 min [38]. The HFIP was evaporated using a gentle stream of oxygen-free nitrogen gas and, alternatively, argon gas can be used. Based on an HFIP volume of 500 µl in each vial prior to drying with nitrogen gas, the peptide/HFIP films were redissolved in 500 µl dimethyl sulfoxide (DMSO). Samples were mixed using a vortex for 1 min and visually inspected for efficient solubilization. Immediately thereafter, the Aβ peptide solutions were separated from the DMSO by means of a desalting column that was pre-equilibrated with 25 ml of a 50 mM Tris-HCl, 1 mM EDTA buffer, pH 7.4. Other buffer systems, including phosphate-buffered saline can also be used. The 500 µl sample was applied to the column using a 1 ml syringe followed by additional injection of 1 ml buffer, the flow-through was discarded. Subsequently, the peptide was eluted from the column by the additional injection of 1 ml buffer. Typically, the first 500 µl flow-through contained ± 100-120 µM peptide and the second 500 µl contained lower Aβ concentrations (40-50 µM), which results in a yield of original Aβ peptide of 80% based on Bradford determination of the peptide concentration. The Aβ-containing samples were collected in pre-cooled low adhesion resin-coated polypropylene centrifuge tubes. After concentration measurement using the Bradford assay for protein determination [39], both fractions were combined to yield the required concentration of Aβ. Samples were kept on ice directly on elution and further experiments were proceeded with within 20 min after elution from the desalting column.

2.4.2 Oligomerization and fibrillization of Aβ

Oligomer-enriched fractions (1.5-2 h incubation) or amyloid fibrils (>1 week incubation) of Aβ were prepared by incubation of 50-100 µM Aβ at 25 °C under quiescent conditions in 50 mM Tris-HCl, 1 mM EDTA, pH 7.4 using low-adhesion resin-coated polypropylene centrifuge tubes.

2.4.3 Sodium dodecyl sulfate-polyacrylamide gel electrophoresis

Non-reducing SDS-PAGE was performed by incubating 10 µl Aβ-containing solution in 15 µl Novex Tris-Glycine SDS sample buffer. Samples were then loaded onto a 10-20% Tricine gel and the gel was run at 170 V for 40 min followed by staining with Imperial Protein Stain.

2.4.4 Thioflavin T fluorescence

Aggregate-free Aβ$_{42}$ solutions at a concentration of 50 μM were prepared as described above by further dilution using 50 mM Tris-HCl, 1 mM EDTA containing buffer and a final concentration of 12 μM thioT. In order to evaluate the effect of DMSO on the aggregation kinetics, various concentrations of DMSO (1-10%) were added to the elution buffer of Aβ. In order to validate the effectiveness of the proposed three-step solubilization procedure, Aβ$_{42}$ was also directly dissolved into buffer without organic solvent treatment. The fibrillization kinetics of Aβ were monitored *in situ* at an excitation wavelength of 440 nm and an emission wavelength of 480 nm. Fluorescence readings were recorded every 10 min for a period of 7 h. Measurements were performed in triplicate, the recorded values were averaged and standard deviations were calculated. Background measurements included buffer or buffer containing DMSO and 12 μM thioT.

2.4.5 Transmission electron microscopy

Aliquots (5 μl) of the Aβ preparation were adsorbed to carboncoated FormVar film on 400-mesh copper grids for 1 min. The grids were blotted, washed twice in droplets of Milli-Q water and stained with 1% (wt/vol) uranyl acetate. Samples were studied with a JEOL JEM-1400 microscope at 80 kV.

2.4.6 Fourier transform infraRed spectroscopy

An aggregate-free Aβ$_{42}$ solution was prepared as described in section 2.4.1. The Aβ concentration was adjusted to 100 μM by dilution using 50 mM Tris-HCl, 1 mM EDTA containing buffer. Spectra of Aβ$_{42}$ were recorded directly on elution from the column and after 24 h incubation at 25 °C under quiescent conditions. To evaluate the contribution of organic solvent components to the FTIR spectrum, 1% DMSO or 1% HFIP were directly dissolved into 50 mM Tris-HCl, 1 mM EDTA containing buffer. Buffer was used to record a blank signal. The InfraRed spectra were recorded using a Bruker Tensor 27 infrared spectrophotometer equipped with a Bio-ATR II accessory. Spectra were recorded at a spectral resolution of 4 cm^{-1} and 120 accumulations were performed per measurement at a wavenumber range from 900 to 3500 cm^{-1}. Analysis of the spectra involved blank (buffer) and baseline subtraction from the obtained spectra and rescaling in a wavenumber range from 900 to 1800 cm^{-1}.

2.4.7 Electrospray-ionization mass spectrometry

Aβ$_{42}$ was prepared as described in section 2.4.1, but the column elution step was disregarded. The concentrated Aβ$_{42}$ solution in DMSO was diluted 100x in acetonitrile:water (1:1) containing 1% acetic acid to a final concentration of 2 μM Aβ. Positive-ion mass spectra were recorded on an orthogonal acceleration quadrupole time-of-flight mass spectrometer equipped with a standard electrospray probe (Z-spray) and controlled by a datasystem running MassLynx 3.4 and cone voltage was set to 30 V, capillary voltage was 3 kV. Spectra were recorded from *m/z* 600 to *m/z* 1600. Scan time was set to 4.9 s with an interscan time of 0.1 s. At least 10 spectra were acquired and averaged. Deconvolution was performed using the MaxEnt algorithm included in the software.

2.4.8 Nuclear magnetic resonance spectroscopy

Uniformly ^{15}N-labeled $A\beta_{40}$ and $A\beta_{42}$ peptides were treated as described above using 1 ml HFIP and 1 ml DMSO. Peptide concentrations were adjusted to 60 μM for $A\beta_{42}$ and 100 μM for $A\beta_{40}$ with 50 mM Tris-HCl, 1 mM EDTA (pH 7.4) buffer and the samples contained 10% (vol/vol) $^{2}H_2O$. A ^{15}N-^{1}H heteronuclear single quantum coherence (HSQC) spectrum for $A\beta_{42}$ was recorded on a Bruker Avance spectrometer equipped with a cryoprobe and operating at 700 MHz at 5 °C. The $A\beta_{40}$ ^{15}N-^{1}H-HSQC spectrum was recorded at 25 °C on a Varian Inova spectrometer operating at 600 MHz. Spectral assignment was verified using ^{15}N-NOESY-HSQC and ^{1}H,^{1}H-TOCSY experiments. Spectra were processed using NMRPipe/NMRDraw [40] and analyzed by XEASY/CARA software [41].

2.4.9 Cell viability in neuroblastoma cells

Neuroblastoma SH-SY5Y cells were used with a maximum passage number of 15. Cells were cultured in Dulbecco's modified eagle medium (DMEM) 1x, 1% (vol/vol) penicillin/streptomycin and 10% (vol/vol) fetal calf serum at 37 °C, 5% CO_2 to a confluency of 85% in a 75 cm^2 flask. On trypsinization, cells were resuspended at a concentration of 200 000 cells/ml in DMEM/F12 (1:1), containing 1% (vol/vol) penicillin/streptomycin. The resuspended cells were plated at a volume of 100 μl and a cell density of 20 000 cells/well in a 96-well plate. The plated cells were incubated for 48 h at 37 °C at 5% CO_2. $A\beta_{40}$ and $A\beta_{42}$ oligomer-enriched fractions were prepared at a concentration of 100 μM as described under section 2.4.2 and incubation for 1.5 h under quiescent conditions at 25 °C. After incubation, the Aβ was diluted to final concentrations of 1-50 μM in buffer and then diluted 1:1 with prewarmed (37 °C) DMEM/F12 (1:1), containing 1% (vol/vol) penicillin/streptomycin. The Aβ or medium as a control was added at a volume of 100 μl in medium to each well and left to incubate for 48 h. After 48 h, 10 μl Cell Titer-Blue Cell Viability Assay compound was added to each well and incubated for 4-6 h at 37 °C to allow viable cells to convert resazurin into resorufin. Fluorescence intensity of resorufin was measured on a 96-well plate reader at an excitation wavelength of 544 nm and an emission wavelength of 590 nm. Measurements were performed in three independent experiments and statistical analysis was performed to calculate average values and standard deviations.

Author contribution

AV contributed to this manuscript by recording thioT fluorescence data, and by validating fibril morphology and cytotoxicity of the Aβ preparations.

2.5 References

[1] Suzuki N, Cheung T, Cai X, Odaka A, Otvos L, Eckman C, Golde T, Younkin S (1994). An increased percentage of long amyloid β protein secreted by familial amyloid β protein precursor (β APP717) mutants. *Science*, 264:1336-1340.

[2] Scheuner D, Eckman C, Jensen M, Song X, Citron M, Suzuki N, Bird T, Hardy J, Hutton M, Kukull W, Larson E, Levy-Lahad E, Viitanen M, Peskind E, Poorkaj P, Schellenberg G, Tanzi R, Wasco W, Lannfelt L, Selkoe D, Younkin S (1996). Secreted amyloid β-protein similar to that in the senile plaques of Alzheimer's disease is increased in vivo by the presenilin 1 and 2 and APP mutations linked to familial Alzheimer's disease. *Nat. med.*, 2:864-870.

[3] Wiltfang J, Esselmann H, Bibl M, Smirov A, Otto M, Paul S, Schmidt B, Klafki H-W, Maler M, Dyrks T, Bienert M, Beyermann M, R:uther E, Kornhuber J (2002). Highly conserved and disease-specific patterns of carboxyterminally truncated Aβ peptides 1-37/38/39 in addition to 1-40/42 in Alzheimer's disease and in patients with chronic neuroinflammation. *J. Neurochem.*, 81:481-496.

[4] Lewczuk P, Esselmann H, Meyer M, Wollscheid V, Neumann M, Otto M, Maler J, Rüther E, Kornhuber J, Wiltfang J (2003). The amyloid-β (Aβ) peptide pattern in cerebrospinal fluid in Alzheimer's disease: evidence of a novel carboxyterminally elongated Aβ peptide. *Rapid Commun. Mass Spectrom.*, 17:1291-1296.

[5] Bentahir M, Nyabi O, Verhamme J, Tolia A, Horré K, Wiltfang J, Esselmann H, De Strooper B (2006). Presenilin clinical mutations can affect γ-secretase activity by different mechanisms. *J. Neurochem.*, 96:732-742.

[6] Jarrett J, Berger E, Lansbury P (1993). The carboxy terminus of the β amyloid protein is critical for the seeding of amyloid formation: implications for the pathogenesis of Alzheimer's disease. *Biochem.*, 32:4693-4697.

[7] Chiti F, Stefani M, Taddei N, Ramponi G, Dobson C (2003). Rationalization of the effects of mutations on peptide an protein aggregation rates. *Nature*, 424:805-808.

[8] DuBay K, Pawar A, Chiti F, Zurdo J, Dobson C, Vendruscolo M (2004). Prediction of the absolute aggregation rates of amyloidogenic polypeptide chains. *J. Mol. Biol.*, 341:1317-1326.

[9] Fernandez-Escamilla A, Rousseau F, Schymkowitz J, Serrano L (2004). Prediction of sequence-dependent and mutational effects on the aggregation of peptides and proteins. *Nat. Biotechnol.*, 22:1302-1306.

[10] Linding R, Schymkowitz J, Rousseau F, Diella F, Serrano L (2004). A comparative study of the relationship between protein structure and beta-aggregation in globular and intrinsically disordered proteins. *J. Mol. Biol.*, 342:345-353.

[11] Fezoui Y, Hartley D, Harper J, Khurana R, Walsh D, Condron M, Selkoe D, Lansbury P, Fink A, Teplow D (2000). An improved method of preparing the amyloid beta-protein for fibrillogenesis and neurotoxicity experiments. *Amyloid*, 7:166-178.

[12] Ward R, Jennings K, Jepras R, Neville W, Owen D, Hawkins J, Christie G, Davis J, George A, Karran E, Howlett D (2000). Fractionation and characterization of oligomeric, protofibrillar and fibrillar forms of β-amyloid peptide. *Biochem. J.*, 348:137-144.

[13] Bitan G & Teplow D (2004). Preparation of aggregate-free, low molecular weight amyloid-β for assembly and toxicity assays. In: E Sigurdsson ed. (2004). *Amyloid Proteins: Methods and Protocols*. Totowa, NJ: Humana Press, pp 3-9.

[14] Bernstein S, Wyttenbach T, Baumketner A, Shea J, Bitan G, Teplow D, Bowers M (2005). Amyloid β-protein: monomer structure and early aggregation states of Aβ42 and its Pro19 alloform. *J. Am. Chem. Soc.*, 127:2075-2084.

[15] Miyazawa T & Blout E (1961). The infrared spectra of polypeptides in various conformations: amide I and II bands, *Anal. Biochem.*, 177:244-249.

[16] Hirota N, Mizuno K, Goto Y (1997). Cooperative α-helix formation of β-lactoglobulin and melittin induced by hexafluoroisopropanol. *Protein Sci.*, 6:416-421.

[17] Padrick S & Miranker A (2002). Islet amyloid: phase partitioning and secondary nucleation are central to the mechanism of fibrillogenesis. *Biochemistry*, 41:4694-4703.

[18] Buck M (1998). Trifluoroethanol and colleagues: cosolvents come of age. Recent studies with peptides and proteins. *Q. Rev. Biophys.*, 31:297-355.

[19] Zagorski M, Yang J, Shao H, Ma K, Zeng H, Hong A (1999). Methodological and chemical factors affecting amyloid β peptide amyloidogenicity. *Methods Enzymol.*, 309:189-204.

[20] Nichols M, Moss M, Reed D, Cratic-McDaniel S, Hoh J, Rosenberry T (2005). Amyloid-β protofibrils differ from amyloid-β aggregates induced in dilute hexafluoroisopropanol in stability and morphology. *J. Biol. Chem.*, 280:2471-2480.

[21] Hirota-Nakaoka N, Hasegawa K, Naiki H, Goto Y (2003).Dissolution of β2-microglobulin amyloid fibrils by dimethylsulfoxide. *J. Biochem.*,134:159-164.
[22] Tomaseli S, Esposito V, Vangone P, van Nuland N, Bonvin A, Guerrini R, Tancredi T, Temussi P, Picone D (2006). The α-to-β conformational transition of Alzheimer's Aβ-(1-42) peptide in aqueous media is reversible: a step by step conformational analysis suggests the location of β conformation seeding. *Chembiochem*, 7:257-267.
[23] Kosower E (1958). The effect of solvent on spectra. 1. A new emperical measure of solvent polarity: Z-values. *J. Am. Chem. Soc.*, 80:3253-3260.
[24] Butterfield D & Bush A (2004). Alzheimer's amyloid β-peptide (1-42): involvement of methionine residue 35 in the oxidative stress and neurotoxicity properties of this peptide. *Neurobiol. Aging*, 25:563-568.
[25] Zheng Y & Ornstein R (1996). A molecular dynamics and quantum mechanics analysis of the effect of DMSO on enzyme structure and dynamics: subtilisin. *J. Am. Chem. Soc.*, 118:4175-4180.
[26] Shen C & Murphy R (1995). Solvent effects on self-assembly of β-amyloid peptide. *Biophys. J.*, 69:640-651.
[27] Czarnik-Matusewicz B, Pilorz S, Zhang L, Wu Y (2008). Structure of hexafluoroisopropanol-water mixture studied by FTIR-ATR spectra and selected chemometric methods. *J. Mol. Struct.*, 883–884:195-202.
[28] Yoburn J, Tian W, Brower J, Nowick J, Glabe C, Van Vranken D (2003). Dityrosine cross-linked Aβ peptides: fibrillar β-structure in Aβ(1-40) is conductive to formation of dityrosine cross-links but a dityrosine cross-link in Aβ(8-14) does not induce β-structure. *Chem. Res. Toxicol.*, 16:531-535.
[29] Hayashi H, Kimura N, Yamaguchi H, Hasegawa K, Yokoseki T, Shibata M, Yamamoto N, Michikawa M, Yoshikawa Y, Terao K, Matsuzaki K, Lemere C, Selkoe D, Naiki H, Yanagisawa K (2004). A seed for Alzheimer amyloid in the brain. *J. Neurosci.*, 24:4894-4902.
[30] Martins I, Kuperstein I, Wilkinson H, Maes E, Vanbrabant M, Jonckheere W, Van Gelder P, Harmann D, D'Hooge R, De Strooper B, Schymkowitz J, Rousseau F (2008). Lipids revert inert Aβ amyloid fibrils to neurotoxic protofibrils that affect learning in mice. *EMBO J.*, 27:224-233.
[31] Nerelius C, Sandegren A, Sargsyan H, Raunak R, Leijonmarck H, Chatterjee U, Fisahn A, Imarisio S, Lomas D, Crowther D, Strömberg R, Johansson J (2009). α-Helix targeting reduces amyloid-β peptide toxicity. *Proc. Natl. Acad. Sci. USA*, 106:9191-9196.
[32] Cerf E, Sarroukh R, Tamamizu-Kato S, Breydo L, Derclaye S, Dufrêne Y, Narayanaswami V, Goormaghtigh E, Ruysschaert J-M, Raussens V (2009). Anti-parallel β-sheet - a signature structure of the oligomeric amyloid-β peptide. *Biochem. J.*, 421:415-423.
[33] Chromy B, Nowak R, Lambert M, Viola K, Chang L, Velasco P, Jones B, Fernandez S, Lacor P, Horowitz P, Finch C, Krafft G, Klein W (2003). Self-assembly of Aβ1-42 into globular neurotoxins. *Biochemistry*, 42:12749-12760.
[34] Lambert M, Barlow A, Chromy B, Edwards C, Freed R, Liosatos M, Morgan T, Rozovsky I, Trommer B, Viola K, Wals P, Zhang C, Finch C, Krafft G, Klein W (1998). Diffusible, nonfibrillar ligands derived from Aβ1-42 are potent central nervous system neurotoxins. *Proc. Natl. Acad. Sci. USA*, 95:6448-6453.
[35] Hou L, Shao H, Zhang Y, Li H, Menon N, Neuhaus E, Brewer J, Byeon I-J, Ray D, Vitek M, Iwashita T, Makula R, Przybyla A, Zagorski M (2004). Solution NMR studies of the Aβ(1-40) and Aβ(1-42) peptides establish that the Met35 oxidation state affects the mechanism of amyloid formation. *J. Am. Chem. Soc.*, 126:1992-2005.
[36] Naiki H, Higuchi K, Hosokawa M, Takeda T (1989). Fluorimetric determination of amyloid fibrils in vitro using the fluorescent dye, thioflavine T. *Anal. Biochem.*,177:244-249.
[37] Jiménez J, Nettleton E, Bouchard M, Robinson C, Dobson C, Saibil H (2002). The protofilanent structure of insulin amyloid fibrils. *Proc. Natl. Acad. Sci. USA*, 99:9196-201.
[38] Kuperstein I, Broersen K, Benilova I, Rozenski J, Jonckheere W, Debulpaep M, Vandersteen A, Segers-Nolten I, van der Werf K, Subramaniam V, Braeken D, Callewaert G, Bartic C, D'Hooge R, Martins I, Rousseau F, Schymkowitz J, De Strooper B (2010). Neurotoxicity of Alzheimer's disease Aβ peptides is induced by small changes in the Aβ42 to Aβ42 ratio. *EMBO J.*, 29:3408-3420.
[39] Bradford M (1976). A rapid and sensitive method for the quantitation of microgram quantities of protein utilizing the principle of protein-dye binding. *Anal. Biochem.*, 72:248-254.
[40] Delaglio F, Grzesiek S, Vuister G, Zhu G, Pfeifer J, Bax A (1995). NMRPipe: A multidimensional spectral processing system based on UNIX pipes. *J. Biomol. NMR*, 6:277-293.
[41] Bartels C, Xia T, Billeter M, Güntert P, Wüthrich K (1995). The program XEASY for computer-supported NMR spectral analysis of biological macromolecules. *J. Biomol. NMR*, 6:1-10.

3

A comparative analysis of the aggregation behavior of Aβ variants.

Early aggregated forms of the amyloid-β peptide are hypothesized to act as the prime toxic agents in Alzheimer disease. The *in vivo* Aβ peptide pool consists of both C- and N-terminally truncated or mutated peptides, and the composition thereof significantly determines risk of Alzheimer disease. Other variations, such as biotinylation, are introduced as molecular tools to aid the understanding of disease mechanisms. Since these modifications have the potential to alter key aggregation properties of the Aβ peptide, we present a comparative study of the aggregation of a substantial set of the most common *in vivo* identified and *in vitro* produced Aβ peptides.

The results described in this chapter have been published in:
Vandersteen A*, Hubin E*, Sarroukh R, De Baets G, Schymkowitz J, Rousseau F, Subramaniam V, Raussens V, Wenschuh H, Wildemann D, and Broersen K (2012). *FEBS Letters, first published online on October 24, 2012.*
* Annelies Vandersteen and Ellen Hubin are joint first authors.

3.1 Introduction

Early aggregated forms of Aβ have been considered the basis for development of Alzheimer disease [1,2]. Despite extensive research, the exact link between Aβ and Alzheimer disease remains elusive. One of the underlying reasons is that APP processing *in vivo* does not generate a single, well-defined species. The main cause for peptide heterogeneity stems from the identification of two main APP processing pathways, termed 'non-amyloidogenic' and 'amyloidogenic'. The non-amyloidogenic pathway involves APP cleavage by α- and γ-secretase and generates the p3 peptide, a N-terminally truncated form of Aβ, while the amyloidogenic pathway releases Aβ by action of β- and γ-secretase [3]. Besides the dual processing of APP generating either p3 or Aβ, the γ-secretase cleavage site is ill-defined resulting in variation at the C-terminus of Aβ [4,5]. As a result thereof, released Aβ peptides vary in length from 27 to 49 amino acids [6,7]. Additional variation in the *in vivo* Aβ pool is attained by mutations within the Aβ domain of APP. Known mutations inducing familial Alzheimer disease (FAD) include the Flemish (Ala21 to Gly), Dutch (Glu22 to Gln), Italian (Glu22 to Lys), Arctic (Glu22 to Gly), Iowa (Asp23 to Asn), and Tottori (Asp7 to Asn) mutations (reviewed by [8]). An additional source of peptide variation results from the introduction of biotinylation as a research tool for interaction studies [9-12]. All modifications described above could affect peptide behavior due to altered aggregation properties. In this study we systematically compared the aggregation behavior of p3 and Aβ peptides resulting from heterogeneous APP processing as well as a selection of FAD-associated Aβ mutants and biotinylated variants.

3.2 Results

We present a comparison of the aggregation profiles of an extensive set of Aβ peptides with N- or C-terminal variation [p3$_{17-40}$, p3$_{17-42}$, Aβ$_{37}$, Aβ$_{38}$, Aβ$_{40}$, Aβ$_{42}$, Aβ$_{43}$], FAD-related mutations [Aβ$_{42}$ D7N, A21G, E22G, E22K, E22Q, D23N], and biotinylated forms of Aβ [biotin-Aβ$_{40}$, biotin-Aβ$_{42}$, Aβ$_{40}$-K-biotin, Aβ$_{42}$-K-biotin]. Aβ peptides were prepared by peptide synthesis. Identity and purity were confirmed by MALDI-TOF MS and LC-MS (see appendix A).

3.2.1 C-terminal elongation increases aggregation propensity and induces an amorphous fibrillar state.

Aggregation kinetics of various Aβ lengths were recorded by thioT fluorescence and two different aggregation profiles could be distinguished: slow aggregation accompanied with long nucleation times and high final fluorescence intensity were detected for Aβ$_{37}$, Aβ$_{38}$ and Aβ$_{40}$, while Aβ$_{42}$ and Aβ$_{43}$ aggregated rapidly with almost immediate onset resulting in low final fluorescence intensity (Figure 3.1 a,b). Fibril morphology has been related to different affinities for thioT binding, affecting the extent of thioT fluorescence intensity [13,14]. Visualization of fibrils by TEM indeed revealed morphologically distinct aggregates, showing extended negatively-stained fibrils for Aβ$_{37}$, Aβ$_{38}$ and Aβ$_{40}$, and heavily intertwined networks for Aβ$_{42}$ and Aβ$_{43}$ (Figure 3.1c). Structural analysis by ATR-FTIR at early time points confirmed that these peptides adopted a β-sheet conformation, as seen by strong absorption at 1630 cm^{-1} (Figure 3.1e). Apart from affecting fibril properties, increasing peptide length also leads to a more pronounced oligomerization as detected through dotblotting with the

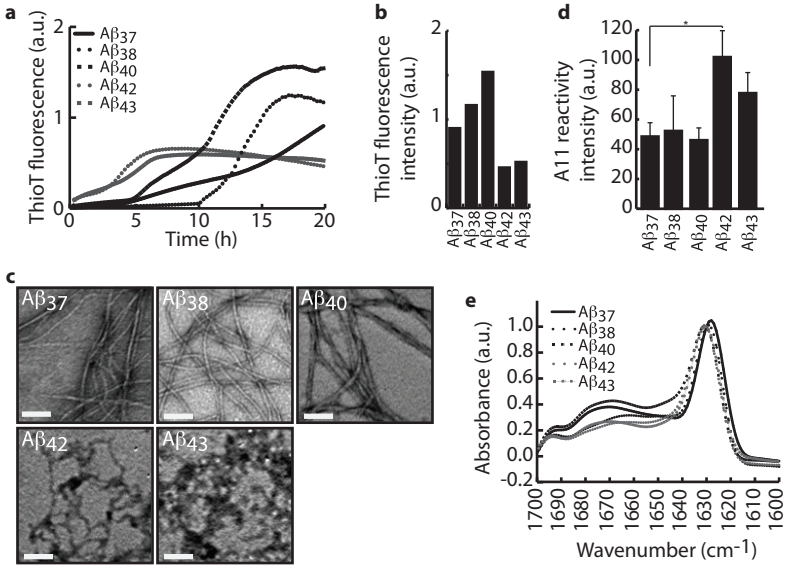

Figure 3.1 Increased aggregation and oligomerization of Aβ with increasing peptide length
(a) Aggregation of C-terminal varying Aβ peptides monitored by ThioT fluorescence. (b) ThioT fluorescence intensities after 20 h of incubation. (c) TEM images of 2 week incubated Aβ at 25 °C. The scale bar represents 0.1 μm. (d) A11-reactivity of 0.5 h pre-incubated Aβ in a dotblot assay. (e) Deconvoluted ATR-FTIR spectra of Aβ peptides (2 μg) recorded after 1.5 h incubation at 25 °C.

oligomer-specific A11 antibody (Figure 3.1d). $A\beta_{37}$, $A\beta_{38}$ and $A\beta_{40}$ showed less oligomer accumulation after 0.5 h of incubation than $A\beta_{42}$ and $A\beta_{43}$. Accordingly, ATR-FTIR spectra observed for pre-fibrillar $A\beta_{42}$ and $A\beta_{43}$ suggested higher β-sheet content compared to oligomers produced from shorter Aβ peptides which appeared more as a mixture of β-sheet, random coil and α-helical secondary structure elements (Table 3.1). This confirms the earlier report that the conversion of monomeric Aβ peptide into oligomers and mature fibrils coincides with the accumulation of a β-sheet enriched conformation [15]. The shorter $A\beta_{37}$, $A\beta_{38}$ and $A\beta_{40}$ displayed a higher β-sheet index [calculated as the ratio of the (1695 cm^{-1}/1630 cm^{-1}) intensities] than the longer $A\beta_{42}$ and $A\beta_{43}$. This suggests a higher content of antiparallel β-strands which reflects a less extended conversion from the oligomeric, antiparallel conformation into the fibrillar, parallel conformation after 1.5 h of incubation [16].

3.2.2 FAD mutations affect the aggregation rate to various extents but have little effect on fibril morphology and secondary structure.

Familial mutations of $A\beta_{42}$ displayed a short nucleation phase similar to that observed for wild type $A\beta_{42}$, but affected the rate of fibril elongation and final thioT fluorescence intensity (Figure 3.2 a,b). The slow polymerization of the D23N mutation coincided with a very low final thioT fluorescence, while A21G and E22Q mutations of $A\beta_{42}$ aggregated at a higher rate with an increased final thioT fluorescence intensity compared to wild type $A\beta_{42}$. All mutants of $A\beta_{42}$ displayed a β-sheet enriched conformation (Figure 3.2e, Table 3.1) and eventually formed similar dense fibrillar networks (Figure 3.2c).

	Secondary structure element (%)			
Peptide identity	β-sheet	Random coil + α-helix	Turn	β-sheet index
$A\beta_{37}$	36	44	20	0.28
$A\beta_{38}$	37	43	20	0.26
$A\beta_{40}$	47	33	20	0.27
$A\beta_{42}$	55	32	13	0.18
$A\beta_{43}$	56	28	16	0.14
D7N $A\beta_{42}$	55	30	15	0.19
A21G $A\beta_{42}$	51	33	16	0.22
E22G $A\beta_{42}$	41	37	22	0.18
E22K $A\beta_{42}$	45	39	16	0.16
E22Q $A\beta_{42}$	50	32	19	0.21
D23N $A\beta_{42}$	46	32	23	0.14
biotin-$A\beta_{40}$	34	44	22	0.31
$A\beta_{40}$-K-biotin	42	39	19	0.21
biotin-$A\beta_{42}$	54	34	12	0.17
$A\beta_{42}$-K-biotin	44	38	17	0.15
$p3_{17-40}$	39	40	20	0.25
$p3_{17-42}$	49	34	17	0.19

Table 3.1 Quantification of the secondary structure content using ATR-FTIR.
Curve-fitting was performed on the non-deconvoluted FTIR spectra and resulted in estimated contributions of β-sheets (1613-1637 cm^{-1} and 1682-1689 cm^{-1}),α-helices and random coil (1637-1662 cm^{-1}), and turns (1662-1682 cm^{-1}) to the secondary structure content of every Aβ peptide sample. The β-sheet index is defined as the ratio of the (1695 cm^{-1}/1630 cm^{-1}) intensities.

Oligomerization of the mutated $A\beta_{42}$ peptides showed little variability as seen by A11-reactivity (Figure 3.2d), with exception of D23N $A\beta_{42}$, and β-sheet index analysis indicated similar oligomer-content for the various peptides (Table 3.1).

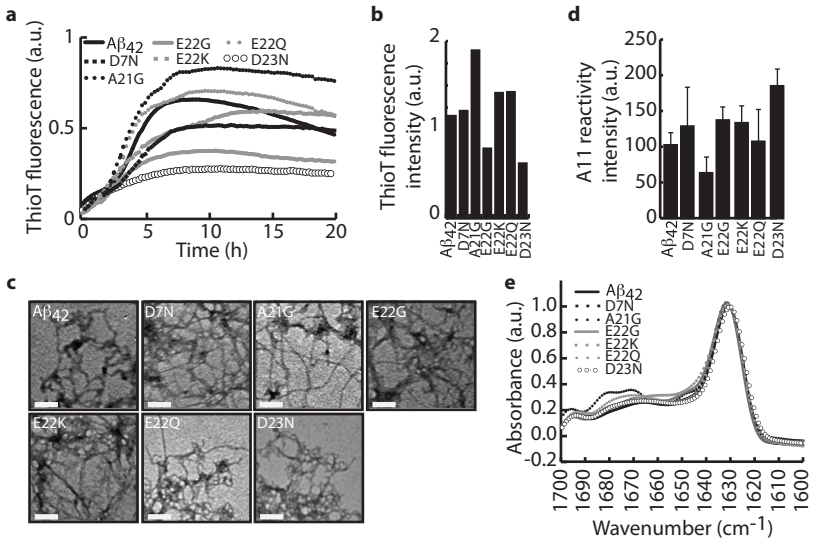

Figure 3.2 Some FAD-mutations affect aggregation and oligomerization of $A\beta_{42}$
(a) Aggregation of $A\beta_{42}$ FAD mutations monitored by thioT fluorescence. (b) ThioT fluorescence intensities after 20 h of incubation. (c) TEM images of 2 week incubated Aβ at 25 °C. The scale bar represents 0.1 μm. (d) A11-reactivity of 0.5 h pre-incubated Aβ in a dotblot assay. (e) Deconvoluted ATR-FTIR spectra of Aβ peptides (2 μg) recorded after 1.5 h incubation at 25 °C.

3.2.3 Biotinylation affects aggregation of Aβ40 and Aβ42.

N- and C-terminal biotinylation increased the lag time of aggregation (Figure 3.3a) while decreasing final thioT fluorescence for Aβ40 (Figure 3.3 a,b), indicative of inhibited aggregation, without affecting fibril morphology (Figure 3.3c). Oligomerization of biotinylated Aβ40, as probed by A11-reactivity, was unaffected (Figure 3.3d). Structural analysis of the peptides by ATR-FTIR however revealed absorption differences in the 1680-1640 cm^{-1} region (Figure 3.3e, Table 3.1). Biotinylation of Aβ42 reduced polymerization of the peptide compared to wild type Aβ42 (Figure 3.3a) without significantly affecting final ThioT fluorescence (Figure 3.3b), fibril morphology (Figure 3.3c) or secondary structure content (Figure 3.3e, Table 3.1). For Aβ42 the impact of biotinylation on oligomerization depended on the location of the modification. C-terminal biotinylation did not affect A11-reactivity (Figure 3.3d) but resulted in a reduced β-sheet index (Table 3.1). N-terminal modification on the other hand strongly impaired A11-reactivity (Figure 3.3d) but did not influence the β-sheet index (Table 3.1). The β-sheet index of biotinylated peptides however needs to be interpreted with caution as the biotin tag might absorb around 1695 cm^{-1}, leading to an overestimation of this value.

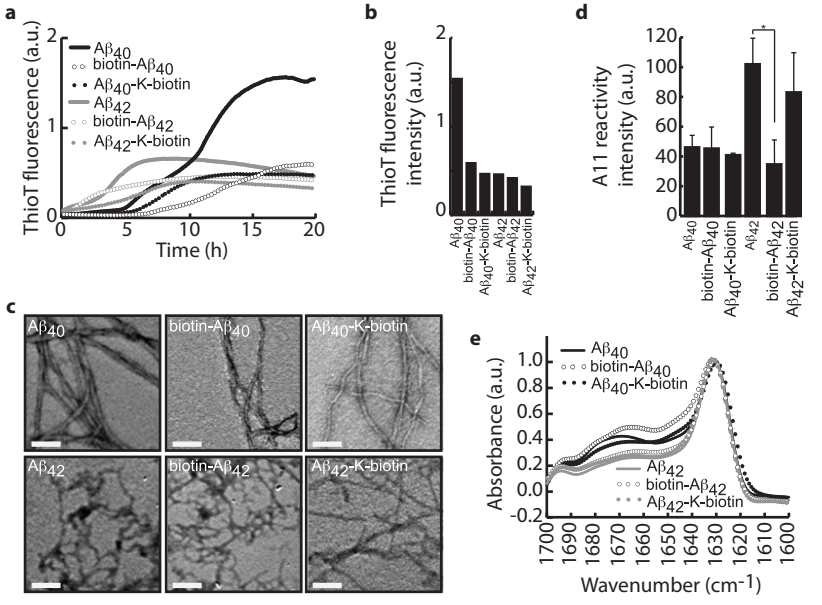

Figure 3.3 C- and N-terminal biotinylation of Aβ42 and Aβ40 differentially affect aggregation

(a) Aggregation of C- and N-terminally biotinylated forms of Aβ40 and Aβ42 monitored by thioT fluorescence. (b) ThioT fluorescence intensities after 20 h of incubation. (c) TEM images of 2 week incubated Aβ at 25 °C. The scale bar represents 0.1 μm. (d) A11-reactivity of 0.5 h pre-incubated Aβ in a dotblot assay. (e) Deconvoluted ATR-FTIR spectra of Aβ peptides (2 μg) recorded after 1.5 h incubation at 25 °C.

3.2.4 N-terminal truncation of Aβ induces rapid onset aggregation.

Both N-terminally truncated forms of Aβ40 and Aβ42, p3$_{17-40}$ and p3$_{17-42}$ respectively, were characterized by rapid onset of aggregation compared to their corresponding full-length forms with decreased final thioT fluorescence intensity (Figure

3.4 a,b). From a morphological perspective, visualization by TEM revealed short fibrillar fragments for $p3_{17-40}$ dissimilar from the long extended networks observed for full-length $A\beta_{40}$ (Figure 3.4c). Truncation of $A\beta_{42}$ to $p3_{17-42}$ only slightly affected fibril morphology resulting in less curly fibrils (Figure 3.4c). Structural analysis by ATR-FTIR indicated that $p3_{17-40}$ displayed less β-sheets and more random coil and α-helical content than full-length $A\beta_{40}$. A similar observation was made for $p3_{17-42}$ compared to $A\beta_{42}$ (Figure 3.4e, Table 3.1). Oligomerization of the truncated p3 peptides, as analyzed by A11-reactivity and the β-sheet index, was not significantly affected compared to the full-length counterparts (Figure 3.4d, Table 3.1).

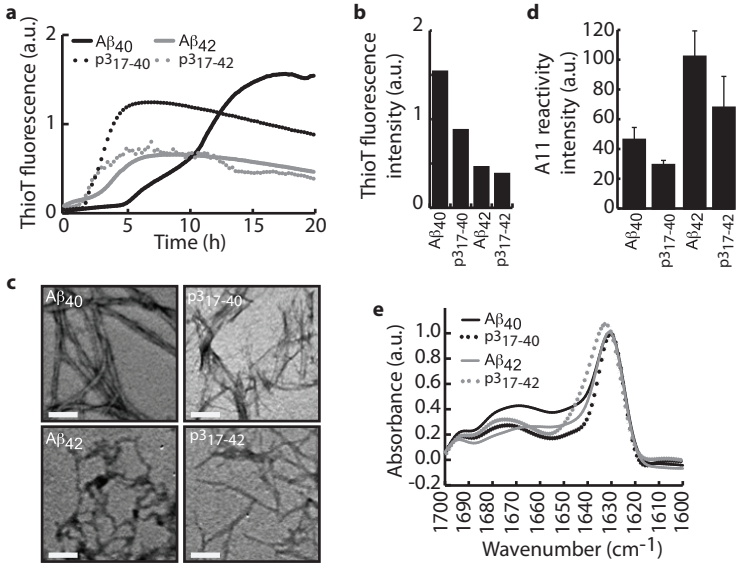

Figure 3.4 p3 peptides show pronounced aggregation
(a) Aggregation of $p3_{17-40}$ and $p3_{17-42}$ monitored by thioT fluorescence. (b) ThioT fluorescence intensities after 20 h of incubation. (c) TEM images of 2 week incubated Aβ at 25 °C. The scale bar represents 0.1 μm. (d) A11-reactivity of 0.5 h pre-incubated Aβ in a dotblot assay. (e) Deconvoluted ATR-FTIR spectra of Aβ peptides (2 μg) recorded after 1.5 h incubation at 25 °C.

3.3 Discussion

The *in vivo* Aβ pool contains a high degree of variability, consisting of peptides with C-terminal variations, mutations related to familial Alzheimer disease, and N-terminal truncations. To elucidate the mechanisms leading to Alzheimer disease some peptides have been additionally modified, e.g. biotinylated, to enable their investigation in experimental research. The chemically synthesized Aβ peptide variants were compare in terms of aggregation and oligomerization behavior using biophysical techniques. Our observations show that variations in the Aβ sequence can have consequences for the propensity of the Aβ peptide to aggregate and oligomerize.

C-terminal variation was previously shown to affect aggregation propensity, and it has been generally reported that $A\beta_{42}$ aggregates at a higher rate than $A\beta_{40}$ [17,18]. Even though approximately 90% of the Aβ peptide pool is composed of these two

peptides, it was recently recognized that also $A\beta_{37}$, $A\beta_{38}$, and $A\beta_{43}$ are present in the brain and may modulate disease progress [19]. We show that C-terminal extension generally results in faster aggregation and gradual transformation into densely networked β-sheet rich aggregates compared to shorter peptides, which form extended fibrils characterized by a primarily disordered structure. We further observed that $A\beta_{37}$ and $A\beta_{38}$ generally behave similar to $A\beta_{40}$ while the behavior of $A\beta_{43}$ strongly resembles that of $A\beta_{42}$. The dense fibril networks formed by $A\beta_{42}$ and $A\beta_{43}$ possibly provide less access to the thioT dye compared to the more extended fibrils of shorter peptides, resulting in a lower final thioT fluorescence intensity. Alternatively, the denser peptide networks can be more prone to precipitation in the test tube which would lead to a similar observation. Although the effect of mutations of $A\beta_{42}$ related to familial Alzheimer disease on aggregation has been investigated in the past [20-23], no comprehensive study has been reported that directly compares the majority of the currently known mutations. Different Aβ preparation methods and experimental conditions have led to considerable variation in reported effects of these mutations. ThioT fluorescence data in this study were measured at a physiologically relevant Aβ concentration of 1 μM. Most mutations related to familial Alzheimer disease are located in or near the central hydrophobic cluster of the Aβ peptide, which has been predicted and reported to play an important role in aggregation [24-28]. These mutations can thus either inhibit or induce aggregation depending on the suitability of the replacing amino acid to accommodate an amyloidogenic or aggregated structure. Molecular dynamics simulations have suggested the depletion of the E22-K28 salt bridge to explain the enhanced aggregation of E22Q $A\beta_{42}$, while the switch of a bend motif to a turn in the region 22-28 could result in slower aggregation of the D23N $A\beta_{42}$ mutant [22]. Overall fibril morphology is however not affected, as has been shown previously for a subset of mutants leading to familial Alzheimer disease [20]. The central hydrophobic region is however not the absolute key in determining aggregation tendency as a subset of the mutations in this region has no effect on the aggregation rate and most likely exert their pathological function through aberrant APP processing or reduced proteolytic Aβ degradation [29-31]. We further show that C-terminal elongation, which does not affect the central region of Aβ, also affects aggregation. Moreover, complete destruction of the central aggregation zone by deletion of the first 17 N-terminal amino acids, as naturally occurs by APP processing via the non-amyloidogenic pathway, does not abolish the aggregating character of the peptides, as was observed before [32] and upregulation of the α-secretase cleavage pathway initiating the non-amyloidogenic processing of APP has served as a template for the generation of various potential disease modulating drugs [33]. It is thus likely to suggest that, even though the central Aβ region can play a regulating role in the aggregation process, the C-terminal region may dominate this effect by determining fibril morphology. Biotinylation of Aβ can be used as a tool to pool or detect via interaction with streptavidin. Our data show that this modification can affect the onset of aggregation substantially depending on the type of biotinylation applied and its location, either N- or C-terminally, without affecting fibril morphology or oligomer formation. These observations underline the importance of selecting and validating the type of labeling required for experiments without inducing changes in the peptide behavior that are subject to study.

In this work we systematically compared a wide range of Aβ peptides for their aggregation properties. The overall aggregation profile was determined by thioT

fluorescence while we attempted to gain insight in early aggregation events by probing oligomerization of the peptides. We therefore used A11-reactivity as well as analysis of secondary structure content which were however not always completely in agreement. This could be attributed to the polyclonal nature of the A11 antibody [34] that can be hypothesized to recognize more than one conformation. On the other hand, it might be likely that both methods detect different oligomeric species. In conclusion, the results highlight that minor sequential variations may have consequences for the aggregation of Aβ.

3.4 Experimental procedures

3.4.1 Aβ peptide synthesis

Aβ and p3 peptides were produced by JPT Peptide Technologies. Peptides were synthesized on preloaded TentaGel® S TRT resins using an ABI 433A peptide synthesizer. Synthesis was performed using 2-(1H-7-azabenzotriazol-1-yl)-1,1,3,3-tetramethyl uronium hexafluorophosphate as an activation reagent and standard procedures of Fmoc-based solid phase peptide synthesis were applied. Peptides were cleaved from the resin with trifluoroacetic acid and purified by preparative high performance liquid chromatography. Following synthesis the purity and identity of Aβ peptides was assessed by matrix-assisted laser desorption/ionization time-of-flight mass spectrometry and LC-MS (see appendix A). The LC-MS system was used in combination with a C18 Gemini-NX column at a flow rate of 1 ml min^{-1} and a gradient of 5-95% acetonitrile was set in 6 minutes.

3.4.2 Solubilization of Aβ peptides

Peptides were dissolved according to the standard procedure described in Chapter 2. In short, Aβ peptides were dissolved in HFIP which was evaporated and the resulting peptide film was redissolved using DMSO. The peptide was separated from DMSO by elution from a desalting column into a 50mM Tris pH 7.5 buffer containing 1mM EDTA. The resulting samples were kept on ice until experiments started with a maximum lag time of 30 min. Peptide concentration was determined using the Coomassie (Bradford) Protein Assay kit and diluted to 25 μM in 50mM Tris pH 7.5 buffer containing 1mM EDTA. Incubation of Aβ peptides occurred for the given time periods at 25 °C under quiescent conditions.

3.4.3 Thioflavin T fluorescence

Aβ concentrations were adjusted to 1 μM using 50mM Tris pH 7.5 buffer containing 1mM EDTA and a final concentration of 12 μM thioT. The fibrillation kinetics of the various Aβ preparations were monitored *in situ* at excitation and emission wavelengths of 440 and 480 nm respectively. Fluorescence readings were recorded every 5 min for a period of 20 h. Measurements were performed as independent triplicates. Recorded values were averaged and background measurements (buffer containing 12 μM ThT) were subtracted.

3.4.4 Transmission electron microscopy

After 2 weeks of incubation, Aβ aliquots (5 μL) were adsorbed to carbon-coated

Formvar 400-mesh copper grids for 1 min. The grids were blotted, washed, and stained with 1% (wt/vol) uranyl acetate. Samples were studied with a JEOL JEM-1400 microscope at 80 kV. Images were collected from three independently prepared Aβ solutions.

3.4.5 Dotblot

After 0.5 h of incubation a volume of 5 μL Aβ was spotted onto a nitrocellulose membrane. The membranes were blocked in phosphate buffered saline (PBS) containing 0.2% Tween-20 (1 h, 25 °C), and incubated (1 h, 25 °C) with primary A11 antibody, diluted 1:4000 in 100mM Hepes, pH 7.0 [34]. After incubation (0.5 h, 25 °C) with a secondary anti-rabbit-HRP-tagged antibody, diluted 1:5000 in PBS containing 0.05% Tween-20, the membranes were visualized using the Immobilon^{TM} Western chemiluminescent HRP substrate system. Spots were manually selected and their intensities were analyzed as mean grey values using ImageJ software [35]. Images were background subtracted.

3.4.6 Attenuated total reflectance-Fourier-transform infrared spectroscopy

ATR-FTIR spectra were recorded on an Equinox 55 IR spectrophotometer. The Aβ solubilization procedure and buffer composition were slightly adapted to obtain ATR-FTIR spectra with sufficient intensity and without interference by EDTA or salts. In short, Aβ peptide samples were dissolved in HFIP. HFIP was evaporated and the resulting peptide film was redissolved in 10mM Tris pH 7.5 to a concentration of 1 mg ml^{-1}. Samples were incubated for 1.5 h at room temperature under quiescent conditions. Two μg of Aβ was spread on the diamond surface of the internal reflection element and was washed with excess milliQ water to eliminate salts. Excess water was evaporated under nitrogen flow. Each spectrum represents the mean of 128 repetitions, recorded at a resolution of 2 cm^{-1}. The ATR-FTIR data were processed by subtracting the water vapor contribution with 1562-1555 cm^{-1} as reference peak and spectra were baseline corrected. Spectral intensities were normalized to the intensity of the 1630 cm^{-1} peak, and were smoothed at a final resolution of 4 cm^{-1}. All spectra were self-deconvoluted and curve-fitting was performed on the non-deconvoluted ATR-FTIR spectra. The proportion of a particular structure is computed to be the sum of the area of all the fitted bands divided by the area of all the Lorentzian bands. The β-sheet index was defined as the ratio of the 1695 cm^{-1}/1630 cm^{-1} intensities.

3.4.7 Statistical Analysis

The intensities of A11-positive spots as determined with ImageJ software were further analyzed using the two-tailed unpaired t-test for significance. Significant differences are denoted by a star: *p<0.05, **p<0.01, ***p<0.001.

author contributions

KB designed the study; JS, FR, VS suggested experiments and discussed the results; AV, EH performed the experiments and wrote the manuscript; GDB made computational analyses; HW, DW produced the peptides and assessed their purity.

3.5 References

[1] Glenner G & Wong C (1984). Alzheimer's disease: initial report of the purification and characterization of a novel cerebrovascular amyloid protein. *Biochem. Bioph. Res. Co.*, 120:885-890.

[2] Pike C, Walencewicz A, Glabe C (1991). In vitro aging of β-amyloid protein causes peptide aggregation and neurotoxicity. *Brain Res.*, 563:311-314.

[3] Nunan J & Small D (2000). Regulation of APP cleavage by α-, β- and γ-secretases. *FEBS Lett.*, 483:6-10.

[4] Weidemann A, Eggert S, Reinhard F, Vogel M, Paliga K, Baier G, Masters C, Beyreuther K, Evin G (2002). A novel ε-cleavage within the transmembrane domain of the Alzheimer amyloid precursor protein demonstrates homology with Notch processing. *Biochemistry,* 41:2825-2835.

[5] Zhao G, Mao G, Tan J, Dong Y, Cui M-Z, Kim S-H, Xu X (2004). Identification of a new presenilin-dependent ζ-cleavage site within the transmembrane domain of amyloid precursor protein. *J. Biol. Chem.*, 279:50647-50650.

[6] Vigo-Pelfrey C, Lee D, Keim P, Lieberburg I, Schenk D (1993). Characterization of β-amyloid peptide from human cerebrospinal fluid. *J. Neurochem.*, 61:1965-1968.

[7] Takami M, Nagashima Y, Sano Y, Ishihara S, Morishima-Kawashima M, Funamoto S, Ihara Y (2009). γ-Secretase: successive tripeptide and tetrapeptide release from the transmembrane domain of β carboxyl terminal fragment. *J. Neurosci.*, 29:13042-13052.

[8] Van Dam D & De Deyn P (2006). Drug discovery in dementia: the role of rodent models. *Nat. Rev. Drug Discov.*, 5:956-970.

[9] Bohrmann B, Tjernberg L, Kuner P, Poli S, Levet-Trafit B, Näslund J, Richards G, Huber W, Döbeli H, Nordstedt C (1999). Endogenous proteins controlling amyloid β-peptide polymerization. Possible implications for β-amyloid formation in the central nervous system and in peripheral tissues. *J. Biol. Chem.*, 274:15990-15995.

[10] Leissring M, Lu A, Condron M, Teplow D, Stein R, Farris W, Selkoe D (2003). Kinetics of amyloid β-protein degradation determined by novel fluorescence- and fluorescence polarization-based assays. *J. Biol. Chem.*, 278:37314-37320.

[11] Liu R, Barkhordarian H, Emadi S, Park C, Sierks M. (2005). Trehalose differentially inhibits aggregation and neurotoxicity of β-amyloid 40 and 42. *Neurobiol. Dis.*, 20:74-81.

[12] Nelson T & Alkon D (2007). Protection against β-amyloid-induced apoptosis by peptides interacting with β-amyloid. *J. Biol. Chem.*, 282:31238- 31249.

[13] Groenning M (2010). Binding mode of Thioflavin T and other molecular probes in the context of amyloid fibrils-current status. *J. Chem. Biol.*, 3:1-18.

[14] Biancalana M & Koide S (2010). Molecular mechanism of Thioflavin-T binding to amyloid fibrils. *Biochim. Biophys. Acta.*, 1804:1405-1412.

[15] Barrow C, Yasuda A, Kenny P, Zagorski M (1992). Solution conformations and aggregational properties of synthetic amyloid β-peptides of Alzheimer's disease. Analysis of circular dichroism spectra. *J. Mol. Biol.*, 225:1075-1093.

[16] Cerf E, Sarroukh R, Tamamizu-Kato S, Breydo L, Derclaye S, Dufrêne Y, Naratanaswami V, Goormaghtigh E, Ruysschaert J, Raussens V (2009). Antiparallel β-sheet: a signature structure of the oligomeric amyloid β-peptide. *Biochem. J.*, 421:415-423.

[17] Jarrett J, Berger E, Lansbury P (1993). The carboxy terminus of the β amyloid protein is critical for the seeding of amyloid formation: implications for the pathogenesis of Alzheimer's disease. *Biochemistry,* 32:4693-4697.

[18] Snyder S, Ladror U, Wade W, Wang G, Barrett L, Matayoshi E, Huffaker H, Krafft G, Holzman T (1994). Amyloid-β aggregation: selective inhibition of aggregation in mixtures of amyloid with different chain lengths. *Biophys. J.*, 67:1216-1228.

[19] Portelius E, Bogdanovic N, Gustavsson M, Volkmann I, Brinkmalm G, Zetterberg H, Winblad B, Blennow K (2010). Mass spectrometric characterization of brain amyloid β isoform signatures in familial and sporadic Alzheimer's disease. *Acta Neuropathol.*, 120:185-193.

[20] Murakami K, Irie K, Morimoto A, Ohigashi H, Shindo M, Nagao M, Shimizu T, Shirasawa T (2003). Neurotoxicity and physicochemical properties of Aβ mutant peptides from cerebral amyloid angiopathy: implication for the pathogenesis of cerebral 1 amyloid angiopathy and Alzheimer's disease. *J. Biol. Chem.*, 278:46179-46187.

[21] Baumketner A, Krone M, Shea J (2008). Role of the familial Dutch mutation E22Q in the folding and aggregation of the 15–28 fragment of the Alzheimer amyloid-β protein. *Proc. Natl. Acad. Sci. USA*, 105:6027-6032.

[22] Krone M, Baumketner A, Bernstein S, Wyttenbach T, Lazo N, Teplow D, Bowers M, Shea J (2008).

Effects of familial Alzheimer's disease mutations on the folding nucleation of the amyloid β-protein. *J. Mol. Biol.*, 381:221-228.
[23] Ono K, Condron M, Teplow D (2010). Effects of the English (H6R) and Tottori (D7N) familial Alzheimer disease mutations on amyloid β-protein assembly and toxicity. *J. Biol. Chem.*, 285:23186-23197.
[24] Fernandez-Escamilla A, Rousseau F, Schymkowitz J, Serrano L (2004). Prediction of sequence-dependent and mutational effects on the aggregation of peptides and proteins. *Nature Biotechnol.*, 22:1302-1306.
[25] Liu R, McAllister C, Lyubchenko Y, Sierks M (2004). Residues 17-20 and 30-35 of β-amyloid play critical roles in aggregation. *J. Neurosci. Res.*, 75:162-71.
[26] Lopez-De la Paz M, Goldie K, Zurdo J, Lacroix E, Dobson C, Hoenger A, Serrano L (2002). De novo designed peptide-based amyloid fibrils. *Proc. Natl. Acad. Sci. USA*, 99:16052-16057.
[27] Sánchez de Groot N, Pallarés I, Avilés F, Vendrell J, Ventura S. (2005). Prediction of "hot spots" of aggregation in disease-linked polypeptides. *BMC Struct. Biol.*, 5:18.
[28] Chiti F, Stefani M, Taddei N, Ramponi G, Dobson C (2003). Rationalization of the effects of mutations on peptide and protein aggregation rates. *Nature,* 424:805-808.
[29] Tian Y, Bassit B, Chau D, Li, Y (2010). An APP inhibitory domain containing the Flemish mutation residue modulates γ-secretase activity for Aβ production. *Nat. Struct. Mol. Biol.*, 17:151-158.
[30] Betts V, Leissring M, Dolios G, Wang R, Selkoe D, Walsh D (2008). Aggregation and catabolism of disease-associated intra-Aβ mutations: reduced proteolysis of AβA21G by neprilysin. *Neurobiol. Dis.*, 31:442-450.
[31] Morelli L, Llovera R, Gonzalez S, Affranchino J, Prelli F, Frangione B, Ghiso J, Castano E (2003). Differential degradation of amyloid β genetic variants associated with hereditary dementia or stroke by insulin-degrading enzyme. *J. Biol. Chem.*, 278:23221-23226.
[32] Pike C, Overman M, Cotman C (1995). Amino-terminal deletions enhance aggregation of β-amyloid peptides in vitro. *J. Biol. Chem.*, 270:23895-23898.
[33] Fahrenholz F (2007). α-Secretase as a therapeutic target. *Curr. Alzheimer Res.*, 4:412-417.
[34] Kayed R, Head E, Thompson J, McIntire T, Milton S, Cotman C, Glabe C (2003). Common structure of soluble amyloid oligomers implies common mechanism of pathogenesis. *Science*, 300:486- 489.
[35] Abramoff M, Magalhaes P, Ram S (2004). Image processing with ImageJ. *Biophotonics International,* 11:36-42.

4

Amyloid precursor protein mutation E682K at the alternative β-secretase cleavage β'-site increases Aβ generation.

BACE1 cleaves the amyloid precursor protein (APP) at the β-cleavage site to initiate the generation of amyloid peptide Aβ. Besides, BACE1 is also known to cleave at a much less well-characterized β'-cleavage site. The novel APP mutation E682K is located at this β'-site in an early onset Alzheimer disease case. Functional analysis revealed that this E682K mutation blocked the β'-site and shifted all cleavage of APP to the β-site, causing increased Aβ production. This work demonstrates the functional importance of APP processing at the β'-site and shows how disruption of the balance between β- and β'-site cleavage may enhance the amyloidogenic processing and consequentially the risk for Alzheimer disease. Increasing exon- and exome-based sequencing efforts will identify many more putative pathogenic mutations without comclusive segregation-based evidence in a single family. This study shows how functional analysis of such mutations allows to determine the potential pathogenic nature of these mutations. We propose to classify the E682K mutation as probable pathogenic awaiting further independent confirmation of its association with Alzheimer disease in other patients.

The results described in this chapter have been published in:
Zhou L, Brouwers N, Benilova I, Vandersteen A, Mercken M, Van Laere K, Van Damme P, Demedts D, Van Leuven F, Sleegers K, Broersen K, Van Broeckhoven C, Vandenberghe R, and De Strooper B (2011). *EMBO Mol. Med.*, 3:1-12.

4.1 Introduction

BACE1, a membrane-bound aspartic protease, is the β-secretase which cleaves APP at the β-site Met_{671}-Asp_{672} of APP (Asp_1 of the Aβ sequence) [1-5]. This cleavage generates the APP carboxyterminal fragment CTF_{99}, which is a substrate for the γ-secretase complex, an intramembrane cleaving protease [6]. γ-Secretase processing of CTF_{99} yields a mixture of Aβ peptides including $Aβ_{38}$, $Aβ_{40}$, and $Aβ_{42}$ as the most abundantly detected species in cell culture and biological fluids [7].

Additionally BACE1 cleaves APP at a β'-site, a secondary cleavage site between Tyr_{681} and Glu_{682} (Glu_{11} of Aβ) to generate CTF_{89}, which is further processed by γ-secretase to produce truncated $Aβ_{11\text{-}40/42}$ species. BACE1 cleavage at the β'-site was originally discovered in cell cultures overexpressing this protease [3]. An *in vitro* study showed that purified BACE1 cleaves synthetic peptides mimicking the sequence around the human APP β'-site in an enzymatic assay, but the enzymatic efficiency was lower than towards peptides containing the 'canonic' β-site sequence [8]. Additional evidence suggested that the relative abundance of BACE1 cleavage at these two adjacent sites is governed by the expression levels of the protease: when BACE1 levels are low, β-site cleavage products are the major species, when BACE1 levels are high, β'-site cleavage products become predominant [9,10]. These findings were also taken to suggest that β'-site processing was only a minor event in APP processing [9]. The abundance of the β'-site cleavage for human APP processing as well as the functional significance of this alternative β-secretase cleavage site remains, therefore, elusive.

In this work, we identify a novel and unusual APP mutation in a Belgian patient showing early onset Alzheimer disease and seen in the University Hospital in Leuven. This mutation - E682K - is located at the β'-site within the Aβ sequence (Figure 4.1). We examined the effect of this mutation on the proteolytic processing of APP and found that this mutation caused significant increases in total Aβ and in $Aβ_{42/40}$ levels. We further analysed APP processing in neuronal cultures by short metabolic labelling experiments demonstrating that β'-site cleavage is a major processing event of wild-type (wt) human APP in neuronal cultures. The E682K mutation blocked this processing step and consequentially shifted BACE1 cleavage towards the β-site. The data demonstrate the functional significance of β'-site cleavage in preventing overproduction of Aβ, which may potentially cause Alzheimer disease.

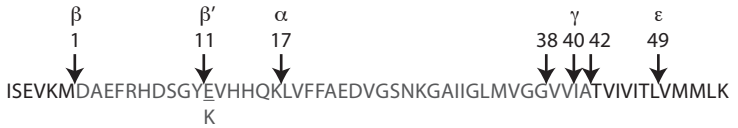

Figure 4.1 Schematic overview of APP E682K mutation and secretase cleavage sites.
Numbers were indicated according to the Aβ sequence (in grey).

4.2 Results

4.2.1 Clinical description of the index patient carrying the APP E682K mutation

The index patient presented at the Memory Clinic, University Hospitals Leuven, at the age of 50 years with a prior diagnosis of early onset clinically probable Alzheimer

disease. Around the age of 47, she had developed symptoms of depression followed by gradually progressive cognitive decline with significant impact on her instrumental activities of daily living. At presentation, the index patient was on citalopram 10 mg twice per day and donepezil 10 mg once per day. Neuropsychological evaluation of the patient revealed a significant memory deficit as indicated by the standard testing. Magnetic resonance imaging T2-weighted sequence revealed bilateral hippocampal volume loss. Analysis of cerebrospinal fluid revealed decreased $A\beta_{42}$ and increased total and 181T-phosphorylated tau (Table 4.1), a pattern corresponding to Alzheimer disease. Sequencing of the APP gene revealed a G to A substitution at g.278228G, which is predicted to result in an amino acid substitution at codon 682 (E682K). Such mutation was absent in 940 control samples.

	control	AD control	patient (E682K)
n (male/female)	7 (5/2)	10 (6/4)	
age	62.3 ± 4.4	66.6 ± 5.0	51
$A\beta_{1-42}$ (pg/ml)	986.8 ± 255.8	368.2 ± 63.7	165
total-tau (pg/ml)	168.7 ± 63.7	926.8 ± 487.8	834
phospho-tau (pg/ml)	57.8 ± 16.17	122.2 ± 34.1	104

values are mean ± SD

Table 4.1 Aβ and tau protein levels in cerebrospinal fluid.

The patient is from a small family. Her father received a diagnosis of dementia at the age of 75 and died at the age of 83 years. His genetic status is unknown as no sample was available for genomic analysis. The patient's brother, however, is clinically, at the age of 53, an asymptomatic carrier. We considered the possibility that the APP E682K mutation could have a variable penetrance in this family. A strong variation in age of onset (range 45-88 years) has previously been observed with Alzheimer disease causing mutations in *PS2* as well [11]. We thus turned to functional assays to evaluate whether the identified mutation could be a genetic risk factor for Alzheimer disease or not.

4.2.2 E682K mutation increased Aβ generation

We introduced the E682K mutation by site directed mutagenesis into human WT APP695 and expressed WT or mutant APP in mouse primary neuronal cultures and in transiently transfected CHO cells. The expression levels of WT and mutant full length APP were checked by Western blotting, and neuronal or CHO cell cultures expressing similar amounts of APP were subjected to further analysis. Conditioned media were analysed using Aβ enzyme-linked immunosorbent assay (ELISA) (Table 4.2). In both neuronal and CHO cell cultures, the E682K mutation caused a two- to three-fold increase in $A\beta_{40}$ and $A\beta_{42}$ levels, but also a slightly higher $A\beta_{42}$:$A\beta_{40}$ ratio (Table 4.2). The alterations are quantitatively and qualitatively comparable to those caused by the previously characterized disease-causing 'Flemish' A692G mutation, which also caused increases in the Aβ levels and a slightly higher $A\beta_{42}$:$A\beta_{40}$ ratio (Table 4.2) [12-17].

4.2.3 E682K mutation enhanced β-site cleavage of APP

We next analysed the effects of the E682K mutation on APP processing in further detail. In primary neuronal cultures, this mutation increased CTF_{99} and $APP_{s\beta}$ levels

	$A\beta_{42}$ (pg/ml)	$A\beta_{40}$ (pg/ml)	$A\beta_{42}/A\beta_{40}$ ratio
CHO cells			
APPwt	37.7 ± 1.2	355.6 ± 17.2	0.1065 ± 0.0051
E682K	94.6 ± 4.7	604.6 ± 18.0	0.1563 ± 0.0049**
A692G (Flemish)	77.5 ± 2.4	621.3 ± 27.2	0.1251 ± 0.0039*
primary neurons			
APPwt	60.0 ± 1.9	546.3 ± 14.3	0.1101 ± 0.0046
E682K	189.9 ± 5.1	1005.3 ± 10.1	0.1890 ± 0.0040**
A692G (Flemish)	131.7 ± 1.5	1049.2 ± 42.7	0.1257 ± 0.0037*

Data were normalized to APP expression level (**p<0.001, *p<0.05; mean ± SEM; n=3)

Table 4.2 $A\beta_{42}$ and $A\beta_{40}$ levels as well as $A\beta_{42}$:$A\beta_{40}$ ratio in conditioned media from transfected CHO cells or transduced neurons

two- to three-fold (Figure 4.2 a-c), which correlates well with the overall increases in Aβ levels as measured by ELISA. Similar effects were observed in transiently transfected CHO cells, in which the E682K mutation caused a two- to three-fold increase in CTF_{99} and $APP_{S\beta}$ levels (Figure 4.2 d-f). These data show that the E682K mutation increased Aβ generation by favouring the β-site cleavage of APP. In contrast to the E682K mutation, the 'Flemish' A692G mutation did not significantly affect the β-secretase processing (as measured by CTF_{99} and $APP_{S\beta}$ generation), confirming that the increased Aβ generation with this mutant is caused by a different mechanism. It has indeed been shown that the 'Flemish' mutation affects an inhibitory domain in the APP sequence that modulates γ-secretase activity [17].

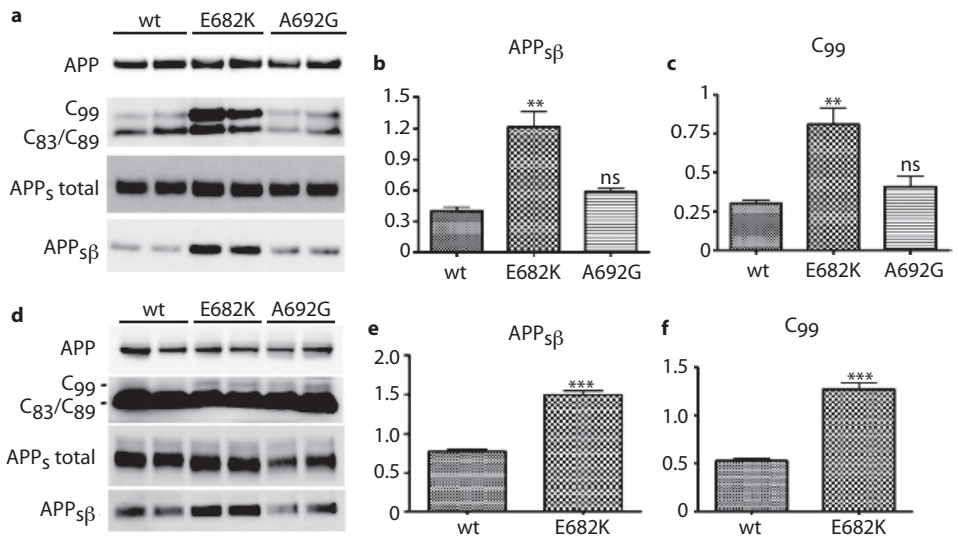

Figure 4.2 Effects of E682K mutation on APP processing in cultured neurons (a-c) and in CHO cells (d-f).

(a) Primary cultured neurons were transduced with SFV expressing WT or mutant APP and (d) CHO cells were transiently transfected with constructs expressing WT or mutant APP. Cell lysates were analysed by Western blotting using APP C-terminal antibody B63. Conditioned medium was analysed by Western blotting to determine secreted total APPs (using 22C11 antibody) and $APP_{S\beta}$ (using anti-$APP_{S\beta}$ antibody).

(b,c)(e,f). Semi-quantification of $APP_{S\beta}$ and CTF_{99} levels from Western blotting, data were normalized to APP levels (b,c) **p<0.01; ns, statistically not significant; mean±SEM; n=4 (e,f) **p<0.01; mean ±SEM; n=3

4.2.4 E682K mutation blocked the β'-site cleavage, which is a major processing event of human APP in neuronal cultures

We further examined how the E682K mutation might enhance β-site cleavage. This mutation is located at the previously identified β'-site in APP and the WT residue Glu_{11} is known to occupy the P1' subsite of BACE1 involved in β'-site cleavage. A previous kinetic study has shown that the P1' subsite of BACE1 favours several residues including Asp, Glu, Met, Ala, Ser, and Gln, but that positively charged residues like Lys or Arg decrease affinity [18]. The E682K mutation was thus predicted to block the β'-site cleavage. However, until now, β'-cleavage of human APP is considered as a minor processing event in cells expressing endogenous levels of BACE1, and has been mainly documented in cells overexpressing BACE1 [9,10,19,20].

Here, we reanalyse the metabolism of human APP in neuronal cultures. We expressed WT or mutant human APP in neuronal cultures using the SFV system and then metabolically labelled the cells for 4 h. The carboxyterminal fragments (CTFs) of APP were immunoprecipitated from cell lysates using an APP carboxyterminal-specific antibody and separated by gel electrophoresis for further analysis. We identified five species of CTFs (Figure 4.3a), as previously described [21,22]. We conclude that the two highest molecular weight bands are phosphorylated CTF_{99} and nonphosphorylated CTF_{99}; the next faint band is phosphorylated CTF_{89}; the fourth band is a mixture of non-phosphorylated CTF_{89} and phosphorylated CTF_{83}; and the lowest molecular weight band is non-phosphorylated CTF_{83}. In another group of experiments, we treated the immunoprecipitates with lambda protein phosphatase (LPP) (Figure 4.3b) to remove the confounding phosphorylation, and this resulted, as predicted, in three species of CTFs, i.e. non-phosphorylated CTF_{99}, CTF_{89}, and CTF_{83}. Quantification of phosphor images showed that CTF_{99}, CTF_{89}, and CTF_{83} accounted for 51.7, 24.9, and 23.4%, respectively, of the total of the three species (Figure 4.3c). These data indicate that β'-site cleavage is a major processing event that occurs with human APP in neuronal cultures. Interestingly, the E682K mutation (Figure 4.3a), when expressed in neuronal cultures, generated more CTF_{99} (both phosphorylated and non-phosphorylated), no detectable phosphorylated CTF_{89}, and apparently less of the mixture of non-phosphorylated CTF_{89} and phosphorylated CTF_{83} compared to WT APP (Figure 4.3a). The level of the latter band was equal to that of the band isolated from neuronal cultures treated with a highly selective BACE1 inhibitor compound 3 (Figure 4.3a), which is in accordance with our hypothesis that the E682K mutation blocked CTF_{89} generation. After treatment with LPP, this hypothesis was confirmed as only CTF_{99} and CTF_{83} were detected (Figure 4.3b).

We also immunoprecipitated Aβ related peptides from the conditioned medium using $Aβ_{40/42}$ carboxyterminal specific monoclonal antibodies (mAbs). WT APP generated two major species (Figure 4.3d), and both peptides were eliminated after treatment with BACE1 inhibitor (Figure 4.3d), but remained after treatment with α-secretase inhibitor TAPI-1 (Figure 4.3d). We thus concluded that these two peptides were products from BACE1 cleavage, i.e. they are $Aβ_{40/42}$ and $Aβ_{11–40/42}$ species. In agreement with the results obtained from analyzing the CTF levels, the E682K mutation blocked the generation of the $Aβ_{11\text{-}40/42}$ peptide while it enhanced generation of $Aβ_{40/42}$ peptide (Figure 4.3d).

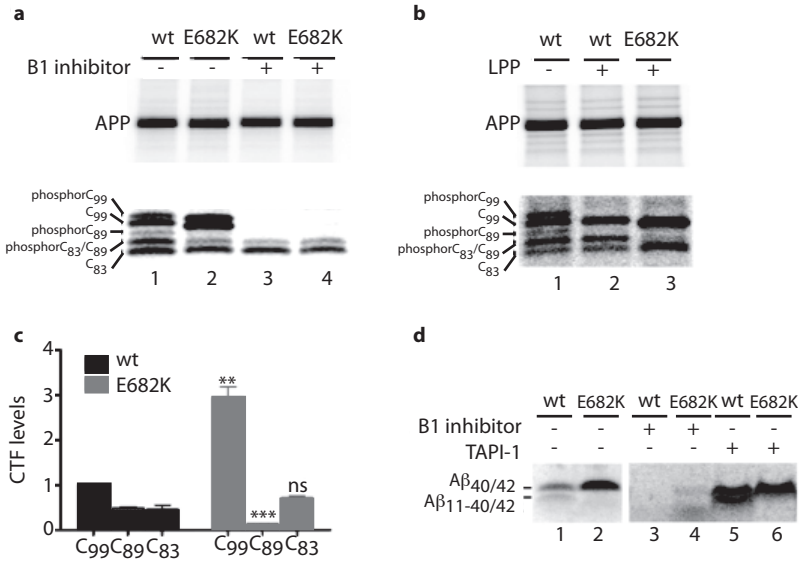

Figure 4.3 E682K mutation blocked β'-cleavage of human APP by BACE1 in cultured neurons.
Primary cultured neurons were transduced with SFV expressing WT or E682K mutant APP and were metabolically labelled with [^{35}S] cysteine/methionine for 4 h.
(a) Cell lysates were subjected to IP with antibody B63 specific to the C-terminus of APP. Eluates were separated on 16% Tricine gels and analysed by phosphorimager. Five species of CTFs were detected from neurons expressing WT APP (lane 1), including phosphorylated CTF_{99}, CTF_{99}, phosphorylated CTF_{89}, CTF_{89}/phosphorylated CTF_{83}, and CTF_{83} (from high to low MW). Neurons expressing E682K APP (lane 2) eliminated the generation of phosphorylated CTF_{89} and CTF_{89}. CTF_{89} can bemeasured by subtracting the density of the phosphorylated CTF_{83} band (lane 4) from the CTF_{89}/phosphorylated CTF_{83} band (lane 2). In lanes 3 and 4, neurons were treated with BACE1 inhibitor, therefore, only phosphorylated and non-phosphorylated CTF_{83} is observed.
(b) Immunoprecipitates from cell lysates were treated with LPP. Neurons expressing WT APP (lane 2) generated CTF_{99}, CTF_{89}, and CTF_{83}, while neurons expressing E682K APP (lane 3) largely eliminated the generation of CTF_{89}.
(c) Quantification of radioactive bands of CTFs. Statistics were analysed by comparing each CTF species generated from E682K APP with that generated from WT APP (**p<0.01; ***p<0.0001; ns, statistically not significant; mean±SEM; n=4).
(d) Conditioned media were subjected to IP with JRFcAβ40/42 antibodies specific to the C-terminus of $Aβ_{40}$ or $Aβ_{42}$, eluates were resolved on 10% Bis–Tris gels and analysed by phosphorimager. Neurons expressing WT APP generated $Aβ_{40/42}$ and $Aβ_{11–40/42}$ species (lane 1), and production of both peptides was eliminated after treatment with BACE1 inhibitor (lane 3), but was unaffected by the treatment with α-secretase inhibitor TAPI-1 (lane 5). E682K mutation enhanced the generation of $Aβ_{40/42}$ but eliminated the generation of $Aβ_{11–40/42}$ (lanes 2 and 6).

4.2.5 E682K MUTATION HAD LITTLE EFFECTS ON α-SECRETASE CLEAVAGE

The E682K mutation (Glu_{11} to Lys) is located close to the α-secretase cleavage site Lys_{17}. Therefore, we decided to investigate whether this mutation affected α-secretase cleavage as well. Typical α-secretase generated CTF_{83} which remained unchanged (Figure 4.3c), while total APP_S levels showed a slight increase probably due to the increase in $APP_{Sβ}$ (Figure 4.2a), suggesting that this mutation had little effects on the α-site cleavage of APP. In contrast, the 'Flemish' A692G mutation appeared to slightly

affect the generation of CTF_{α} (Figure 4.2a), as published before [13,15].

4.2.6 E682K mutation modulated γ-secretase activity

One interesting observation is that the E682K mutation increased the $A\beta_{42}$:$A\beta_{40}$ ratio in neuronal and CHO cell cultures. It is known that pathogenic mutations near the C-terminus of the Aβ sequence in APP can lead to increased generation of $A\beta_{42}$ by modulating the active sites of γ-secretase. A recent report has shown that the 'Flemish' A692G mutation, which is located in the middle of Aβ, has unexpectedly, in addition to its slight inhibitory effect on α-secretase processing [13,15], a quite pronounced effect on γ-secretase activity [17], suggesting that the interaction between γ-secretase and CTF_{99} may also occur at sites that are remote from the actual cleavage site in CTF_{99}. Therefore, we wondered whether the increase in the $A\beta_{42}$:$A\beta_{40}$ ratio caused by the E682K mutation might be caused by an additional effect on the modulation of γ-secretase. We transiently transfected CHO cells with WT or E682K mutant CTF_{99}. This APP fragment is the direct substrate of γ-secretase and its processing will, therefore, largely be determined by γ-secretase. The expression levels of both CTF_{99}WT and CTF_{99}E682K were investigated by Western blotting, no difference was observed. Conditioned media were analysed by Aβ ELISA (Figure 4.4). The E682K mutation generated the same amounts of $A\beta_{42}$ but significantly less $A\beta_{40}$, leading to an increased $A\beta_{42}$:$A\beta_{40}$ ratio. These data suggested that the E682K mutation affects also to a certain extent the $A\beta_{42}$:$A\beta_{40}$ ratio via modulation of γ-secretase.

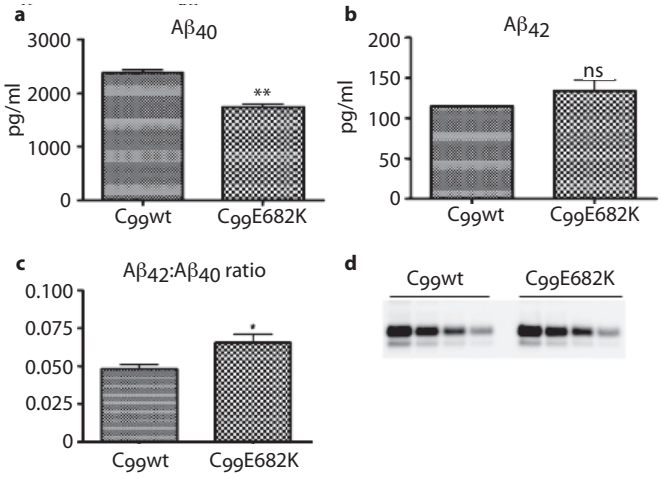

Figure 4.4 Effects of E682K mutant CTF_{99} on γ-secretase activity in cell-based assay. (a-c) CHO cells were transfected with WT or E682K mutant CTF_{99}, conditioned media were analysed by Aβ ELISAs (**p<0.01; *p<0.05; ns, statistically not significant; mean±SEM; n=3). (d) Western blotting analysis of CTF_{99} expression levels. Cell lysates containing either CTF_{99}WT or CTF_{99}E682K were loaded in a series of two times dilution.

4.2.7 Limited effects of E682K mutation on the aggregation kinetics and cytotoxicity of Aβ peptide

We studied the *in vitro* aggregation properties of synthetic Aβ peptide carrying the E682K mutation (E11K mutant Aβ). The aggregation kinetics of WT and mutant

Aβ42 peptide were monitored by a thioT fluorescence assay. Compared with WT $A\beta_{42}$ peptide, E11K mutant $A\beta_{42}$ showed a slight increase in the initial aggregation rate during the first 3 h of the aggregation process (Figure 4.5a); however, the overall change in aggregation kinetics was small. TEM images further underlined that the aggregation process of E11K mutant $A\beta_{42}$ was not significantly different from that of the WT $A\beta_{42}$ peptide (Figure 4.5b). In parallel, we also analysed the cytotoxicity of E11K mutant and WT $A\beta_{42}$, no significant difference was detected (Figure 4.5c).

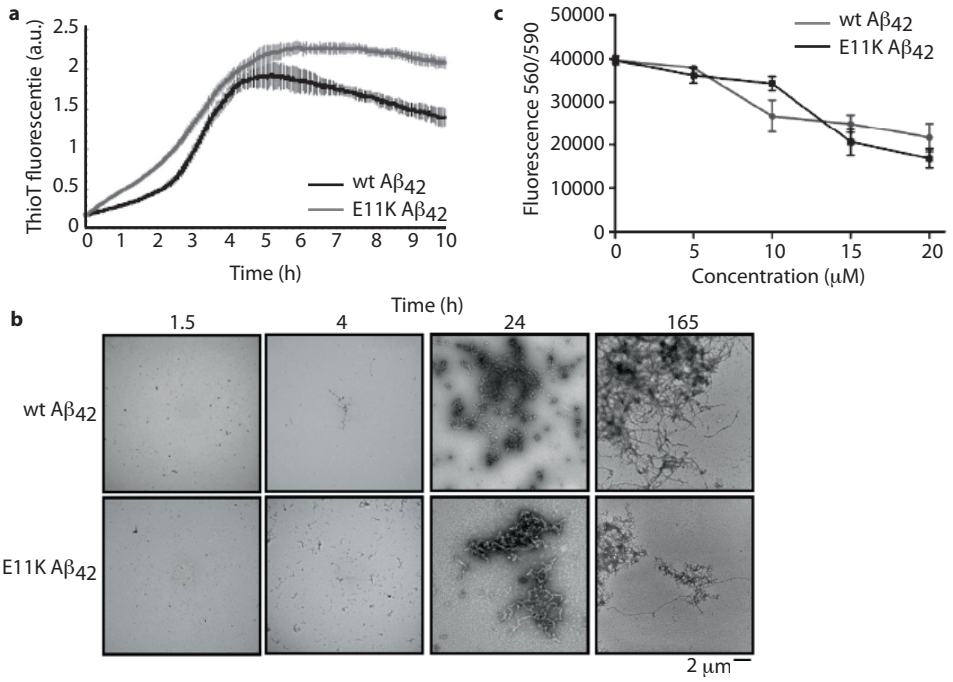

Figure 4.5 Biophysical determination of the aggregation kinetics of WT $A\beta_{42}$ and mutant E11K $A\beta_{42}$.
(a) ThioT fluorescence of aggregating WT $A\beta_{42}$ (black) and mutant $A\beta_{42}$ E11K (grey). Indicated are the error bars for each time point based on three measurements. The aggregation kinetics is not dramatically affected by the E11K mutation, apart from a small increase in the initial rate during the first 3 h of aggregation process.
(b) TEM images further underline that the aggregation process of $A\beta_{42}$ upon introduction of the E11K mutation is not significantly modified. After 1.5 h aggregates are observed which become larger upon further incubation.
(c) Neurotoxicity of wild type and E682K (E11K) $A\beta_{42}$ peptide. One week old mouse hippocampal neurons were treated with wild type or E682 (E11) $A\beta_{42}$ preaggregated for 1.5 hours, and cell viability was determined by cell titer blue assay after 72 hours treatment (mean ±SEM; n=6; the difference between wt and mutant $A\beta_{42}$ peptide is not statistically significant; $p>0.05$ as evaluated by unpaired two-tailed Student's t test).

4.3 Discussion

This work describes the identification and characterization of a novel APP mutation E682K from a single case of early onset Alzheimer disease. The index patient is a Belgian female; she was diagnosed as probable Alzheimer disease at the age of 49 years. Neuropsychological evaluation and CSF biomarkers ($A\beta_{42}$, total-tau and phospho-

tau) confirmed the diagnosis of Alzheimer disease. The patient's father developed late onset Alzheimer disease, while the brother is an asymptomatic mutation carrier currently at the age of 53, and there is no extended familial information. This raised the interesting question whether the identified mutation is a benign polymorphism or should be considered a genuine genetic risk factor for disease. The issue of rare genetic variants contributing moderate risk to disease is hotly debated in genetic research, as it is very difficult to detect such mutations while they are likely to contribute significantly to the total genetic risk for disease [23]. We hypothesized that the APP E682K mutation could have variable penetrance, which has previously also been proposed for disease causing mutations in *PS2*, carriers of which display a strong variation in age of onset [11] and decided to use functional assays to test whether the identified mutation could be considered as pathogenic or not.

Our analysis showed that this novel mutation increased full length Aβ release and also the Aβ42:Aβ40 ratio to similar extents as found with a previously well characterized disease associated APP A692G or 'Flemish' mutation. While the observed effects on Aβ processing suggest the possibility that this novel mutation is pathogenic, the genetic support is inconclusive. According to the criteria discussed by Guerreiro and coworkers [24], the APP E682K mutation was found in a single case of early onset Alzheimer disease. This mutation was absent from 940 healthy controls and affects Aβ generation. Although strictly spoken a second case with this mutation needs to be identified as independent confirmation [24], we propose that the accumulated evidence is clearly in favour to classify this mutation as probable pathogenic. Further follow up of the brother of the index case could yield final confirmation, but because of the study design, we are not allowed to contact the brother for further investigation. Therefore, we will have to wait for additional cases from other investigations in the future to classify this mutation as definitively pathogenic. Nevertheless, the functional analysis of this mutation provided an important and interesting novel insight in the biological significance of the β'-site processing of APP, which appeared quantitatively much more important for normal APP metabolism than previously thought.

Our data indicate indeed that processing at this site should be considered anti-amyloidogenic, counteracting partially the amyloidogenic β-secretase cleavage of APP. In agreement with this assumption, rodents, which tend to cleave their endogenous APP at the β'-site [15], do not spontaneously develop amyloid plaques. The functional significance of β'-site cleavage of APP by BACE1 has indeed been debated since a long time. On the one hand, it was previously suggested that this cleavage is a minor part of physiological APP processing [9]. Our new study now clarifies that this is not the case and that about one-fourth of the major APP CTF species is generated by this pathway under our experimental conditions. Second, it was reported that N-terminal truncation of Aβ may enhance the aggregation properties as well as the cytotoxic effects of Aβ [25] and that in sporadic Alzheimer disease cases, significant amounts of Aβ11–40/42 species were found in the plaques in the brain [19,26]. Therefore, β'-site cleavage was proposed to contribute to Alzheimer's pathogenesis [19,26]. However, our data argues for a protective role of β'-site cleavage, as blocking this cleavage disrupted the balance of APP processing by BACE1 leading to increased full length Aβ. The fact that the β'-site mutation E682K is associated with early onset Alzheimer disease speaks clearly in favour of this argument.

Of note, our data suggest additional effects of the E682K mutation on γ-secretase

activity as well. APP carrying the E682K mutation increased significantly the $A\beta_{42}$:$A\beta_{40}$ ratio in cell-based assays. This effect occurs at the γ-secretase level because expressing a CTF99 construct that bypasses the ectodomain shedding step needed for γ-secretase [27] led to a similar increase in this ratio. It has been recently reported that a substrate inhibitory domain (ASID) located at the middle of Aβ (residues 17–23) is modulating γ-secretase activity by binding to an allosteric site within the γ-secretase complex and that the 'Flemish' mutant CTF99 increased γ-secretase activity via disruption of this ASID [17]. The E682K mutation is located at the $A\beta_{11}$ site, which is not part of the previously delineated ASID, but had nevertheless a significant effect on $A\beta_{40}$ levels and little effects on $A\beta_{42}$ levels. We suggest the possibility that the interaction domain between γ-secretase and CTF99 is more extended than ASID and mutations such as the E682K mutation, as well as other similar substitutions, may be considered as new tools to investigate the possible allosteric modulation of γ-secretase by APP substrate.

The current data indicate that BACE1 cleaves APP at two distinct sites and that both are physiologically significant events in APP processing. So far, BACE1 is the most attractive drug target for Alzheimer disease treatments, and the evaluation of inhibitors under development for treatment of the disease focuses on the effect of blocking the β-site cleavage. This could be problematic because BACE1 inhibitors will also affect β'-site cleavage. Kinetic data showed that the BACE1 has a much higher enzymatic efficiency towards peptide containing the β-site than peptide containing the β'-site sequence [8], which raises a theoretical possibility that BACE1 inhibitors may have differential inhibition effects on the two distinct sites depending on the concentrations used. This could cause relative shifts from β'- to β-site cleavage, as observed with the current mutation. We thus propose that inhibitor drugs should be carefully monitored for their dose-effect on both BACE1 cleavage sites and to measure, therefore, the effects on $A\beta_{11–40/42}$ of any such drug when used in patients.

Finally it is likely that in the near future, increasing exon- and also exome-based sequencing efforts will increase the number of putative pathogenic mutations identified without further conclusive segregation-based evidence in a single family. Functional analysis of such mutations as demonstrated here will allow to determine the putative pathogenic nature of some of these mutations as more extensively discussed by Guerreiro and colleagues [24]. Such functional study may also be crucial to fill part of the existing gap in genetic research with regard to the postulated low frequency, moderate risk genetic loci that are now very difficult to identify and were called the 'dark matter of disease risk' [23,28].

4.4 Experimental procedures

4.4.1 Plasmids and site-directed mutagenesis

The plasmids pSG5-huAPP695, pSFV-huAPP695 [15] and pSG5-APPC99-FLAG [30] have been described previously. Mutagenesis was performed using the Quick-Change site-directed mutagenesis kit according to the manufacturer's instructions. Following primers were used to introduce the E682K mutation: 50-CCGACATGACTCAGGATATAAAGTTCATCATCAAAAATTGGTG-30 (forward) and 50-CACCAATTTTTGATGATGAACTTTATATCCTGAGTCATGTCGG-30 (reverse).

Antibodies and compounds

Rabbit polyclonal antibody B63 raised against the C-terminus of APP has been described previously [31]. mAbs JRFcAβ40/28, JRFcAβ42/26 recognizing the C-terminus of Aβ species terminating at 40 or 42, respectively, and JRFAβN/25 recognizing the N-terminal 1–7 amino acids of human Aβ were provided by Janssens Pharmaceutica. The following antibodies were purchased: mAb 22C11 recognizing the N-terminus of APP; $APP_{s}\beta$ polyclonal antibody recognizing the N-terminus to the β-secretase cleavage site of APP. Compound TAPI-1 was purchased from Calbiochem; BACE1 inhibitor compound 3 was kindly provided by Merck Research Laboratories.

4.4.2 Cell culture and transfection

CHO cells were maintained at 37 °C in a humidified, 5% CO_2 controlled atmosphere in DMEM supplemented with 10% foetal bovine serum (FBS). Transfections were performed using Fugene according to the manufacturer's instructions. When 80% confluence was reached, cells were transiently transfected with APP or C99 cDNA constructs. After 24 h, media were replaced with DMEM supplemented with 5% FBS and conditioned for 16-24 h and then collected for Aβ ELISA assays in the presence of complete protease inhibitor cocktail. Conditioned media were also analysed by Western blot for the detection of APPs, while cell lysates were analysed by Western blot for the detection of APP CTFs.

4.4.3 Neuronal cultures and Semliki Forest virus transfection

Primary cortical neurons were derived from E14 embryos from C57BL/6 mice, the preparation procedures have been described previously [32]. Briefly, the brains of E14 embryos were dissected in HBSS medium, trypsinized and plated on 6-cm dishes precoated with poly-L-lysine. Cultures were maintained in neurobasal medium supplemented with B27. A 5 μM cytosine arabinoside was added to prevent glial cell prolification. Semliki Forest viruses (SFV) were produced as described [32]. Three days cultured neurons were transduced with SFV expressing WT or mutant human APP695. After 1 h, media were replaced with normal culture media and left for 2 h. Media were refreshed and conditioned for ~6 h. Conditioned media were analysed by Aβ ELISA or Western blot for the detection of APPs, while cell lysates were analysed by Western blotting for the detection of APP CTFs.

4.4.4 Metabolic labelling and immunoprecipitation

Neuronal cultures were transduced with SFV for 1 h and left in normal culture medium for 2 h as described above. Media were then replaced with methionine-free MEM containing 100 μCi/μl [^{35}S] methionine. After 4 h metabolic labelling, supernatants were collected, cells were washed and lysed in DIP buffer (20mM Tris-HCl pH 7.4, 150mM NaCl, 1% Triton X-100, 1% sodium deoxycholate, 0.1% SDS) supplemented with complete protease inhibitors. Supernatants were immunoprecipitated using a combination of JRFcAβ40 and JRFcAβ42 antibodies and incubated with protein G-Sepharose at 4 °C overnight. The immunoprecipitants were resolved on 10% NuPAGE gels running with MES buffer. Cell extracts were immunoprecipitated using APP C-terminal antibody B63. The immunoprecipitants were resolved on 16% Tricine gels running with Tricine-SDS buffer. The intensity of the radioactive bands was

quantified using a phosphorimager and Aida Image Analyzer v.4.22 software.

4.4.5 Aβ ELISA

The concentration of Aβ in conditioned medium was measured by end-specific ELISAs. JRFcAβ40/28 or JRFcAβ42/26 was used as capturing antibodies for Aβ species terminating at 40 or 42, respectively. HRP-conjugated JRFAβN/25 recognizing the N-terminal 1–7 amino acids of human Aβ was used as detecting antibody for full length Aβ. The affinity of JRFAβN/25 for E11K mutant Aβ peptide was not different from its affinity for WT Aβ peptide. Plates were coated with 60 µl capturing antibodies at 2 µg ml^{-1} at 4 °C overnight in coating buffer (10mM Tris-HCl, 10mM NaCl, 10mM NaN3, pH 8.5). The next day, plates were rinsed once in phosphate buffer saline (PBS) and blocked with blocking buffer (0.1% casein in PBS, pH7.4) either at 4 °C overnight or at room temperature for 4 h. Plates were then rinsed twice with PBS. Thirty µl of detecting antibody diluted in blocking buffer was first added to each well, followed by adding 30 µl conditioned medium diluted in blocking buffer. Plates were incubated at 4 °C overnight, and rinsed and developed the next day using 60 µl mixture of 3,3',5,5'-tetramethylbenzidine (TMB) solution. The reaction was stopped by addition of 60 µl of 2N H_2SO_4. Plates were read immediately at 450nm.

4.4.6 Preparation of Aβ peptide

Aβ peptide (JPT Peptide Technologies GmbH) was dissolved using the procedure described in chapter 2. Briefly, Aβ was dissolved in HFIP which was evaporated using a gentle stream of argon gas and the peptide film was resolved using DMSO. The peptide was separated from DMSO with a 5 ml HiTrap^{TM} Desalting column and eluted into a 50mM Tris, 1mM EDTA buffer, pH 7.5. The peptide concentration was measured using Bradford assay. The samples were kept on ice until experiments started, with a maximum lag time of 20 min.

4.4.7 Thioflavin T fluorescence

Aβ protein concentrations were normalized to 25 µM by further dilution using 50mM Tris, 1mM EDTA containing buffer and a final concentration of 12 µM ThioT was added. The fibrillation kinetics were followed *in situ* using a Fluostar OPTIMA fluorescence plate reader at an excitation wavelength of 440nm and an emission wavelength of 480 nm. Readings were recorded in triplicate every 10 min for a period of 10 h.

4.4.8 Transmission electron microscopy

Aliquots (5 µl) of the Aβ preparation were adsorbed to carbon-coated FormVar film on 400-mesh copper grids for 1 min. The grids were blotted, washed twice in droplets of Milli-Q water, and stained with 1% w/v uranyl acetate. Samples were studied with a JEOL JEM-1400 microscope at 80 kV.

4.4.9 Cell viability assay

Mouse primary hippocampal neurons were grown in neurobasal medium for 1 week, and then were treated with different concentrations of $Aβ_{42}$ (wt or mutant) pre-aggregated for 1.5 h. After 72 h treatment, 10 µl Cell-Titer-Blue dye (Promega) was added to 200 µl of the growth culture medium on the cells. After 3 h, the fluorescence

intensity of the samples was measured at an excitation wavelength of 560 nm and an emission wavelength of 590 nm.

4.4.10 Statistical analyses

Statistical significance was determined by the Student's t-test.

AUTHOR CONTRIBUTIONS

LZ analysed the effects of APP mutants in Aβ generation and wrote the manuscript. NB and KS performed the genetic analysis. MM suggested experiments and contributed to Aβ ELISA measurements. KVL, PVD, DD and FVL analysed patient's brain image and blood samples. AV, KB, and IB characterized the aggregation property and cytotoxicity of mutant Aβ peptide *in vitro*. CVB and RV identified the Alzheimer disease case and the APP mutation. BDS designed the study and wrote the manuscript.

4.5 References

[1] Hussain I, Powell D, Howlett D, Tew D, Meek T, Chapman C, Gloger I, Murphy K, Southan C, Ryan D, Smith T, Simmons D, Walsh F, Dingwall C, Christie G (1999). Identification of a novel aspartic protease (Asp 2) as β-secretase. *Mol. Cell Neurosci.*, 14:419-427.

[2] Sinha S, Anderson J, Barbour R, Basi G, Caccavello R, Davis D, Doan M, Dovey H, Frigon N, Hong J, Jacobson-Croak K, Jewett N, Keim P, Knops J, Lieberburg I, Power M, Tan H, Tatsuno G, Tung J, Schenk D, Seubert P, Suomensaari S, Wang S, Walker D, Zhao J, McConlogue L, John V (1999). Purification and cloning of amyloid precursor protein β-secretase from human brain. *Nature,* 402:537-540.

[3] Vassar R, Bennett B, Babu-Khan S, Kahn S, Mendiaz E, Denis P, Teplow D, Ross S, Amarante P, Loeloff R, Luo Y, Fisher S, Fuller J, Edenson S, Lile J, Jarosinski M, Biere A, Curran E, Burgess T, Louis J-C, Collins F, Treanor J, Rogers G, Citron M (1999). β-Secretase cleavage of Alzheimer's amyloid precursor protein by the transmembrane aspartic protease BACE. *Science,* 286:735-741.

[4] Yan R, Bienkowski M, Shuck M, Miao H, Tory M, Pauley A, Brashier J, Stratman N, Mathews W, Buhl A, Carter D, Tomasselli A, Parodi L, Heinrikson R, Gurney M (1999). Membrane-anchored aspartyl protease with Alzheimer's disease β-secretase activity. *Nature,* 402:533-537.

[5] Lin X, Koelsch G, Wu S, Downs D, Dashti A, Tang J (2000). Human aspartic protease memapsin 2 cleaves the β-secretase site of β-amyloid precursor protein. *Proc. Natl. Acad. Sci. USA*, 97:1456-1460.

[6] De Strooper B (2003) Aph-1, Pen-2, and nicastrin with presenilin generate an active γ-secretase complex. *Neuron,* 38:9-12.

[7] Takami M, Nagashima Y, Sano Y, Ishihara S, Morishima-Kawashima Y, Funamoto S, Ihara Y (2009). γ-Secretase: successive tripeptide and tetrapeptide release from the transmembrane domain of β-carboxyl terminal fragment. *J. Neurosci.*, 29:13042-13052.

[8] Yang H, Chai X, Mosior M, Kohn W, Boggs L, Erickson J, McClure D, Yeh W-K, Zhang L, Gonzalez-DeWhitt P, Mayer J, Martin J, Hu J, Chen S, Bueno A, Little S, McCarthy J, May P (2004). Biochemical and kinetic characterization of BACE1: investigation into the putative species-specificity for β- and β'-cleavage sites by human and murine BACE1. *J. Neurochem.*, 91:1249-1259.

[9] Creemers J, Ines Dominguez D, Plets E, Serneels L, Taylor N, Multhaup G, Craessaerts K, Annaert W, De Strooper B (2001). Processing of β-secretase by furin and other members of the proprotein convertase family. *J. Biol. Chem.*, 276:4211-4217.

[10] Qahwash I, He W, Tomasselli A, Kletzien R, Yan R (2004). Processing amyloid precursor protein at the β-site requires proper orientation to be accessed by BACE1. *J. Biol. Chem.*, 279:39010-39016.

[11] Sherrington R, Froelich S, Sorbi S, Campion D, Chi H, Rogaeva E, Levesque G, Rogaev E, Lin C, Liang Y, Ikeda M, Mar L, Brice A, Agid Y, Percy M, Clerget-Darpoux F, Piacentini S, Marcon G, Nacmias B, Amaducci L, Frebourg T, Lannfelt L, Rommens J, St George-Hyslop P (1996). Alzheimer's disease associated with mutations in presenilin 2 is rare and variably penetrant. *Hum. Mol. Genet.*, 5:985-988.

[12] Hendriks L, van Duijn C, Cras P, Cruts M, Van Hul W, van Harskamp F, Warren A, McInnis M, Antonarakis S, Martin J, Hofman A, Van Broeckhoven C (1992). Presenile dementia and cerebral haemorrhage linked to a mutation at codon 692 of the β-amyloid precursor protein gene. *Nat. Genet.*, 1:218-221.

[13] Haass C, Hung A, Selkoe D, Teplow D (1994). Mutations associated with a locus for familial Alzheimer's disease result in alternative processing of amyloid β-protein precursor. *J. Biol. Chem.*, 269:17741-17748.

[14] Suzuki N, Cheung T, Cai X, Odaka A, Otvos L, Eckman C, Golde T, Younkin S (1994). An increased percentage of long amyloid β protein secreted by familial amyloid β protein precursor (β APP717) mutants. *Science* 264:1336-1340.

[15] De Strooper B, Simons M, Multhaup G, Van Leuven F, Beyreuther K, Dotti C (1995). Production of intracellular amyloid-containing fragments in hippocampal neurons expressing human amyloid precursor protein and protection against amyloidogenesis by subtle amino acid substitutions in the rodent sequence. *EMBO J.*, 14:4932-4938.

[16] Nilsberth C, Westlind-Danielsson A, Eckman C, Condron M, Axelman K, Forsell C, Stenh C, Luthman J, Teplow D, Younkin S, Näslund J, Lannfelt L (2001). The 'Arctic' APP mutation (E693G) causes Alzheimer's disease by enhanced Aβ protofibril formation. *Nat. Neurosci.*, 4:887-893.

[17] Tian Y, Bassit B, Chau D, Li Y (2010). An APP inhibitory domain containing the Flemish mutation residue modulates γ-secretase activity for Aβ production. *Nat. Struct. Mol. Biol.*, 17:151-158.

[18] Turner R, Koelsch G, Hong L, Castanheira P, Ermolieff J, Ghosh A, Tang J (2001). Subsite specificity

of memapsin 2 (β-secretase): implications for inhibitor design. *Biochemistry,* 40:10001-10006.

[19] Huse J, Liu K, Pijak D, Carlin D, Lee V, Doms R (2002). β-Secretase processing in the trans-golgi network preferentially generates truncated amyloid species that accumulate in Alzheimer's disease brain. *J. Biol. Chem.*, 277:16278-16284.

[20] Liu K, Doms R, Lee V (2002). Glu11 site cleavage and N-terminally truncated Aβ production upon BACE overexpression. *Biochemistry,* 41:3128-3136.

[21] Kimberly W, Zheng J, Town T, Flavell R, Selkoe D (2005). Physiological regulation of the β-amyloid precursor protein signaling domain by c-Jun N-terminal kinase JNK3 during neuronal differentiation. *J. Neurosci.*, 25:5533-5543.

[22] Hoey S, Williams R, Perkinton M (2009). Synaptic NMDA receptor activation stimulates α-secretase amyloid precursor protein processing and inhibits amyloid-β production. *J. Neurosci.*, 29:4442-4460.

[23] Singleton A, Hardy J, Traynor B, Houlden H (2010). Towards a complete resolution of the genetic architecture of disease. *Trends Genet.*, 26:438- 442.

[24] Guerreiro R, Baquero M, Blesa R, Boada M, Bras J, Bullido M, Calado A, Crook R, Ferreira C, Frank A, Gomez-Isla T, Hernandez I, Lleo A, Machado A, Martinez-Lage P, Masdeu J, Molina-Porcel L, Molinuevo J, Pastor P, Perez-Tur J, Relvas R, Oliveira C, Ribeiro M, Rogaeva E, Sa A, Samaranch L, Sanchez-Valle R, Santana I, Tarraga L, Valdivieso F, Singleton A, Hardy J, Clarimon J (2010). Genetic screening of Alzheimer's disease genes in Iberian and African samples yields novel mutations in presenilins and APP. *Neurobiol. Aging*, 31:725-731.

[25] Demeester N, Mertens C, Caster H, Goethals M, Vandekerckhove J, Rosseneu M, Labeur C (2001). Comparison of the aggregation properties, secondary structure and apoptotic effects of wild-type, Flemish and Dutch N-terminally truncated amyloid β peptides. *Eur. J. Neurosci.*, 13:2015-2024.

[26] Liu K, Solano I, Mann D, Lemere C, Mercken M, Trojanowski J, Lee V (2006). Characterization of Aβ11-40/42 peptide deposition in Alzheimer's disease and young Down's syndrome brains: implication of N-terminally truncated Aβ species in the pathogenesis of Alzheimer's disease. *Acta Neuropathol.,* 112:163-174.

[27] Lichtenthaler S, Multhaup G, Masters C, Beyreuther K (1999). A novel substrate for analyzing Alzheimer's disease γ-secretase. *FEBS Lett.,* 453:288-292.

[28] Manolio T, Collins F, Cox N, Goldstein D, Hindorff L, Hunter D, McCarthy M, Ramos E, Cardon L, Chakravarti A, Cho J, Guttmacher A, Kong A, Kruglyak L, Mardis E, Rotimi C, Slatkin M, Valle D, Whittemore A, Boehnke M, Clark A, Eichler E, Gibson G, Haines J, Mackay T, McCarroll S, Visscher P (2009). Finding the missing heritability of complex diseases. *Nature* 461:747-753.

[29] Weckx S, Del-Favero J, Rademakers R, Claes L, Cruts M, De Jonghe P, Van Broeckhoven C, De Rijk P (2005). NovoSNP, a novel computational tool for sequence variation discovery. *Genome Res.*, 15:436-442.

[30] Bentahir M, Nyabi O, Verhamme J, Tolia A, Horré K, Wiltfang J, Esselmann H, De Strooper B (2006). Presenilin clinical mutations can affect γ-secretase activity by different mechanisms. *J. Neurochem.*, 96:732-742.

[31] Annaert W, Esselens C, Baert V, Boeve C, Snellings G, Cupers P, Craessaerts K, De Strooper B (2001). Interaction with telencephalin and the amyloid precursor protein predicts a ring structure for presenilins. *Neuron,* 32:579-589.

[32] Annaert W, Levesque L, Craessaert K, Dierinck L, Snellings G, Westaway D, George-Hyslop P, Cordell B, Fraser P, De Strooper B (1999). Presenilin 1 controls γ-secretase processing of amyloid precursor protein in pre-golgi compartments of hippocampal neurons. *J. Cell Biol.*, 147:277-294.

5

Neurotoxicity of Alzheimer disease Aβ peptides is induced by small changes in the Aβ42 to Aβ40 ratio.

The amyloid peptides Aβ40 and Aβ42 involved in Alzheimer disease are thought to contribute differentially to the disease process. Although Aβ42 seems more pathogenic than Aβ40, the reason for this is not well understood. The results described in this chapter show that small alterations in the Aβ42:Aβ40 ratio dramatically affect the biophysical and biological properties of the Aβ mixtures reflected in their aggregation kinetics, the morphology of the resulting amyloid fibrils and synaptic function tested *in vitro* and *in vivo*. A minor increase in the Aβ42:Aβ40 ratio stabilizes toxic oligomeric species with intermediate conformations. The initial toxic impact of these Aβ species is synaptic in nature, but this can spread into the cells leading to neuronal cell death. The fact that the relative ratio of Aβ peptides is more crucial than the absolute amounts of peptides for the induction of neurotoxic conformations has important implications for anti-amyloid therapy. Our work also suggests the dynamic nature of the equilibrium between toxic and non-toxic intermediates.

The results described in this chapter have been published in:
Kuperstein I, Broersen K, Benilova I, Rozenski J, Jonckheere W, Debulpaep M, Vandersteen A, Segers-Nolten I, van der Werf K, Subramaniam V, Braeken D, Callewaert G, Bartic C, D'Hooge R, Martins I, Rousseau F, Schymkowitz J, and De Strooper B (2010). *EMBO J.*, 29:3408-3420.

5.1 Introduction

$A\beta_{40}$ is the major species recovered from serum, cerebrospinal fluid and cell culture supernatants [1,2]. Interest in a second peptide, $A\beta_{42}$, which is detected at about 10-fold lower levels, was strongly stimulated by the observation that familial Alzheimer disesase causing mutations increased the relative production of $A\beta_{42}$ relative to $A\beta_{40}$ [2-4]. We reported earlier [5] that clinical mutations in presenilin mainly affect the spectrum of the Aβ peptides generated by γ-secretase. As patients with such mutations present an early and aggressive form of the disease, it seems then logical to propose that the absolute quantity of Aβ peptides produced in the brain might be less important than the quality of the Aβ peptides (reflected in a changed $A\beta_{42}$ to $A\beta_{40}$ ratio) for the generation of elusive toxic Aβ species [6]. The implication of such hypothesis for current efforts in drug development is important because lowering the absolute amounts of Aβ in patients would then be less crucial than the restoration of the correct ratios of Aβ peptides. Earlier studies have already provided evidence that $A\beta_{40}$ and $A\beta_{42}$ affect each other's aggregation rates and toxic effects [7-13]. Generally, it is found that $A\beta_{42}$ has fast aggregation kinetics, which can be inhibited by $A\beta_{40}$ in a concentration-dependent manner. Interesting *in vivo* studies have further shown that increased levels of $A\beta_{40}$ peptides in the brain actually might have a protective effect [10,11].

More recently, the discrepancy between the total burden of Aβ peptide deposited into plaques in the brain and the degree of neurodegeneration in the patients has been confirmed with modern amyloid imaging techniques [14,15]. Obviously, it is possible that these patients are in a preclinical phase of the disease, and follow-up studies are underway to investigate this. Nevertheless, these observations support the concept that the amyloid fibrils are biologically largely inert and that not all conformations of Aβ are equally toxic [16,17]. A series of intermediate soluble aggregates of Aβ peptides have recently been identified [18,19]. The mechanism of their neurotoxic activity remains not only subject of intense investigation, but also the precise conformation(s) of the toxic species remains uncertain [20,21]. Various oligomeric conformations were reported to exert toxicity to various extent, affect synapse function and even impair memory formation in mice [16-18,22-26]. It should be noted that in many of the publications, the identified toxic species are presented as stable, defined structures, although it seems logical to assume that their assembly and disassembly is a dynamic and continuous process, at least in the initial stages. Hence the alternative possibility that toxicity is present over a series of conformers or sizes should not be disregarded [16,21,27]. The question is thus how biophysical parameters influence this process *in vivo* and affect the relative distribution of Aβ species over toxic and non-toxic conformations over time. Given the complexity of the biophysical environment in which Aβ aggregation occurs *in vivo*, such question is extremely difficult to address. Nevertheless, it is possible to analyse the dynamic features of this process in simplified and controlled conditions *in vitro*, and to evaluate the effect of the relative concentrations of $A\beta_{40}$ and $A\beta_{42}$ to the generation of neurotoxic species over time.

We hypothesized here that the early onset of Alzheimer disease by APP and/or presenilin mutations that increase the $A\beta_{42}$:$A\beta_{40}$ ratios can be explained by interactions between $A\beta_{40}$ and $A\beta_{42}$, which provide stability to intermediate, neurotoxic species. Using biophysical methods and a novel cellular assay we analysed the

establishment of neurotoxicity over time in different Aβ mixtures. We found that very minor changes in the relative amount of Aβ42 versus Aβ40 has dramatic effects on the dynamic behaviour of toxic Aβ species. Our findings provide an important biological addition to the original 'Aβ42 seeding hypothesis' [28], which focused on amyloid fibril formation. These dynamic oligomeric species exhibit initial synaptotoxicity and cause later neurotoxicity in primary hippocampal neurons and affect memory formation in mice, underlining their potential importance for the understanding of Alzheimer disease.

5.2 Result

As the objective of this study was to investigate how Aβ40 and Aβ42 affect each others' biophysical and biological properties, it was important to prepare a pre-aggregate-free Aβ solution and to validate the mixtures using mass spectrometry (see appendix B) and anti-Aβ40- and anti-Aβ42-specific antibodies (Figure 5.1). Peptides were dissolved in HFIP and mixtures of Aβ were prepared. Further handling of the solutions was according to the procedure described in Chapter 2.

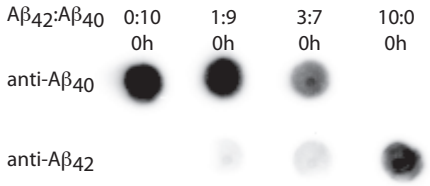

Figure 5.1 Preparation of Aβ ratios.
Dot blot confirming the presence of both Aβ40 and Aβ42 in ratios by employing carboxy-terminus specific antibodies

5.2.1 Aggregation rate of Aβ peptides is strongly influenced by the ratio Aβ42:Aβ40

Aβ peptide was incubated at a concentration of 50 μM in 50 mM Tris-HCl, 1 mM EDTA, pH 7.5 at 25 °C. The aggregation process of a range of Aβ42:Aβ40 ratios (10:0 to 0:10) tested by thioT fluorescence yielded a typical sigmoidal curve as generally observed for aggregating proteins and peptides (Figure 5.2a) [29]. Both the length of the lag phase and the rate of aggregation were affected by the ratio of Aβ42:Aβ40 (Figure 5.2 b,c). The lag phase for pure Aβ40 was ~2.5 h (±0.3 h). Addition of 10% Aβ42 (Aβ42:Aβ40 1:9) resulted in a small, but reproducible increase in the lag phase (~2.9±0.3 h) (Figure 5.2B). A further increase in the Aβ42:Aβ40 ratio decreased paradoxically the length of the lag phase to ~0.5±0.01 h. From a ratio of 3:7 onwards, no difference was observed compared with Aβ42 alone. The elongation rate was fastest for pure Aβ40 and was slowed down by addition of Aβ42 (Figure 5.2c). Remarkably, judging from the lag phase of aggregation, the 1:9 and the 3:7 ratio showed two opposite ends of the spectrum (Figure 5.2b). These ratios, in addition to 10:0 and 0:10 were selected for our further studies. The choice for 3:7 can be also rationalized as it reflects roughly the ratio of Aβ42 and Aβ40 in patients with familial Alzheimer disease [2,4,30,31]. Thus, both time and the Aβ42:Aβ40 ratios are two important parameters when considering the biophysical properties of Aβ, and we decided to investigate how these parameters determine Aβ-oligomer toxicity. We describe in the rest of the paper the different Aβ mixtures as an Aβ42:Aβ40 ratio,

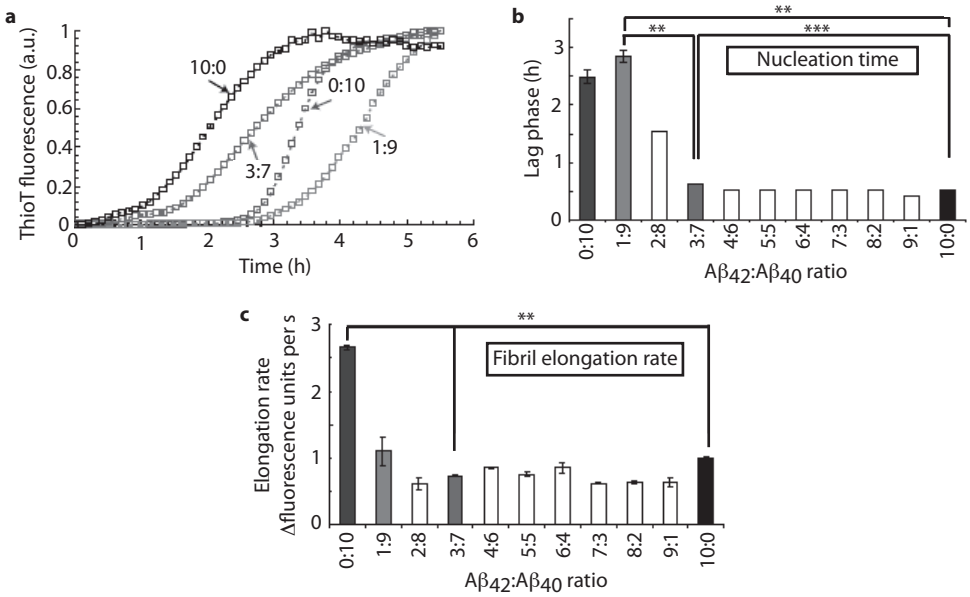

Figure 5.2 $A\beta_{42}$ determines the kinetics of Aβ aggregation.
(a) Aggregation kinetics of 50 μM Aβ ratios in 50mM Tris, 1mM EDTA at 25 °C for 6 h by thioT assay shows how the ratio of $A\beta_{42}$:$A\beta_{40}$ (e.g. 3:7) influences the aggregation kinetics. (b) Quantitative analysis of lag phase, showing the time (hours) of the initial part of curves as in (a), during which no increase in thioT fluorescence signal is detected using different $A\beta_{42}$:$A\beta_{40}$ ratios as indicated.
(c) Quantitative analysis of the elongation rate, derived from (a) as rate of fluorescence change, which is the slope of the linear phase of exponential growth in (a), using different Aβ ratios as indicated.
Numbers are averages of three independent experiments. Error flags indicate s.d. calculated over the three independent experiments. Statistical significance of the results was established by p-values using paired two-tailed t-tests, and only shown for the four ratios further studied in the text. Statistical significance levels were in (b,c): *p<0.005, **p<0.001, ***p<0.0001. p-value of $A\beta_{40}$ (0:10) and (1:9)=0.09, and p-value of $A\beta_{40}$ (0:10) and (1:9)=0.0058 in panels (b) and (c), respectively.

incubated for an indicated time at an Aβ concentration of 100 μM in 50 mM Tris-HCl, 1 mM EDTA, pH 7.5 at 25 °C. Thus, (3:7, 2 h) means a ratio of three $A\beta_{42}$ versus seven $A\beta_{40}$ peptides incubated for 2 h under given buffer conditions before addition to the cell culture. Final concentration of Aβ in cell culture is in most experiments 1 μM apart from a few in which 10 μM was used as indicated. On the basis of our further experiments, it appeared that at any time point only a small fraction of the peptides is in a toxic active conformation.

5.2.2 The $A\beta_{42}$:$A\beta_{40}$ ratio is a driver of acute synaptic alterations

One problem with Aβ toxicity assays is the delay between the actual preparation of the oligomer samples used for the biophysical analysis and the moment when the biological read out becomes available to assess the neurotoxicity. We, therefore, sought to set up an assay that allows verifying biological effects of Aβ preparations within the time frame of the biophysical experiments. We plated mouse hippocampal neurons on microelectrode array (MEA)-based chips (Figure 5.3a) [32] and recorded

spontaneous firing rates in the neuronal networks before and after treatment with Aβ mixtures at a final concentration of 1 μM. Representative traces of responses of cultures treated with different Aβ mixtures are displayed in Figure 5.3b. Interestingly, treatment with pure $A\beta_{40}$ mixtures (0:10, 2h) appeared to enhance synaptic activity measured as spontaneous firing rate, whereas (1:9, 2 h) mixtures had no effect on spontaneous synaptic activity (Figure 5.3 b,c). In contrast, $A\beta_{42}$ alone (10:0, 2 h) or with $A\beta_{40}$ (3:7, 2 h) readily suppressed spontaneous neuronal activity within 40 min after addition of the peptides (Figure 5.3 b,c). As a control of the oligomeric species status during the course of the recording, we followed changes in fluorescent thioT emission over 40 min of Aβ mixtures at 1 μM in neuronal culture medium at 37 °C, which mimics the conditions of the cell culture experiments (Figure 5.3d). The Aβ mixtures appeared stable over the time frame of the experiment at least as far as it concerns thioT incorporation. We next assayed how different $A\beta_{42}$:$A\beta_{40}$ ratios evolve over time with regard to synaptotoxic properties. $A\beta_{42}$:$A\beta_{40}$ ratio mixtures were incubated for 0, 1.5, 4, 6 and 20 h before addition to the cultures. Synaptic firing rates were recorded for 40 min as above using MEA. Figure 5.3e shows that synaptic effects were little after treatment of the cells with mixtures of Aβ shortly after dissolving them in buffer (0 h, Figure 5.3e). Toxicity was, however, already significantly high after 1.5 h of aggregation in the (3:7, 1.5 h) and the (10:0, 1.5 h) mixtures. The synaptotoxic potential in the (3:7) and (10:0) ratios remained stable up to 20 h (Figure 5.3e). Remarkably, (1:9) or (0:10) ratios did not result in major synaptic effects at any incubation point (Figure 5.3e). To validate the findings, we performed double immunostaining for the synaptic marker synaptophysin and Aβ oligomers using the A11 antibody [20]. Figure 5.3f shows that Aβ (3:7) and (10:0) mainly co-localized with the synaptic marker, whereas staining was not observed with the (1:9) and (0:10) ratio. Extensive washing of the neurons to remove Aβ species did not interfere with consecutive A11 staining, indicating the rather irreversible nature of the binding of these synaptic active species to the neurons (not shown).

To prove Aβ specificity of the observed effects, we pre-incubated cells with anti-oligomer A11 or anti-Aβ antibody 6E10 before treatment with Aβ (10:0, 2 h) ratio. The alterations in the synaptic activity by toxic intermediates are indeed Aβ specific, as cells pre-incubated with antibodies are no longer susceptible to the neurotoxic effects (Figure 5.3g). We also further explored the reversibility of these Aβ effects on synaptic function. Removal of Aβ (3:7, 2 h) and Aβ (10:0, 2 h) after 40 min of incubation on the neuronal cultures by extensive washes with medium did not restore synaptic activity over the next 6h in line with the immunofluorescence data (Figure 5.3h). However, 18 h after the wash out of Aβ (3:7, 2 h) and Aβ (10:0, 2 h), we found partial synaptic activity recovery at some electrodes, although the profile of the action potentials (AP) displayed a slightly different character than the ones recorded before the treatment (Figure 5.3h). Given the long time needed for some recovery and the fact that the profiles after recovery were different from those before, it seems likely that this partial restoration of neuronal activity is due to the generation of novel synaptic contacts rather than recovery of existing synapses.

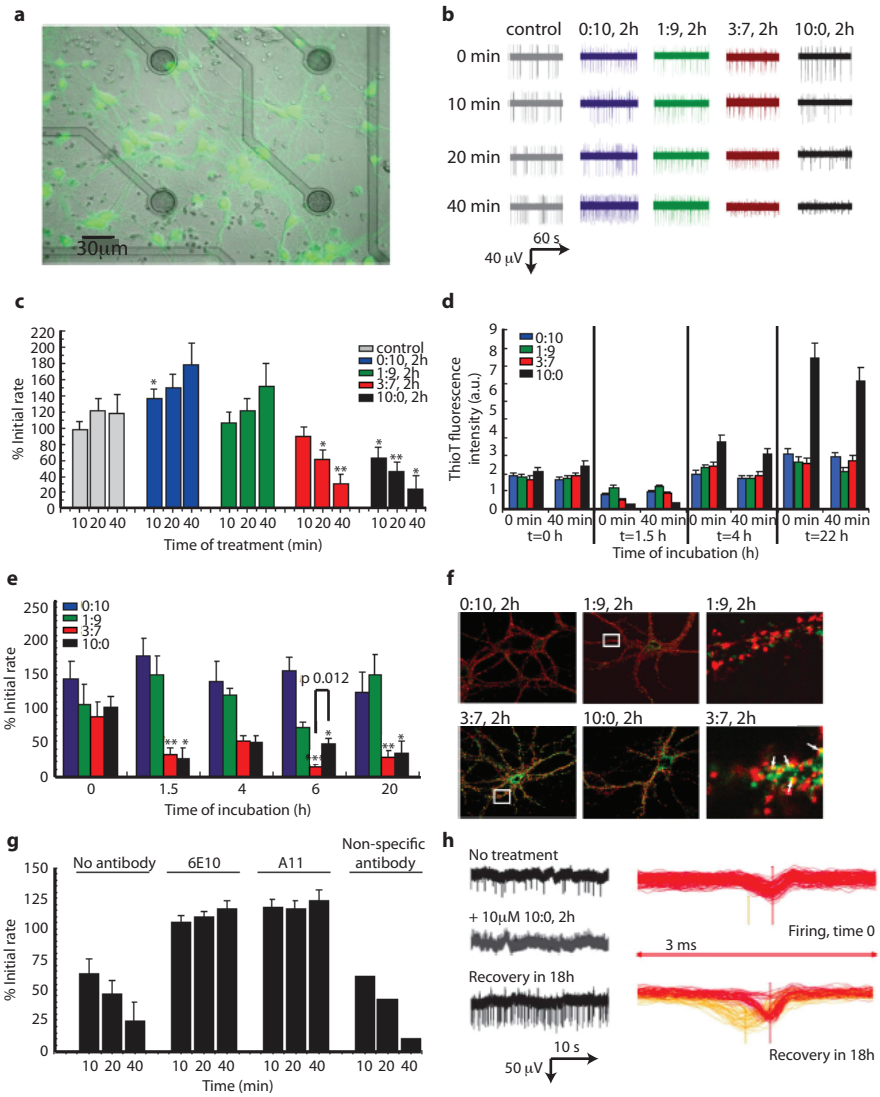

Figure 5.3 Mixed Aβ oligomers result in a rapid synaptotoxic response in primary neurons. (a) Neurons stained with Fluo-4 were cultured 8 days *in vitro* (DIV) on the MEA chip. (b) Firing pattern of neurons from representative electrodes at 0, 10, 20 and 40 min treatment with different Aβ ratios prepared as indicated. Note the significantly decreased firing rate and amplitude for $A\beta_{42}$:$A\beta_{40}$ ratios 10:0 and 3:7 after 20 min of treatment. (c) Spontaneous electrical synaptic activity recordings of hippocampal neurons during 40 min of treatment with 1 μM Aβ ratios incubated for 2 h prior to the addition to cells. Values are % of initial firing rate±s.e.m. of 3–5 independent experiments. Statistical significance (unpaired two-tailed t-test) of the data versus control is indicated by *p<0.01 or **p<0.001 in the figure. Notice that a strong reduction in spontaneous synaptic firing versus correspondent control (buffer-treated chips) can be observed after 20 and 40 min in the medium of the 3:7 and 10:0 $A\beta_{42}$:$A\beta_{40}$ ratios. (d) Oligomers dissolved in culture medium remain stable with regard to thioT tinctorial properties for at least 40 min. Aβ ratios were prepared and at specific time intervals of incubation, that is 0, 1.5, 4 and 22 h, Aβ aliquots were removed and diluted to 1 μM in

cell culture medium containing thioT. The stability of the aggregates at 37 °C in cell culture medium was deduced from the stability of the thioT signal over 40 min. Blue bars represent different $A\beta_{42}$:$A\beta_{40}$ ratios as indicated in the figure. Compare signals directly upon dilution into cell culture medium ('0 min') at 37 °C with signals obtained after 40 min incubation at 37 °C ('40 min'). Values are averages of three experiments.
(e) Different ratios of Aβ peptides were generated and added to neuronal cultures diluted to a final concentration of 1 μM, either immediately (0 h) or after 1.5 h; 4 h, 6 h or 20 h of incubation. Synaptotoxicity was measured by recording a decreased rate of firing 40 min after adding the Aβ mixtures to the neurons. Statistical significance levels determined as a function of s.e.m.: ***p<0.0001, n=6 chips, **p<0.001, n=3 chips, *p<0.01, n=3 chips, difference between 6 h ratio (3:7) and (10:0): *p<0.012 (unpaired two-tailed t-test).
(f) Synaptic localization of mixed Aβ oligomers. Fluorescence microscopy images of hippocampal neurons stained for synaptophysin (red) and Aβ oligomers (A11 antibody) (green) after 1 h treatment with 1 μM of the indicated Aβ ratios, incubated for 2 h prior the addition to cells. Right panel: magnification of selected region stained with synaptophysin (red) and Aβ oligomers (A11 antibody, green). Oligomeric Aβ co-localizes with synapses.
(g) Rescue of spontaneous electrical synaptic activity after the treatment with ratio (10:0, 2 h) in the presence or absence of anti-oligomer A11 or anti-Aβ 6E10 antibody, final concentration 10 μg ml^{-1}. Values are % of initial firing rate±s.e.m., of three independent experiments, except for the control with non-specific antibody, which was performed only once.
(h) Example of firing recovery after treatment with 10 μM (10:0, 2 h). Raw data streams are shown in black, and corresponding spike shapes are in red. The treatment completely inhibited spontaneous activity in 6 min. Then the medium was refreshed, and signals were measured after overnight recovery (18 h). Note partial restoration of initial firing profile along with appearance of another spike population endowed with slightly different waveform and amplitude. Spike sorting is performed in MC Rack software.

In an alternative paradigm to validate the MEA measurements and to evaluate the effect of Aβ on the postsynaptic response only, we performed patch-clamp experiments on 2-week-old neurons and recorded spontaneous electrical activity comprising APs and excitatory postsynaptic potentials (EPSP) (Figure 5.4). The effects of Aβ addition were already observed after a few minutes [33] and the changes in AP and EPSP frequency were, therefore, assessed at 7 min and compared with those measured during 1 min before Aβ was applied (time point '-1 min'). It is clear that the Aβ (3:7, 2 h) has a profound effect on the EPSP frequency, indicating a block of spontaneous postsynaptic depolarizations. Neither AP nor EPSP were affected by Aβ (1:9, 2 h), and significant increase in AP rate was observed in case of Aβ (0:10, 2 h), in line with the MEA data. As it can be seen, synaptotoxic signatures of $A\beta_{42}$:$A\beta_{40}$ ratios are similar regardless of extra- or intracellular mode of measurement.

5.2.3 Toxic Aβ species are oligomeric and dynamic structures

We used transmission electron microscopy (TEM) to characterize the morphology of the species populated during fibril formation. At the starting point of incubation, no fibrils are detected with any of the different Aβ ratios (Figure 5.5a, column 0 h). With time, the pure $A\beta_{42}$ (10:0) solution showed mature fibril formation consistent with the fast nucleation observed by thioT fluorescence. The fibrils have typical long, negatively stained amyloid fibril morphology as is frequently observed for other amyloid-forming proteins or peptides [34]. Upon longer incubation, these fibrils progressively transform into a dense network of clustered fibrils. $A\beta_{42}$:$A\beta_{40}$ (0:10) and (1:9) ratios developed fibrils after ~6 h, which have similar characteristics to the fibrils observed in the (10:0) ratio, but display in addition a regular twist pattern, which is not observed in the $A\beta_{42}$ fibrils (Figure 5.5a, most right column, arrows indicate twist pattern). The (3:7) ratio in

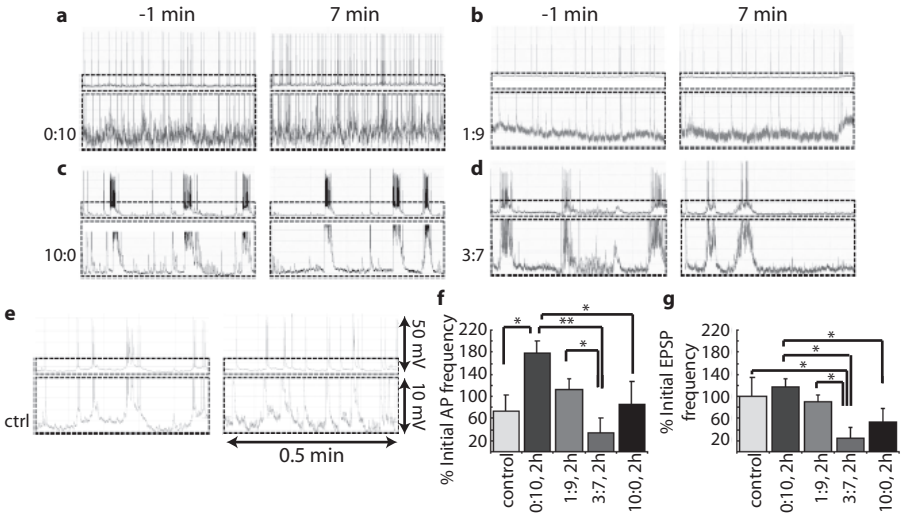

Figure 5.4 Patch-clamp measurements in primary cultures of neurons.
(a-d) Firing pattern of spontaneously active patch-clamped neurons 1 min before and 7 min after the treatment with different Aβ ratios (2 h) as indicated.
(e) Measurement in control conditions (only buffer)
(f) Relative changes in spontaneous AP frequency expressed as % of initial (1 min) rate. Note the early increase in AP rate for $A\beta_{40}$ (0:10)-treated neurons. The other ratios do not reach statistical significance as compared with control likely because of the comparatively short time of treatment.
(g) Relative change in single EPSP. Note the significantly decreased EPSPs rate for $A\beta_{42}$:$A\beta_{40}$ ratio 3:7 ($p<0.03$ versus control, unpaired two-tailed t-test) after only 7 min of treatment. Values are % of initial firing rate±s.e.m. of at least three independent experiments. Statistical significance of the data is indicated by *$p<0.035$ or **$p<0.01$ in (f) and (g).

contrast showed no fibrils at this time point, and the first aggregates appeared only after ~9 h. These aggregates differed markedly in their morphologies as they interacted heavily with the uranyl acetate stain used to visualize the aggregates in TEM and also formed densely fibrous and fractured networks in which individual fibrils cannot be distinguished, which is similar to the later stages of $A\beta_{42}$ aggregation (not shown). Interestingly, the fast nucleation and aggregation kinetics of the (3:7) ratio as observed using thioT fluorescence assays (Figure 5.2) did not coincide with the early appearance of mature aggregates using EM (Figure 5.5a). This suggested that the (3:7) ratio rapidly generates small thioT-positive oligomers, but that these do not propagate towards assemblies that are sufficiently large to allow visualization with EM. Although EM experiments confirmed clearly the dramatic differences in the aggregation properties of the different mixtures, they did not allow visualizing the postulated toxic species responsible for the synaptic effects observed in the MEA experiments with the (3:7) ratio. We hence set out to further identify the presence of smaller oligomeric Aβ using the complementary technique of tapping mode atomic force microscopy (AFM). The various Aβ ratios under investigation were screened at 1.5 h incubation, which is a time point that yields strong synaptotoxicity for ratios (3:7) and (10:0), but not for ratios (1:9) and (0:10) (Figure 5.3e). Interestingly, we observed oligomer formation for all four ratios of $A\beta_{42}$:$A\beta_{40}$ (Figure 5.5b), even for the two non-synaptotoxic ratios (1:9) and (0:10).

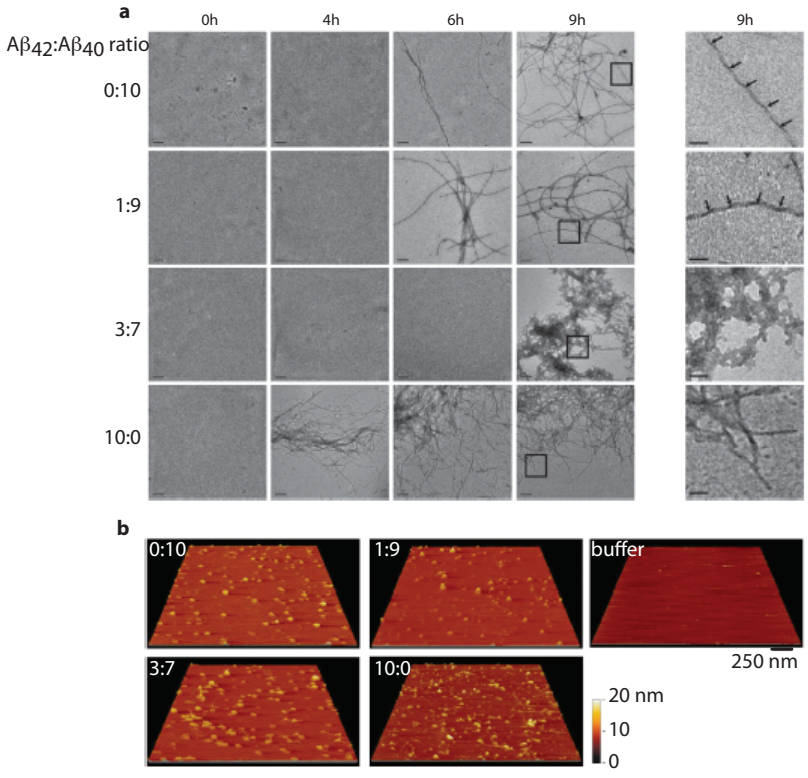

Figure 5.5 Characterization of Aβ oligomers with transmission electron microscopy and atomic force microscopy.
(a) Transmission electron microscopy images of Aβ ratios incubated for 0, 4, 6 and 9 h. Images shown are representative for two experiments. Time of appearance and fibril morphology are affected by $A\beta_{42}$:$A\beta_{40}$ ratio and mature fibril formation is delayed for the synaptotoxic 3:7 ratio. The bars represent 0.2 μm size. The last column shows a magnification of the area indicated by squares in the panels of 9 h. The bars represent 0.04 μm size. The arrows indicate a regular twist pattern observed in the 1:9 and 0:10 fibrils. (b) AFM height images of Aβ oligomers formed by incubation of 70 μM Aβ for 1.5 h at 25 °C in 50mM Tris, 1mM EDTA. The buffer image is shown as a control. The bar represents 250 μm size.

This finding implies that oligomer formation *per se* is not directly linked to the toxic effects of Aβ. We infer that the internal organization of the oligomers might make them toxic to neuronal cells. Native PAGE showed that (10:0) and (3:7) already display a wide range of oligomers and fibrillar material that did not enter the gel after 4 h incubation. SDS PAGE in contrast shows at the same time points only low-molecular weight oligomers (Figure 5.6). It, therefore, seems that SDS PAGE dissociates the larger native structures in the toxic mixtures. The smaller oligomeric SDS-resistant structures can only be considered 'building blocks' of larger structures. As no clear differences were observed in oligomerization state between the four different ratios that could explain the variation in cytotoxicity, we used *in situ* FTIR spectroscopy to obtain information on the conformation of the Aβ peptides and aggregates in solution. We found that the initial spectra of the different Aβ mixtures at t=0 h, when peptides

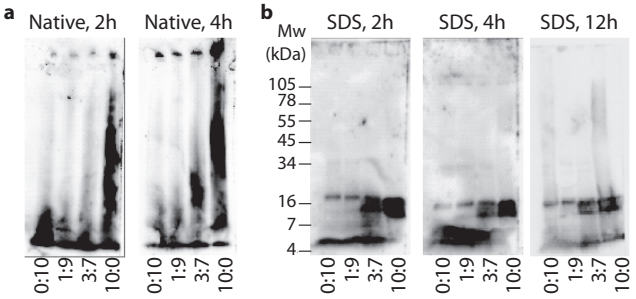

Figure 5.6 Native PAGE and SDS PAGE of Aβ ratios show a range of different oligomeric sizes of Aβ present throughout the aggregation process.
(a) Native PAGE and (b) SDS PAGE (10-20% tris-tricine) and subsequent staining by mAb 6E10. Native PAGE shows large oligomers and fibrils (comparable with EM) especially upon longer incubation for synaptotoxic (3:7) and (10:0). SDS PAGE only shows primarily monomeric and some trimeric and tetrameric species indicating that the oligomers and fibrils detected by Native PAGE are constructed from similar building blocks and that the detection of these oligomeric species is dependent on the particular technology used.

are mainly monomeric, are characterized by a broad peak at 1654 cm^{-1} indicative of random coil structure [35]. This spectrum gradually converts into a defined and sharper peak at 1627 cm^{-1} (Figure 5.7). The intensity at 1627 cm^{-1} is indicative for β-sheet-organized aggregates [36] and the concomitant increases of the FTIR signal at 1627 cm^{-1} with a decreased signal at 1654 cm^{-1} suggested a transition from disordered monomeric structures to β-sheet enriched-oligomeric structures in all mixtures (Figure 5.7 a-d). Conformational changes are rapidly evolving for the three Aβ ratios that contain $Aβ_{42}$, but the rate of this change does not seem to predict toxicity: $Aβ_{42}$ is toxic at 1.5 h, whereas ratio (1:9) is not. For $Aβ_{40}$ alone (Figure 5.7a) and for Aβ (1:9) (Figure 5.7b), it appears that the loss of unordered structure (1654 cm^{-1}) coincided with a prompt transition into amyloid fibrillar β-sheet structure (1627 cm^{-1}), suggesting a two-state manner in the mixtures that develop at inverse rates. This is not observed for Aβ (3:7) and (10:0), suggesting that there is an intermediate, which seems to correlate with toxicity.

5.2.4 Long-term cellular toxicity of Aβ mixtures

Although the changes in synaptic activity are clearly an early effect of the toxic conformations in the Aβ preparations, it remained unclear whether these initial hits on the synapse could also evolve to full cellular neurotoxicity. This is an important question with regard to Alzheimer disease as it is characterized in essence by neuronal cell loss. We investigated, therefore, the effects of the different $Aβ_{42}$:$Aβ_{40}$ ratios over two distinct concentrations (1 μM, which appeared sub-lethal and 10 μM, which appeared lethal) on the staining pattern of primary hippocampal neurons with the synaptic marker synaptophysin or with the early apoptotic markers cleaved caspase-3 and annexinV/propidium iodide (PI). Treatment of cells with 1 μM concentration of Aβ ratios (the same as used for the MEA experiments) for 12 h clearly decreased synaptophysin staining for the Aβ (3:7, 2 h) and (10:0, 2h) ratios. At this concentration, no or little effect on appearance of apoptotic markers in the neuronal cells was observed (Figure 5.8a; quantified in Figure 5.8c), further indicating that the initial effect of the Aβ toxic intermediates is at the synapses. However, 10-fold higher concentration of Aβ (3:7, 2h)

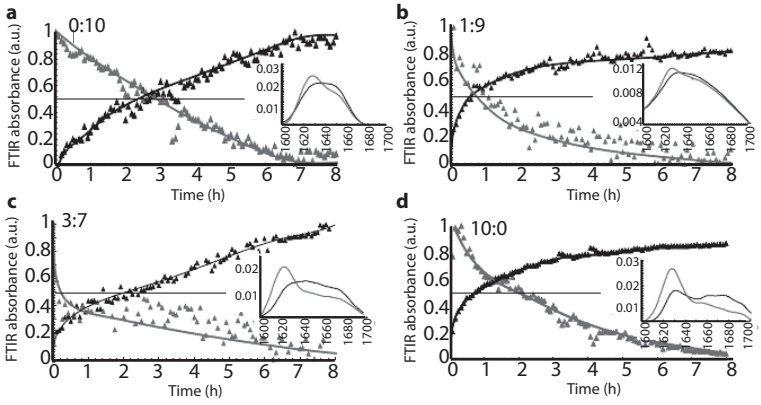

Figure 5.7 Conformational transitions observed using Fourier transform infrared (FTIR) spectroscopy.

FTIR spectra were collected continuously upon incubation of Aβ ratios at 25 °C to investigate conformational changes over time. $A\beta_{42}$:$A\beta_{40}$ (a) (0:10), (b) (1:9), (c) (3:7), (d) (10:0). Intensity at 1654 cm^{-1} in grey characteristic for disordered structure and intensity at 1627 cm^{-1} in black characteristic for amyloid fibril structure. Intensities are averages of three independent experiments and normalized against buffer. Notice that the transition of ratio (3:7) and (10:0) cannot be explained by a two-state transition model (the two curves do not cross at the 50% intersection), whereas (0:10) and (1:9) can completely be accounted for by the two states. Insets show typical spectra for the different Aβ ratios recorded at 0 h (black) and after incubation for 8 h (grey).

and (10:0, 2h) ratios resulted not only in the loss of synaptophysin staining, but was accompanied by a strong increase in the early apoptotic markers, annexin V/PI and cleaved caspase-3 staining (Figure 5.8b; quantified in Figure 5.8d). In contrast, synapses remained intact and no early apoptotic marker induction was caused by Aβ (0:10, 2 h) and (1:9, 2 h) ratios at both 1 and 10 μM concentrations after 12 h of treatment (Figure 5.8 c,d). This finding indicates that synaptotoxic and cytotoxic effects of Aβ intermediates are both ratio and concentration dependent.

We evaluated the time course of caspase-3 activation and its subcellular localization versus the synaptic marker synaptophysin in both sub-lethal (1 μM) and lethal (10 μM) concentrations of the (3:7, 2 h) ratio (Figure 5.8e). Cells treated with 1 μM (3:7, 2 h) showed that cleaved caspase-3 after 2 and 6 h was mostly observed in areas positive for synaptophysin staining. Further treatment up to 12 h resulted in loss of synapses as indicated by loss of staining for synaptophysin; however, the cleaved caspase-3 immunostaining did not propagate to the soma and nucleus. Treatment with 10 μM (3:7, 2 h) caused in contrast strong activation of caspase-3 at the synapses already after 2h (Figure 5.8e). In addition, immunostaining for activated caspase-3 was clearly detectable after 6 h in the soma of the cells. At 12 h, this concentration resulted in loss of synaptic staining with synaptophysin antibodies and strong staining of activated caspase-3 in the soma and nucleus indicative of cell apoptosis (Figure 5.8e). These data indicate that the Aβ toxicity observed at the level of the synapses can spread towards the cell body depending on the type of Aβ species and concentration of toxic intermediates. In addition, the observation suggests that synapse toxicity and cellular toxicity are related.

To further confirm that the different Aβ preparations exerted cellular toxicity, we used a Cell-Titer Blue viability assay on neurons 48 h after they had been exposed to

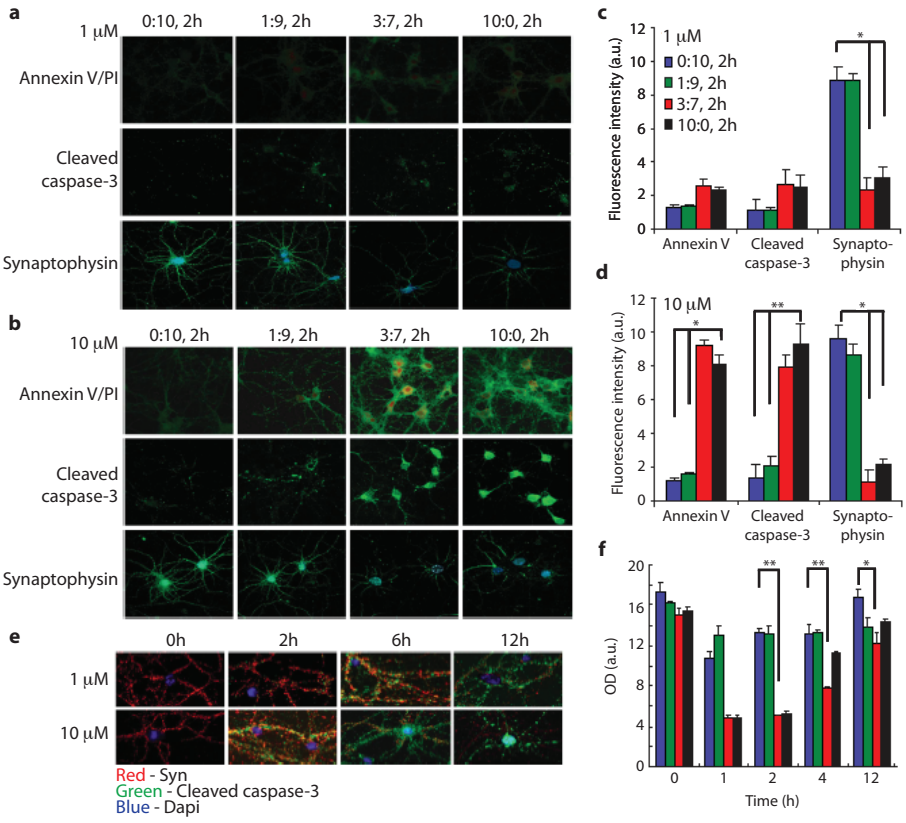

Figure 5.8 Mixed Aβ oligomers affect synapses at low concentration and induce cell death at higher concentrations.

(a,b) Fluorescence microscopy images of hippocampal neurons stained for annexin V (green)/PI (red) (upper row), cleaved caspase-3 (middle row) and synaptophysin (green)/ DAPI (blue) (bottom row) after 12 h treatment with (a) 1 μM Aβ ratios and (b) 10 μM Aβ ratios incubated for 2 h before the addition to cells. Fluorescence intensity quantification for annexin V, cleaved caspase-3 and synaptophysin staining

(c) 1 μM and (d) 10 μM of Aβ ratios. Values are intensity±s.e.m., **p<0.001 and *p<0.003, of five different areas from two independent experiments.

(e) Time course of fluorescence microscopy study of hippocampal neurons stained for synaptophysin (red) and cleaved caspase-3 (green) after treatment with 1 and 10 μM (3:7) ratio Aβ oligomers incubated for 2 h prior the addition to cells (blue: DAPI) figure representative for two independent experiments.

(f) Cell-Titer Blue viability assay of hippocampal neurons treated with 10 μM Aβ ratios incubated for different time periods before the addition to cells. The Cell-Titer Blue reagent conversion was determined 48 h after the treatment. Values are OD±s.e.m., **p<0.01, three independent experiments performed in triplicates.

10 μM of different Aβ ratios, taken at the start of the aggregation process (0 h in Figure 5.8f) and during the propagation reaction (1, 2, 4 and 12 h in Figure 5.8f). In agreement with the previous studies, monomers (Figure 5.8f, 0 h) and mature fibril preparations (Figure 5.8, 12h) are largely inert towards neurons [16,37]. In contrast, the $A\beta_{42}$:$A\beta_{40}$ (3:7, 1 and 2 h) and (10:0, 1 and 2 h) exhibited clear neurotoxicity (Figure 5.8f). Both (1:9) and (0:10) did not exhibit neurotoxicity at any stage of the aggregation process (Figure 5.8f). Collectively, these data indicate that stabilized intermediates in

the Aβ (10:0) and (3:7) ratios bind to synapses and inhibit synaptic activity, and affect neuronal viability at higher concentrations.

5.2.5 Aβ ratio affects behaviour and learning alteration in mice

We finally evaluated to what extent the different Aβ ratio mixtures affected memory formation in mice *in vivo*. We injected mice intraventricularly with 6 µl of 100 µM Aβ mixtures allowed to aggregate for 1.5 h before the injection. The effect of these Aβ preparations on memory formation was tested using passive avoidance and contextual/auditory-cue fear conditioning as described previously [16]. In a light–dark step-through task (passive avoidance test), animals were trained to memorize an electrical shock that followed entrance to a dark compartment. When the test was repeated 24 h later, animals injected with (0:10, 1.5 h) or (1:9, 1.5 h) recalled the electroshock correctly and showed a latency to enter the dark room of 232±15 and 273±16s, respectively, which was not significantly different from control mice injected with buffer (256±20s)-control group not shown. Injection of (10:0, 1.5 h) or (3:7, 1.5 h) before the shock, however, inhibited strongly the formation of new memory. These animals showed significantly faster entrance latencies of 134±12 and 165±19 s, respectively ($p<0.002$) (Figure 5.9a). Contextual and auditory-cue fear conditioning experiments confirmed these results. Injection of (10:0) and (3:7) 90 min before conditioning disturbed the typical freezing behaviour observed 24 h after the training when the animals were exposed again to the contextual stimulus (~50%, $p<0.006$) or the auditory-cue fear conditioning experiment (39%, $p<0.004$) (Figure 5.9b). These results show that also in the complex environment of a living animal clear differences can be observed between the different Aβ ratios similar to those observed in biophysical and cellular assays.

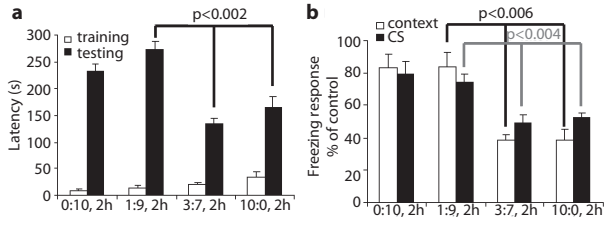

Figure 5.9 Toxic Aβ affects behaviour and learning of mice.
(a) Passive avoidance; 1.5 h after intraventricular injection with 6 µl of Aβ ratios incubated for 2 h before the injection, latency of entrance in the dark cage during the training (white) was tested. The latency of entrance during the testing was performed 24 h later (black) (values are latency mean±s.e.m., $p<0.002$, control (n=13), $Aβ_{40}$ and ratio 1:9 (n=12), ratio 3:7 and $Aβ_{42}$ (n=11)).
(b) Conditional fear response; 1 h after intraventricular injection with 6 µl of Aβ ratios, habituation was induced. Animals were exposed to the training after an additional 4 h. The freezing response was recorded 24 h later for context-dependent (white bars) and auditory cue-dependent (black bars) memory formation. Values are % freezing mean±s.e.m., Aβ ratios (0:10) and (1:9): n=13 for ratio (3:7) and (10:0): n=14.

5.3 Discussion

One of the most challenging issues in Alzheimer disease research is the unresolved nature of the Aβ peptide conformation(s) that exert neurotoxicity. Our current work shows that Aβ-associated toxicity is a dynamic property and that a critical equilibrium

between the two major Aβ species, $A\beta_{40}$ and $A\beta_{42}$, exists, which determines the rate of appearance of these toxic properties as assessed in neuronal cell culture and in brains of animals *in vivo*. Our study design has taken this dynamic behaviour into account by indicating the time of aggregation of the peptides used in each experiment. We found that relative high concentrations of Aβ are needed to induce fibrillization and toxic-oligomer conformation. Although this might seem an artificial situation, one should realize that by increasing the Aβ concentrations, processes which otherwise take decades become accelerated to the extent that they can be studied in laboratory conditions. Most importantly, such high concentrations of Aβ might actually be even quite relevant for what happens *in vivo*. A recent publication suggested indeed that intracellular compartments accumulate Aβ at high μM concentrations, which could create the conditions for the local formation of the elusive toxic conformations of Aβ peptides [38].

It turns out that a small relative increase of $A\beta_{42}$, comparable with those observed in patients with familial cases of Alzheimer disease [2,4,30,31], dramatically influenced the final effects on spontaneous synaptic activity and viability of neuronal cells and on memory formation in animals. This correlated with remarkable changes in the biophysical behaviour of the Aβ peptides as assessed in a variety of approaches. Thus, we find that shifting the ratio of $A\beta_{42}$:$A\beta_{40}$ from (1:9) to (3:7) shortened nucleation time strongly, whereas fibril elongation time remained similar as measured by thioT incorporation. In EM, the (3:7) ratio revealed only visible fibrillar structures after prolonged incubation compared with the other three ratios investigated. Both experiments together suggested that intermediary assemblies of Aβ peptides became stabilized in the (3:7) ratio, which were too small to be observed in EM, but which, as evaluated in MEA, exerted strong effects on synaptic activity. In SDSPAGE, these assemblies apparently fall apart in small multimeric Aβ oligomers as observed by others [17,19], but from non-denaturing PAGE analysis, we deduced that these 'building blocks' are part of larger structures present in the toxic mixtures on the neuronal cultures. Investigation by AFM further underlined that oligomeric Aβ was present in all Aβ ratio preparations, suggesting that the presence of oligomers *per se* are not directly linked with toxic effects. We suggest, therefore, that the toxic aggregates of Aβ in our assays were dynamic in nature and could assemble and disassemble when in solution in the culture medium of the cells. In addition, based on the results obtained by AFM, one can assume that not the size but the structure of the intermediate oligomers dictates their stability and synaptotoxic potential. Indeed, with FTIR spectroscopy, we found indications for particular conformational transitions in the peptides that are specific for this postulated toxic intermediate situation. Going from monomeric Aβ (disordered at 1654 cm^{-1}) to fibrillar Aβ (parallel β-sheet at 1627cm^{-1}) [35,36], we find in the $A\beta_{40}$ (0:10) or $A\beta_{42}$:$A\beta_{40}$ (1:9) preparations that the unstructured state converted to the β-sheet conformation without intermediary structures. In contrast, the patterns of conversion in the $A\beta_{42}$:$A\beta_{40}$ (3:7) and the $A\beta_{42}$ (10:0) ratios indicated the existence of an intermediate conformation (Figure 5.5d, Figure 5.7c). The current work also suggests the prolonged time window of existence of such intermediate states in the (3:7) ratio.

$A\beta_{42}$ drives apparently this reaction, interactions of $A\beta_{40}$ and $A\beta_{42}$ occur random. Previously, it has been shown that $A\beta_{42}$ induces indeed the aggregation of $A\beta_{40}$ [7,9,12,13,28]. We show here that the relative amount of $A\beta_{42}$ is most crucial in

this regard as shown by the dramatic shift in properties from Aβ42:Aβ40 ratio (1:9) towards the FAD-like Aβ42:Aβ40 ratio (3:7). In fact, ratio (1:9) is nucleating very late (Figure 5.2), but once the nucleation occurs, this mixture rapidly forms mature and well-organized fibrils (Figure 5.5a), in which oligomer formation is observed by AFM (Figure 5.5b), but not by TEM. Collectively, the data suggest that the Aβ (1:9) and (0:10) ratios most probably bypassed the synaptotoxic stage and aggregated quite rapidly into non-toxic mature fibrils once nucleation had been induced (Figure 5.3 e,f, Figure 5.5a) and, therefore, did not bind and affect synapses. In contrary, Aβ (3:7) and (10:0) ratios were enriched with synaptotoxic intermediates that bind to synapses and inhibit spontaneous synaptic activity. It should be mentioned that it has been already suggested that neurotoxicity by Aβ is not exerted by a specific species, but that in contrast the polymerization reaction itself, which depends on monomer concentration and nucleation rate, drives toxicity [39]. Our data seem indeed more compatible with a dynamic interpretation of Aβ toxicity, and argue against a simple receptor-ligand mechanism mediated by a precise Aβ species as has been proposed by several others; e.g. [40].

A wide range of evidences indicate that Aβ oligomers and protofibrillar intermediates, regardless of their origin or preparation, attack synapses, block LTP and disrupt cognitive functions [16,19,23,25,41-43]. One of the questions in these assays is whether the species that exerts the toxicity as measured in the biological assay is the same as the one that is analysed in the biophysical assays. We developed, therefore, an acute cellular assay to measure synaptic effects very early after addition of the Aβ preparations. We observed changes in the spontaneous firing rate of neurons in culture already within 20 min incubation with Aβ ratio mixtures (Figure 5.3 d,e). We confirmed that the thioT tinctorial properties of the different Aβ preparations used were minimally changed over the time frame of 40 min. This assay was performed in neuronal culture medium and at the same dilution and temperature used in the cellular assays, further strengthening our assumption that the toxicity measured in the MEA cellular assay was indeed associated with the Aβ aggregation state characterized in the biophysical assays. This acute toxicity was further confirmed by measuring EPSPs of neurons in culture: as early as 7 min after addition of the Aβ mixtures toxicity, measured as decreased rate of EPSP, was detected.

We addressed the question of synaptotoxic versus cytotoxic effects of Aβ intermediates. We show that intermediates from the Aβ (3:7) ratio specifically bind synapses (Figure 5.3f) without major cytotoxicity as assessed by caspase-3 and annexin staining (Figure 5.8). Our data also provide some preliminary evidence that the initial synaptotoxicity is accompanied by some local synaptic activation of caspase-3 (Figure 5.8) occurring in parallel to the functional inactivation of synapses (Figure 5.3), which needs further exploration. Interestingly, higher concentrations of the Aβ (3:7) ratio caused caspase-3 activation in the soma as well (Figure 5.8).

The findings in this chapter impact on our understanding of the function of the different Aβ species and their relative contribution to synapse toxicity and neuronal cell death in the brain of patients with Alzheimer disease. The paradox of loss of function of several presenilin mutations causing Alzheimer disease (reviewed in [6]) indicates that at least in these FAD cases, a lower generation of Aβ peptide can still be associated with disease and progressive amyloid accumulation. *In vivo* experiments are in line with this conclusion: more amyloid pathology was observed in transgenic mice expressing

a PS1 mutant allele over a PS1 null allele than over a PS1 wild-type allele [10]. Our work explains that it is indeed possible to come to very different, pathologically relevant, situations with the same quantitative Aβ load, but with a qualitatively different Aβ mix. This could potentially explain the early and aggressive neurodegeneration in the brain of presenilin FAD patients, even with a loss of function of γ-secretase [5]. If indeed the specific mix of the different Aβ peptides with specific conformation in the brain dictates the synapse and neuronal toxicity potential of the Aβ load in FAD and, by extrapolation, in SAD brain, these observations have obviously important implications for the development of anti-amyloid medication.

5.4 Experimental procedures

5.4.1 Preparation of Aβ peptide ratios

Aβ peptide was dissolved as described in Chapter 2 and the peptide concentration was measured using Bradford assay. The samples were kept on ice until experiments started, with a maximum lag time of 20 min.

5.4.2 ThioT fluorescence

Aβ protein concentrations were normalized to 50 μM by further dilution using 50mM Tris, 1mM EDTA containing buffer and a final concentration of 12 μM thioT was added. The fibrillation kinetics were followed *in situ* at excitation and emission wavelengths of 440 and 480 nm resp. Readings were recorded in triplicate every 10 min during 6h.

5.4.3 Time-resolved Western blot and dotblot

Aggregation of $A\beta_{40}$, $A\beta_{42}$ and ratios (1:9) and (3:7) ($A\beta_{42}$:$A\beta_{40}$) was studied using Western blot analysis. Aggregates were prepared at 100 μM and incubated at 25 °C. At various time points, aliquots of Aβ were mixed 2x Novex Tricine SDS sample buffer (for SDS PAGE) or with 4x native PAGE sample buffer with G-250 and loaded onto a 10% bis-tris gel (SDS-PAGE) or a 3-12% bis-tris gel (native PAGE). The SDS-gel was run at 125 V for 75 min and the native-gel at a fixed voltage of 100 V for 120 min, Subsequently the peptides were transferred onto a nitrocellulose membrane (SDS PAGE) or to PVDF membrane (native PAGE) for 2 h at 25 V at 4 °C using Towbin blot buffer (25mM Tris, 192mM Glycine, 20% MeOH, 0.1% SDS) (SDS PAGE) or for 70 min at 0.09 A at 4 °C using NuPAGE transfer buffer (native PAGE). For dotblot, 5 μL sample was blotted onto nitrocellulose membrane followed by boiling of the membrane in PBST. Membranes were blocked and incubated with primary antibodies 6E10, and A11 for PAGE and anti-$A\beta_{40}$ and anti-$A\beta_{42}$ for dotblots. After blotting with HRP-tagged secondary antibodies the membranes were visualized using an electrochemical luminescence (ECL) system.

5.4.4 Transmission electron microscopy

Aliquots (5 μl) of the Aβ preparation were adsorbed to carboncoated FormVar film on 400-mesh copper grids for 1 min. The grids were blotted, washed twice in droplets of Milli-Q water and stained with 1% (wt/vol) uranyl acetate. Samples were studied with a JEOL JEM-2100 microscope at 200 kV.

5.4.5 Atomic force microscopy

Atomic force microscopy imaging was performed on a custom built instrument using Si_3N_4 tips with a spring constant of 0.5 N/m and a nominal tip radius of 10 nm. The measurements were made in tapping mode in liquid, with a tapping amplitude of less than 4 nm. The AFM scan settings were optimized to minimum force interaction with the sample. All AFM images have 512x512 pixels. Aβ ratios were incubated at 25 °C at 70 μM for 1.5h. AFM samples were prepared by placing 4 μL of sample on freshly cleaved mica. After 4 min adsorption time, unbound Aβ was gently washed off with twice 100 μL buffer (filtered 10mM Tris, 1mM EDTA, pH 7.5). The sample was then mounted on the AFM stage with application of 300 μL extra buffer, a volume sufficient to keep the sample in buffer throughout the experiment. The images are represented in 3D after removal of height discontinuities between subsequent scan lines and compensation for piezo drift using SPIP software.

5.4.6 Fourier transform infrared spectroscopy

Aβ solutions were applied to the FTIR sample holder and incubated for 8 h at 25 °C. InfraRed spectra were recorded on a Bruker Tensor 27 infrared spectrophotometer equipped with a Bio-ATR II accessory. The spectrophotometer was continuously purged with dried air. Spectra were recorded at a spectral resolution of 4 cm^{-1} and 120 accumulations were performed per measurement. FTIR spectra were recorded every 5 min *in situ* at a wavelength range from 900 to 3500 cm^{-1}. The obtained spectra were baseline subtracted and rescaled in the amide I area, which spans from ~1600 to ~1700 cm^{-1}.

5.4.7 Primary hippocampal cultures

Hippocampal neuronal cultures were generated from trypsinized brains obtained from 17-days-old embryos and were maintained in Neurobasal medium supplemented with B27 and 12.5 μM L-glutamate After 3 days of culturing, the medium was changed to Neurobasal medium without glutamate. Cultures were maintained at 37 °C in a humidified 5% CO_2 atmosphere for 8-10 days prior to further experiments.

5.4.8 Spontaneous synaptic activity recording by MEA

Neurons were plated at 1000 cells mm^{-2} on an MEA substrate and grown for 8-10 days. The spontaneous firing rate of the neuronal network was recorded simultaneously from at least 10 successful electrodes (out of 60 available). During the recording experiment, a temperature controller was used to maintain the MEA platform temperature at 37 °C. The basal firing rate was recorded during 5 min. Upon treatment with Aβ, the spontaneous synaptic activity was continuously recorded during 40 min. Raw signals from MEA electrodes were amplified with a gain of 1200 and digitized at a sampling rate of 25 kHz; MC_Rack 3.5.10 software was used for data recording and processing. The raw data stream was high-pass filtered at 200 Hz, and the threshold for spike detection was set to 5 SD of the average noise amplitude computed during the first 1000 ms of recording. A number of spikes detected by every electrode per time bin of 60 s was normalized to baseline (firing rate in the absence of treatment). After data analysis, the firing rates at 10, 20 and 40 min of treatment were extracted and presented as percentage of initial rate.

5.4.9 Immunocytochemistry

Slides were washed with PBS, fixed with 4% paraformaldehyde/PBS and immunostained with anti-cleaved caspase 3 antibody (1:100) or anti-synaptophysin (1:200) followed by staining with Alexa-Fluor 488-conjugated GaM secondary antibody (1:200). For double staining anti-oligomer A11 antibody (1:200) and anti-synaptophysin (1:200) were used and subsequently stained with Alexa-Fluor 564-conjugated GaR and Alexa-Fluor 488-conjugated GaM secondary antibodies (1:200), respectively. Microscopic analysis was performed on a Confocal microscope.

5.4.10 Cell-titer-blue cell viability assay

Ten μL of Cell-Titer-Blue dye was added directly to the growth medium on the cells. After 3 h incubation the fluorescence intensity of the samples was measured at an excitation wavelength of 560 nm and an emission wavelength of 590 nm.

5.4.11 Annexin V/Propidium iodide (PI) staining

Hippocampal cultures on slides were incubated with annexin V/PI dye mixture from the ApoAlert apoptosis kit for 15 min according to manufacture recommendations. Microscopic analysis was performed using confocal microscope as described above.

5.4.12 Patch-clamp experiments

Two-week-old neurons from at least five independent hippocampal cultures were patch clamped, and spontaneous electrical activity comprising APs and EPSPs was recorded. Quartz glass pipettes with an inner diameter of 1mm were pulled using a P-2000 Laser Puller to obtain pipettes with series resistance of 2-4MΩ. The pipette solution consisted of 140mM KCl, 5mM EGTA, 5mM NaCl, 5mM Na_2ATP, 10mM HEPES, 1mM $MgCl_2$, pH 7.2. After the formation of a gigaseal, the cell membrane was ruptured using ZAP pulses to obtain the whole-cell configuration. Then, APs and EPSPs were recorded in current clamp mode. Neurons were kept in neurobasal cell medium supplemented with 10% HEPES. Different ratios of Aβ were added to the measurement chamber by manual pipetting. The number of EPSPs before and after the treatment were analysed in 1 min segments by means of the Clampfit software.

5.4.13 Mouse care

Female 3 month old mice of comparable weight were maintained in a specific pathogen-free facility that meets Belgian and European Union requirements for animal care. Mice were group housed in a climate-controlled animal colony with a 12 h light/dark cycle (light on 6:00 A.M.) with access to food and water *ad libitum*, except during some of the behavioral testing. Adequate measures were taken to minimize pain or discomfort.

5.4.14 Brain intraventricular injections

Animals were locally anesthetized by subcutaneous injection of 5 μL of 2% Xylocaine. The needle was inserted unilaterally 1 mm to the right of the midline point equidistant from each eye, at an equal distance between the eyes and the ears and perpendicular to the plane of the skull and 6 μg Aβ from an aged (2 h) solution was injected using a Hamilton syringe. The surgery was completed within 8 min. Animals

were followed-up for their post-surgery recovery and normally showed unimpaired behavior and motility. 1-1.5 h after the injections the animals were exposed to behavior tests. Different experimental groups of transiently injected animals were used for each behavioral test.

5.4.15 Learning and memory tests

Passive avoidance learning was tested in a step-through box. During training, dark-adapted mice were placed in the small illuminated compartment of the box. After 5 s, a sliding door to the larger dark compartment was opened, and entry latency was recorded. The door was closed as soon as all four feet were on the grid floor, and a slight foot shock (0.3 mA, 2 s) was delivered using a constant current shocker. Retention was tested 24 h later using the same procedure, and entry was recorded up to 300 s cutoff. The results are expressed as latency to enter the dark compartment before and after the foot shock. In cue- and context-dependent fear conditioning the unconditioned stimulus (US) (an electric shock) is paired with a CS (the tone) to elicit a freezing response, a reliable measure of fear in rodents. On the first day, the animals were placed in the testing chamber (22.5x32.5x33.3 cm; Plexiglas cage with a grid floor) and were allowed to acclimatize for 5 min. On day 2, they were first allowed to explore the testing chamber for 2 min (pre-US score). A 30-s tone (conditioned stimulus (CS)) was delivered (frequency, 2150±200 Hz), which coterminated with a 2 s, 0.35mA foot shock (the US). Two minutes later, a second pairing of the CS and US was presented, followed by another 30 s exploration (post-US score). Twenty-four hours later, the animals were returned to the testing chamber for 5 min exploration in the same context as the previous day (context score). Ninety minutes later, the animals were returned to the test chamber, but now the grid floor was hidden with a Plexiglas plate and odourized sawdust to alter the context of the testing chamber. The animals were observed for 6 min. During the first 3 min, no stimulus was delivered (pre-CS score). During the next 3 min phase, the auditory cue was delivered (CS score). Freezings were automatically recorded. A freezing score was expressed as the percentage of freezing, when the threshold was defined equally through all experiments in each of the five trial blocks.

5.4.16 Statistics

Differences between groups were examined using unpaired two-tailed t-tests, and one-way or two-way repeated measurements ANOVA procedures with Fisher's method. Significance levels for each experiment are indicated in the figure legends. Significance in Cell-Titer Blue viability assay, MEA assay, ThioT assays and immunofluorescence intensity assay was established using two-tailed t-tests.

AUTHOR CONTRIBUTION

AV contributed to this manuscript by validating thioT fluorescence, fibril morphology and cytotoxicity of the Aβ preparations.

5.5 References

[1] Haass C & Selkoe D (1993). Cellular processing of β-amyloid precursor protein and the genesis of amyloid β-peptide. *Cell*, 75:1039-1042.

[2] Scheuner D, Eckman C, Jensen M, Song X, Citron M, Suzuki N, Bird T, Hardy J, Hutton M, Kukull W, Larson E, Levy-Lahad E, Viitanen M, Peskind E, Poorkaj P, Schellenberg G, Tanzi R, Wasco W, Lannfelt L, Selkoe D, Younkin S (1996). Secreted amyloid β-protein similar to that in the senile plaques of Alzheimer's disease is increased in vivo by the presenilin 1 and 2 and APP mutations linked to familial Alzheimer's disease. *Nat. Med.*, 2:864-870.

[3] Suzuki N, Cheung T, Cai X, Odaka A, Otvos L, Eckman C, Golde T, Younkin S (1994). An increased percentage of long amyloid β protein secreted by familial amyloid β protein precursor (β APP717) mutants. *Science*, 264:1336-1340.

[4] Duff K, Eckman C, Zehr C, Yu X, Prada C, Perez-Tur J, Hutton M, Buee L, Harigaya Y, Yager D, Morgan D, Gordon M, Holcomb L, Refolo L, Zenk B, Hardy J, Younkin S (1996). Increased amyloid-β42(43) in brains of mice expressing mutant presenilin 1. *Nature*, 383:710-713.

[5] Bentahir M, Nyabi O, Verhamme J, Tolia A, Horré K, Wiltfang J, Esselmann H, De Strooper B (2006). Presenilin clinical mutations can affect γ-secretase activity by different mechanisms. *J. Neurochem.*, 96:732-742.

[6] De Strooper B (2007). Loss-of-function presenilin mutations in Alzheimer disease. Talking Point on the role of presenilin mutations in Alzheimer disease. *EMBO Rep.*, 8:141-146.

[7] Snyder S, Ladror U, Wade W, Wang G, Barrett L, Matayoshi E, Huffaker H, Krafft G, Holzman T (1994). Amyloid-β aggregation: selective inhibition of aggregation in mixtures of amyloid with different chain lengths. *Biophys. J.*, 67:1216-1228.

[8] Frost D, Gorman P, Yip C, Chakrabartty A (2003). Co-incorporation of Aβ 40 and Aβ 42 to form mixed pre-fibrillar aggregates. *Eur. J. Biochem.*, 270:654-663.

[9] Yoshiike Y, Chui D, Akagi T, Tanaka N, Takashima A (2003). Specific compositions of amyloid-β peptides as the determinant of toxic β-aggregation. *J. Biol. Chem.*, 278:23648-23655.

[10] Wang R, Wang B, He W, Zheng H (2006). Wild-type presenilin 1 protects against Alzheimer's disease mutation-induced amyloid pathology. *J. Biol. Chem.*, 29:29.

[11] Kim J, Onstead L, Randle S, Price R, Smithson L, Zwizinski C, Dickson D, Golde T, McGowan E (2007). Aβ40 inhibits amyloid deposition in vivo. *J. Neurosci.*, 27:627-633.

[12] Yan Y & Wang C (2007). Aβ40 protects non-toxic Aβ42 monomer from aggregation. *J. Mol. Biol.*, 369:909-916.

[13] Jan A, Gokce O, Luthi-Carter R, Lashuel HA (2008). The ratio of monomeric to aggregated forms of Aβ40 and Aβ42 is an important determinant of amyloid-β aggregation, fibrillogenesis, and toxicity. *J. Biol. Chem.*, 283:28176-28189.

[14] Aizenstein H, Nebes R, Saxton J, Price J, Mathis C, Tsopelas N, Ziolko S, James J, Snitz B, Houck P, Bi W, Cohen A, Lopresti B, DeKosky S, Halligan E, Klunk W (2008). Frequent amyloid deposition without significant cognitive impairment among the elderly. *Arch. Neurol.*, 65:1509-1517.

[15] Reiman E, Chen K, Liu X, Bandy D, Yu M, Lee W, Ayutyanont N, Keppler J, Reeder S, Langbaum J, Alexander G, Klunk W, Mathis C, Price J, Aizenstein H, DeKosky S, Caselli R (2009). Fibrillar amyloid-β burden in cognitively normal people at 3 levels of genetic risk for Alzheimer's disease. *Proc. Natl. Acad. Sci. USA*, 106:6820-6825.

[16] Martins I, Kuperstein I, Wilkinson H, Maes E, Vanbrabant M, Jonckheere W, Van Gelder P, Hartmann D, D'Hooge R, De Strooper B, Schymkowitz J, Rousseau F (2008). Lipids revert inert Aβ amyloid fibrils to neurotoxic protofibrils that affect learning in mice. *EMBO J.*, 27:224-233.

[17] Shankar G, Li S, Mehta T, Garcia-Munoz A, Shepardson N, Smith I, Brett F, Farrell M, Rowan M, Lemere C, Regan C, Walsh D, Sabatini B, Selkoe D (2008). Amyloid-β protein dimers isolated directly from Alzheimer's brains impair synaptic plasticity and memory. *Nat. Med.*, 14:837-842.

[18] Lambert M, Barlow A, Chromy B, Edwards C, Freed R, Liosatos M, Morgan T, Rozovsky I, Trommer B, Viola K, Wals P, Zhang C, Finch C, Krafft G, Klein W (1998). Diffusible, nonfibrillar ligands derived from Aβ1-42 are potent central nervous system neurotoxins. *Proc. Natl. Acad. Sci. USA*, 95:6448-6453.

[19] Walsh D, Klyubin I, Fadeeva J, Cullen W, Anwyl R, Wolfe M, Rowan M, Selkoe D (2002). Naturally secreted oligomers of amyloid β protein potently inhibit hippocampal long-term potentiation in vivo. *Nature*, 416:535-539.

[20] Kayed R, Head E, Thompson J, McIntire T, Milton S, Cotman C, Glabe C (2003). Common structure of soluble amyloid oligomers implies common mechanism of pathogenesis. *Science*, 300:486-489.

[21] Hepler R, Grimm K, Nahas D, Breese R, Dodson E, Acton P, Keller P, Yeager M, Wang H, Shughrue P, Kinney G, Joyce J (2006). Solution state characterization of amyloid β-derived diffusible ligands. *Biochemistry*, 45:15157-15167.

[22] Lashuel H, Hartley D, Petre B, Walz T, Lansbury P (2002). Neurodegenerative disease: amyloid pores

from pathogenic mutations. *Nature,* 418:291.
[23] Gong Y, Chang L, Viola K, Lacor P, Lambert M, Finch C, Krafft G, Klein W (2003). Alzheimer's disease-affected brain: presence of oligomeric Aβ ligands (ADDLs) suggests a molecular basis for reversible memory loss. *Proc. Natl. Acad. Sci. USA*, 100:10417-10422.
[24] Lesné S, Koh M, Kotilinek L, Kayed R, Glabe C, Yang A (2006). A specific amyloid-β protein assembly in the brain impairs memory. *Nature*, 440:352-357.
[25] Lacor P, Buniel M, Furlow P, Clemente A, Velasco P, Wood M, Viola K, Klein W (2007). Aβ oligomer-induced aberrations in synapse composition, shape, and density provide a molecular basis for loss of connectivity in Alzheimer's disease. *J. Neurosci.*, 27:796-807.
[26] Klyubin I, Betts V, Welzel A, Blennow K, Zetterberg H, Wallin A, Lemere C, Cullen W, Peng Y, Wisniewski T, Selkoe D, Anwyl R, Walsh D, Rowan M (2008). Amyloid β protein dimer-containing human CSF disrupts synaptic plasticity: prevention by systemic passive immunization. *J. Neurosci.*, 28:4231-4237.
[27] Ono K, Condron M, Teplow D (2009). Structure-neurotoxicity relationships of amyloid β-protein oligomers. *Proc. Natl. Acad. Sci. USA*, 106:14745-14750.
[28] Jarrett J & Lansbury P (1993). Seeding 'one-dimensional crystallization' of amyloid: a pathogenic mechanism in Alzheimer's disease and scrapie? *Cell*, 73:1055-1058.
[29] Harper J & Lansbury P (1997). Models of amyloid seeding in Alzheimer's disease and scrapie: mechanistic truths and physiological consequences of the time-dependent solubility of amyloid proteins. *Annu. Rev. Biochem.*, 66:385-407.
[30] Mann D, Iwatsubo T, Cairns N, Lantos P, Nochlin D, Sumi S, Bird T, Poorkaj P, Hardy J, Hutton M, Prihar G, Crook R, Rossor M, Haltia M (1996). Amyloid β protein (Aβ) deposition in chromosome 14-linked Alzheimer's disease: predominance of Aβ42(43). *Ann. Neurol.*, 40:149-156.
[31] Citron M, Westaway D, Xia W, Carlson G, Diehl T, Levesque G, Johnson-Wood K, Lee M, Suebert P, Davis A, Kholodenko D, Motter R, Sherrington R, Perry B, Yao H, Strome R, Lieberburg I, Rommens J, Kim S, Schenk D, Fraser P, St George-Hyslop P, Selkoe D (1997). Mutant presenilins of Alzheimer's disease increase production of 42-residue amyloid β-protein in both transfected cells and transgenic mice. *Nat. Med.*, 3:67-72.
[32] Stett A, Egert U, Guenther E, Hofmann F, Meyer T, Nisch W, Haemmerle H (2003). Biological application of microelectrode arrays in drug discovery and basic research. *Anal. Bioanal. Chem.*, 377:486-495.
[33] Hartley D, Walsh D, Ye C, Diehl T, Vasquez S, Vassilev P, Teplow D, Selkoe D (1999). Protofibrillar intermediates of amyloid β-protein induce acute electrophysiological changes and progressive neurotoxicity in cortical neurons. *J. Neurosci.*, 19:8876-8884.
[34] Chamberlain A, MacPhee C, Zurdo J, Morozova-Roche L, Hill HA, Dobson C, Davis J (2000). Ultrastructural organization of amyloid fibrils by atomic force microscopy. *Biophys. J.*, 79:3282-3293.
[35] Goormaghtigh E, Cabiaux V, Ruysschaert J (1994). Determination of soluble and membrane protein structure by Fourier transform infrared spectroscopy. II. Experimental aspects, side chain structure, and H/D exchange. *Subcell. Biochem.*, 23:363-403.
[36] Chirgadze Y & Nevskaya N (1976). Infrared spectra and resonance interaction of amide-I vibration of the paraellel-chain pleated sheets. *Biopolymers*, 15:627-636.
[37] Aksenov M, Aksenova M, Butterfield D, Hensley K, Vigo-Pelfrey C, Carney J (1996). Glutamine synthetase-induced enhancement of β-amyloid peptide Aβ (1–40) neurotoxicity accompanied by abrogation of fibril formation and Aβ fragmentation. *J. Neurochem.*, 66:2050-2056.
[38] Hu X, Crick S, Bu G, Frieden C, Pappu R, Lee J-M (2009). Amyloid seeds formed by cellular uptake, concentration, and aggregation of the amyloid-β peptide. *Proc. Natl. Acad. Sci. USA.*, 106:20324-20329.
[39] Wogulis M, Wright S, Cunningham D, Chilcote T, Powell K, Rydel R (2005). Nucleation-dependent polymerization is an essential component of amyloid-mediated neuronal cell death. *J. Neurosci.*, 25:1071-1080.
[40] Lauren J, Gimbel D, Nygaard H, Gilbert J, Strittmatter S (2009). Cellular prion protein mediates impairment of synaptic plasticity by amyloid-β oligomers. *Nature*, 457:1128-1132.
[41] Cleary J, Walsh D, Hofmeister J, Shankar G, Kuskowski MA, Selkoe D, Ashe K (2005). Natural oligomers of the amyloid-β protein specifically disrupt cognitive function. *Nat. Neurosci.*, 8:79-84.
[42] Calabrese B, Shaked G, Tabarean I, Braga J, Koo E, Halpain S (2007). Rapid, concurrent alterations in pre- and postsynaptic structure induced by naturally-secreted amyloid-β protein. *Mol. Cell. Neurosci.*, 35:183-193.
[43] Tew D, Bottomley S, Smith D, Ciccotosto G, Babon J, Hinds M, Masters C, Cappai R, Barnham K (2008). Stabilization of neurotoxic soluble β-sheet-rich conformations of the Alzheimer's disease amyloid-β peptide. *Biophys. J.*, 94:2752-2766.

6

Structural basis for increased toxicity of pathological Aβ42:Aβ40 ratios in Alzheimer disease.

Aβ is directly related to neurotoxicity in Alzheimer disease. The two most abundant alloforms of the peptide co-exist under normal physiological conditions in the brain in an $A\beta_{42}$:$A\beta_{40}$ ratio of ~ 1:9. This ratio is often shifted to a higher percentage of $A\beta_{42}$ in brains of patients with familial Alzheimer disease and this has recently been shown to lead to increased synaptotoxicity. The molecular basis for this phenomenon remains unclear. Although the aggregation characteristics of $A\beta_{40}$ and $A\beta_{42}$ individually are well established, little is known about the properties of mixtures. We have explored the biophysical and structural properties of physiologically relevant $A\beta_{42}$:$A\beta_{40}$ ratios by several techniques. We show that $A\beta_{40}$ and $A\beta_{42}$ directly interact as well as modify the behavior of the other. The structures of monomeric and fibrillar assemblies formed from $A\beta_{40}$ and $A\beta_{42}$ mixtures do not differ from those formed from either of these peptides alone. Instead, the co-assembly of $A\beta_{40}$ and $A\beta_{42}$ influences the aggregation kinetics by altering the pattern of oligomer formation as evidenced by a unique combination of solution nuclear magnetic resonance spectroscopy, high molecular weight mass spectrometry, and cross-seeding experiments. We relate these observations to the observed enhanced toxicity of relevant ratios of $A\beta_{42}$:$A\beta_{40}$ in synaptotoxicity assays and in Alzheimer disease patients.

The results described in this chapter have been published in:
Pauwels K, Williams T, Morris K, Jonckheere W, Vandersteen A, Kelly G, Schymkowitz J, Rousseau F, Pastore A, Serpell L, and Broersen K (2012). *J. Biol. Chem.*, 287:5650-5660.

6.1 Introduction

Alzheimer disease is a multifactorial neurodegenerative disease that mainly affects the growing population of the elderly. The primary agents of Alzheimer disease, the Aβ peptides, are released from the amyloid precursor protein by sequential endoproteolytic cleavages. The severity of dementia correlates with soluble assemblies of Aβ peptides rather than with the final fibrillar Aβ deposits observed in the brain [1] and a plethora of different toxic oligomers have been identified [2-5].

Imprecise cleavage of the amyloid precursor protein substrate by γ-secretase or altered catabolism of the Aβ peptides affect the relative amounts of $A\beta_{40}$ and $A\beta_{42}$, the two main Aβ fragments [6-8]. An increased $A\beta_{42}$:$A\beta_{40}$ ratio seems to coincide with more aggressive forms of the disease compared with cases of sporadic Alzheimer disease [9] and affects synaptic activity, viability of neuronal cells, and memory formation in animals [7,8,10-12]. Minor shifts in the $A\beta_{42}$:$A\beta_{40}$ ratio have been reported to drastically influence the formation of neurotoxic oligomers [13,14]. Despite the very similar chemical nature of the two peptides, they seem to have quite different structural and biophysical properties. $A\beta_{42}$ is known to be highly fibrillogenic and more prone than $A\beta_{40}$ to form neurotoxic assemblies [13,15-17]. Different architectures of *in vitro* generated amyloid fibrils from pure $A\beta_{40}$ and $A\beta_{42}$ peptides have been revealed by nuclear magnetic resonance (NMR) [18], electron microscopy (EM) [19], and x-ray fiber diffraction methods [20-22]. A limited number of studies have demonstrated that $A\beta_{40}$ and $A\beta_{42}$ each affect the aggregation rates of the other, and it is generally reported that $A\beta_{40}$ inhibits the aggregation of $A\beta_{42}$ [12,14,23-27].

To date, most structural and biophysical studies have been performed using $A\beta_{40}$ or $A\beta_{42}$ in isolation. However, the aberrant behavior of neurotoxic Aβ peptides directed by the $A\beta_{42}$:$A\beta_{40}$ ratio requires the need to simultaneously investigate $A\beta_{40}$ and $A\beta_{42}$. In this chapter, we address how $A\beta_{40}$ and $A\beta_{42}$ influence and modulate assembly and consider how structural aspects of intermediates along the aggregation pathway can direct the cytotoxic response of $A\beta_{42}$:$A\beta_{40}$ ratios. By combining transmission electron microscopy (TEM), x-ray fiber diffraction, surface plasmon resonance (SPR), solution NMR, and high molecular weight mass spectrometry, we have characterized the start and end states of different relevant $A\beta_{42}$:$A\beta_{40}$ ratios. Using the unique combination of ^{15}N-edited and ^{15}N-filtered NMR experiments, we have been able to isolate the specific behavior of either $A\beta_{40}$ or $A\beta_{42}$ in mixtures. We show that $A\beta_{40}$ and $A\beta_{42}$ can interact and that they mutually influence their aggregation behavior. Interestingly, cross-seeding and mass spectrometry experiments reveal differences in the prefibrillar stage of aggregation, which are reflected by different aggregation kinetics.

6.2 Results

6.2.1 Direct interactions between $A\beta_{40}$ and $A\beta_{42}$

SPR was used to explore whether $A\beta_{40}$ and $A\beta_{42}$ are able to directly associate. Either biotinylated $A\beta_{40}$ or $A\beta_{42}$ were tethered to a chip and measurements of interactions between $A\beta_{40}$-$A\beta_{40}$ and $A\beta_{42}$-$A\beta_{42}$ adsorption resulted in initial fast adsorption of the Aβ peptides, followed by a slower kinetics phase of peptide binding, characteristic for high affinity binding (Figure 6.1). A similar binding profile has been reported for the aggregation and fibrillization of isolated $A\beta_{42}$, where a high incidence

of specific binding is observed between 11-mercaptoundecanoic acid tethered Aβ42 and monomeric Aβ42 in bulk solution [28]. The interaction between tethered Aβ42 with Aβ40 monomers showed a similar binding profile but slightly weaker binding. Binding between the same Aβ alloform resulted in greater mass adsorption to the sensor surface compared with mixed Aβ oligomeric interactions. These data show that the strongest binding occurs between the same alloform such as Aβ40-Aβ40 or Aβ42-Aβ42. However, strong specific binding was also observed between Aβ42-Aβ40.

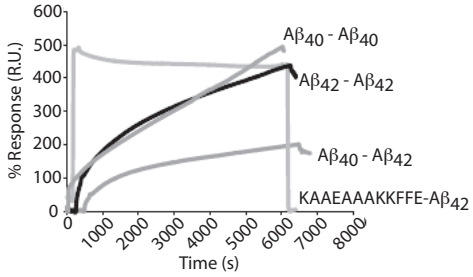

Figure 6.1 Aβ40 and Aβ42 interact directly.
10 μM covalently tethered biotinylated Aβ40 or Aβ42 to streptavidin-coated SA chips show binding between 10 μM Aβ variants. The sensorgram presents the interaction between Aβ40-Aβ42, Aβ42-Aβ42, Aβ40-Aβ40, and the negative control nonspecific binding between Aβ42-KAAEAAAKKFFE.

6.2.2 Different molar Aβ42:Aβ40 ratios are structurally similar at beginning of aggregation process

Because Aβ42 and Aβ40 were found to interact directly, we used NMR to explore whether the interactions could influence the conformation of Aβ at different Aβ42:Aβ40 ratios immediately following their preparation. The peptides were treated according to a new protocol designed to yield completely solubilized samples without solvent contamination [13]. ^{15}N-labeling of one Aβ alloform at a time allowed us to monitor the individual structural behavior of each alloform within the context of different molar ratios. The structural fingerprints of pure Aβ40 and Aβ42 peptides by the ^{15}N-^{1}H$_N$ HSQC spectra are in excellent agreement with data shown in the literature (Figure 6.2) [27,29]. The spectra of ^{15}N-labeled Aβ42 at different molar ratios do not present chemical shift variations, not even for the resonances of the C terminus, which should be the most sensitive to even a small change of environment (Figure 6.2b). This indicates that the co-presence of the two alloforms has no influence on the structure at an atomic level, as expected for the monomeric state. The same is observed for Aβ40 (Figure 6.2a). We conclude that samples with different Aβ ratios are structurally equivalent to samples of pure individual peptides prior to aggregation.

6.2.3 Fibers formed by different Aβ ratios have similar morphology and cross-β structure

Negative stain TEM was used for a morphological characterization of the end states of the Aβ aggregation reactions. Upon long term incubation, all Aβ ratios display a similar morphology with long, unbranched amyloid fibrils with detectable helicity and uniform diameters of 5.4, 10.2, and 16 nm, depending on the number of laterally associated protofilaments (Figure 6.3a). At a qualitative level, the fibrillar structure of the (3:7) ratio of Aβ42:Aβ40 appeared to be slightly more polymorphic compared with the other ratios.

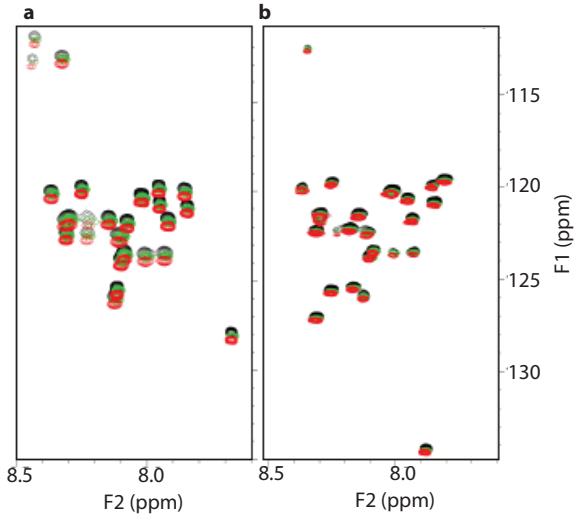

Figure 6.2 The monomeric structures of Aβ42:Aβ40 ratios are identical at atomic level. Shown is the overlay of the ^{1}H-^{15}N HSQC spectra immediately after sample preparation of (a) ^{15}N-labeled Aβ40 in pure Aβ40 sample (black), ratio 1:9(^{15}N) (green) and ratio 3:7(^{15}N) (red). (b) ^{15}N-labeled Aβ42 in pure Aβ42 sample (black), ratio 1(^{15}N):9 (red), and ratio 3(^{15}N):7 (green). For representation purposes and clarity, we have artificially introduced a systematic shift of the spectra of the 1:9 and 3:7 Aβ42:Aβ40 ratios.

X-ray fiber diffraction showed that the samples of pure Aβ and mixed ratios all exhibit the classic cross-β fiber diffraction patterns described in the literature [30,31], showing a strong meridional reflection at 4.7 Å and a major equatorial reflection at ~10 Å consistent with a cross-β architecture (Figure 6.3b). The patterns arising from Aβ40 and Aβ42 fibrils both share the same 9.7-9.8 Å major equatorial reflection, which we attribute to the β-sheet spacing perpendicular to the fiber axis. The fiber diffraction pattern obtained from Aβ42 fibrils was distinguishable from Aβ40 fibrils only by the sharper signals likely to arise from a higher degree of order in the Aβ42 fibers, whereas the mixtures of the two peptides give rise to patterns that are virtually indistinguishable from that of Aβ40. This could be due to the large amount of Aβ40 relative to Aβ42 such that the signal from Aβ40 dominates the pattern. Although subtle differences in the fiber diffraction patterns likely arise from differing degrees of order and composition of the samples, the equatorial signal positions and relative intensities of signals are largely comparable for all samples (Figure 6.3c).

To confirm structural similarity of fiber architecture of various Aβ ratios at a higher resolution, we measured the protection factors of the Aβ peptides by acquiring ^{15}N-$^{1}H_N$ HSQC spectra for monomeric Aβ40 and Aβ42 after resolubilizing amyloid fibers that were subjected to hydrogen-deuterium exchange (HDX) (Figure 6.4). Amide protection factors were measured by comparing the amide peak intensities obtained for the sample in H_2O and the sample in D_2O after the exchange period. The backbone amide chemical shift data are consistent with those previously reported in acidified DMSO-d_6 [32], although we observed (partial) overlaps in the cross-peaks of residues 11/23, 12/18, 13/27, 19/40, and 32/41 for Aβ42. Only residues 11/23 and 13/27 have overlapping cross-peaks in the Aβ40 spectrum.

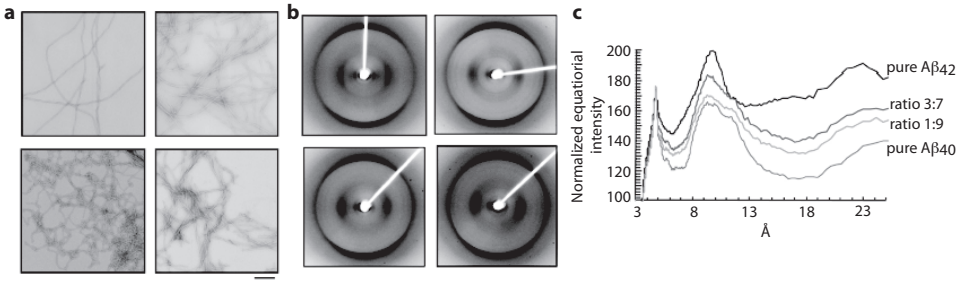

Figure 6.3 Morphology and detailed structure analysis of fibrils of Aβ42:Aβ40 ratios reveals similar structural characteristics.
(a) TEM images of Aβ ratios obtained upon aggregation for 2 weeks at 25 °C without agitation. Top left panel, pure $A\beta_{40}$; top right panel, ratio 1:9; bottom left panel, ratio 3:7; bottom right panel, pure $A\beta_{42}$. Bar, 200 nm.
(b) fiber diffraction patterns of Aβ ratios obtained upon aggregation for 4 weeks at 25 °C without agitation. Top left panel, pure $A\beta_{40}$; top right panel, ratio 1:9; bottom left panel, ratio 3:7; bottom right panel, pure $A\beta_{42}$.
(c) overlay showing the normalized x-ray scattering intensity function of D-spacing plotted from b.

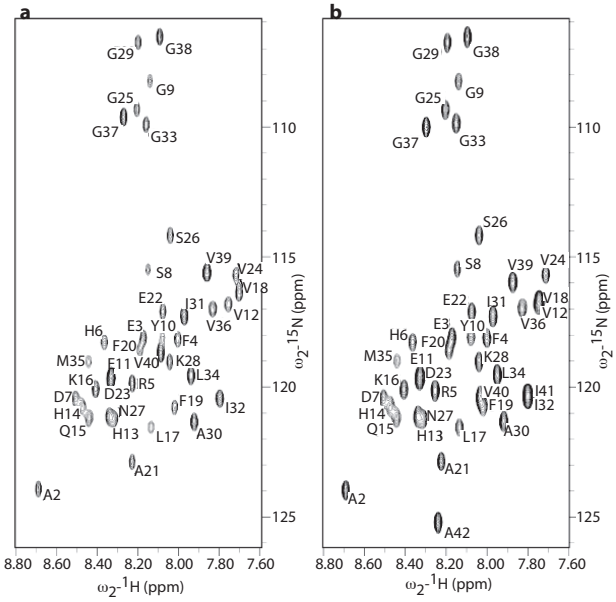

Figure 6.4 HSQC spectra obtained after redissolving Aβ fibrils in perdeuterated dimethylsulfoxide containing 0.01% deuterated trifluoroacetic acid.
(a) HSQC spectrum of ^{15}N-labeled monomeric $A\beta_{40}$ obtained from resolubilized fully protonated amyloid fibrils. The cross-peaks of residues 11/23 and 13/27 overlap in the $A\beta_{40}$ spectrum. (b) HSQC spectrum of ^{15}N-labeled monomeric $A\beta_{42}$ obtained from fully protonated fibrils. For $A\beta_{42}$, there are (partial) overlaps in the cross-peaks of residues 11/23, 12/18, 13/27, 19/40 and 32/41. The sequence-specific assignment of the peptide backbone amides is indicated next to each cross-peak. The presence of the unlabeled Aβ alloform in the mixtures does not influence the spectra as expected for monomeric peptides, since the cross-peaks of labeled peptides in the 1:9 and 3:7 ratios display identical chemical shifts. For the HDX interpretation, the intensities of the peaks are determined by the height of the spectral signals.

The HDX pattern of ^{15}N-labeled Aβ$_{40}$ for the (1:9$_{15N}$) and (3:7$_{15N}$) ratios and for pure Aβ$_{40}$ fibers shows that the stretches comprising residues 18-22 and 30-34 are more protected from solvent exchange than the N terminus (Figure 6.5). The C-terminal residues 37-40 also appear more accessible to solvent exchange. This agrees with earlier observations and proposed models for Aβ$_{40}$ fibrils [18,33-35]. The HDX patterns of ^{15}N-labeled Aβ$_{40}$, Aβ$_{42}$, and the ratios showed only small differences. Extensive exchange times (up to 672h) (Figure 6.5) of Aβ$_{42}$ showed no noticeable effects in agreement with the suggestion that Aβ$_{42}$ fibrils are highly resistant to solvent exchange [32,36]. The pattern for pure Aβ$_{42}$ and the (3$_{15N}$:7) and (1$_{15N}$:9) ratios is less distinct but indicates a clear distinction between the N- and the C-terminal halves with higher protection of the C-terminal half.

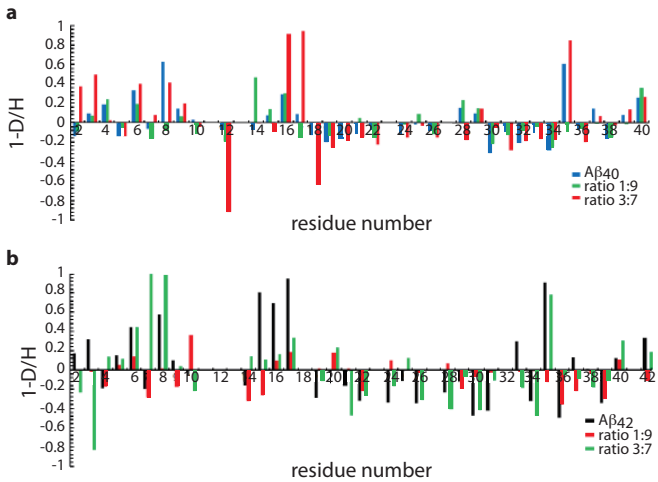

Figure 6.5 Atomic resolution HDX using NMR reveals that small differences at atomic level may be present between fibrillar Aβ ratios.
The protection factor of each residue is derived from comparing the corresponding peak intensities observed under fully protonated conditions to the signal intensities after exchange with D_2O. The results are shown as bar plots. In these plots no data is available for residues 11, 12, 13, 18, 19, 23, 27, 32, 40 and 41 for Aβ$_{42}$, and 11, 13, 23 and 27 for Aβ$_{40}$ due to (partial) overlapping peaks (and therefore ambiguous N-H cross-peak assignments).
(a) signals for the ^{15}N-labeled Aβ$_{40}$ alloform in the ratios;
(b) signals for the ^{15}N-labeled Aβ$_{42}$ alloform.

We conclude that the architecture of Aβ fibers in pure or mixed form is overall indistinguishable both at a macromolecular and high resolution level, although small differences at atomic level may be present. As these mature fibrils have been shown to have weak toxicity, we will focus on differences in the oligomeric regime.

6.2.4 Aβ$_{40}$ and Aβ$_{42}$ affect aggregation kinetics of the other

To address whether aggregation kinetics are affected by different ratios, we monitored the intensity of NMR spectra as a function of time, exploiting the disappearance of the resonances due to the increased molecular weight, typical of events in a slow exchange regime. We exploited again the possibility of ^{15}N-isotope labeling only one of the Aβ alloforms, in combination with ^{15}N-edited filter experiments to monitor

the aggregation of both the ^{15}N-labeled and unlabeled peptides simultaneously. This experimental setup offers the advantage that the individual Aβ alloforms are selectively observed in parallel and within the same sample preparation, thereby circumventing any uncertainty that might arise from different sample preparations or peptide batches. In all cases, we observed the concomitant disappearance of all peaks according to a cooperative behavior along the whole peptide or at least the region of it visible in the NMR spectrum. No sufficiently populated lower molecular weight assemblies were observed, indicating that Aβ aggregates directly into NMR invisible assemblies under these experimental conditions. Due to the long apparent lag phase, we did not detect a sigmoidal transition for Aβ40 and the (1:9) ratio over a time scale of 180 h (Figure 6.6 a,e,f). In contrast, pure Aβ42 aggregates very rapidly with a sigmoidal signal disappearance (Figure 6.6b). Interestingly, the Aβ42 component of the (1:9) ratio remains in solution significantly longer in the presence of Aβ40. The kinetics recorded for Aβ40 and Aβ42 within the (3:7) ratios with either ^{15}N-labeled Aβ42 or ^{15}N-labeled Aβ40 (named ($3_{^{15}N}$:7) and (3:$7_{^{15}N}$), respectively) indicate that Aβ40 remains longer in solution compared with Aβ42, which aggregates more rapidly (Figure 6.6 c,d). However, the complete loss of signal for Aβ42 in the presence of Aβ40 is delayed in comparison with pure Aβ42, suggesting that the shorter Aβ40 alloform reduces the aggregation propensity of the longer Aβ42 alloform. To make sure that these observations could not be explained as the average of populations containing only the same alloforms, we analyzed a (5:5) ratio where ^{15}N-labeled Aβ42 or Aβ40 are present in equimolar amounts of the unlabeled alloform (Figure 6.6 g,h). We observed a nearly simultaneous disappearance of the signals of Aβ42 and Aβ40, which strongly suggests co-aggregation of both peptides into mixed fibers. We conclude that Aβ40 and Aβ42 mutually influence the aggregation kinetics of the other.

6.2.5 Aβ40 and Aβ42 ratios both form complex but different ensembles of oligomers

To investigate whether the observed alloform influence on the aggregation arises from an impact on the formation of intermediates along the aggregation pathway, we followed aggregation of the Aβ mixtures using high molecular weight mass spectrometry, a technique that uses high voltages to enable detection of high molecular weight species. Because non-covalent complexes disassemble at these voltages, we incubated our samples prior to analysis with glutaraldehyde as cross-linking agent. The resulting masses reveal various interesting features (Figure 6.7). First, the masses of Aβ42 and of the two mixtures are consistently larger than those of Aβ40, in support of the hypothesis that there are appreciable populations of oligomers that contain both alloforms. Second, early aggregation proceeds through a monomer addition process during which oligomers gradually grow by the addition of one monomer at a time. Third, in all cases we observed that assemblies accumulate during aggregation, the maximum size of which depends on the Aβ42:Aβ40 ratio. At an incubation time of 1 h, Aβ40 samples contain oligomers with a range of sizes from dimers up to 13-mers. As the process continues, larger oligomers are formed and after 6 h of incubation, 25-mer assemblies are detected together with larger oligomers at apparent molecular weights of 186 up to 852 kDa. For (1:9) ratios, we observe formation of much smaller oligomers with a maximum of 8-mers and accumulation of larger sized oligomers at apparent molecular masses of 171 up to 515 kDa. The (3:7) ratios aggregate in a similar manner but share features closer to the pattern observed for Aβ42. No very

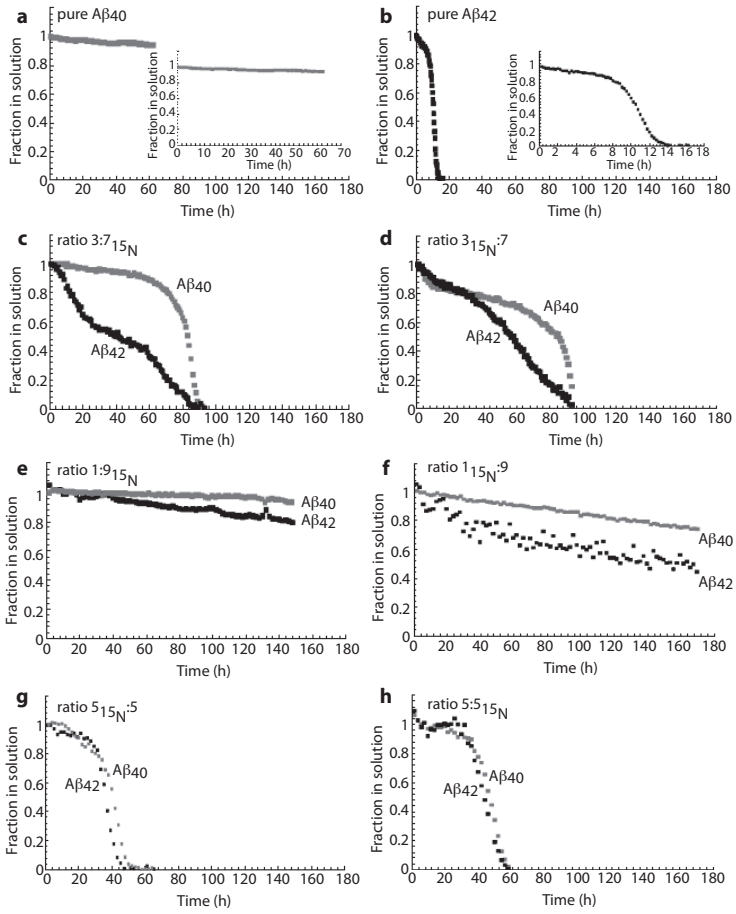

Figure 6.6 $A\beta_{40}$ and $A\beta_{42}$ show different aggregation behavior in different $A\beta_{42}$:$A\beta_{40}$ ratios.

(a) pure $A\beta_{40}$ at a concentration of 180 μM does not aggregate within the timeframe of data collection. (b) pure $A\beta_{42}$ at a concentration of 20 μM displays a lag phase and a sigmoidal transition from monomeric species into NMR invisible aggregates. (c) 3:7(^{15}N) ratio, whereby the Aβ sample is composed of 70% ^{15}N-labeled $A\beta_{40}$, which is monitored via HSQC (140 μM $A\beta_{40}$ monomer concentration) and 30% unlabeled $A\beta_{42}$ (at a monomer concentration of 60 μM), which is simultaneously monitored via the amide region ^{15}N-filtered one-dimensional NMR spectrum. (d) the 3(^{15}N):7 ratio whereby the Aβ sample is composed of 30% ^{15}N-labeled $A\beta_{42}$ and 70% unlabeled $A\beta_{40}$. (e), the 1:9(^{15}N) ratio with 10% unlabeled $A\beta_{42}$ (20 μM) and 90% ^{15}N-labeled $A\beta_{40}$ (180 μM). (f) the 1(^{15}N):9 ratio with 10% ^{15}N-labeled $A\beta_{42}$ and 90% unlabeled $A\beta_{40}$. (g) the 5(^{15}N):5 ratio whereby the ^{15}N-labeled $A\beta_{42}$ and unlabeled $A\beta_{40}$ are present in equimolar amounts (60 μM of each alloform). (h) the 5:5(^{15}N) ratio whereby equimolar amounts (60 μM) of unlabeled $A\beta_{42}$ and ^{15}N-labeled $A\beta_{40}$ are present. The grey symbols represent $A\beta_{40}$, and the black symbols correspond to $A\beta_{42}$.

large molecular weight oligomers are observed after 6 h of incubation, presumably because they become so large that either they cannot become mobile or are not efficiently cross-linked. These results reveal clear differences in the pattern of small oligomeric species formed under different ratio conditions, indicating a potential basis for the difference in toxic effect [13].

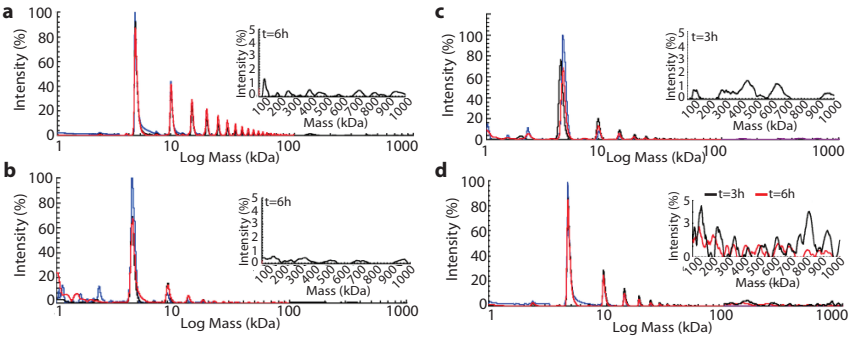

Figure 6.7 Oligomer formation by Aβ42:Aβ40 ratios shows a monomer addition process and a dynamic distribution of oligomeric species.
Mass spectra of the different ratios with the high molecular weight detection spectra as insets whereby the blue trace is t = 1 h, the black trace is t = 3 h, and the red trace is t = 6 h. (a) pure Aβ40; (b) 1:9 ratio; (c) 3:7 ratio; (d) pure Aβ42.

6.2.6 Differences between Aβ42:Aβ40 ratios reside along the aggregation pathway

The influence of the Aβ40 and Aβ42 ratios on aggregation kinetics is also evident from cross-seeding experiments where sonicated protofibrils were added to monomeric solutions of different Aβ42:Aβ40 ratios. Seed preparations were verified by TEM (Figure 6.8a) and added to freshly prepared monomeric Aβ solutions. The aggregation kinetics were followed by *in situ* thioT fluorescence (Figure 6.8 b-e). Aβ40 aggregation was efficiently seeded by Aβ40 seeds and the (1:9) ratio seeds leading to elimination of the lag phase (Figure 6.8b). The initial parts of the two curves overlap, indicating that the properties of Aβ40 are predominant, also in the (1:9) mixture. Addition of (3:7) seeds also induces aggregation, but some lag phase is retained. Addition of pure Aβ42 not only does not seed aggregation, but even lengthens the lag phase. Seeding of Aβ40 therefore appears to proceed in a highly specific manner with preference for the same alloform seeds. The (1:9) ratio is seeded by any seed but, as for pure Aβ40, Aβ40 and (1:9) seeds have a similar strong seeding effect, whereas Aβ42 and (3:7) seeds have a milder effect, which, however, still preferentially selects the same alloform (Figure 6.8c). In contrast, pure Aβ42 and the (3:7) ratio were equally effectively seeded by any Aβ seed, regardless of whether they were formed from Aβ40 or Aβ42 or a mixture (Figure 6.8 d,e). Therefore, it appears that Aβ42 monomers have a higher degree of plasticity so that they may use a less specific surface as a template, whereas Aβ40 oligomers have higher selectivity.

The effect of cross-seeding on the disappearance of the NMR signals of the different Aβ alloforms was also studied. In these experiments, we limited ourselves to the addition of seeds of pure Aβ40 or pure Aβ42 to the preincubated samples of which the NMR signals were monitored. In all cases, adding seeds resulted in appreciable aggregation irrespectively of the time point at which the addition was made. The control experiments were performed without any addition and this ensured that the effect is the direct consequence of the addition. Pure Aβ42 monomers could be easily seeded by both peptides (Figure 6.9 c,d). Induction of aggregation of Aβ40 with Aβ40 seeds was also highly efficient (Figure 6.9b), whereas Aβ42 seeds induced some initial signal disappearance but with a delayed aggregation (Figure 6.9a).

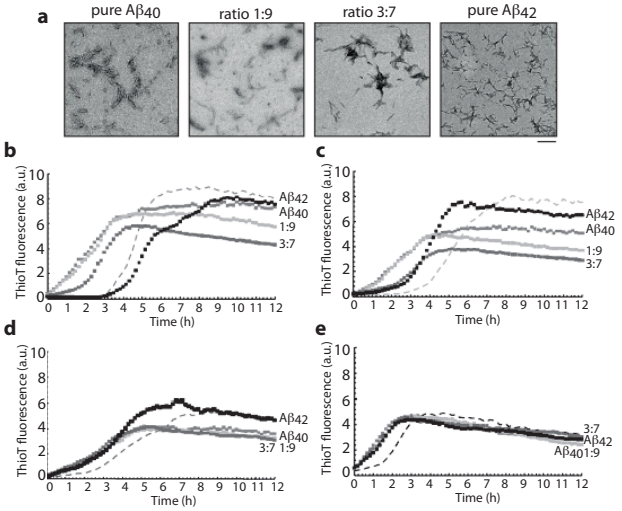

Figure 6.8 Cross-seeding reveals that $A\beta_{42}$ oligomers show plasticity, whereas $A\beta_{40}$ oligomers display a higher selectivity.

(a) TEM of seed preparations. Seeds were prepared by incubation of 50 μM Aβ ratios for 24 h followed by sonication at maximum power for 10 min. From left to right: pure $A\beta_{40}$, ratio 1:9; ratio 3:7, pure $A\beta_{42}$. Bar, 0.2 μm. Freshly prepared seeds were added to monomeric solutions of $A\beta_{42}$:$A\beta_{40}$ ratios at final concentrations of 0.5 μM and 25 μM, respectively. (b) thioT of $A\beta_{40}$ monomers seeded with pure $A\beta_{40}$ seeds; with seeds from ratio 1:9, with seeds from ratio 3:7, and with seeds from pure $A\beta_{42}$. The dashed line represents the unseeded $A\beta_{40}$ control. (c) thioT of ratio 1:9 monomers seeded with Aβ ratios as compared with the non-seeded aggregation curve. (d) thioT of ratio 3:7 monomers seeded with Aβ ratios as compared with the non-seeded aggregation curve (dashed line). (e) thioT of $A\beta_{42}$ monomers seeded with Aβ ratios in comparison with the non-seeded sample (dashed line).

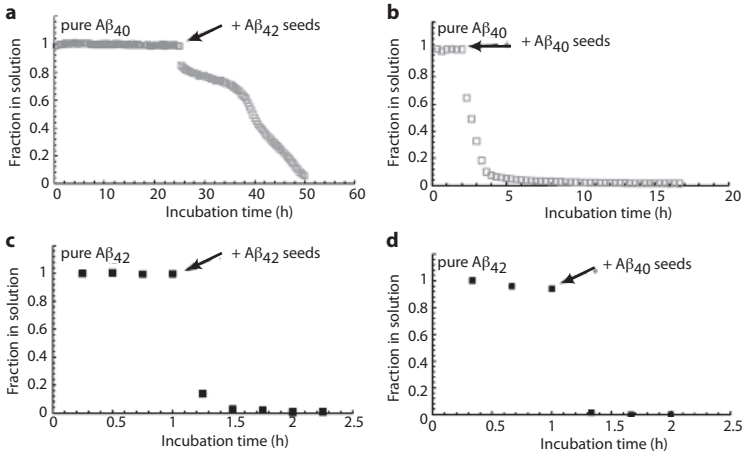

Figure 6.9 Cross-seeding was monitored by NMR by recording one-dimensional proton spectra as a function of time

(a,b) with unlabeled pure $A\beta_{40}$ and (c,d) pure $A\beta_{42}$ monomers using preformed $A\beta_{40}$ seeds (b,d) and $A\beta_{42}$ seeds (a,c). Pure $A\beta_{40}$ samples (grey) were prepared at a concentration of 180 μM, whereas pure $A\beta_{42}$ samples (black) were at a concentration of 20 μM. The addition of 10% (v/v) of a 50 μM (monomeric equivalent) seed preparation was added at the time points indicated by the arrow.

In the (1:9) and (3:7) ratios, Aβ40 seeds could efficiently induce aggregation of the two Aβ alloforms in the mixtures, while the Aβ42 seeds efficiently seeded the Aβ42 alloform, whereas the Aβ40 alloform lags behind in the aggregation. This implies that the presence of Aβ42 monomers in the ratios influences the behavior of the Aβ40 alloform. Overall, it is observed that the Aβ40 seeds can efficiently induce aggregation of Aβ samples, whereas the Aβ40 alloform responds less efficiently to the Aβ42 seeds (Figure 6.10 and Table 6.1). These data show a genuine difference between the two peptides at the level of the oligomeric state. They reveal that even a relatively small increase in Aβ42 in the mixture confers aggregation properties to Aβ40 that are markedly more similar to pure Aβ42.

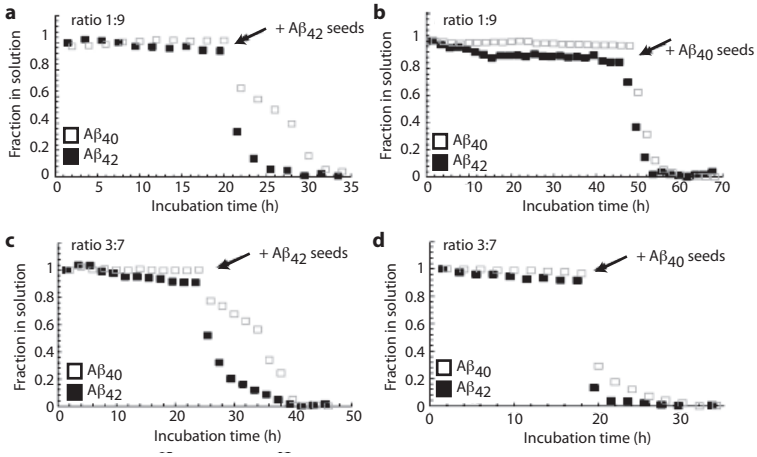

Figure 6.10 Cross-seeding was monitored by ^{15}N-filtered and ^{15}N-edited NMR experiments. with Aβ samples composed of the (a,b) Aβ42:Aβ40 ratio 1(^{15}N):9, whereby 20 μM ^{15}N-labeled Aβ42 is present with 180 μM unlabeled Aβ40 and the (c,d) Aβ42:Aβ40 ratio 3(^{15}N):7 with 60 μM ^{15}N-labeled Aβ42 and 140 μM unlabeled Aβ40. The addition of 10% (v/v) of a 50 μM (monomeric equivalent) preparation of preformed Aβ40 seeds (b,d) and Aβ42 seeds (a,c) is indicated by the arrows.

Efficiency of seeding monitored by NMR			
Monomeric sample	seeds	Aβ42	Aβ40
pure Aβ42	Aβ40	+++	NA
	Aβ42	+++	NA
Aβ42:Aβ40 3:7	Aβ40	+++	+++
	Aβ42	+++	+
Aβ42:Aβ40 1:9	Aβ40	+++	+++
	Aβ42	+++	+
pure Aβ40	Aβ40	NA	+++
	Aβ42	NA	+

Table 6.1 Efficiency of cross-seeding on Aβ alloforms as monitored by isotope-labeled NMR

NA not applicable, + seeding induces aggregation, +++ seeding induces aggregation very efficiently.

6.3 Discussion

Although previous structural studies have mostly focused on pure Aβ alloforms and the identification of a single oligomeric species, the present work aims to understand the determinants of the toxicity of different $A\beta_{42}$:$A\beta_{40}$ ratios. We demonstrate by independent evidence from mass spec, NMR, and SPR that the two peptides interact, although recognition between the same alloforms is preferred over interactions between different ones. We therefore expect that the populations of the two peptides in the aggregates will be mixed. This explains and expands previous data [23,25,27] that indicate that $A\beta_{40}$ and $A\beta_{42}$ influence their respective aggregation properties.

To understand which step along the aggregation pathway is responsible for this effect, we compared the structures and morphologies of all the species formed. We show that the initial monomeric and final fibrillar states do not differ to a large extent. NMR analysis of freshly prepared samples at different $A\beta_{42}$:$A\beta_{40}$ ratios conclusively reveals the presence of predominant monomeric species that lack a regular and well defined structure. Therefore, at this stage, the peptides are not affected by the presence of the other alloform. Likewise, we do not observe appreciable differences between the mature fibrillar states by TEM, HDX, and fiber diffraction: fibers formed during long incubation times are virtually identical. The absence of significant differences in the start and end points of Aβ fibrillation directed our focus to the formation of transient oligomeric intermediates. Previous data had indicated differences in the protofibrillar morphologies and FTIR data following short term incubation, which, together with the present data, underline the importance of the aggregation pathway and of the dynamics of the oligomeric state [13,37,38].

We observed subtle but clear differences between the different Aβ ratios along the aggregation pathway. NMR experiments visualizing the spontaneous aggregation (Figure 6.6) showed that the presence of monomeric $A\beta_{40}$ slows down the aggregation kinetics of $A\beta_{42}$, increasing the time frame that soluble forms are found in solution for any peptide ratio. *Vice versa* $A\beta_{42}$ stimulates $A\beta_{40}$ aggregation as revealed by comparing the (3:7) and (1:9) ratios with pure $A\beta_{40}$. This is compatible with the view that $A\beta_{42}$ drives aggregation and acts as a template by lowering the kinetic barriers that prevent $A\beta_{40}$ from aggregating [15,25,39]. $A\beta_{40}$ potentially delays $A\beta_{42}$ aggregation through "non-productive" interactions. Although these conclusions are in agreement with previous reports [25,27,39], our cross-seeding data suggest that $A\beta_{40}$ monomers specifically require $A\beta_{40}$ oligomers to induce growth of mature fibrils, whereas $A\beta_{42}$ monomers are less selective and are stimulated by all types of seeds.

It might be argued that there is an apparent discrepancy between the progressive Aβ aggregation as monitored by NMR (Figure 6.6) and the cross-seeding data (Figure 6.8, 6.7, 6.8). By NMR, we observe that $A\beta_{42}$ stimulates $A\beta_{40}$ to aggregate while $A\beta_{40}$ simultaneously delays $A\beta_{42}$ aggregation. Vice versa, the cross-seeding data reveal that monomeric $A\beta_{40}$ is not efficiently seeded by sonicated $A\beta_{42}$ protofibrils. It is reasonable to explain this discrepancy by assuming that the oligomers formed during the aggregation process have features that are distinct from the sonicated protofibrillar species (seeds) that may have undergone advanced structural maturation. For pure $A\beta_{42}$, these seeds would not be the optimal templates to directly incorporate $A\beta_{40}$ monomers and perhaps even entail a conformational restructuring to lead to productive aggregation. We cannot rule out the possibility that monomeric $A\beta_{40}$

could be able to resolubilize Aβ42 seeds, thereby bringing Aβ42 into solution and promoting in this way productive aggregation, as hinted by Yan and Wang [27]. Because our observations with high molecular weight mass spectrometry underline that the aggregation process proceeds through a monomer addition mechanism, the dynamic interplay (productive and non-productive) of monomeric Aβ with soluble Aβ assemblies seems appropriate to explain toxicity of the Aβ42:Aβ40 ratios. This relevance of monomer addition processes for neurotoxicity was recently described by Jan and colleagues for pure Aβ42 aggregation [37]. Thus, the modulation of the Aβ oligomer formation by the Aβ42:Aβ40 ratio adds to the cause of neurotoxicity and the Alzheimer disease pathology.

In conclusion, our work indicates that the Aβ42:Aβ40 ratio behavior cannot be simply interpreted by stating that Aβ42 can induce Aβ40 aggregation while at the same time, Aβ40 can prevent or delay Aβ42 aggregation. Rather than the morphology of the amyloid fibrils, the Aβ42:Aβ40 ratio modulates the Aβ oligomer formation. Our data indicate that neurotoxicity is more likely to be explained by the dynamic nature of the ongoing Aβ aggregation rather than by the prevailing view that Aβ toxicity is associated with a distinct assembly. A change in the Aβ42:Aβ40 ratio induces differences in conformational plasticity of the oligomeric peptide mixtures and the pattern of detectable oligomeric species. That the oligomer formation along the amyloid assembly pathway is affected by the different Aβ ratios emphasizes the necessity to further expand our understanding of the exact compositional, temporal, and structural properties of the homo- and hetero-oligomers. The implications of this finding for Alzheimer disease therapy are fundamental: the results imply that it is less important to focus on lowering the total amyloid burden in patients, although it appears crucial to affect the relative ratios of the peptides.

6.4 Experimental procedures

6.4.1 Preparation of Aβ Peptide Ratios

The Aβ40 and Aβ42 peptides and their uniformly ^{15}N-labeled variants were purchased from rPeptide. The Aβ40 and Aβ42 peptides were combined in monomeric form in the desired ratios as described in detail in chapter 2. In brief, Aβ peptides were dissolved in HFIP, Aβ42 and Aβ40 were then mixed in molar ratios of 1:9 and 3:7 together with pure Aβ42 and Aβ40 samples, and after evaporation of HFIP, they were redissolved in DMSO. The peptide was passed through a desalting column and eluted in a 50mM Tris, 1mM EDTA buffer, pH 7.5. Peptide concentrations were measured by the Bradford assay or by UV absorbance at 280 nm (ε_{280}=1490 $M^{-1}cm^{-1}$). The samples were kept on ice until required, with a maximum lag time of 30 min.

6.4.2 SPR Analysis

N-terminally labeled biotin-linker chain Aβ40 (biotin-Aβ40) and biotin-Aβ42 and Aβ40, Aβ42, and a non-assembling peptide with the sequence KAAEAAAKKFFE [40] were treated as described above except using a 10mM HEPES, 100mM NaCl, 1mM EDTA, and 0.05mM NaN3, pH7.4 buffer, and the peptide was eluted using a 2-ml Zeba spin column for buffer exchange. SPR measurements were carried out on a Biacore® 2000 system using carboxymethylated dextran preimmobilized

with streptavidin sensor chips. A volume of 150 μl of biotin-Aβ$_{40}$ or biotin-Aβ$_{42}$ was immobilized to the sensor surface at a concentration of 10 μM at a flow rate of 30 μl min^{-1}. Concentrations of 10 μM of Aβ$_{40}$, Aβ$_{42}$ or KAAEAAAKKFFE were injected at 3 μl min^{-1}. Measurements were done in triplicate and analyzed with the built-in BIAevaluation software. Curve fitting relied on the Marquardt-Levenberg algorithm, and the change in response was fitted to the binding isotherm $R_{eq} = R_{max}[A]/((k_{off}/k_{on})+[A])$, where R_{eq} is the equilibrium response, R_{max} is the maximum signal response, [A] is the analyte concentration, k_{off} is the dissociation rate constant, and kon is the association rate constant.

6.4.3 Fiber Diffraction

Samples of mature fibers were aligned by suspending a droplet of solution at 4 mg/ml between two waxtipped capillaries positioned end-to-end. Fibers were mounted on a goniometer head, and x-ray diffraction data were collected using a Rigaku CuKα rotating anode with a wavelength of 1.5419 Å and RAxis IV++ detector. Specimen to detector distances were 160 and 250 mm with an exposure time of 10 min. Diffraction patterns were examined in CLEARER [41]. For additional inspection, meridional, and equatorial axes signals were sampled through an angular search width of 60°, exported as a function of distance (pixels), and plotted using Braggs Law.

6.4.4 TEM Analysis

Aliquots of 4 μl Aβ were adsorbed for 30 s onto freshly prepared carbon-coated and glow-discharged copper grids, washed briefly with milli-Q water, and subsequently stained with 1% (w/v) uranyl acetate for 30 s. Samples were examined with a JEOL 1200 transmission electron microscope operating at 100 KV.

6.4.5 Cross-seeding Monitored with thioT

Aliquots (100 μl) of each Aβ ratio at 50 μM were incubated at 25 °C in 50mM Tris, 1 mM EDTA, pH 7.5. After 24 h incubation these samples were sonicated at 4 °C for 10 min at maximum power and mixed with freshly and simultaneously prepared Aβ ratios to induce (cross)-seeding of Aβ aggregation. Final concentrations in these mixtures were 0.5 μM of sonicated Aβ and 25 μM of monomeric Aβ. The seed preparations were examined by TEM.

6.4.6 ThioT Fluorescence

A peptide samples of 25 μM were incubated with 12 μM thioflavin T (thioT) in a total volume of 150 μl. Fibrillization kinetics were followed using a Fluostar OPTIMA fluorescence plate reader using 440 nm excitation wavelength and an emission wavelength of 480 nm. Readings were recorded in triplicate every 10 min for a period of 24 h.

6.4.7 High Molecular Weight MS

High mass measurements were performed at CovalX AG using an ABI 4800 MALDI TOF mass spectrometer retrofitted with CovalX HM2 TUVO high mass system. A phosphate-buffered saline buffer was used to prepare the Aβ ratios, which were subjected to cross-linking with gluteraldehyde at specific time points. Each sample was

mixed with sinapinic acid matrix (10 mg ml^{-1}) in acetonitrile/water (1:1, v/v), TFA 0.1% and spotted on the MALDI plate. High-mass MALDI TOF MS analysis was performed using standard nitrogen laser and focusing on different mass ranges from 8 to 1000 kDa in linear and positive mode and at a gain voltage of 3.14 kV and an acceleration voltage of 20 kV for HM2 High-Mass detection. The instrument was calibrated using insulin, BSA, and IgG. The analysis was repeated in triplicate.

6.4.8 Solution NMR

Aβ samples for NMR studies varied between 20 and 200 μM (monomer concentration) in 50mM Tris-HCl, 1mM EDTA at pH 7.5, supplemented with 10% (v/v) D_2O. The experiments were performed at 25 °C either on a Bruker Avance (equipped with cryoprobe) or on a Varian Inova spectrometer both operating at 14.1 Tesla (600 MHz). ^{15}N sofast heteronuclear single quantum coherence (HSQC) spectra were each collected over 30 min to monitor aggregation. ^{15}N NOESY-HSQC and $^{1}H,^{1}H$ TOCSY experiments were recorded at 5 °C to obtain sequence specific $^{1}H_N,^{15}N$ assignments to identify the HSQC peaks. A combination of ^{15}N-edited and ^{15}N-filtered experiments [42] acquired on samples containing uniformly ^{15}N-labeled and unlabeled Aβ peptides at different ratios was used to selectively monitor Aβ42 and Aβ40 in solution. Protection factors of mature Aβ fibers were measured by comparing the amide peak intensities obtained for Aβ samples incubated in H_2O or in D_2O after for a period of 672 h to allow amide exchange. The fibers were collected by centrifugation, washed, and incubated in D_2O at 25 °C for 48 h, flash-frozen to quench the hydrogen-deuterium exchange (HDX), lyophilized, and redissolved in 100% DMSO-d_6 acidified with 0.1% (v/v) trifluoroacetic acid for 30 s, followed by a 10-fold dilution with perdeuterated DMSO [32]. Amide exchange was measured by collecting two-dimensional ^{15}N-^{1}H HSQC spectra in comparison to control samples that were incubated in H_2O. The ^{15}N-^{1}H HSQC cross-peak assignment was confirmed with a ^{15}N-resolved NOESY experiment.

6.4.9 Cross-seeding Monitored via NMR

Seeds were prepared of pure Aβ40 or pure Aβ42 as described above. An aliquot of 30 μl seeds (50 μM equivalent monomeric concentration) was mixed with 330 μl of the corresponding Aβ samples that were preincubated in an NMR tube, whereas the non-seeded signals were monitored. ^{15}N-edited and ^{15}N-filtered spectra [42] were acquired as a function of time to simultaneously monitor both Aβ alloforms in the 1:9 and 3:7 ratios, whereby Aβ42 was ^{15}N-labeled and Aβ40 was unlabeled. Only one-dimensional proton spectra were recorded as a function of time for the pure Aβ40 or pure Aβ42 unlabeled samples.

AUTHOR CONTRIBUTION

AV contributed to this manuscript by performing cross-seeding experiments, obtaining transmission electron microscopy images and by discussing data.

6.5 References

[1] McLean C, Cherny R, Fraser F, Fuller S, Smith M, Beyreuther K (1999). Soluble pool of Aβ amyloid as a determinant of severity of neurodegeneration in Alzheimer disease. *Ann. Neurol.*, 46:860-866.

[2] Lambert M, Barlow A, Chromy B, Edwards C, Freed R, Liosatos M, Morgan T, Rozovsky I, Trommer B, Viola K, Wals P, Zhang C, Finch C, Krafft G, Klein W (1998). Diffusible, nonfibrillar ligands derived from Aβ1-42 are potent central nervous system neurotoxins. *Proc. Natl. Acad. Sci. USA*, 95:6448-6453.

[3] Klyubin I, Betts V, Welzel A, Blennow K, Zetterberg H, Wallin A, Lemere C, Cullen W, Peng Y, Wisniewski T, Selkoe D, Anwyl R, Walsh D, Rowan M (2008). Amyloid β protein dimer- containing human CSF disrupts synaptic plasticity: prevention by systemic passive immunization. *J. Neurosci.*, 28:4231-4237.

[4] Shankar G, Li S, Mehta T, Garcia-Munoz A, Shepardson N, Smith I, Brett F, Farrell M, Rowan M, Lemere C, Regan C, Walsh D, Sabatini B, Selkoe D (2008). Amyloid β protein dimers isolated directly from Alzheimer brains impair synaptic plasticity and memory. *Nat. Med.*, 14:837-842.

[5] Lashuel H, Hartley D, Petre B, Walz T, Lansbury P (2002). Neurodegenerative disease: amyloid pores from pathogenic mutations. *Nature*, 418:291.

[6] Suzuki N, Cheung T, Cai X, Odaka A, Otvos L, Eckman C, Golde T, Younkin S (1994). An increased percentage of long amyloid β protein secreted by familial amyloid β protein precursor (β APP717) mutants. *Science*, 264:1336-1340.

[7] Duff K, Eckman C, Zehr C, Yu X, Prada C, Perez-Tur J, Hutton M, Buee L, Harigaya Y, Yager D, Morgan D, Gordon M, Holcomb L, Refolo L, Zenk B, Hardy J, Younkin S (1996). Increased amyloid β42(43) in brains of mice expressing mutant presenilin 1. *Nature*, 383:710-713.

[8] Scheuner D, Eckman C, Jensen M, Song X, Citron M, Suzuki N, Bird T, Hardy J, Hutton M, Kukull W, Larson E, Levy-Lahad E, Viitanen M, Peskind E, Poorkaj P, Schellenberg G, Tanzi R, Wasco W, Lannfelt L, Selkoe D, Younkin S (1996). Secreted amyloid β protein similar to that in the senile plaques of Alzheimer disease is increased in vivo by the presenilin 1 and 2 and APP mutations linked to familial Alzheimer disease. *Nat. Med.*, 2:864-870.

[9] Hellström-Lindahl E, Viitanen M, Marutle A (2009). Comparison of Aβ levels in the brain of familial and sporadic Alzheimer disease. *Neurochem. Int.*, 55:243-252.

[10] Citron M, Westaway D, Xia W, Carlson G, Diehl T, Levesque G, Johnson-Wood K, Lee M, Seubert P, Davis A, Kholodenko D, Motter R, Sherrington R, Perry B, Yao H, Strome R, Lieberburg I, Rommens J, Kim S, Schenk D, Fraser P, St George-Hyslop P, Selkoe D (1997). Mutant presenilins of Alzheimer disease increase production of 42-residue amyloid β protein in both transfected cells and transgenic mice. *Nat. Med.*, 3:67-72.

[11] Mann D, Iwatsubo T, Cairns N, Lantos P, Nochlin D, Sumi S, Bird T, Poorkaj P, Hardy J, Hutton M, Prihar G, Crook R, Rossor M, Haltia M (1996). Amyloid β protein (Aβ) deposition in chromosome 14-linked Alzheimer disease: predominance of Aβ42(43). *Ann. Neurol.*, 40:149-156.

[12] Wang R, Wang B, He W, Zheng H (2006). Wild-type presenilin1 protects against Alzheimer disease mutation-induced amyloid pathology. *J. Biol. Chem.,* 281:15330-15336.

[13] Kuperstein I, Broersen K, Benilova I, Rozenski J, Jonckheere W, Debulpaep M, Vandersteen A, Segers-Nolten I, van der Werf K, Subramaniam V, Braeken D, Callewaert G, Bartic C, D'Hooge R, Martins I, Rousseau F, Schymkowitz J, and De Strooper B (2010). Neurotoxicity of Alzheimer disease Aβ peptides is induced by small changes in the $A\beta_{42}$ to $A\beta_{40}$ ratio. *EMBO J.,* 29:3408-4320.

[14] Yoshiike Y, Chui D, Akagi T, Tanaka N, Takashima A (2003) Specific compositions of amyloid β peptides as the determinant of toxic β aggregation. *J. Biol. Chem.,* 278:23648-23655.

[15] Jarrett J & Lansbury P (1993). Seeding "one-dimensional crystallization" of amyloid: a pathogenic mechanism in Alzheimer disease and scrapie? *Cell,* 73:1055-1058.

[16] Bitan G, Vollers S, Teplow D (2003). Elucidation of primary structure elements controlling early amyloid β protein oligomerization. *J. Biol. Chem.*, 278:34882-34889.

[17] Chen Y & Glabe C (2006). Distinct early folding and aggregation properties of Alzheimer amyloid β peptides Aβ40 and Aβ42: stable trimer or tetramer formation by Aβ42. *J. Biol. Chem.*, 281:24414-24422.

[18] Petkova A, Ishii Y, Balbach J, Antzutkin O, Leapman R, Delaglio F, Tycko R (2002). A structural model for Alzheimer β amyloid fibrils based on experimental constraints from solid state NMR. *Proc. Natl. Acad. Sci. USA*, 99:16742-16747.

[19] Schmidt M, Sachse C, Richter W, Xu C, Fändrich M, Grigorieff N (2009). Comparison of Alzheimer Aβ(1-40) and Aβ(1-42) amyloid fibrils reveals similar protofilament structures. *Proc. Natl. Acad. Sci. USA*, 106:19813-19818.

[20] Kirschner D, Abraham C, Selkoe D (1986). X-ray diffraction from intraneuronal paired helical filaments and extraneuronal amyloid fibers in Alzheimer disease indicates cross-β conformation. *Proc. Natl. Acad. Sci. USA*, 83:503-507.
[21] Malinchik S, Inouye H, Szumowski K, Kirschner D (1998). Structural analysis of Alzheimer β(1-40) amyloid: protofilament assembly of tubular fibrils. *Biophys. J.,* 74:537-545.
[22] Sikorski P, Atkins E, Serpell L (2003). Structure and texture of fibrous crystals formed by Alzheimer Aβ(11–25) peptide fragment. *Structure*, 11:915-926.
[23] Snyder S, Ladror U, Wade W, Wang G, Barrett L, Matayoshi E, Huffaker H, Krafft G, Holzman T (1994). Amyloid β aggregation: selective inhibition of aggregation in mixtures of amyloid with different chain lengths. *Biophys. J.*, 67:1216-1228.
[24] Frost D, Gorman P, Yip C, Chakrabartty A (2003). Co-incorporation of Aβ40 and Aβ42 to form mixed prefibrillar aggregates. *Eur. J. Biochem.,* 270:654-663.
[25] Jan A, Gokce O, Luthi-Carter R, Lashuel H (2008). The ratio of monomeric to aggregated forms of Aβ40 and Aβ42 is an important determinant of amyloid-β aggregation, fibrillogenesis, and toxicity. *J. Biol. Chem.*, 283:28176-28189.
[26] Kim J, Onstead L, Randle S, Price R, Smithson L, Zwizinski C, Dickson D, Golde T, McGowan E (2007). Aβ40 inhibits amyloid deposition in vivo. *J. Neurosci.*, 27:627-633.
[27] Yan Y & Wang C (2007). Aβ40 protects non-toxic Aβ42 monomer from aggregation. *J. Mol. Biol.,* 369:909-916.
[28] Ryu J, Joung H, Kim M, Park C (2008). Surface plasmon resonance analysis of Alzheimer β-amyloid aggregation on a solid surface: from monomers to fully grown fibrils. *Anal. Chem.*, 80:2400-2407.
[29] Hou L, Shao H, Zhang Y, Li H, Menon N, Neuhaus E, Brewer J, Byeon I-J, Ray D, Vitek M, Iwashita T, Makula R, Przybyla A, Zagorski M (2004). Solution NMR studies of the Aβ(1- 40) and Aβ(1-42) peptides establish that the Met-35 oxidation state affects the mechanism of amyloid formation. *J. Am. Chem. Soc.*, 126:1992–2005.
[30] Eanes E & Glenner G (1968). X-ray diffraction studies on amyloid filaments. *J. Histochem. Cytochem.,* 16:673-677.
[31] Makin O & Serpell L (2005). Structures for amyloid fibrils. *FEBS J.,* 272:5950-5961.
[32] Luhrs T, Ritter C, Adrian M, Riek-Loher D, Bohrmann B, Döbeli H, Schubert D, Riek R (2005). Three-dimensional structure of Alzheimer amyloid-β(1-42) fibrils. *Proc. Natl. Acad. Sci. USA,* 102:17342-17347.
[33] Whittemore N, Mishra R, Kheterpal I, Williams A, Wetzel R, Serpersu E (2005). Hydrogen-deuterium (H/D) exchange mapping of Aβ1–40 amyloid fibril secondary structure using nuclear magnetic resonance spectroscopy. *Biochemistry,* 44:4434-4441.
[34] Olofsson A, Lindhagen-Persson M, Sauer-Eriksson A, Ohman A (2007). Amide solvent protection analysis demonstrates that amyloid-β(1-40) and amyloid-β(1-42) form different fibrillar structures under identical conditions. *Biochem. J.,* 404:63-70.
[35] Wetzel R, Shivaprasad S, Williams A (2007). Plasticity of amyloid fibrils. *Biochemistry* 46:1-10.
[36] Olofsson A, Sauer-Eriksson A, Ohman A (2006). The solvent protection of Alzheimer amyloid β-(1-42) fibrils as determined by solution NMR spectroscopy. *J. Biol. Chem.,* 281:477-483.
[37] Jan A, Adolfsson O, Allaman I, Buccarello A, Magistretti P, Pfeifer A, Muhs A, Lashuel H (2011). Aβ42 neurotoxicity is mediated by ongoing nucleated polymerization process rather than by discrete Aβ42 species. *J. Biol. Chem.,* 286:8585-8596.
[38] Wogulis M, Wright S, Cunningham D, Chilcote T, Powell K, Rydel R (2005). Nucleation-dependent polymerization is an essential component of amyloid-mediated neuronal cell death. *J. Neurosci.,* 25:1071-1080.
[39] Myszka D, Wood S, Biere A (1999). Analysis of fibril elongation using surface plasmon resonance biosensors. *Methods Enzymol.,* 309:386-402.
[40] Marshall K, Morris K, Charlton D, O'Reilly N, Lewis L, Walden H, Serpell L (2011). Hydrophobic, aromatic, and electrostatic interactions play a central role in amyloid fibril formation and stability. *Biochemistry*, 50:2061-2071.
[41] Makin O, Sikorski S, Serpell L (2007). CLEARER: a new tool for the analysis of x-ray fibre diffraction patterns and diffraction simulation from atomic structural models. *J. Appl. Cryst.*, 40:966-972.
[42] Ikura M & Bax A (1992). Isotope-filtered 2D NMR of a protein-peptide complex: study of a skeletal muscle myosin light chain kinase fragment bound to calmodulin. *J. Am. Chem. Soc.*, 114:2433-2440.

7

The mechanism of γ-secretase dysfunction in familial Alzheimer disease.

The mechanisms by which mutations in the presenilins or the amyloid precursor protein genes cause familial Alzheimer disease are controversial. Those mutations increase the release of $A\beta_{42}$ relative to $A\beta_{40}$ by an unknown, possibly gain-of-toxic-function, mechanism. However, many PS mutations paradoxically impair γ-secretase and 'loss-of-function' mechanisms have also been postulated. Here, we use kinetic studies to demonstrate that mutations related to familial Alzheimer disease affect Aβ generation via three different mechanisms, resulting in qualitative changes in the Aβ profiles, which are not limited to $A\beta_{42}$. Loss of ε-cleavage function is not generally observed among the mutations related to familial Alzheimer disease. On the other hand, γ-secretase inhibitors used in the clinic appear to block the initial ε-cleavage step, but unexpectedly affect more selectively Notch than APP processing, while modulators act as activators of the carboxypeptidase-like (γ) activity. Overall, this chapter provides a coherent explanation for the effect of different FAD mutations, demonstrating the importance of qualitative rather than quantitative changes in the Aβ products, and suggest fundamental improvements for current drug development efforts.

The results described in this chapter have been published in:
Chávez-Gutiérrez L, Bammens L, Benilova I, Vandersteen A, Benurwar M, Borgers M, Lismont S, Zhou L, Van Cleynenbruegel S, Esselmann H, Wiltfang J, Serneels L, Karran E, Gijsen H, Schymkowitz J, Rousseau F, Broersen K, and De Strooper B (2012). *EMBO J.*, 31:2261-2274.

7.1 Introduction

A central and still unresolved debate with important therapeutic implications in the field of Alzheimer disease research revolves around the question of how mutations in presenilin (PS), the catalytic core of the γ-secretases [1], cause disease. More than 150 familial Alzheimer disease mutations have been mapped to the genes encoding *PS1* or *PS2* (http://www.molgen.ua.ac.be/ADMutations), pointing to a crucial role of the γ-secretase complexes in the disease. As a rule, PS mutations leading to familial Alzheimer disease increase the relative amount of $A\beta_{42}$ versus $A\beta_{40}$ in *in vivo* and *in vitro* paradigms [2-5], which led to propose that PS mutations act via a toxic gain-of-function mechanism. However, more refined analyses have made clear that the change in Aβ ratio does not necessarily reflect an increase in $A\beta_{42}$ production, but can also be the consequence of a decrease in $A\beta_{40}$ levels. Actually, many mutations reduce one or both products of the γ-secretase in steady-state conditions [6-10]. These observations have led to an opposite hypothesis in which those mutations in PS cause dementia through a loss-of-function of γ-secretase, resulting in decreased proteolytic processing of different substrates and compromising intracellular signalling pathways [8,11]. In fact, the current model for γ-secretase successive proteolysis [12] may link a loss of function to misprocessing of APP and abnormal generation of Aβ [13,14]. However, the fact that less efficient proteolytic processing of APP may lead to alterations in the Aβ profile and Alzheimer disease is contraintuitive in the light of the classical amyloid hypothesis, which stresses the importance of quantitative accumulation of either total Aβ or $A\beta_{42}$ [15]. Moreover, a recent report has shown that reduced γ-secretase activity does not increase the production (accumulation) of longer Aβ peptides [16].

Importantly, the biophysical and biochemical properties of Aβ vary strongly with its length. Whereas $A\beta_{40}$ appears to act protectively in various toxicity assays [17,18], longer Aβ peptides promote aggregation and neurotoxicity [19]. In fact, it has been suggested that the ratio ($A\beta_{42}$:$A\beta_{40}$) is more important than the absolute amounts of $A\beta_{42}$ [20]. Similar to $A\beta_{42}$, $A\beta_{43}$ is potently amyloidogenic and neurotoxic [21]. Thus, qualitative changes in Aβ [13,14] are at least as important as the quantitative alterations proposed by the original amyloid hypothesis [15].

In contrast, the 'simple' loss-of-function hypothesis proposes that Aβ alterations are only an epiphenomenon of the *PS* mutations, and that inefficient cleavage of membrane proteins by γ-secretase complexes is the fundamental upstream cause of the neurodegenerative process [8,11].

On the other hand, recent observations in patients suffering from familial acne inversa in China [22] and independently in Great Britain [23] raise doubts about the validity of the 'simple' γ-secretase loss-of-function hypothesis. This condition appears to be associated with the haploinsufficiency of γ-secretase subunit genes (*Nicastrin*, *Pen2*) and most likely involves a deficiency in Notch cell signalling. However, none of the acne-affected individuals had Alzheimer disease symptoms. These observations indicate that reduced γ-secretase activity is not sufficient to cause Alzheimer disease, although further follow-up studies in these families are needed. Alternative mechanisms for the loss-of-function hypothesis have been proposed over the years (for an overview, see [24]). For instance, several reports indicate alterations in subcellular trafficking or turnover of selected membrane proteins [25,26], defective acidification of

phagolysosomal compartments [27] or disturbances in cellular Ca^{2+} homeostasis [28] (reviewed in [29]) associated to PS loss of function. However, these hypotheses do not provide an explanation for the mutations in APP and also do not take into account that all tested mutations related to familial Alzheimer disease affect the prime function of PS, which is proteolysis.

From this brief overview it is clear that further in-depth investigation of the effects of clinical mutations on the function and structure of γ-secretase is required, especially given the relevance of such analysis for further drug development.

Addressing this important question implies multidisciplinary approaches, in which deep structural and functional studies dissect the mechanisms of the mutations linked to hereditary Alzheimer disease. On the other hand, dissecting γ-secretase activity by kinetic analysis can yield important mechanistic insights into how those mutations regulate enzyme function. *In vitro* reconstitution of γ-secretase activity has provided initial insights into the enzymatic mechanism. Ihara and co-workers have provided compelling evidence for sequential processing of substrates by γ-secretase [30-33]. Their model proposes that APP can be sequentially cut along two production lines: Aβ49>Aβ46>Aβ43>Aβ40 and Aβ48>Aβ45>Aβ42>Aβ38 (Figure 7.1a) In agreement, it has been shown that the endoproteolytic cleavage site determines the product line preference of the γ-secretase *in vivo* [34], and therefore the series of Aβ products.

In the current study, we used a cell-free assay to analyse how clinical mutations in *PS1*, *PS2* and *APP* affect the activity of the γ-secretase complex. Dissection of the different activities of the γ-secretase complex allowed us to reach a coherent explanation for the effects of the tested mutations linked to familial Alzheimer disease. We coupled kinetic studies of the endopeptidase activity to the analysis of the carboxypeptidase-like cleavage to show that these mutations have widely variable effects on the efficiency of the first cleavage, which releases the intracellular signalling domains of substrates. This observation rules out an impairment in the endopeptidase (ε) mechanism as necessary for the pathological effect of these mutations. In contrast, all mutations in PS and APP linked to hereditary Alzheimer disease alter the processing of APP, regulating the generation of Aβ by three different mechanisms.

7.2 Results

7.2.1 PS1 mutations do not consistently impair the endopeptidase activity of the γ-secretase

We analysed the effects of mutations PS1-Y115H, - M139V, -L166P, -I213T, -G384A and delta-exon9 (DE9) on the kinetic constants of the ε-cleavage of APP, Notch, ErB4 and N-cadherin substrates. The selected mutations are spread throughout the PS1 primary sequence (Figure 7.1b). Importantly, blockage by the transition state analogue L-685,458 (TSA, InhX) demonstrated the specificity of the assays (Figure 7.2). To determine the kinetic constants of wt and mutated γ-secretase complexes, we used CHAPSO-extracted membranes from *Ps1/2*$^{-/-}$, rescued with wt or mutant *PS1* as source of enzyme (Figure 7.1c) and purified APP C99-3XFlag, Notch-3XFlag, Erb4-3XFlag or N-Cadherin-3XFlag as substrates. The kinetic data fit the Michaelis-Menten reaction curves (Figure 7.1 d,f), and K_m (affinity constant) as well as V_{max} (maximal velocity) were determined (Table 7.1). Since γ-secretase activities are normalized to enzyme levels, V_{max} can be taken as k_{cat} and enzymatic efficiencies calculated as

k_{cat}/K_m. The results reveal diverse effects of the *PS1* mutations on this important kinetic parameter. Y115H, L166P and G384A mutants decrease γ-secretase efficiencies by 75% for both APP and Notch, while I213T and DE9 only affect APP, and M139V does not show any effect on the ε-cleavage (Figure 7.1e). Moreover, *PS1* mutations that do not affect Notch endoproteolysis do not impair ErB4 cleavage either, while only the M139V significantly increases the processing of N-cadherin (Figure 7.1g). Thus, the tested FAD-PS1 mutations have no consistent inhibitory effect on the endoproteolytic cleavage of γ-secretase substrates, indicating that reduced release of intracellular domains and signalling cannot explain their Alzheimer disease-causing effects.

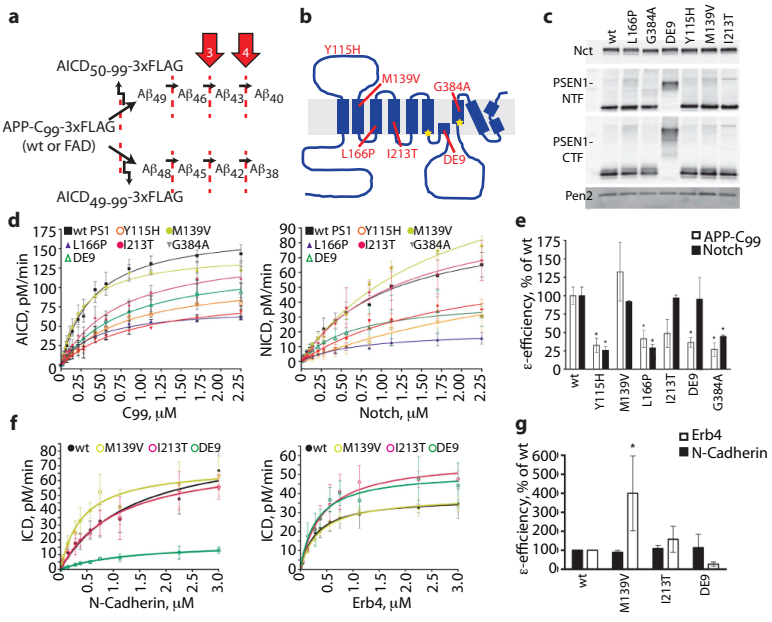

Figure 7.1 FAD–*PS1* mutations do not consistently decrease the enzymatic efficiency of the endopeptidase cleavage.

(a,b) Schematic overviews of APP processing and location of FAD–PS1 mutations used in the current study. (c) Expression levels of Nct, PS1–NTF, PS1–CTF and Pen-2 in Ps1/2/ mEFs transduced with human wt or FAD–*PS1* mutants using a replication-defective recombinant retroviral expression system and selected with puromycin (5 μg ml^{-1}). Western blotting and densitometric analysis of the CHAPSO-solubilized membrane proteins from the different PS1 cell lines indicate that wt and mutant PS1 rescued γ-secretase complex to similar extents. In order to determine specific activities for the wt or FAD complexes, γ-secretase activities were normalized to PS CTF fragment levels or full-length PS1 levels for the DE9 mutant. (d) Kinetic curves for wt and PS1–FAD mutants using purified APP-C99-3XFLAG or Notch- 3XFLAG substrates (mean±s.e.) or (f) ErB4-3XFLAG and N-Cadherin-3XFLAG substrates (mean±s.d.). Detergent-extracted membranes were incubated in 0.25% CHAPSO reaction buffer with varying concentrations of purified substrate for 4 h at 37 °C. *In vitro* generated ICD-3XFLAG were analysed by quantitative western blot analysis. (e) FAD–*PS1* ε-enzymatic efficiencies for APP-C99 and Notch substrates (mean±s.e.). Enzymatic efficiencies unequivocally demonstrate that loss of function at the ε-cleavage is not a constant among *PS1* mutations. (g) FAD–*PS1* mutations that did not affect the generation of NICD did not change significantly the processing of ErB4 (mean±s.d.) either. In contrast, N-Cadherin processing was significantly upregulated by the M139V (mean±s.d.). (e,g) Experiments were repeated 3–5 times. Statistical significance of the data was tested with one-way analysis of variance (ANOVA) and Dunnett's post test, taking the corresponding WT efficiency as control group, *p<0.05.

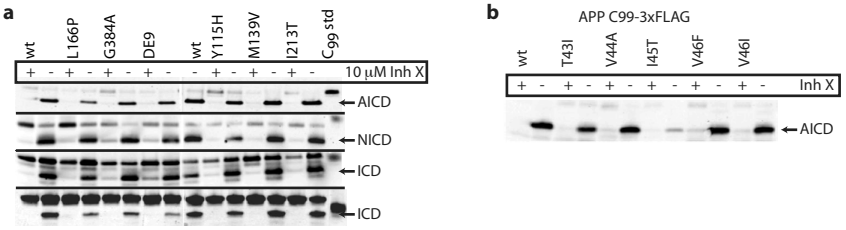

Figure 7.2 *In vitro* generation of ICD products from APPC99, Notch, ErB4 and N-Cadherin is γ-secretase dependent.

In vitro activity assays using CHAPSO extracted membranes from (a) *Ps1/2*$^{-/-}$ mEFs stably transduced with human wt or FAD *PS1* mutants and purified substrates-3XFlag. Substrate concentrations: 1,125 μM APP-C99 or 2 μM for the other substrates. (b) *Ps1/2*$^{-/-}$ mEFs stably transduced with human wt PS1 and purified wt- or FAD-APP-C99-3XFlag. Addition of the transition state analog inhibitor L-685,458 demonstrates that ICD products are generated in a γ-secretase dependent manner.

	APP-C99 substrate		Notch substrate		Erb4 substrate		N-Cadherin substrate	
	K_m ± s.e. μM	V_{max} ± s.e. pM/min	K_m ± s.e. μM	V_{max} ± s.e. pM/min	K_m ± s.d. μM	V_{max} ± s.d. pM/min	K_m ± s.d. μM	V_{max} ± s.d. pM/min
PS1 wt	0.40 ± 0.05	175.6 ± 8.4	1.08 ± 0.17	95.7 ± 7.5	0.31 ± 0.07	37.72 ± 6.18	1.46 ± 0.36	88.37 ± 10.95
Y115H	0.81 ± 0.18	113.3 ± 11.3*	3.92 ± 1.97	86.49 ± 31.4	-	-	-	-
M139V	0.27 ± 0.04*	144.5 ± 6.8*	1.78 ± 0.21*	146.9 ± 10.1*	0.40 ± 0.23	39.76 ± 6.36	0.42 ± 0.19*	71.16 ± 20.14
L166P	0.43 ± 0.07	74.03 ± 4.2*	0.97 ± 0.2	23.76 ± 2.4*	-	-	-	-
I213T	0.73 ± 0.18	151.1 ± 14.7	1.26 ± 0.26	106.1 ± 11.2	0.45 ± 0.13	58.68 ± 5.83*	1.02 ± 0.11	74.95 ± 11.76
DeltaE9	0.82 ± 0.18*	133.5 ± 13.5*	0.67 ± 0.24	42.8 ± 6.5*	0.33 ± 0.06	40.84 ± 8.12	1.70 ± 0.43	21.97 ± 8.39*
G384A	0.92 ± 0.18	93.87 ± 8.7*	1.85 ± 0.42	71.04 ± 9.5	-	-	-	-

Table 7.1 Kinetic parameters for human PS1 γ-secretase complexes using APP-C99, Notch, ErB4 or N-Cadherin as substrates

Kinetic values are derived from the curves displayed in Figure 7.1 and were determined by nonlinear curve-fitting using GraphPad Prism4 software. * Significant changes according to the 95% CI ($p<0.05$). *In vitro* activity assays were performed using CHAPSO-extracted membranes from PS1/2-/- mEFS stably transduced with human wt or FAD PS1 mutants and purified substrates-3XFlag, n≥3.

7.2.2 PS MUTATIONS IMPAIR THE FOURTH γ-SECRETASE CLEAVAGE IN BOTH PRODUCT LINES

Next, we asked whether *PS1* mutations lead to APP misprocessing at the γ-cleavage sites. We use Ihara's model (see Introduction) for further description of our work since it explains very well our observations. Kinetic analysis of the carboxypeptidase-like activity is challenging to perform since controlling substrate concentrations, that is, the intermediary Aβ products, is experimentally not possible yet. Nevertheless, we measured two γ-products in each production line: Aβ43, Aβ42, Aβ40 and Aβ38 (Figure 7.1a) at saturating APP-substrate concentration. Thus, substrates (Aβ43 and Aβ42) and products (Aβ40 and Aβ38) of the fourth γ-secretase cleavage in both pathways are analysed and provide a relative number for the γ-cleavage efficiency. Importantly, as some of the clinical mutants affect the ε-cleavage, we normalized the Aβ product levels (Aβ38, Aβ40, Aβ42 or Aβ43) towards total AICD (Figure 7.3 a,b). AICD reflects the total initial Aβ substrate (Aβ49 + Aβ48) produced and processed in each reaction. Low Aβ40 and Aβ38 levels and high, long Aβ levels (>Aβ42) are found in all the mutations linked to familial Alzheimer disease tested, including the M139V, which does not affect the ε-efficiency. Interestingly, the M139V mutation affects the processing of APP only at the level of Aβ, indicating that endo- and carboxypeptidase-like activities of the γ-secretase can be dissociated.

Total 'secreted' Aβ, defined as the sum of $Aβ_{38}$, $Aβ_{40}$, $Aβ_{42}$ and $Aβ_{43}$, decreases significantly in the Y115H, L166P, DE9 and G384A mutations (Figure 7.3b), implying the concomitant accumulation of longer Aβ precursors generated in cycles 2 and 3. Qualitative analysis of the Aβ profiles in urea-based SDS PAGE confirmed this observation (Figure 7.3c). We finally determine product:substrate ratios for the fourth enzymatic turnover ($Aβ_{38}$:$Aβ_{42}$ and $Aβ_{40}$:$Aβ_{43}$) (Figure 7.3d), which demonstrates that the *PS1* mutations investigated here dramatically impair the fourth γ-secretase cleavage in both product lines. Our data imply that *PS1* mutations cause Alzheimer disease by qualitative shifts in Aβ profiles and not by general loss of function of the enzyme complex [8,14]. The dysfunction at the carboxypeptidase-like activity of the complex not only explains the widely documented increase of the $Aβ_{42}$:$Aβ_{40}$ ratio, but also suggests a pathological relevance of an increase in $Aβ_{43}$, which has been reported recently *in vivo* with the *PS-R278I* [21].

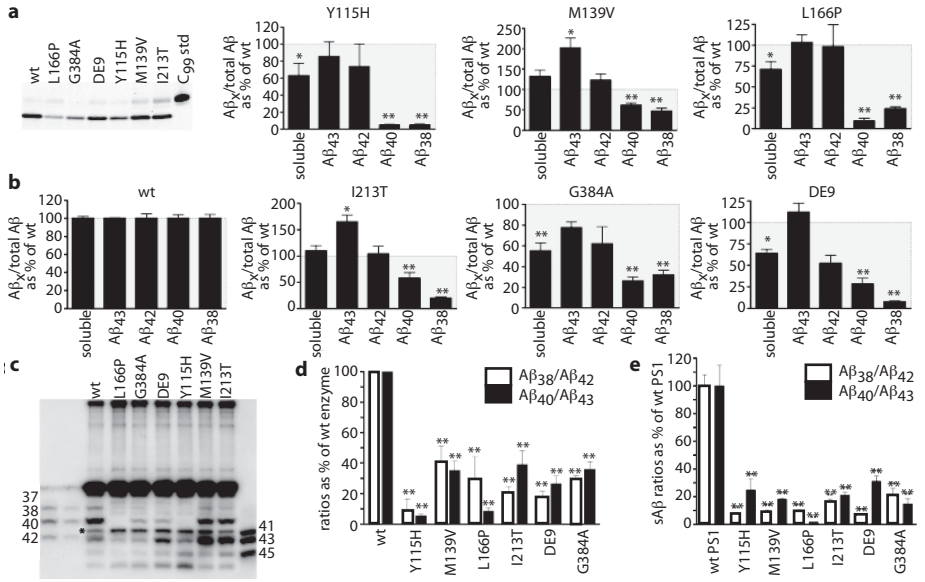

Figure 7.3 FAD–*PS1* mutations impair the fourth enzymatic turnover. AICD levels (moles per min) generated by the wt or FAD mutant complexes

(a) were used to normalize Aβ products (moles per min) in order to determine accurately Aβ generation relative to C_{99} substrate. Aβ profiles (b) thus represent Aβ products corrected for the initial endoprotease activities, plotted as percentage of the wt Aβ products (mean±s.e.). Soluble Aβ (sum of $Aβ_{38}$, $Aβ_{40}$, $Aβ_{42}$ and $Aβ_{43}$ peptides) gives information about the efficiency of the γ-cleavages: lower levels (<100%, grey box) suggest that longer peptides (>$Aβ_{43}$) accumulate in the reactions. (c) In agreement with the ELISA quantifications, total Aβ analysed in urea-based gels show increments in $Aβ_{42}$ and $Aβ_{43}$, and reductions in $Aβ_{40}$ and $Aβ_{38}$ in FAD–*PS1* mutations, relative to wt. (*) Indicates a non product band that is present in the C_{99} substrate. (d) Aβ product:substrate ratios determined *in vitro* for the FAD–*PS1* mutations show an impairment at the fourth γ-secretase turnover (mean±s.e.). Experiments in (b) and (d) were repeated 4-6 times. Statistical significance of the data tested with one-way ANOVA and Dunnett's post test taking the corresponding WT as control group; *p<0.05, **p<0.01. (e) Aβ product:substrate ratios determined *in vivo* confirm impairment at the fourth enzymatic cycle: wt or FAD–PS1 mEF cell lines were transiently transduced with APPswe, extracellular media collected at 24 h after infection and sAβ measured by ELISA (mean±s.e.). Statistical significance: n=4, ANOVA and Dunnett's post test, **p<0.01.

In order to confirm our *in vitro* data, mouse embryonic fibroblasts (MEFs) derived from *Ps1/2*$^{-/-}$ mice [35] rescued with human *WT-* or *mutant-PS1* were transiently transduced with APPsw. Secreted Aβ levels (sAβ) were quantified by ELISA. Figure 7.3e shows drastic reductions in the Aβ$_{38}$:Aβ$_{42}$ and Aβ$_{40}$:Aβ$_{43}$ ratios for all *PS1* mutations, confirming that the fourth enzymatic turnover of the γ-secretase is actually impaired in cells (native γ-secretase conditions). To investigate whether *PS2* mutations also affect the fourth enzymatic turn-over of the γ-secretase, we performed kinetic analyses with human *WT-PS2* or *FAD N141I-PS2* mutant. The effect of the mutation on the endopeptidase efficiency of the γ-secretase complex does not reach statistical significance (Figure 7.4a) (mean±s.e.: 100±39.9, n=4 or 46.6±3.9, n=3 for *WT- or FAD N141I-PS2*, respectively, two-tailed t-test, p=0.3). Although we cannot discard that this difference is biologically meaningful, the effect on the fourth catalytic cycle is unequivocal. In particular, the Aβ$_{40}$ product was decreased to undetectable levels (Figure 7.4b). Similar to the mutations in *PS1*, the N141I–*PS2* reduces the Aβ$_{38}$:Aβ$_{42}$ and Aβ$_{40}$:Aβ$_{43}$ ratios (Figure 7.4c), confirming an impairment in the carboxypeptidase-like activity.

Since high Aβ$_{42}$ and Aβ$_{43}$ (substrates in this cycle) accumulate *in vitro* or are released *in vivo*, we speculate that *FAD-PS* mutations promote a premature release of the Aβ$_{43}$:Aβ$_{42}$ peptides.

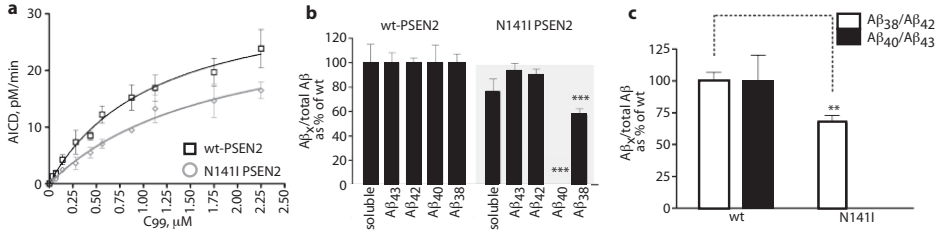

Figure 7.4 FAD–*PS2* N141I impairs the fourth enzymatic turnover.
(a) Kinetic curves for wt and *PS2*–FAD N141I mutant using purified APP-C99-3XFLAG as substrate (mean±s.e.). (b) Aβ profiles represent Aβ products corrected for the initial endoprotease activities, plotted as % of the wt Aβ products (mean±s.e.). Soluble Aβ (sum of Aβ$_{38}$, Aβ$_{40}$, Aβ$_{42}$ and Aβ$_{43}$ peptides) suggests accumulation of longer peptides (>Aβ$_{43}$) in the mutant reactions. (c) Aβ product/substrate ratios determined *in vitro* for the FAD– *PS2* mutation show an impairment at the fourth γ-secretase turnover (mean±s.e.). In (b) and (c) statistical significance (two tailed t-test) is indicated by **p<0.005 and ***p<0.001. Note that N141I abolishes Aβ$_{40}$ generation.

7.2.3 APP MUTATIONS CHANGE THE PRODUCT LINE PREFERENCE OF THE γ-SECRETASE

We then asked whether similar mechanisms could explain the effect of mutations in the APP substrate. The tested mutations are located close to the γ-secretase cleavage site, that is, T43I, V44A, I45T, V46F and V46I (Figure 7.5a) and all produce wild-type Aβ$_{38}$, Aβ$_{40}$, Aβ$_{42}$ and Aβ$_{43}$ peptides, except for the T43I mutation. Kinetic analyses of the ε-cleavage show that APP-T43I, V44A and I45T mutants produce less AICD per mol mutant APP compared to wt substrate, while the other mutations do not affect the ε-enzymatic efficiency (Figure 7.5 b,c). In order to analyse accurately the Aβ profiles from wt and disease-related substrates, Aβ levels were normalized to the amount of AICD generated in the reaction. FAD Aβ levels, corrected for the initial amounts of substrates, were then plotted as a percentage of the wt enzyme (Figure 7.5d).

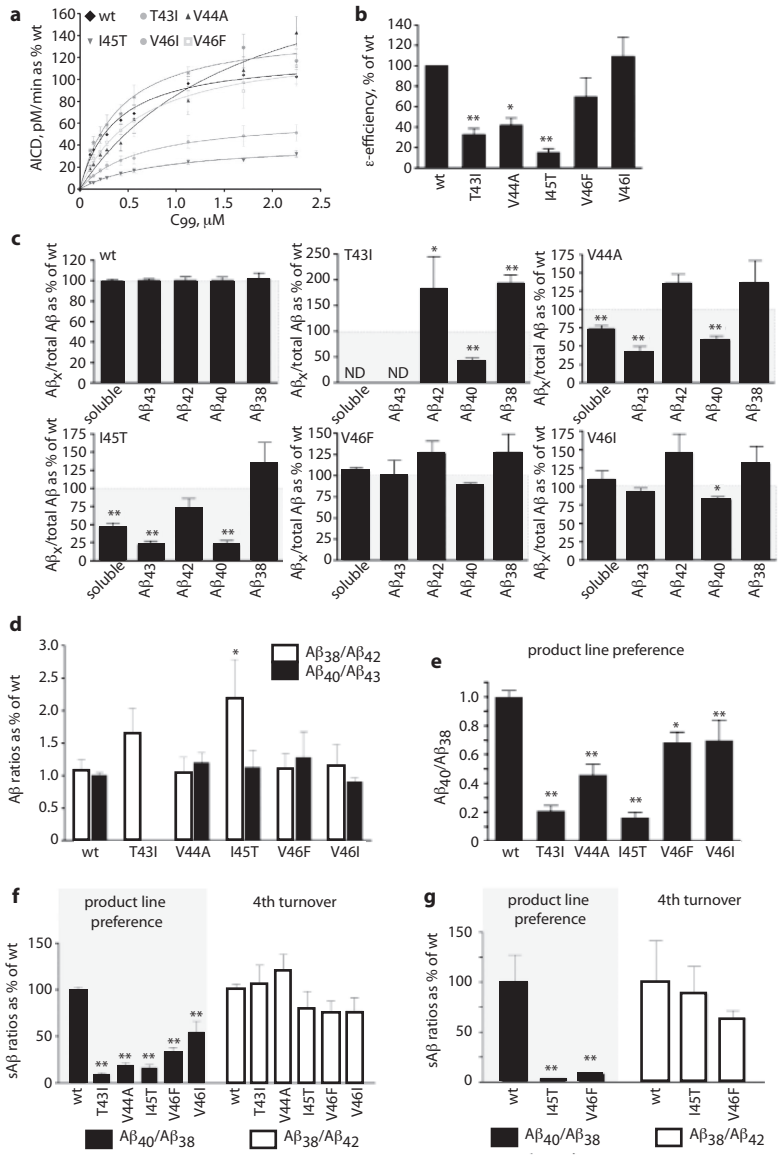

Figure 7.5 FAD substrate mutations shift APP processing towards the $A\beta_{38}$ product line. (a) Kinetic curves for the ε-processing of APP. Detergent-extracted membranes from *Ps1/2*$^{-/-}$ mEFs rescued with human wt *PS1* were incubated in 0.25% CHAPSO reaction buffer, with varying concentrations of purified wt or FAD–APP substrates. AICD-3XFLAG levels were analysed by quantitative western blot analysis. (b) Enzymatic efficiencies for FAD–APP-C_{99} substrates (mean±s.e.) prove that AICD generation is affected in three out of five FAD-mutant substrates. (c) FAD Aβ product profiles suggest consistent increments in $A\beta_{42}$ and $A\beta_{38}$. Soluble Aβ levels (sum of $A\beta_{38}$, $A\beta_{40}$, $A\beta_{42}$ and $A\beta_{43}$ peptides) suggest accumulations of longer Aβ peptides in the γ-processing of the V44A and I45T mutants. The T43I mutation disrupts the epitope for the anti-$A\beta_{43}$-specific antibody, thus neither $A\beta_{43}$ nor soluble Aβ levels could be determined (ND). (d) Aβ product:substrate ratios reveal that APP mutations do not consistently affect the fourth γ-secretase turnover, but change the product-line preference as indicated by the $A\beta_{40}$:$A\beta_{38}$ ratio (e). (f) sAβ in the conditioned

media of HEK293 cells transiently transfected with wt or FAD-C_{99} mutants were quantified by ELISA. sAβ ratios indicate that APP–FAD substrate mutants change the product-line preference towards the $Aβ_{48}$>$Aβ_{38}$ ($Aβ_{40}/Aβ_{38}$) in living cells, but do not affect the fourth catalytic turnover of the γ-secretase ($Aβ_{38}/Aβ_{42}$) (mean±s.e., n=5). (g) Primary cultured neurons were transduced with SFV expressing WT APP or the indicated mutant substrates (mean±s.d., n=3). (b-g) Statistical significance tested with one-way ANOVA and Dunnett's post-test, taking the corresponding WT as control group; *p<0.05,**p<0.01.

Importantly, and in contrast to mutated *PS*, none of the tested *APP* mutations affect $Aβ_{38}$:$Aβ_{42}$ or $Aβ_{40}$:$Aβ_{43}$ ratios (Figure 7.5e). The I45T mutant is the exception, showing increased $Aβ_{38}$:$Aβ_{42}$ ratio, which would be consistent with an impairment in the processing of $Aβ_{45}$ (mutant peptide) to $Aβ_{42}$. However, *APP* mutations result in high $Aβ_{40}$:$Aβ_{38}$ compared to wt *APP* (Figure 7.5f). Thus, all investigated mutations change the product line preference by shifting APP processing towards the $Aβ_{38}$ production line. The APP-V44A and I45T substrates in particular show an additional accumulation of longer Aβ precursors (generated in cycles 2 and 3), as deduced from soluble Aβ in Figure 7.5d. The change in the product line can be explained if these APP mutations shift the position of the ε-cleavage to generate more $Aβ_{48}$, the initial substrate in the $Aβ_{38}$ production line. A neo-epitope antibody against $AICD_{50–99}$ (Figure 7.6) was generated, and allowed us to confirm the product line preference (Figure 7.7 a,b).

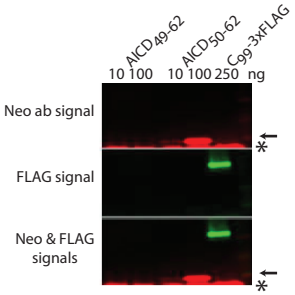

Figure 7.6 $AICD_{50-99}$ neo-antibody specificity.
$AICD_{50}$ neo-antibody was tested against 10 or 100 ng $AICD_{50-62}$ and $AICD_{49-62}$ synthetic peptides in Western blot analysis. The neo-epitope antibody is able to interact with the $AICD_{50-62}$ but not with the $AICD_{49-62}$ peptide (lanes 1-2 vs. 3-4). Neo-epitope and FLAG antibodies were detected with secondary antibodies coupled to different fluorophores. Signals in red and green for the neo and anti-Flag antibodies; respectively. As expected, the neo-epitope antibody does not recognize C99-FLAG substrate (lane 5). Arrow indicates the neo-antibody specific signals. * Dye front.

Figure 7.7c shows that the *APP* mutations consistently shift the position of the ε-cleavage towards $AICD_{49–99}$, promoting the $Aβ_{38}$ product line, and therefore causing increments in the $Aβ_{42}$ and $Aβ_{38}$ products. Importantly, HEK cells transiently transfected with FAD-mutant C_{99} substrates increase the $Aβ_{42}$ and $Aβ_{38}$ levels in the extracellular medium while decreasing $Aβ_{40}$, compared to control (wt C_{99}) (Figure 7.8). Figure 7.5g actually shows that *APP* mutations change the product line preference ($Aβ_{40}$:$Aβ_{38}$ ratio), but do not alter the fourth enzymatic turnover ($Aβ_{38}$:$Aβ_{42}$ ratio). Similar results were obtained from primary neuronal cultures transiently expressing wt, I45T or V46F-APP (Figure 7.5h). These results indicate that our observations in the cell-free assay can be extrapolated to the *in vivo* situation. The *APP* data imply that promoting the $Aβ_{38}$ production line is pathogenic.

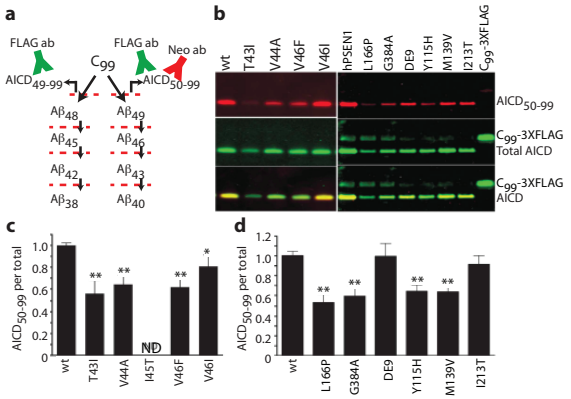

Figure 7.7 Shift in the ε-cleavage position contributes to the FAD-associated phenotype.
(a) Detection of AICD50–99 and total AICD using a neoepitope antibody and the FLAG-M2 antibody, respectively. (b) SDS PAGE/western blot analysis of AICD products from either wt and FAD substrates (left panel) or wt and FAD–*PS1* mutants (right panel). Signals for the AICD50–99 neo-epitope antibody or the FLAG-M2 antibody are shown in red and green, respectively. Overlapping neo-epitope and FLAG antibody signals are displayed in yellow. (c) AICD50–99/total AICD ratios indicate that FAD–*APP* mutations promote the $A\beta_{38}$ product line by shifting the ε-cleavage position. The I45T could not be included in the analysis because of extremely low AICD signals (ND, not determined). (d) This pathogenic mechanism is also observed in some FAD–*PS1* mutations. Statistical significance of the data (n=5) tested with ANOVA and Dunnett's post test, taking AICD generated in WT conditions as control group; *p<0.05,**p<0.01.

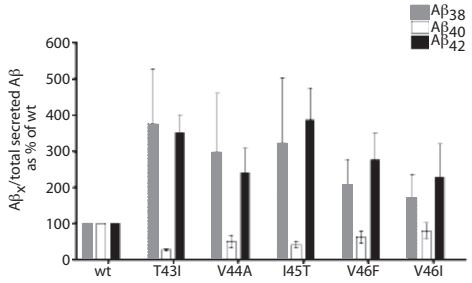

Figure 7.8 Aβ products in the conditioned media of HEK293 cells transfected with wt or C99 mutants.
HEK293 cells transiently transfected with human wt C99 or mutants were maintained in DMEM supplemented with 2% serum. Media were collected at 48 h post-transfection and Aβ levels determined by ELISA. Secreted $A\beta_{43}$ was at undetectable levels in the media. Plot shows mean ± s.d. Notice the same shifts in profiles (increase of the $A\beta_{38}$ pathway, decrease of the $A\beta_{40}$ pathway) as measured with the cell free assays.

We therefore investigated the effects of different Aβ peptides on spontaneous synaptic transmission in the primary mouse hippocampal neurons. Our results show that $A\beta_{38}$, similar to $A\beta_{42}$ and $A\beta_{43}$, but to a lesser extent, elicits acute synaptotoxicity. Although further work is needed to investigate the effects of $A\beta_{38}$ *in vivo*, these data confirm that individual Aβ peptides have widely divergent biophysical and biochemical properties (Figure 7.9).

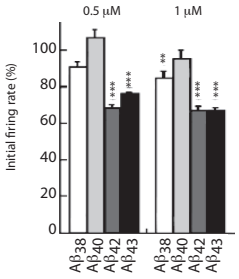

Figure 7.9 $A\beta_{38}$ elicits acute synaptotoxicity.
Aβ synaptotoxicity on primary neurons. Primary mouse hippocampal neurons were cultured on MicroElectrode Array (MEA) substrate for 7-10 days. Synaptic activity was recorded as a function of increasing Aβ concentration. $A\beta_{42}$ (dark grey) and $A\beta_{43}$ (black) are significantly synaptotoxic at a concentration of 0.5 μM. At a concentration of 1 μM $A\beta_{38}$ (white) inhibits activity with 15%. Values are percent of initial firing rate ± SEM; culture response was first normalized to the initial basal firing rate. Recorded values were averaged over all active electrodes from different chips. Different buffer treatments were each normalized to 100%. Statistical significance (unpaired 2-tailed t-test) is indicated by ***p<0.0001 or **p<0.0005. (5 independent cultures, n=3 MEA substrates for $A\beta_{38}$ and $A\beta_{42}$, n=4 MEA substrates for $A\beta_{40}$ and $A\beta_{43}$).

7.2.4 Effects of inhibitors and modulators on the γ-secretase activity

Our data indicate that the various mechanisms affecting the Aβ spectrum generated by γ-secretase are responsible for the pathogenic effects of the FAD mutations. Therefore, we asked to what extent γ-secretase inhibitors (GSI) and modulators (GSM) that were tested in clinical trial or are under development [37] affected the different parameters discussed above. To evaluate γ-secretase inhibition under equal kinetic conditions, we took advantage of the *in vitro* system and performed activity assays at 1x K_m substrate concentrations for APP C99 or Notch substrates (0.4 and 1.1 μM, respectively). Under these conditions, the GSI semagacestat (LY-450139), begacestat (Notch sparing GSI) and avagecestat (Notch sparing GSI) efficiently inhibit Aβ generation in the two production lines (Figure 7.10).

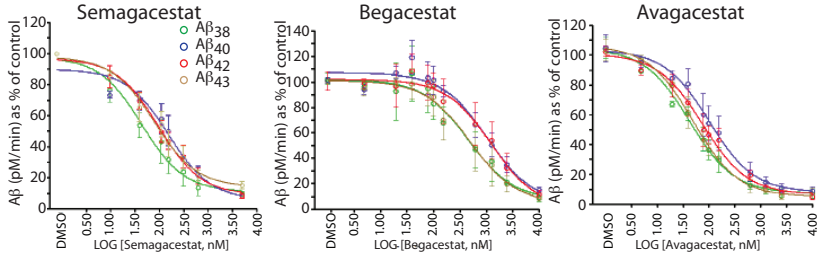

Figure 7.10 Dose-response inhibitory assays for semagacestat, begacestat and avagacestat.
IC_{50} curves for GSI using CHAPSO extracted membranes from *Ps1/2*$^{-/-}$ MEFs stably expressing human wt PS1 mutants and 400 nM mutant-C99 substrate (1x Km concentration). All GSI inhibit $A\beta_{38}$, $A\beta_{40}$, $A\beta_{42}$ and $A\beta_{43}$ production to similar extents. Aβ products are plotted as percentage of control reaction (DMSO). Error bars indicate S.D. (n=3); except for semagacestat plot (S.E., n=5).

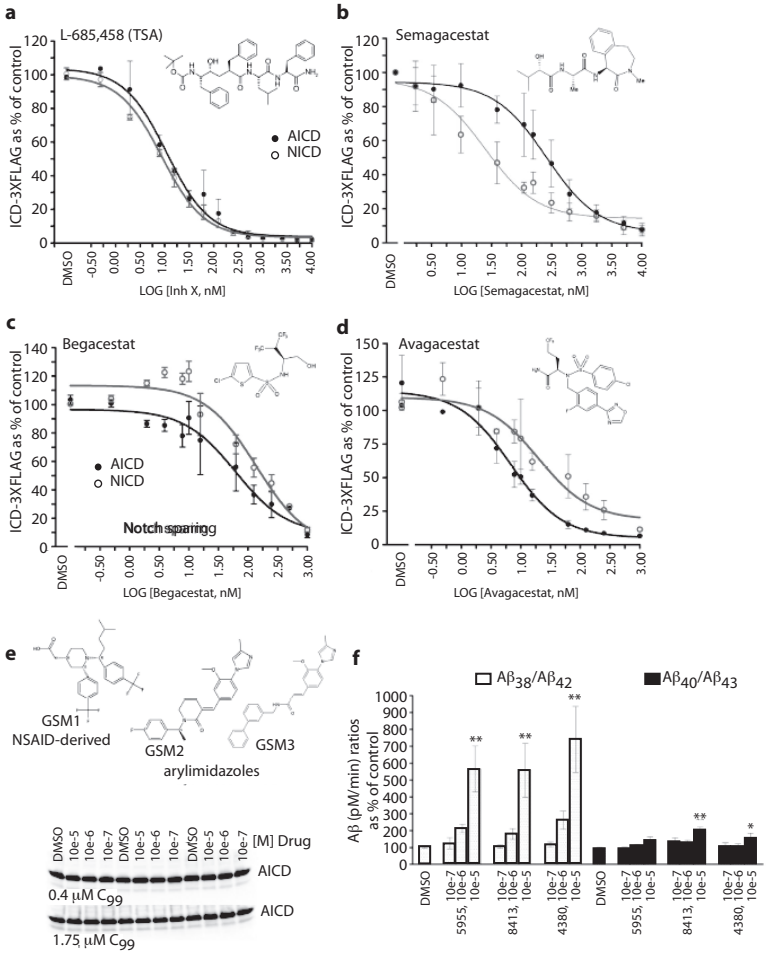

Figure 7.11 Analysis of GSI and GSM. Dose-response inhibitory assays for (a) the transition state analogue (TSA) L-685,458 (InhX), (b) semagacestat, and the Notch-sparing compounds (c) begacestat and (d) avagacestat were performed using CHAPSO-extracted membranes from dKO PS1/2 MEFs stably expressing human wt PS1 as source of γ-secretase and 1x Km substrate concentrations (400 nM APP-C99-3XFLAG or 1 mM Notch-3XFLAG). Structures of the different compounds are displayed. *In vitro* generated AICD (in black) or NICD (in grey) are plotted as percentage of control reaction (DMSO). Error bars indicate s.d. (n=3); except for semagacestat plot (s.e., n=5). (e) Top panel: structures of the GSM tested. Low panel: increasing concentrations of GSM 1–3 did not change *in vitro* AICD generation, neither at 0.4 μM APP-C99 substrate (1x Km) nor at saturating conditions (1.75 μM C99-3XFLAG). (f) Effect of increasing concentrations of GSM 1–3 on Aβ production at 1x Km APP-C_{99} substrate (0.4 μM): Aβ product:substrate ratios show that GSM 1–3 specifically activate the fourth cycle of the γ-secretase complex. In particular, GSM activate the $Aβ_{38}$ product line. Panel shows mean±s.e.; statistical significance of the data (n=4) tested with ANOVA and Dunnett's post test, vehicle (DMSO) as control group; *p<0.05,**p<0.01.

However, semagacestat, which failed in phase III trial (https://www.investor.lilly.com/releasedetail2.cfm?releaseid=592438) because of cognition and skin problems,

is more selective for Notch than for APP (AICD IC_{50}=257.8 nM and Notch intracellular domain (NICD) IC_{50}=24.62 nM (95% confidence interval (CI): 190.2-349.5 nM for APP and 15.74-38.51 nM for Notch, n=5), whereas the transition state inhibitor L-685,458 affects both substrates to an equal extent (Figure 7.11 a,b). Surprisingly, and in contrast to previous claims [38,39], the selectivity of both of the 'Notch sparing' GSI is not significantly different for APP and Notch substrates (Begacestat: AICD IC_{50}=61.71 nM and NICD IC_{50}=138.4 nM (95% CI: 24.77-153.7 nM for AICD and 73.29-261.3 for NICD, n=3) and BMS708163: AICD IC_{50}=6.82 nM and NICD IC_{50}=20.03 nM (95% CI: 4.06-11.46 nM for AICD and 7.76–51.7 nM for NICD, n=3)) (Figure 7.11 c,d).

Recently, γ-secretase modulators (GSM) have been evaluated as an alternative to GSI [40]. GSM lower $A\beta_{42}$ and increase $A\beta_{38}$, but the precise mechanism of action has not been elucidated. One NSAID and two arylimidazole-derived GSM [41] (E-2012 and a close analogue) did not affect the endopeptidase activity (Figure 7.11e, Figure 7.12a) but, as expected, reduced $A\beta_{42}$ and increased $A\beta_{38}$. Analysis of the product:substrate ratios for the fourth enzymatic turnover shows that these drugs increase specifically this cycle (Figure 7.11f, Figure 7.12b) and act, therefore, in the opposite way to the clinical FAD-PS mutations. The Aβ ratios indicated that the GSM evaluated in this study act mainly on the fourth cycle of the $A\beta_{38}$ production line. In fact, our data show them as activators of the γ-secretase (GSA). Taking into account the changes in the mutant APP Aβ profiles and the possibility that $A\beta_{38}$ may be part of the pathogenic mechanism, it is crucial to evaluate to what extent the differential effects of the GSA on the Aβ production lines are problematic.

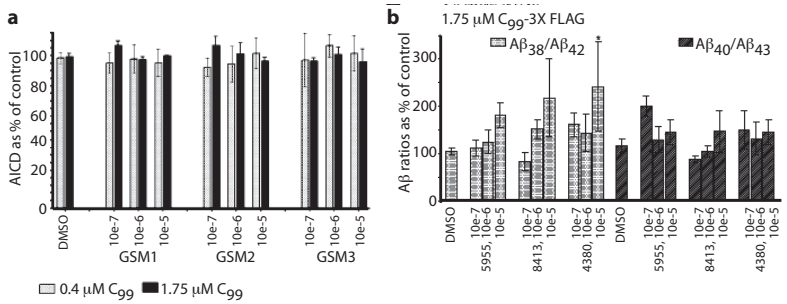

Figure 7.12 Effects of increasing concentrations of GSM 1-3 on γ-secretase activity.
(a) *In vitro* activity assays using CHAPSO extracted membranes from *Ps1/2*$^{-/-}$ mEFs stably expressing human wt PS1 and 0.4 or 1.75 μM APP-C99 substrate (1x Km or saturating concentrations, respectively). The three GSM (at $1x10^{-5}$, $1x10^{-6}$, $1x10^{-7}$ M) do not affect the endopeptidese activity of the γ-secretase (no effect on AICD production). AICD production is plotted as percentage of control reaction (DMSO). (b) Increasing concentrations of GSM 1-3 on $A\beta_{38}$:$A\beta_{42}$ and $A\beta_{40}$:$A\beta_{43}$ ratios show that GSM 1-3 activate the 4th catalytic cycle of the γ-secretase; in particular, the $A\beta_{48}$>$A\beta_{38}$ product line. Panels a,b show mean±s.d.; statistical significance of the data (n=3) tested with ANOVA and Dunnett's post test, vehicle (DMSO) as control group; *p<0.05.

7.3 Discussion

This study settles several issues that have been heavily debated in the literature. Dissection of the different activities of the γ-secretase complex allowed us to characterize the mechanisms that are regulated in a consistent fashion by FAD mutations in PS and APP. Previous reports have employed steady-state analyses to evaluate the

effect of these mutations on the γ-secretase. In general, these studies have employed transfected cells to measure, in culture or *in vitro*, changes in secreted product levels or follow the intracellular generation of ICD products by coupling it to reporter systems. Although these approaches are informative, they do not truly reflect the kinetic features of the mutated γ-secretase complexes or APP substrates. For instance, substrate concentration and accessibility is not controlled in such assays.

By analysing the catalytic efficiency of the γ-secretase complex (wt or mutated) in an *in vitro* assay, with both enzyme and substrate in solution, we find here that mutations in PS1 and PS2 affect γ-secretase at three levels. We see (i) a variable inhibitory effect at the initial endoproteolytic ε-cleavage step, which releases the intracellular domains of substrates such as APP, Notch, Erb4 and N-cadherin. (ii) A consistent effect on the consecutive carboxypeptidase-like γ-cleavage with all PS mutations causing a 'premature' release of (intermediary) substrates/products, explaining why longer Aβ is generated by these mutants. Interestingly, our data suggest that both $A\beta_{42}$:$A\beta_{38}$ and $A\beta_{43}$:$A\beta_{40}$ ratio increments are pathologically relevant. (iii) Additionally, some of the mutations in PS and all mutations investigated here in the APP sequence (selected for their close position to the γ-cleavage site in APP) affect the initial position of the ε-site, that is, whether γ-secretase cleaves preferentially at position 49-50 or 51-50 in the APP sequence. While these three mechanisms explain for the first time the abundantly documented increase in $A\beta_{42}$:$A\beta_{40}$ ratio associated with all mutations leading to familial Alzheimer disease, they also provide a set of entirely novel insights, as we discuss in the following paragraphs.

Our study gives definite numbers on the catalytic efficiency of the γ-secretase complex at the ε-site and unequivocally shows that 'loss of function' - lower catalytic efficiency - is not consistent across the hereditary mutations tested. In this regard, we wish to draw attention to the fact that point mutations in PS might affect protein stability, and therefore solubilization of 'less stable' mutated γ-secretase complexes might result in an accentuated 'loss of function'. Thus, we cannot exclude that the enzymatic efficiencies of particular mutated complexes (less stable) are underestimated in the conditions used in the current work, which would even strengthen our conclusion that 'loss of function' is not necessary for the pathogenic mechanism. Taking all into consideration, our results indeed rule out the possibility that loss of intracellular signalling is necessary and sufficient to cause Alzheimer disease, as postulated by the 'simple' loss-of- function hypothesis. Interestingly, the effects at the ε-cleavage site are also variable for different substrates tested (K_m values for APP, Notch, Erb4 and N-cadherin, Table 7.1), suggesting that some of the clinical mutations affect the substrate specificity mechanism. This is in particular clear for the M139V and DE9 mutations. DE9 removes part of the hydrophobic domain VII (HDVII) of PS1, which is located in the active site of the γ-secretase [42], while the M139 residue is located in the second transmembrane domain of PS, which contributes to the formation of the initial substrate-binding site [43]. On the contrary, our results show that the L166P mutation affects the catalytic rate of the enzyme but does not change the substrate specificity of the complex, explaining why steady-state levels of NICD and AICD products *in vivo* are equally affected by different amino-acid substitutions in the position 166 [44].

We analysed in considerable detail the effects of PS1 and PS2 mutations on the γ-secretase (carboxypeptidase-like) mechanism that follows the initial ε-endoproteolytic

cleavage of the APP substrate. We find that PS mutations impair dramatically the fourth turnover in both Aβ49>Aβ40 and Aβ48>Aβ38 product lines, resulting in decreased Aβ40:Aβ43 and Aβ38:Aβ42 ratios. Our data therefore give a mechanistic explanation for the decrease in short Aβs (<40) reported in the cerebrospinal fluid of carriers of PS-A431E10 [45] or the alterations in the lengths of Aβ peptides produced *in vitro* by mutated PS-containing complexes [46]. Moreover, biophysical observations have shown that PS mutations alter the conformation of the γ-secretase complex [47]. Based on our biochemical data we propose that changes in the active site of PS mutations promote the premature release of the Aβ43 or the Aβ42 peptides from the γ-secretase complexes.

A third mechanism by which APP mutations act in particular is the shift in the initial ε-cleavage site resulting in an increased Aβ48>Aβ38. Likely, the product preference results from differential docking modes of the APP substrate into the active site. We confirmed the shift towards Aβ48>Aβ38 in living cells expressing wt or mutant APP substrates. This result corroborates our claim that the product line preference is an intrinsic property of the γ-secretase complex that remains unaltered in our cell-free assay. Interestingly, this shift in initial docking and production lines is also observed in four of the six PS1 mutants (Figure 7.7 c,d). The fact that some PS1 mutations combine these two mechanisms (impaired fourth cycle and change in the product line preference) explains the direct and indirect correlations between Aβ38 and Aβ42 levels reported in the past [48,49].

Our study thus demonstrates that mutations linked to familial Alzheimer disease cause qualitative changes in the Aβ profiles by various mechanisms [7,13], and that decreased release of intracellular domains [11] is not an essential part of the Alzheimer disease pathogenic mechanism. Nevertheless, as indicated above, the most aggressive PS1 mutations, for example, the L166P, negatively impact the endopeptidase activity as well, and therefore it is not unlikely that 'partial loss' of γ-secretase function at Notch or other γ-secretase substrates acts as an aggravating factor in familial Alzheimer disease.

Moreover, our Aβ product profiles evidence the generation of longer Aβ peptides (>Aβ43) by the most aggressive mutated complexes. However, whether particular changes in the Aβ profiles can be correlated to the age of onset is an interesting but unaddressed question.

In a final series of experiments, we have also assessed to what extent different γ-secretase-directed drugs such as GSI and GSM affect the three mechanisms identified in the current work. When investigating the transition state analogue L-685,458 (InhX), semagacestat, and the Notch-sparing begacestat and avagacestat, we found that the four compounds lowered all γ-cleavages to a similar extent and did not change the Aβ ratios. However, when we assayed the effects of these GSI on Notch processing, which is considered to be the major liability of GSI, we surprisingly found that semagacestat was more effective in inhibiting Notch than APP. This is particularly significant when considering that a phase III clinical trial with semagacestat was interrupted last year because of severe side effects including worsened cognition and increased incidence of skin cancer. Similarly, the Notch-sparing compounds begacestat and avagacestat did not show significant higher selectivity for APP compared to the Notch substrate in our assay. These data raise serious concerns about the interpretation of inhibitory studies that relied on cellular or *in vivo* data, which in general do not allow direct

quantitative comparisons as done with our assay. Importantly, our data do not discard the selective inhibition of APP at the ε-cleavage as a plausible strategy for drug development, but basically indicates that the approaches that have been used to reach this aim need to be revisited.

We also tested GSMs and found that all three candidates keep full functionality at the endopeptidase cleavage and regulate the carboxypeptidase-like activity by activating the fourth cycle of the γ-secretase, resulting in an increased processing of the aggregation-prone Aβs towards shorter Aβ peptides. Our data, however, suggest some caution with this strategy as the tested compounds differentially affect the $A\beta_{48}$>$A\beta_{38}$ versus the $A\beta_{49}$>$A\beta_{40}$ pathway. The relative increase of $A\beta_{38}$ observed with all compounds needs further scrutiny, as APP clinical mutations also promote this production line.

In conclusion, our work provides an important step forward towards the understanding of the mechanisms by which early-onset familial mutations in *PS* and *APP* cause Alzheimer disease. Our findings support strongly the hypothesis that although these mutations affect γ-secretase in various ways, they all lead to qualitative shifts in the Aβ profiles, which provides a common denominator for the pathogenic effect of all mutations leading to hereditary Alzheimer disease.

7.4 Experimental procedures

7.4.1 Cell culture

Ps1/Ps2-deficient ($^{-/-}$) MEF ($Ps1/2^{-/-}$ mEF) [35] were cultured in Dulbecco's modified Eagle's medium/ F-12 containing 10% fetal bovine serum. $Ps1/2^{-/-}$ mEF rescued with wt (human) *PS1* or L166P, G384A and DE9 as well as wt (human) *PS2* or N141I were reported before [7]. The Y115H, M139V and I213T FAD–*PS1* cell lines were generated accordingly. mEF–*PS1* cell lines were transduced with a recombinant adenovirus Ad5/CMV-APP bearing human APP-swe, as previously described [50]. Neuronal cultures derived from E14 embryos and Semiliki Forest virus transfection procedures have been described previously and Semliki Forest viruses (SFV) were produced as described [51]. Briefly, brains from E14 embryos were trypsinized and plated on 6-cm dishes precoated with poly-L-lysine. Cultures were maintained in neurobasal medium supplemented with B27 and 5mM cytosine arabinoside to prevent glial cell prolification. After 3 days, neurons were transduced with SFV expressing wt or FAD mutant APP. After 1 and 3 h, post-infection media were refreshed. After 24 h, sAβ were analysed by ELISA.

7.4.2 Expression and purification of substrates-3xflag

Substrate purification was performed as previously described [50]. Notch-, ErB4- and N-Cadherinbased substrates were designed to be similar in size to the APP substrate (C99–3XFLAG). Purity was assessed by SDS PAGE and Coomassie staining.

7.4.3 In vitro activity assays using solubilized γ-secretase

In vitro activity assays were done as previously described [50], with minor modifications. MEF's microsomal fractions were prepared in 50mM citric acid, pH 6.7,

0.25M sucrose, 1 mM EGTA, complete protease inhibitor and 1% CHAPSO. *In vitro* reactions were carried out in 50mM citric acid, pH 6.7, 0.25M sucrose, 1 mM EGTA, 1 EDTA-free complete proteinase inhibitor, 2.5% DMSO and 0.05% phosphatidylcholine. Reactions were incubated for 4 h at 37 °C unless otherwise mentioned. Lipids and substrates were extracted by adding 1 volume chloroform:methanol (2:1, v/v). Then, the aqueous fraction (ICD products) was taken and subjected to SDS PAGE and quantitative western immunoblot. Known amounts of C99-3XFLAG were included as standards for absolute quantifications. ICD-3XFLAG and standards were determined with the anti-FLAG M2 and goat anti-mouse IR800 antibodies, whereas the $AICD_{50–99}$ product was determined with a neo-epitope mAb and a goat anti-rabbit Alexa680 secondary antibody.

7.4.4 Calculation of kinetics constants

Kinetic constants were estimated by nonlinear curve-fitting using GraphPad Prism 4 software. The equation $V=(V_{max}[S])/(K_m+[S])$ was used to calculate apparent K_m and V_{max} values for the different enzymes, where V was experimentally determined using a range of substrate concentrations [S]. γ-Secretase activities were normalized to PS–CTF fragment levels or full-length PS1 levels for the DE9 mutant.

7.4.5 Quantification of soluble Aβ using sandwich ELISA

Ninety-six-well plates were coated with 1.5 μg ml^{-1} Aβ capture antibody, excepting $Aβ_{43}$-ab coated at 7.5 μg ml^{-1}, in a final volume of 50 μl buffer (10mM Tris HCl, 10mM NaCl, 10 mM NaN3, pH 8.5). After overnight incubation at 4 °C, the plates were rinsed with PBS+0.05% Tween20 and blocked with 100 μl per well of casein buffer (1g casein in 1L 1xPBS, pH7.4) for 4 h at room temperature. Samples and standards (synthetic human $Aβ_{38}$, $Aβ_{40}$, $Aβ_{42}$ or $Aβ_{43}$ peptides) were diluted in casein buffer. After overnight incubation at 4 °C, plates were rinsed and developed using 50 μl per well of 100mM NaAC pH 4.9/TMB/H_2O_2. Reactions were stopped with 50 μl per well of 2N H_2SO_4 and read on a Perkin Elmer Envision 2103 multilabel reader at 450 nm.

7.4.6 Urea gels

Aβ-peptides were analysed by a modified version of the urea-based SDS PAGE [52]. Western immunoblot was done using 1E8, amplifying the signal with biotinylated anti-mouse IgG and streptavidin-HRP. Signals were detected using ECL chemiluminescence with an Intas Imager.

7.4.7 Synaptotoxicity on primary neurons

Trypsinized brain from 17-days-old FVB mice embryos was used to generate hippocampal neurons. Cultures were plated at 1,000 cells/mm^2 on a MEA substrate and maintained in neurobasal medium supplemented with B27 for 3 days at 37 °C in a humidified 5% CO_2 atmosphere. Then, medium was changed to neurobasal medium supplemented with B27, without L-glutamate and cells were cultured for 8-10 days prior to further experiments. During the recording experiment, a temperature controller was used to maintain the MEA platform temperature at 37 °C. The basal firing rate was recorded during 500 sec. Subsequently, cultures were titrated with pre-aggregated Aβ (1.5 h, 25 °C) at final concentrations of 0.5 and 1 μM at 500 sec

intervals. The spontaneous synaptic activity was continuously recorded during these 500 sec. Raw signals from MEA electrodes were amplified (gain 1200) and digitized at a sampling rate of 25 kHz. The raw data stream was high-pass filtered at 200 Hz, and the threshold for spike detection was set to 5 SD of the average noise amplitude computed during the first 1000 ms of recording. The firing rates recorded by all electrodes were averaged over the 500-sec time bins and were normalized to buffer treatment. Experiments were performed using 5 independent cultures, n=3 MEA-chips for $A\beta_{38}$ and $A\beta_{42}$, and n=4 MEA-chips for $A\beta_{40}$ and $A\beta_{43}$. Results were analyzed using two-tailed unpaired t-test for significance. Significance is indicated by ***p<0.0001 and **p<0.0005.

7.4.8 QUANTIFICATION OF TOTAL Aβ USING SANDWICH ELISA

Sandwich ELISA were done using 4G8 as capture antibody at final concentrations of 1.5 μg/mL in a final volume of 50 μL coating buffer (10mM Tris HCl, 10mM NaCl, 10mM NaN3, pH8.5). Synthetic human $A\beta_{40}$ peptide was used for the preparation of the standard curve.

AUTHOR CONTRIBUTIONS

LC-G and BDS designed the study and wrote the manuscript. LB and LZ contributed to the analysis of APP mutations. AV, IB, JS, FR, and KB contributed to Aβ aggregation assays and characterized the synaptotoxicity of Aβ peptides on primary neurons. MBo, MBe, SL and LS provided their technical and experimental assistance. SVC contributed to the experimental analysis of PS mutations. HE and JW characterized Aβ profiles of PS mutants in urea-based gels. HG and EK synthesized and provided the GSI and GSM.

7.5 References

[1] De Strooper B, Saftig P, Craessaerts K, Vanderstichele H, Guhde G, Annaert W, Von Figura K, Van Leuven F (1998). Deficiency of presenilin-1 inhibits the normal cleavage of amyloid precursor protein. *Nature*, 391:387-390.

[2] Borchelt D, Thinakaran G, Eckman C, Lee M, Davenport F, Ratovitsky T, Prada C-M, Kim G, Seekins S, Yager D, Slunt H, Wang R, Seeger M, Levey A, Gandy S, Copeland N, Jenkins N, Price D, Younkin S, Sisodia S (1996). Familial Alzheimer's disease-linked presenilin 1 variants elevate Aβ1-42/1-40 ratio in vitro and in vivo. *Neuron*, 17:1005-1013.

[3] Duff K, Eckman C, Zehr C, Yu X, Prada C, Perez-Tur J, Hutton M, Buee L, Harigaya Y, Yager D, Morgan D, Gordon M, Holcomb L, Refolo L, Zenk B, Hardy J, Younkin S (1996). Increased amyloid-β42(43). in brains of mice expressing mutant presenilin 1. *Nature*, 383:710-713.

[4] Scheuner D, Eckman C, Jensen M, Song X, Citron M, Suzuki N, Bird T, Hardy J, Hutton M, Kukull W, Larson E, Levy-Lahad E, Viitanen M, Peskind E, Poorkaj P, Schellenberg G, Tanzi R, Wasco W, Lannfelt L, Selkoe D, Younkin S (1996). Secreted amyloid β-protein similar to that in the senile plaques of Alzheimer's disease is increased in vivo by the presenilin 1 and 2 and APP mutations linked to familial Alzheimer's disease. *Nat. Med.*, 2:864-870.

[5] Murayama O, Tomita T, Nihonmatsu N, Murayama M, Sun X, Honda T, Iwatsubo T, Takashima A (1999). Enhancement of amyloid β 42 secretion by 28 different presenilin 1 mutations of familial Alzheimer's disease. *Neurosci. Lett.*, 265:61-63.

[6] Song W, Nadeau P, Yuan M, Yang X, Shen J, Yankner B (1999). Proteolytic release and nuclear translocation of Notch-1 are induced by presenilin-1 and impaired by pathogenic presenilin-1 mutations. *Proc. Natl. Acad. Sci. USA*, 96:6959-6963.

[7] Bentahir M, Nyabi O, Verhamme J, Tolia A, Horré K, Wiltfang J, Esselmann H, De Strooper B (2006). Presenilin clinical mutations can affect γ-secretase activity by different mechanisms. J. *Neurochem.*, 96:732-742.

[8] Shen J & Kelleher R (2007). The presenilin hypothesis of Alzheimer's disease: evidence for a loss-of-function pathogenic mechanism. *Proc. Natl. Acad. Sci. USA*, 104:403-409.

[9] Shimojo M, Sahara N, Murayama M, Ichinose H, Takashima A (2007). Decreased Aβ secretion by cells expressing familial Alzheimer's disease-linked mutant presenilin 1. *Neurosci. Res.*, 57:446-453.

[10] Heilig E, Xia W, Shen J, Kelleher R (2010). A presenilin-1 mutation identified in familial Alzheimer disease with cotton wool plaques causes a nearly complete loss of γ-secretase activity. *J. Biol. Chem.*, 285:22350-22359.

[11] Kelleher R & Shen J (2010). Genetics. γ-Secretase and human disease. *Science*, 330:1055-1056.

[12] Takami M, Nagashima Y, Sano Y, Ishihara S, Morishima-Kawashima Y, Funamoto S, Ihara Y (2009). γ-Secretase: successive tripeptide and tetrapeptide release from the transmembrane domain of β-carboxyl terminal fragment. *J. Neurosci.*, 29:13042-13052.

[13] De Strooper B (2007). Loss-of-function presenilin mutations in Alzheimer disease. Talking Point on the role of presenilin mutations in Alzheimer disease. *EMBO Rep.*, 8:141-146.

[14] Wolfe M (2007). When loss is gain: reduced presenilin proteolytic function leads to increased Aβ42/Aβ40. Talking Point on the role of presenilin mutations in Alzheimer disease. *EMBO Rep.*, 8:136-140.

[15] Hardy J & Selkoe D (2002). The amyloid hypothesis of Alzheimer's disease: progress and problems on the road to therapeutics. *Science*, 297:353-356.

[16] Quintero-Monzon O, Martin M, Fernandez M, Cappello C, Krzysiak A, Osenkowski P, Wolfe M (2011). Dissociation between the processivity and total activity of γ-secretase: implications for the mechanism of Alzheimer's disease-causing presenilin mutations. *Biochemistry*, 50:9023-9035.

[17] Wang R, Wang B, He W, Zheng H (2006). Wild-type presenilin 1 protects against Alzheimer disease mutation-induced amyloid pathology. *J. Biol. Chem.*, 281:15330-15336.

[18] Kim J, Onstead L, Randle S, Price R, Smithson L, Zwizinski C, Dickson D, Golde T, McGowan E (2007). Aβ40 inhibits amyloid deposition in vivo. *J. Neurosci.*, 27:627-633.

[19] McGowan E, Pickford F, Kim J, Onstead L, Eriksen J, Yu C, Skipper L, Murphy M, Beard J, Das P, Jansen K, DeLucia M, Lin W-L, Dolios G, Wang R, Eckman C, Dickson D, Hutton M, Hardy J, Golde T (2005). Aβ42 is essential for parenchymal and vascular amyloid deposition in mice. *Neuron*, 47:191-199.

[20] Tanzi R & Bertram L (2005). Twenty years of the Alzheimer's disease amyloid hypothesis: a genetic perspective. *Cell*, 120:545-555.

[21] Saito T, Suemoto T, Brouwers N, Sleegers K, Funamoto S, Mihira N, Matsuba Y, Yamada K, Nilsson P, Takano J, Nishimura M, Iwata N, Van Broeckhoven C, Ihara Y, Saido T (2011). Potent amyloidogenicity and pathogenicity of Aβ43. *Nat. Neurosci.*, 14:1023-1032.

[22] Wang B, Yang W, Wen W, Sun J, Su B, Liu B, Ma D, Lv D, Wen Y, Qu T, Chen M, Sun M, Shen Y, Zhang X (2010). γ-Secretase gene mutations in familial acne inversa. *Science*, 330:1065.
[23] Pink A, Simpson M, Brice G, Smith C, Desai N, Mortimer P, Barker J, Trembath R (2011). PSENEN and NCSTN mutations in familial hidradenitis suppurativa (acne inversa). *J. Invest. Dermatol.*, 131:1568-1570.
[24] De Strooper B & Annaert W (2010). Novel research horizons for presenilins and γ-secretases in cell biology and disease. *Annu. Rev. Cell. Dev. Biol.*, 26:235-260.
[25] Esselens C, Oorschot V, Baert V, Raemaekers T, Spittaels K, Serneels L, Zheng H, Saftig P, De Strooper B, Klumperman J, Annaert W (2004). Presenilin 1 mediates the turnover of telencephalin in hippocampal neurons via an autophagic degradative pathway. *J. Cell. Biol.*, 166:1041-1054.
[26] Wilson C, Murphy D, Giasson B, Zhang B, Trojanowski J, Lee V (2004). Degradative organelles containing mislocalized α- and β-synuclein proliferate in presenilin-1 null neurons. *J. Cell. Biol.*, 165:335-346.
[27] Lee J, Yu W, Kumar A, Lee S, Mohan P, Peterhoff C, Wolfe D, Martinez-Vicente M, Massey A, Sovak G, Uchiyama Y, Westaway D, Cuervo A, Nixon R (2010). Lysosomal proteolysis and autophagy require presenilin 1 and are disrupted by Alzheimer-related PS1 mutations. *Cell*, 141:1146-1158.
[28] Zhang H, Sun S, Herreman A, De Strooper B, Bezprozvanny I (2010). Role of presenilins in neuronal calcium homeostasis. *J. Neurosci.*, 30:8566-8580.
[29] Bezprozvanny I & Mattson M (2008). Neuronal calcium mishandling and the pathogenesis of Alzheimer's disease. *Trends Neurosci.*, 31:454-463.
[30] Sato T, Dohmae N, Qi Y, Kakuda N, Misonou H, Mitsumori R, Maruyama H, Koo E, Haass C, Takio K, Morishima-Kawashima M, Ishiura S, Ihara Y (2003). Potential link between amyloid β protein 42 and C-terminal fragment γ 49-99 of β-amyloid precursor protein. *J. Biol. Chem.*, 278:24294-24301.
[31] Qi-Takahara Y, Morishima-Kawashima M, Tanimura Y, Dolios G, Hirotani N, Horikoshi Y, Kametani F, Maeda M, Saido T, Wang R, Ihara Y (2005). Longer forms of amyloid β protein: implications for the mechanism of intramembrane cleavage by γ-secretase. *J. Neurosci.*, 25:436-445.
[32] Kakuda N, Funamoto S, Yagishita S, Takami M, Osawa S, Dohmae N, Ihara Y (2006). Equimolar production of amyloid β-protein and amyloid precursor protein intracellular domain from β-carboxyl-terminal fragment by γ-secretase. *J. Biol. Chem.*, 281:14776-14786.
[33] Yagishita S, Morishima-Kawashima M, Ishiura S, Ihara Y (2008). Aβ46 is processed to Aβ40 and Aβ43, but not to Aβ42, in the low density membrane domains. *J. Biol. Chem.*, 283:733-738.
[34] Funamoto S, Morishima-Kawashima M, Tanimura Y, Hirotani N, Saido T, Ihara Y (2004). Truncated carboxyl-terminal fragments of β-amyloid precursor protein are processed to amyloid β-proteins 40 and 42. *Biochemistry*, 43:13532-13540.
[35] Herreman A, Serneels L, Annaert W, Collen D, Schoonjans L, De Strooper B (2000). Total inactivation of γ-secretase activity in presenilin-deficient embryonic stem cells. *Nat. Cell. Biol.*, 2:461-462.
[36] Kuperstein I, Broersen K, Benilova I, Rozenski J, Jonckheere W, Debulpaep M, Vandersteen A, Segers-Nolten I, van der Werf K, Subramaniam V, Braeken D, Callewaert G, Bartic C, D'Hooge R, Martins I, Rousseau F, Schymkowitz J, De Strooper B (2010). Neurotoxicity of Alzheimer's disease Aβ peptides is induced by small changes in the Aβ42 to Aβ40 ratio. *EMBO J.*, 29:3408-3420.
[37] De Strooper B, Vassar R, Golde T (2010). The secretases: enzymes with therapeutic potential in Alzheimer disease. *Nat. Rev. Neurol.*, 6:99-107.
[38] Martone R, Zhou H, Atchison K, Comery T, Xu J, Huang X, Gong X, Jin M, Kreft A, Harrison B, Mayer S, Aschmies S, Gonzales C, Zaleska M, Riddell D, Wagner E, Lu P, Sun S, Sonnenberg-Reines J, Oganesian A, Adkins K, Leach M, Clarke D, Huryn D, Abou-Gharbia M, Magolda R, Bard J, Frick G, Raje S, Forlow S, Balliet C, Burczynski M, Reinhart P, Wan H, Pangalos M, Jacobsen J (2009). Begacestat (GSI-953): a novel, selective thiophene sulfonamide inhibitor of amyloid precursor protein γ-secretase for the treatment of Alzheimer's disease. *J. Pharmacol. Exp. Ther.*, 331:598-608.
[39] Gillman K, Starrett J, Parker M, Xie K, Bronson J Marcin L, McElhone K, Bergstrom C, Mate R, Williams R, Meredith J, Burton C, Barten D, Toyn J, Roberts S, Lentz K, Houston J, Zaczek R, Albright C, Decicco C, Macor J, Olson R (2011). Discovery and evaluation of BMS-708163, a potent, selective and orally bioavailable γ-secretase inhibitor. *ACS Med. Chem. Lett.*, 1:120-124.
[40] Weggen S, Eriksen J, Das P, Sagi S, Wang R, Pietrzik C, Findlay K, Smith T, Murphy M, Bulter T, Kang D, Marquez-Sterling N, Golde T, Koo E (2001). A subset of NSAIDs lower amyloidogenic Aβ42 independently of cyclooxygenase activity. *Nature*, 414:212-216.
[41] Oehlrich D, Berthelot D, Gijsen H (2011). γ-Secretase modulators as potential disease modifying anti-alzheimer's drugs. *J. Med. Chem.*, 54:669-698.
[42] Tolia A, Horre K, De Strooper B (2008). Transmembrane domain 9 of presenilin determines the dynamic conformation of the catalytic site of γ-secretase. *J. Biol. Chem.*, 283:19793-19803.

[43] Watanabe N, Takagi S, Tominaga A, Tomita T, Iwatsubo T (2010). Functional analysis of the transmembrane domains of presenilin 1: participation of transmembrane domains 2 and 6 in the formation of initial substrate-binding site of γ-secretase. *J. Biol. Chem.*, 285:19738-19746.

[44] Moehlmann T, Winkler E, Xia X, Edbauer D, Murrell J, Capell A, Kaether C, Zheng H, Ghetti B, Haass C, Steiner H (2002). Presenilin-1 mutations of leucine 166 equally affect the generation of the Notch and APP intracellular domains independent of their effect on Aβ42 production. *Proc. Natl. Acad. Sci. USA*, 99:8025-8030.

[45] Portelius E, Andreasson U, Ringman J, Buerger K, Daborg J, Buchhave P, Hansson O, Harmsen A, Gustavsson M, Hanse E, Galasko D, Hampel H, Blennow K, Zetterberg H (2010). Distinct cerebrospinal fluid amyloid β peptide signatures in sporadic and PSEN1 A431E-associated familial Alzheimer's disease. *Mol. Neurodegener.*, 5:2.

[46] Murphy M, Uljon S, Golde T, Wang R (2002). FAD-linked mutations in presenilin 1 alter the length of Aβ peptides derived from βAPP transmembrane domain mutants. *Biochim. Biophys. Acta.*, 1586: 199-209.

[47] Berezovska O, Lleo A, Herl L, Frosch M, Stern E, Bacskai B, Hyman B (2005). Familial Alzheimer's disease presenilin 1 mutations cause alterations in the conformation of presenilin and interactions with amyloid precursor protein. *J. Neurosci.*, 25:3009-3017.

[48] Czirr E, Cottrell B, Leuchtenberger S, Kukar T, Ladd T, Esselmann H, Paul S, Schubenel R, Torpey J, Pietrzik C, Golde T, Wiltfang J, Baumann K, Koo E, Weggen S (2008). Independent generation of Aβ42 and Aβ38 peptide species by γ-secretase. *J. Biol. Chem.*, 283:17049-17054.

[49] Page R, Baumann K, Tomioka M, Perez-Revuelta B, Fukumori A, Jacobson H, Flohr A, Luebbers T, Ozmen L, Steiner H, Haass C (2008). Generation of Aβ38 and Aβ42 is independently and differentially affected by familial Alzheimer disease-associated presenilin mutations and γ-secretase modulation. *J. Biol. Chem.*, 283:677-683.

[50] Chavez-Gutierrez L, Tolia A, Maes E, Li T, Wong P, De Strooper B (2008). Glu(332) in the Nicastrin ectodomain is essential for γ-secretase complex maturation but not for its activity. *J. Biol. Chem.*, 283:20096-20105.

[51] Annaert W, Levesque L, Craessaert K, Dierinck L, Snellings G, Westaway D, George-Hyslop P, Cordell B, Fraser P, De Strooper B (1999). Presenilin 1 controls γ-secretase processing of amyloid precursor protein in pre-golgi compartments of hippocampal neurons. *J. Cell Biol.*, 147:277-294.

[52] Wiltfang J, Esselmann H, Bibl M, Smirnov A, Otto M, Paul S, Schmidt B, Klafki H, Maler M, Dyrks T, Bienert M, Beyermann M, Rüther E, Kornhuber J (2002). Highly conserved and disease-specific patterns of carboxyterminally truncated Aβ peptides 1-37/38/39 in addition to 1-40/42 in Alzheimer's disease and in patients with chronic neuroinflammation. *J. Neurochem.*, 81:481-496.

8

Molecular plasticity regulates oligomerization and cytotoxicity of the multipeptide length Aβ pool.

Current therapeutic approaches under development for Alzheimer disease, including γ-secretase modulating therapy, aim at increasing the production of $A\beta_{38}$ and $A\beta_{40}$ at the cost of longer Aβ peptides. Here, we consider the aggregation of $A\beta_{38}$ and $A\beta_{43}$ in addition to $A\beta_{40}$ and $A\beta_{42}$; in particular their behavior in mixtures representing the complex *in vivo* Aβ pool. We demonstrate that $A\beta_{38}$ and $A\beta_{43}$ aggregate similar to $A\beta_{40}$ and $A\beta_{42}$, respectively, but display variation in kinetics of assembly and toxicity due to differences in short timescale conformational plasticity. In biologically relevant mixtures of Aβ, $A\beta_{38}$ and $A\beta_{43}$ significantly affect the behaviors of $A\beta_{40}$ and $A\beta_{42}$. The short timescale conformational flexibility of $A\beta_{38}$ is suggested to be responsible for enhancing toxicity of $A\beta_{40}$ whilst exerting a cyto-protective effect on $A\beta_{42}$. Our results indicate that the complex *in vivo* Aβ peptide array, and variations thereof, is critical in Alzheimer disease, which can influence the selection of current and new therapeutic strategies.

The results described in this chapter have been published in:
Vandersteen A, Masman M, De Baets G, Jonckheere W, van der Werf K, Marrink SJ, Rozenski J, Benilova I, De Strooper B, Subramaniam V, Schymkowitz J, Rousseau F, and Broersen K (2012). *J. Biol. Chem.*, 287:36732-36743.

8.1 Introduction

Extracellular deposits containing Aβ represent one of the hallmarks of Alzheimer disease [1]. Processing of the transmembrane amyloid precursor protein (APP) primarily generates the 40-amino acid $A\beta_{40}$ peptide and smaller amounts of the 42-amino acid $A\beta_{42}$ peptide, in addition to minute quantities of other Aβ peptides ranging in length from 27 to 43 amino acids [2,3]. The observed variation at the Aβ carboxy terminus is a consequence of the heterogeneous γ-secretase processing pattern [4] and the array of Aβ peptides that is produced in this way can be affected by clinical mutations in APP [5,6] or in presenilin-1 (PS1) [5-7]. Mutations of PS1 potently shift the ε-cleavage site on APP towards the $A\beta_{38}$ production pathway [8].

Generally, longer Aβ peptides are more hydrophobic as the carboxy-termini progressively form part of the transmembrane domain of APP and are therefore considered more aggregation prone [9-11]. Recently, γ-secretase modulators (GSMs) have been developed. These fine-tune the action of γ-secretase to shift the production of Aβ peptides towards shorter variants while leaving the total Aβ peptide production and activity of γ-secretase unchanged [12,13]. Given the finding that specifically aggregated Aβ peptide can lead to a neurotoxic response, GSMs offered in this way a promising perspective as a potential agent to slow down the progress of senile plaque deposition in Alzheimer disease by decreasing the production of $A\beta_{42}$ whilst increasing that of $A\beta_{38}$. The first generation of GSMs were classified as non-steroidal anti-inflammatory drugs (NSAIDs) and derivatives thereof. Administration of these drugs to healthy individuals showed positive effects on cognitive function which could be entirely attributed to the cyclo-oxygenase (COX) inhibitory action of the compound without displaying GSM action [14,15]. Clinical trials with non-COX inhibitory NSAIDs did not display protective effects on Alzheimer disease progress possibly as a result of the low potency and poor brain penetrance of the compounds, inhibition of Notch processing or accumulation of APP C-terminal fragments [16]. A next generation of Notch sparing GSMs and non-NSAID derived compounds with improved potency and brain penetration are currently being developed but yet await clinical trials [15].

The reported neurotoxicity of $A\beta_{43}$ [7] as well as the observed increasing [17] and decreasing $A\beta_{38}$ [18] levels in CSF upon Alzheimer disease progress, indicate that the contributions of $A\beta_{38}$ and $A\beta_{43}$ to disease progression require further elucidation. By comparing their pathogenicity, aggregation profiles and biophysical properties with that of well-studied $A\beta_{40}$ and $A\beta_{42}$ we show that $A\beta_{38}$ and $A\beta_{43}$ both form aggregates which differ in cytotoxic potential. We further show that inclusion of $A\beta_{38}$ and $A\beta_{43}$ into complex mixtures containing $A\beta_{40}$ and $A\beta_{42}$ substantially affects the behavior of total Aβ and that $A\beta_{38}$ and $A\beta_{40}$, previously considered non-amyloidogenic, can unexpectedly become toxic in these mixtures. These findings have been related to conformational plasticity of the respective peptides and highlight the relevance of understanding the role of carboxy-terminal variation of Aβ peptides and their potential as therapeutic targets.

8.2 Results

8.2.1 Aβ peptide length determines aggregation, oligomerization and toxicity

It has been reported before that $A\beta_{40}$ and $A\beta_{42}$ display different aggregation

kinetics [9,19]. Consistent with these data, we also observed substantial differences in aggregation kinetics as a function of peptide length (Figure 8.1a) when comparing $A\beta_{38}$, $A\beta_{40}$, $A\beta_{42}$ and $A\beta_{43}$ using thioT fluorescence. While $A\beta_{38}$ and $A\beta_{40}$ showed a delayed onset of aggregation, $A\beta_{42}$ and $A\beta_{43}$ rapidly aggregated as suggested by the immediate rise in thioT fluorescence signal. Even though the aggregation regimes of $A\beta_{38}$ and $A\beta_{40}$ are generally alike with a distinct lag phase and significant and sigmoidal development of thioT signal after 10 h of incubation, $A\beta_{38}$ showed a more rapid onset of aggregation compared to $A\beta_{40}$. The final (10h) thioT fluorescence intensity of both $A\beta_{42}$ and $A\beta_{43}$ aggregates was very low compared to $A\beta_{38}$ and $A\beta_{40}$ (Figure 8.1b) and has been reported to correlate with the weight concentration and the morphology of the formed fibrils [20]. Transmission electron microscopy (TEM) showed that 0.5 h of incubation of $A\beta_{42}$ and $A\beta_{43}$ resulted in networks of intertwined fibrils while for $A\beta_{38}$ and $A\beta_{40}$ aggregates were absent (Figure 8.1c). Upon incubation for 4 h the fibrillar network observed for $A\beta_{43}$ had progressed into polymorphous clusters interconnected by mature fibrils. $A\beta_{42}$ showed a similar organization yet short and aligned fibrils seemed more prevalent compared to $A\beta_{43}$. In contrast, $A\beta_{38}$ and $A\beta_{40}$ both formed long, negatively stained and regularly twisted fibrils with a diameter of 8-12 nm which is typically observed for amyloid-like fibrils [21]. All Aβ peptides formed extensive fibrillar networks upon incubation for 24 h. To establish by which mechanism carboxy-terminal variation affected the observed aggregation characteristics of Aβ, the statistical thermodynamics algorithm TANGO was used to predict aggregating stretches in the various Aβ peptides tested. TANGO scores further showed that, in general, increasing aggregation propensity could be observed with increasing peptide length with the exception of Aβ varying in length from 37 to 40 amino acids (Fig. 1d). A per-residue analysis of the aggregation propensity showed that all Aβ sequences contain a common aggregating stretch ranging from residue 16 to residue 22 [22] (Figure 8.1e). A second aggregating region starts at residue 28 and spans the remaining carboxy-terminal part of the sequence and showed strong variation with Aβ length, owing predominantly to the presence of two subsequent glycine residues, which disfavor aggregation but which are compensated by additional aggregation promoting residues in the longer forms. Our analysis shows that differences in aggregation propensity directly stem from C-terminal variation. In line with our observation that $A\beta_{38}$ aggregates faster than $A\beta_{40}$ (Figure 8.1a), TANGO predicted a slightly higher aggregation propensity for $A\beta_{38}$ than for $A\beta_{40}$ (Figure 8.1 d,e).

ThioT does not interact strongly with oligomeric Aβ [23] while soluble oligomeric Aβ is generally considered to represent the toxic species [24-26]. We used complementary oligomer-sensitive techniques such as the A11 oligomer-specific antibody [27] and atomic force microscopy (AFM) to obtain information on the lifetime of oligomeric Aβ as a function of C-terminal variation. Aβ peptides were allowed to aggregate and were tested for A11-reactivity at various time points of incubation (Figure 8.2a). $A\beta_{42}$ and $A\beta_{43}$ formed A11-positive oligomers already after 0.5 h of incubation while $A\beta_{38}$ and $A\beta_{40}$ only interacted with the A11-antibody after an incubation time of 5 and 6 h, respectively, with $A\beta_{38}$ exhibiting substantially stronger staining with the antibody than $A\beta_{40}$. Complementary to A11 reactivity, AFM imaging of samples upon 1.5 h of incubation showed the presence of small oligomeric species for all Aβ peptides tested, including $A\beta_{38}$ and $A\beta_{40}$ (Figure 8.2b). Even though oligomers were present for all

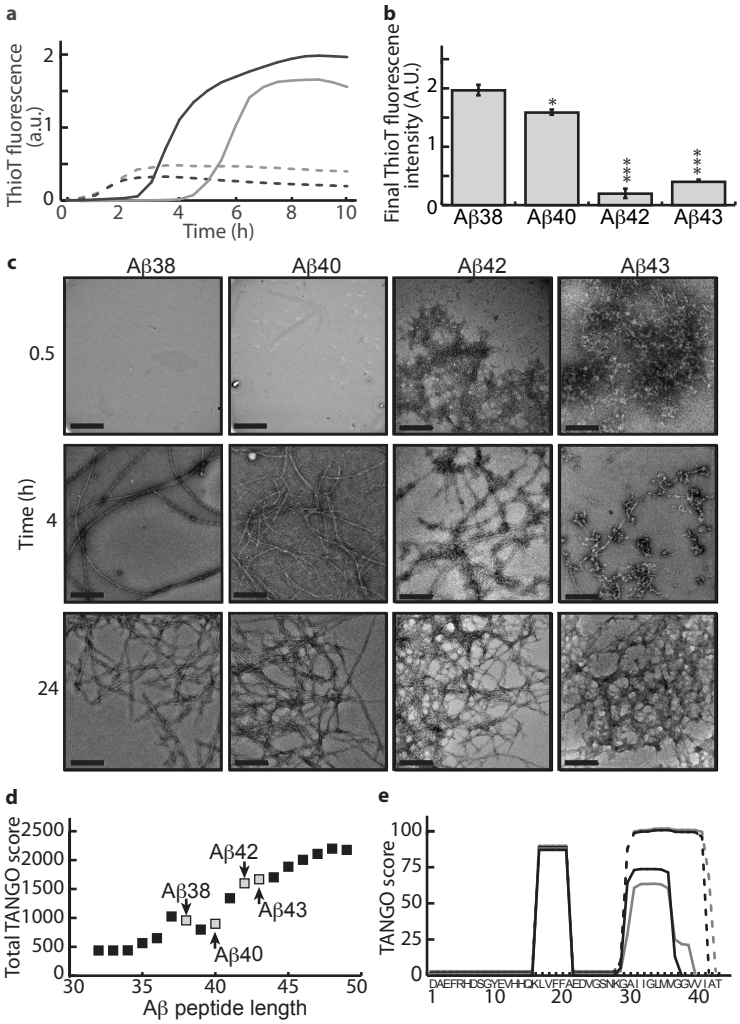

Figure 8.1 Carboxy-terminal heterogeneity affects aggregation kinetics of the Aβ peptide. (a) ThioT fluorescence was recorded *in situ* every 5 min at 25 °C. $A\beta_{38}$ (black line) and $A\beta_{40}$ (grey line) display a lag phase while $A\beta_{42}$ (dotted black line) and $A\beta_{43}$ (dotted grey line) induce ThioT fluorescence almost immediately. The values represent the means of three experiments. (b) Final (10 h) thioT fluorescence intensities derived from panel A. Statistical significance (unpaired 2-tailed t-test) compared to the $A\beta_{38}$ value is indicated by ***p<0.0001, **p<0.0005 or *p<0.005. (c) After 0.5 h incubation $A\beta_{42}$ and $A\beta_{43}$ formed networks while $A\beta_{38}$ and $A\beta_{40}$ did not show visible aggregates. After 4h incubation $A\beta_{38}$ and $A\beta_{40}$ formed 8-12 nm wide, extended, negatively stained fibrils. $A\beta_{42}$ organized into a network of rigid 14-16 nm wide fibrils. For $A\beta_{43}$ a mixture of protofibrils and fibrils was observed. After 24h all Aβ formed similar fibrillar networks. Scalebar: 200 nm. (d) Total TANGO scores indicated an increasing overall aggregation propensity of Aβ with increasing peptide length except for 37 to 40 amino acids long peptides. (e) Sequence based prediction of aggregation prone stretches by TANGO suggests a common aggregating region in the core of the peptide and a second aggregating region at the C-terminus. Differences in total TANGO score (d) are exclusively due to the C-terminal aggregating region. $A\beta_{38}$ (black line) and $A\beta_{40}$ (grey line) display similar predicted aggregation propensity while that of $A\beta_{42}$ (dotted black line) and $A\beta_{43}$ (dotted grey line) were higher.

Aβ peptides tested, $A\beta_{38}$ and $A\beta_{40}$ oligomers only developed into A11-positive oligomers at a later stage compared to $A\beta_{42}$ and $A\beta_{43}$. Cytotoxicity of oligomeric Aβ upon carboxy-terminal variation was assessed using neuroblastoma cell line SH-SY5Y (Figure 8.2c). A11-positive oligomers derived from $A\beta_{42}$ and $A\beta_{43}$ induced loss of cell viability at a concentration of 5 μM while those derived of $A\beta_{38}$ and $A\beta_{40}$ affected cell viability only at a significantly higher concentration of 20 μM.

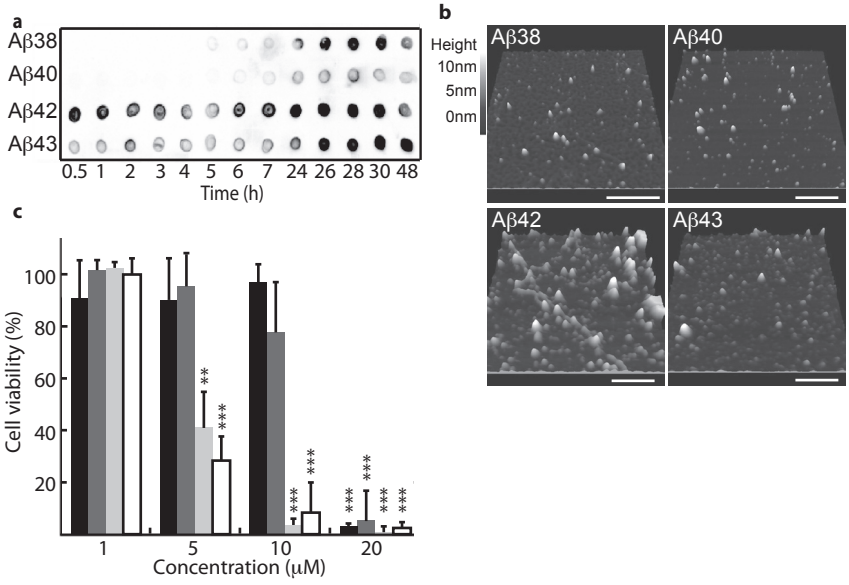

Figure 8.2 Differences in aggregation kinetics due to C-terminal heterogeneity are reflected at toxic oligomer level.
Aβ at 50 μM was allowed to aggregate at 25 °C under quiescent conditions. (a) Analysis with the A11 oligomer-specific antibody detected oligomeric $A\beta_{42}$ and $A\beta_{43}$ after as little as 0.5 h incubation whereas $A\beta_{38}$ and $A\beta_{40}$ became A11-positive after 5 to 6 h of incubation. (b) Imaging using AFM indicated the presence of oligomers for all Aβ samples incubated for 1.5 h. The length of the bar represents 500 nm. (c) Pre-incubated (1.5 h) Aβ was added to cultured SH-SY5Y cells and incubated for 24 h before probing cytotoxicity using Cell Titer Blue viability assay. $A\beta_{38}$ (black) and $A\beta_{40}$ (dark grey) only cause cytotoxicity at a concentration of 20 μM while $A\beta_{42}$ (light grey) and $A\beta_{43}$ (white) are significantly cytotoxic at a concentration of 5 μM. Values are expressed as percent of cell viability ± SD (n=4), buffer signal was normalized to 100%. Statistical significance (unpaired 2-tailed t-test) compared to buffer control values (normalized to 100%) is indicated by p-value analysis similar to Figure 8.1b.

8.2.2 Aβ LENGTHS DISPLAY CONFORMATIONAL DIFFERENCES

Circular dichroism (CD) and Fourier transform infrared (FTIR) spectroscopy were used to evaluate Aβ structure after 1.5 h of incubation. The spectra recorded for $A\beta_{38}$ and $A\beta_{40}$ using CD were very similar, and displayed typical characteristics of a largely unstructured protein while the spectra of $A\beta_{42}$ and $A\beta_{43}$ showed pronounced β-sheet formation with a minimum intensity at a wavelength of 218 nm (Figure 8.3a). As FTIR is more sensitive to β-sheet formation than CD and can distinguish between parallel and anti-parallel β-sheet arrangements, FTIR measurements were performed complementary to CD. Figure 8.3b shows difference spectra obtained by subtraction

of the spectrum of non-aggregated Aβ (time 0) from the spectrum recorded after 1.5 h of incubation. The strong increase of absorbance at a wavelength of 1627 cm^{-1} concurrent with a loss of signal between 1650-1655 cm^{-1} and 1680 cm^{-1} for all four peptides tested, indicated that β-sheet formation took place during the 1.5 h incubation time at the cost of random coil and β-turn structure. The more narrow peak for $A\beta_{38}$ suggests the formation of a more stable β-sheet as a result of more extensive H-bonding, compared to the other peptide lengths investigated although $A\beta_{40}$ was found to form most β-sheet judging from a higher signal intensity at a wavelength of 1627 cm^{-1}. The small increase at 1695 cm^{-1} seen here for $A\beta_{38}$ and $A\beta_{43}$ in addition to the increase at a wavelength of 1627 cm^{-1} reveals the formation of an antiparallel oriented β-sheet which has been typically used as a fingerprint for oligomer formation [28]. Variation in evolution of these regions is observed between the Aβ isoforms. This observation suggests that the various Aβ isoforms display small structural differences during aggregation. Even though CD and FTIR provide useful structural information in terms of an average of the entire protein sequence, they do not provide insight into the behavior of individual residues in the sequence, and, hence, are not able to address the question why the addition of two valines in $A\beta_{40}$ rendered this peptide less aggregation prone than $A\beta_{38}$. Also CD and FTIR spectroscopy were unable to report on short-time scale conformational flexibility of peptides potentially required to trigger the onset of aggregation.

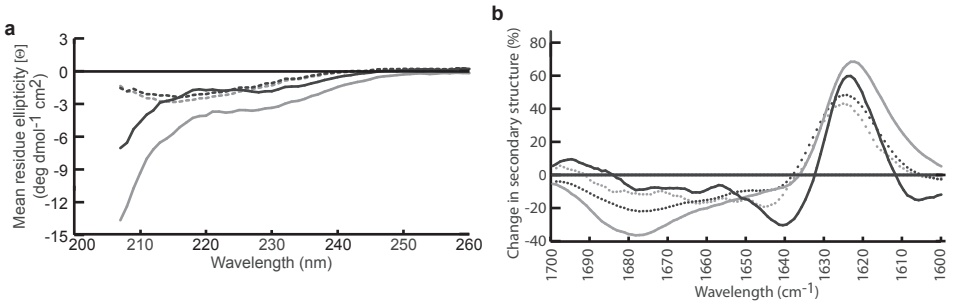

Figure 8.3 Aggregating Aβ peptides show differences on a secondary structural level. (a) CD measurements were performed with pre-incubated (1.5 h) Aβ at 15 μM. Spectra recorded for $A\beta_{38}$ (continuous black line) and $A\beta_{40}$ (continuous grey line) were characteristic of peptides with a large degree of disorder whereas $A\beta_{42}$ (dotted black line) and $A\beta_{43}$ (dotted grey line) displayed curves with a single minimum at 217 nm, suggesting β-sheet formation. High buffer interference was observed at wavelengths < 207 nm (b) FTIR absorbance was measured of monomeric and pre-incubated (1.5 h) Aβ at 200 μM and the difference between both spectra was plotted. The difference spectra showed an intensity increase at a wavelength of 1627 cm^{-1} indicating that all four peptides were converted into a β-sheet conformation. For $A\beta_{38}$ (continuous black line), and $A\beta_{43}$ (dotted grey line) an additional increase in intensity around 1695 cm^{-1} was observed implying an antiparallel oriented β-sheet. $A\beta_{40}$ (continuous grey line) and $A\beta_{42}$ (dotted black line) data were both characterized by a loss of β-turn as observed by the decrease in intensity at 1680 cm^{-1}.

We used molecular dynamics (MD) simulations to establish whether individual residues contributed to changes in peptide conformation which could explain the observed results. We focused our observations on definition of secondary structure of proteins (DSSP) analysis [29]. Here, we report the DSSP results as: coil (unstructured conformation), extended conformation (β-bridge plus β-sheet structures), loop (bend

plus turns), and helical conformation (β-helix plus 3_{10}-helix plus π-helix). All peptides presented a general trend to possess a mixture of a collapsed coil structure and helical conformation for residues 1-20. N-terminal helical structure was partially retained over time, whereas C-terminal helicity, if any, was rapidly lost (Figure 8.4).

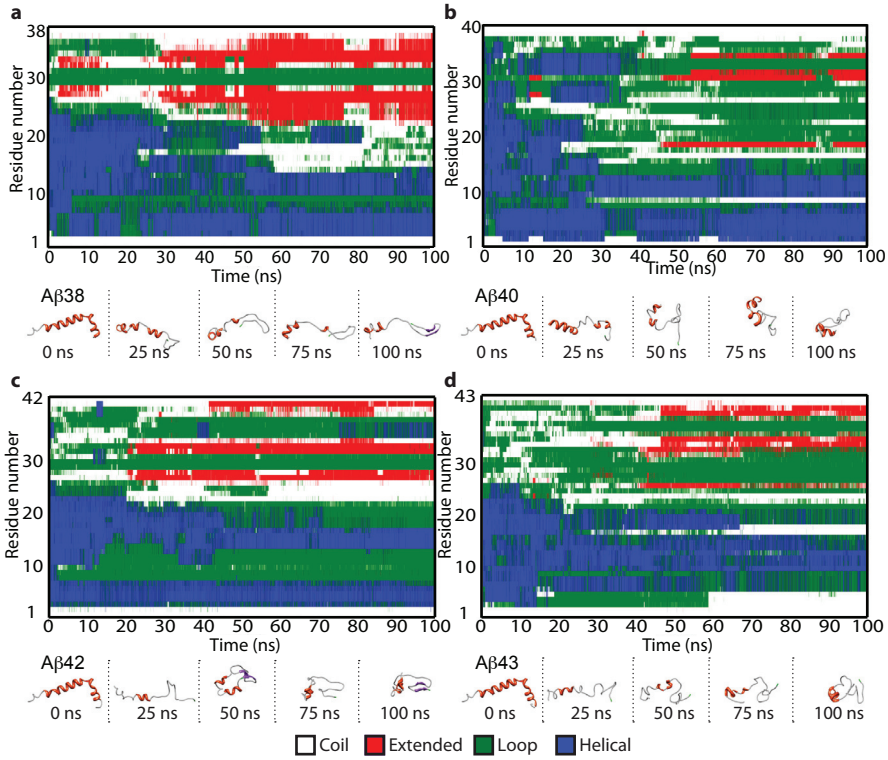

Figure 8.4 At short time scales extended conformations only occur at the C-termini of Aβ, while N-termini retain their helical conformation.
Secondary structure composition per residue in function of time for selected representative MD simulations: (a) $A\beta_{38}$, (b) $A\beta_{40}$, (c) $A\beta_{42}$, $A\beta_{42}$ (d) $A\beta_{43}$. Secondary structure was determined using DSSP criteria. Reported conformations are coil, extended, loop and helical conformation. Snapshots of peptide conformations are shown for 0, 25, 50, 75, and 100 ns of simulation time.

Also as a general observation, all extended conformations occurred between residues 21-28 and residues 32 to the C-terminal amino acid. A loop section comprising residues 29-31 formed flexible links between these extended portions. Contrary to what was expected, $A\beta_{38}$ conformation behavior most closely resembled that of $A\beta_{42}$, rather than $A\beta_{40}$ (Figure 8.4)(Figure 8.5 a,b). Over the 100 ns time scale of the simulations, $A\beta_{38}$ showed a marked tendency to form extended conformations (Figure 8.5 a,b), comparable to $A\beta_{42}$ and $A\beta_{43}$ (Figure 8.5 b,b1). $A\beta_{40}$, on the other hand, exhibited low tendency to form extended conformations (Figure 8.5a). Interestingly, during the first tens of nanoseconds the behavior of $A\beta_{38}$ was erratic and fluctuated between resembling $A\beta_{40}$ and $A\beta_{42}$/$A\beta_{43}$. Only after 50 ns of simulation the content of extended conformation invariably increased (Figure 8.5 a,d). $A\beta_{42}$ and $A\beta_{43}$ seemed

to accumulate and stabilize better their extended conformations, from earlier simulation times onwards (Figure 8.5 b,b1)(Figure 8.6). The same behavior was reflected in the overall helicity of the peptides (Figure 8.5c) revealing a slight, yet statistically significant, higher tendency to retain its helical conformation for $A\beta_{38}$ in comparison to $A\beta_{42}$ and $A\beta_{43}$. A marked increase in the helicity of residues 20-23 and 28 was uniquely observed for $A\beta_{40}$ (Figure 8.5 c,d). Collectively, these data showed that the behaviors of $A\beta_{42}$ and $A\beta_{43}$ were remarkably similar in terms of their high tendency to form an extended β-sheet conformation while $A\beta_{40}$ retained helicity longer. The $A\beta_{38}$ peptide showed very interesting behavior in terms of its highly fluctuating tendency to form extended β-sheet conformation. Over time $A\beta_{38}$ conformation alternated rapidly between $A\beta_{42}$/$A\beta_{43}$-like conformation and $A\beta_{40}$-like conformation before forming stable, extended β-sheet.

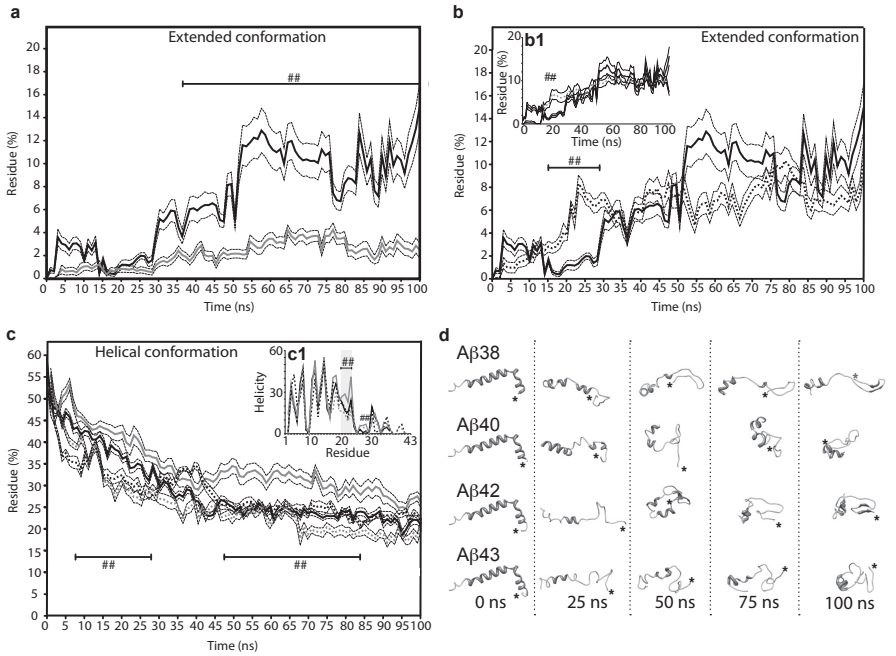

Figure 8.5 Aβ peptides show conformational fluctuations at short time-scales, which vary upon C-terminal elongation.

Secondary structure composition determined by DSSP method: extended conformation (β-bridge plus β-sheet structures), and helical conformation (α-helix plus 3_{10}-helix plus π-helix). Results were averaged over ten independent simulations. The extended conformation content in function of time for $A\beta_{38}$ (continuous black line) is compared to: (a) $A\beta_{40}$ (continuous grey line); and (b) $A\beta_{42}$ (dotted black line); inset plot (b1) $A\beta_{43}$ (dotted grey line), which reveals a similar profile compared to $A\beta_{42}$. Statistically significant differences (SEM) are denoted with a caped-line (##p<0.005). (c) The helical content in function of time is shown for all peptides. Regions of the simulation time wherein there are statistically significant differences are denoted with a caped-line (##p<0.005) compared to $A\beta_{42}$. Inset plot (c1) shows helicity per residue for all Aβ peptides (##p<0.005, compared to all Aβ peptides). Helicity is reported as the percentage of simulation time that a given amino acid residue presented α-helix conformation. (d) Snapshots for all Aβ peptides at 0, 25, 50, 75 and 100 ns of simulation time. C-termini positions are denoted with an asterisk (*).

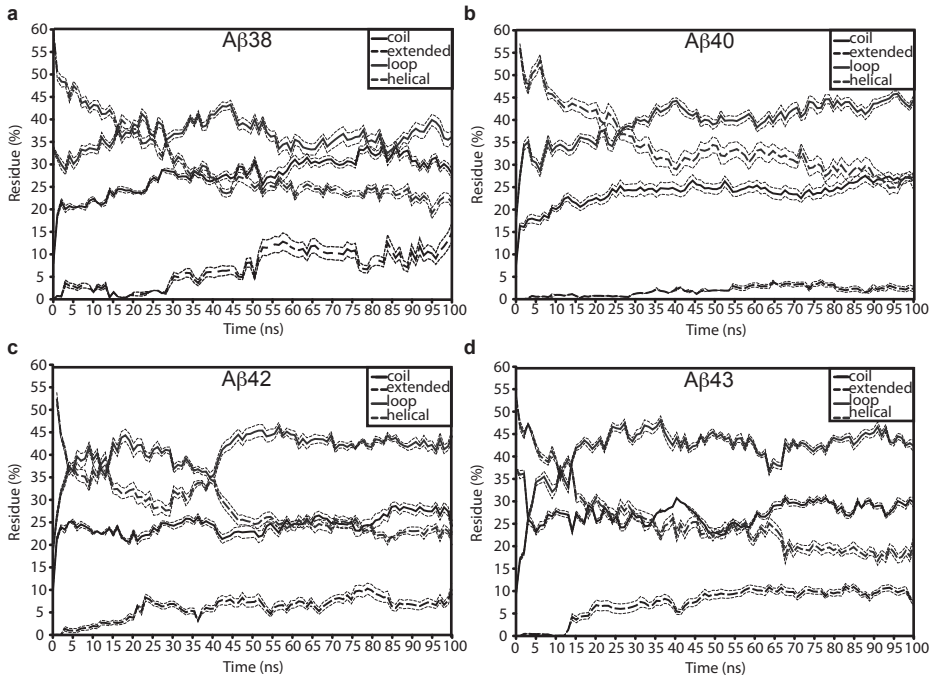

Figure 8.6 Secondary structure composition of Aβ38 correlates better to Aβ42 than to Aβ40.

Overall appearance of secondary structure composition (% of total amount of residues) in function of time for (a) Aβ38, (b) Aβ40, (c) Aβ42 (d) Aβ43. Secondary structure was determined using DSSP criteria, and reported as average of 10 simulations per peptide. Reported conformations correspond to: coil, extended, loop and helical conformation.

8.2.3 Mixtures of Aβ show complex aggregation behavior

To evaluate the influence of the observed differences between Aβ isoforms in a more biologically relevant setting, we mimicked the complex pool of various Aβ peptide lengths as observed *in vivo* by preparing Aβ peptide mixtures containing Aβ40, or Aβ42 and Aβ38, or Aβ43. Increased levels of Aβ38 in the CSF of Alzheimer disease patients are reported [17], as well as an increased generation of this peptide due to PS1 mutations [30]. Some forms of FAD display increased generation of Aβ43 [30], a peptide length frequently present in amyloid plaques [31]. Aβ40 and Aβ43 were shown to directly interact using ESI-MS although these dimeric species only accumulated at a population of ~1% (see appendix B). Effective but low accumulation of mixed dimers was also observed upon mixing Aβ38 and Aβ42 (see appendix B). Mixed dimeric complex formation was further detected for Aβ38:Aβ40 and Aβ42:Aβ43. Along the lines of the earlier identified processing pathways of APP toward the formation of either Aβ40 and Aβ38 with Aβ43 and Aβ42 as intermediates, respectively [8], we mapped dose-response curves of the presence of Aβ43 and Aβ38 on the aggregation kinetics of Aβ40 and Aβ42, respectively, using thioT fluorescence (Figure 8.7). We reported earlier that Aβ42:Aβ40 mixtures behave differently according to their proportional presence (Chapter 5). Titration of Aβ40 with increasing concentrations of Aβ43 substantially reduced the lag phase of aggregation to become similar to that of Aβ43

alone while final fluorescence intensities were not affected (Figure 8.7 a,c). These observations suggest that Aβ43 dominantly influences the nucleation process of Aβ40 while aggregate morphology or mass were presumably determined by Aβ40 (Figure 8.7c). Titration of Aβ38 with Aβ42 similarly lead to a decreased nucleation rate but, in addition, gradually increased the elongation rate and final thioT fluorescence intensity (Figure 8.7 b,d). The complex aggregation characteristics compared to each of these peptides in isolation are highly suggestive of interaction of the Aβ peptides in mixtures.

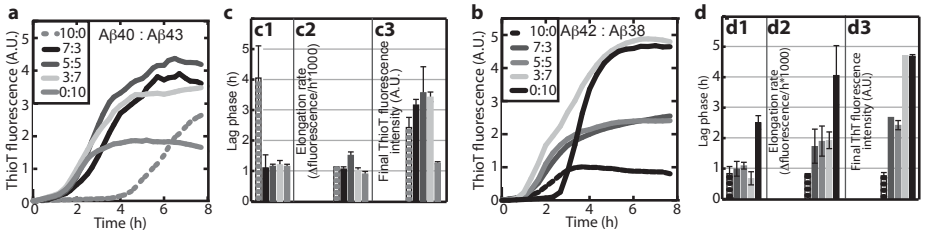

Figure 8.7 Little prevalent Aβ peptides strongly affect the behavior of predominant Aβ. ThioT fluorescence was recorded *in situ* every 5 min at 25 °C with 50 μM Aβ and 12 μM ThioT. Values represent means of two experiments. (a,c) Irrespective of its concentration, Aβ43 (dotted grey line) reduced the lag-phase for aggregation (c1) of Aβ40 (continuous grey line) without affecting elongation rates (c2). Aβ40:Aβ43 mixtures displayed higher fluorescence intensity after 8 h incubation (c3) than Aβ40 and Aβ43 alone. Greyscale code as in Fig. 5a. (b,d) Titration of Aβ42 (dotted black line) with Aβ38 (continuous black line) reduced lag phase (d1), and elongation rate (d2) but increased fluorescence intensity at plateau (d3). Greyscale code as in Fig. 5b.

Aβ40 is the most predominant species recovered from CSF [3,32]. Aβ38 has been reported to be present in CSF at concentrations of 1.26 to 2.78 ng/ml, while concentrations of Aβ42 were 0.46 to 2.07 ng ml^{-1} [3,32,33]. Quantitative detection of Aβ43 has only been performed in brain plaques and, as suitable antibodies are not available, can generally not be distinguished from that of Aβ42. While quantitative information on the released amounts of the four Aβ isoforms of interest from APP is only available for mutations related to familial Alzheimer disease based on *in vitro* observations [6,30,34,35], we performed titration assays (Figure 8.7). Results indicated that 30% of Aβ38 or Aβ43 already caused significant alteration of the aggregation profile of Aβ42 and of the lag phase of Aβ40. Many disease-related mutations accumulate Aβ42 while it can be assumed that in sporadic Alzheimer disease Aβ40 is predominantly produced [36]. We therefore decided to evaluate the effect of small concentrations (10%) of Aβ38 and Aβ43 on predominantly present (90%) Aβ40 and Aβ42 to monitor more subtle influences of the presence of peptides in mixtures. In summary, we evaluated oligomerization, cytotoxicity and aggregation of 9:1 mixtures of Aβ40:Aβ38, Aβ40:Aβ43, Aβ42:Aβ38, and Aβ42:Aβ43. At these low concentrations the effect of the addition of Aβ38 and Aβ43 to either Aβ40 or Aβ42 was limited to a significant decrease in final fluorescence intensity while leaving the nucleation phase unchanged (Figure 8.8 a,b). Visualization of aggregate morphology by TEM further rationalized the observed change in final fluorescence intensity (Figure 8.1c and Figure 8.8c). Even though aggregate formation could not be established at early time points for Aβ38 and Aβ40 in isolation, a 9:1 mixture of these peptides showed the formation of extensive ThioT-negative but A11-positive aggregates that were present for extended periods of time (Figure 8.8 a,c,d). Also at early time points

of incubation the morphologies of both $A\beta_{40}$ and $A\beta_{42}$ in mixtures (Figure 8.8c) appear different from these peptides in isolation (compare with Figure 8.1c). Upon extended incubation all mixtures aggregated into morphologically similar networks of long, interacting fibrils, similar to those observed for peptides in isolation (Figure 8.8c). The observed differences in A11-interaction and aggregate morphology further led us to investigate the cytotoxic response of Aβ mixtures using cultured SH-SY5Y cells. Interestingly, even though $A\beta_{38}$ or $A\beta_{40}$ in isolation induced no cytotoxic response below a concentration of 20 μM, the addition of $A\beta_{38}$ to $A\beta_{40}$ resulted in a pronounced and significant loss of cell viability at a total peptide concentration of 10 μM, consistent with the A11-positive response for this mixture (Figure 8.8 d,e). Strikingly, the addition of $A\beta_{38}$ to $A\beta_{42}$ instead exerted a cytoprotective effect, despite showing the formation of A11-positive oligomers, preventing loss of cell viability up to a total Aβ concentration of 10 μM. In addition to this, even though both $A\beta_{42}$ and $A\beta_{43}$ are similarly cytotoxic at a concentration of 10 μM, the mixture of these two peptides alleviates the cytotoxic response while $A\beta_{43}$ induces cytotoxicity in the presence of $A\beta_{40}$.

Collectively, our data suggest that, apart from distinct propensities to form cytotoxic oligomers and aggregates for individual Aβ peptides, mixtures of various Aβ peptides do not behave in a predictable manner according to a simple additive effect but can actively modulate the behavior of other isoforms present in the mixture to either induce or prevent toxicity or modify their aggregation propensities.

8.3 Discussion

Aβ aggregation is a complex process during which a monomeric population progressively self-assembles first into oligomers and finally into mature fibrils. We show that biologically relevant mixtures of Aβ peptides, containing $A\beta_{38}$, $A\beta_{40}$, $A\beta_{42}$, and $A\beta_{43}$, behave in a more complex manner than can be anticipated from their behaviors in isolation with direct consequences for their oligomerization, aggregation and cytotoxic behavior. We also report that co-occurring Aβ peptides can affect each other by conformational modulation of the C-terminal region which, in turn, is a function of C-terminal flexibility to adopt various conformations. For example, $A\beta_{38}$ in isolation exhibited little cytotoxic potential, similar to $A\beta_{40}$. At the same time, cytotoxic oligomers accumulated rapidly for $A\beta_{42}$, and $A\beta_{43}$. Nevertheless, mixtures of $A\beta_{38}$ and $A\beta_{40}$ were highly toxic while the addition of $A\beta_{38}$ to $A\beta_{42}$ surprisingly induced a cytoprotective effect. The A11 reactivity of the individual Aβ peptides in isolation correlated with the observed cytotoxicity although all isoforms were found to form oligomers. This observation suggests a conformational difference between oligomers of different isoforms. The presence of both toxic, A11-positive and non-toxic, A11-negative oligomers has been reported recently for Aβ as well as for the yeast-sup35 protein [37,38]. The cytotoxicity - A11 reactivity correlation for peptides in isolation could not be extended to mixtures of Aβ isoforms. This lack of correlation can be explained by the polyclonal nature of the antibody to recognize non-toxic oligomers in addition to toxic species. Another possibility is that non-toxic and toxic oligomers are both formed and that the variation in signal intensities, and cytotoxicity, arises from the variation in the distribution between these oligomers. At high concentrations when the level of toxic oligomers is sufficiently high, the shorter Aβ isoforms become similar cytotoxic to the longer Aβ isoforms. While not being able to reveal distinct accumulation of specific conformations using CD, FTIR revealed small structural differences during

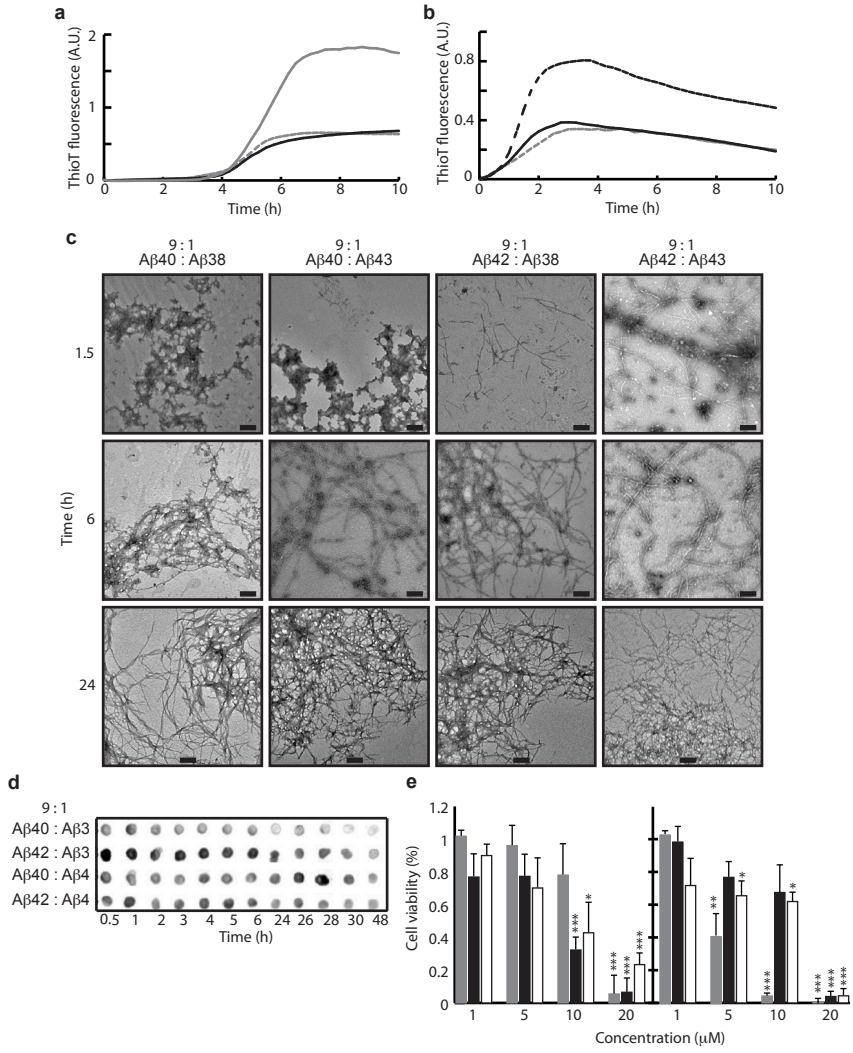

Figure 8.8 Aβ peptides in mixtures display complex aggregation behavior and toxicity. (a,b) Addition of 10% (=5 μM) $A\beta_{38}$ (continuous black line) or $A\beta_{43}$ (dotted grey line) to 90% (=45 μM) $A\beta_{40}$ (continuous grey line) or $A\beta_{42}$ (dotted black line) decreased final (10 h) ThioT fluorescence compared to $A\beta_{40}$ or $A\beta_{42}$ alone. Values represent means of three experiments (c) After 1.5 h of incubation mixtures containing $A\beta_{38}$ formed amorphous aggregates while mixtures containing $A\beta_{43}$ formed short fibrillar structures. Longer incubation for 6 h resulted in fibrillar networks for all mixtures which extended into dense, highly intertwined, stained networks after 24 h of incubation. Length of scale bar is 200 nm. (d) All Aβ mixtures intensively reacted with A11 oligomer-specific antibody after 0.5 h of incubation which gradually decreased upon longer incubation dependent on the Aβ mixture. (e) Aβ was added to cultured SH-SY5Y cells and incubated for 24 h before probing cytotoxicity using the Cell Titer Blue viability assay. Note that non-toxic $A\beta_{40}$ (left, grey) became highly toxic upon mixing with non-toxic $A\beta_{38}$ (left, black) and $A\beta_{43}$ (left, white) at a concentration of 10 μM. Toxicity of $A\beta_{42}$ (right, grey) is reduced upon addition of $A\beta_{38}$ (right, black) or $A\beta_{43}$ (right, white). Values are percent of cell viability ± SD (N=4), buffer signal was normalized to 100%. Statistical significance (unpaired 2-tailed t-test) compared to buffer control is indicated by ***p<0.0001, **p<0.0005, and *p<0.005.

a 1.5 h incubation time. Even though all tested Aβ peptides showed substantial β-sheet formation over time, only for $A\beta_{38}$ and $A\beta_{43}$ anti-parallel β-sheet formation could be identified which has been interpreted previously as typical for oligomer formation [28]. As both FTIR and CD are only informative on an ensemble level, we used MD to elucidate the short-time scale dynamic behavior of the peptides. MD simulations revealed that both $A\beta_{38}$ and $A\beta_{42}$ gained extended β-sheet conformation rapidly while helicity in $A\beta_{40}$ was retained for longer which is in good agreement with earlier reports [39]. In line with our findings, it has previously been reported that stabilization of the central α-helical region of Aβ by ligands or mutations results in significant delay of aggregation [40-42], and that inhibition of unfolding of the central α-helical region increases longevity in a Drosophila model of Alzheimer disease [41]. At the same time, rapid induction of extended β-sheet formation has been found to have strong predictive power in terms of toxic potential rationalizing the development of so-called β-sheet breakers as therapeutic approach (reviewed in [43]). Interestingly, $A\beta_{38}$ showed behavior that could be explained by rapid gain and loss of extended β-sheet conformation, fluctuating in behavior between $A\beta_{40}$ and $A\beta_{42}$/$A\beta_{43}$, respectively. Rapid conformational switching between distinct conformations has been observed before for synaptically confined proteins SNAP-25 and synaptobrevin and was proposed to characterize a specific class of intrinsically disordered proteins [44]. Conformational flexibility was suggested to allow for fast ligand interaction and conformational selection which potentially has functional implications for the findings we report on $A\beta_{38}$ but which warrant further investigation. The presence of other peptides with higher preference of one over another conformation may drive $A\beta_{38}$ to rapidly recognize these as a potential ligand and template for conformational selection, which, in turn, either induces or inhibits aggregation. However, this may be an oversimplification of the actual situation since $A\beta_{42}$ in the presence of $A\beta_{38}$ is in fact less toxic which does not comply with this suggestion. Further research is required to precisely underpin the molecular mechanism of this observation. It has been previously reported that Glu22, Asp23 and Lys28 play a critical role in the aggregation process [45-48]. Presumably, Asp23 (and Lys28), while residing in a helical conformation, may not be able to trigger the formation of extended conformations, at least at early time points, thus retarding the aggregation of $A\beta_{40}$. Therefore, not only the unfolding rate of the C-terminus, as has been previously suggested, can dictate the potential event to trigger aggregation and toxicity of Aβ [47], but also the capability of a given Aβ peptide to retain its helical conformation may be considered to induce such events. Based on the outcome of our molecular dynamics simulations we suggest that the plastic behavior of $A\beta_{38}$, inducing toxicity for $A\beta_{40}$ while eliminating response to $A\beta_{42}$, plays a key role to these observations. Hence, the presence of other peptides may direct the self-assembly process toward at least two possible pathways, one leading to toxic oligomers and the second leading to non-toxic intermediates. $A\beta_{43}$ does not display fluctuating secondary structures, and rapidly forms extended β-sheets. The self-assembly process in presence of other peptides is therefore probably more dependent on the flexibility of the structure of the second peptide. Indeed, it has been shown for the N-terminal domain of the HypF protein from *Escherichia coli* that both toxic and non-toxic oligomers can be formed [49].

Overall, our results can be of major importance for the further development of therapeutic strategies. The current approach of modulating β-secretase activity to

decrease $A\beta_{42}$ generation results in increased $A\beta_{38}$ levels at the same time. This approach is based on the observation that longer Aβ isoforms are more aggregation-prone. Hence, establishing an increased $A\beta_{38}$ level is considered a suitable and non-toxic approach to inhibit Alzheimer disease progress without compromising the important multi-substrate processing by γ-secretase. However, clinical studies still have to confirm their disease-modulating capacity. Whether this is due to the low brain-barrier penetrating potency of the compounds being tested requires further investigation. Together with previously published data [30], our results possibly indicate that another explanation for the lack of clinical evidence to place GSMs firmly on the map as Alzheimer disease therapy may be the induction of adverse, unexpected events as a result of the increased $A\beta_{38}$ levels in combination with other Aβ peptides. In this view, Golde and colleagues [50] recently argued that the efficiency of different GSMs to shift Aβ release towards shorter isoforms could determine their therapeutic potential. We propose that peptide conformational flexibility may confer toxic properties to its oligomers and underline the importance of understanding the interplay between various Aβ isoforms.

8.4 Experimental procedures

8.4.1 Preparation of Aβ peptides and peptide ratios

Aβ peptides (rPeptide) were dissolved, and mixed as described in Chapter 2. Briefly, Aβ was dissolved into HFIP, evaporated with a N_2 stream and redissolved in DMSO. Solvents were removed by elution over a 5 mL HiTrap desalting column into a 50mM Tris buffer pH 7.4 containing 1mM EDTA. Peptide concentrations were measured using the Coomassie (Bradford) Protein Assay kit against a bovine serum albumin standard. Aβ peptide concentrations were diluted to a concentration of 50 μM in 50mM Tris buffer pH 7.4 containing 1mM EDTA and incubated at 25 °C under quiescent conditions for further experiments.

8.4.2 Thioflavin T fluorescence

Fibrillation kinetics of Aβ in the presence of 12 μM thioT were followed *in situ* at 25 °C using a Fluostar OPTIMA fluorescence plate reader at an excitation wavelength of 440 nm and an emission wavelength of 480 nm. Readings were recorded in triplicate every 5 min for a period of 10 h and corrected by subtracting the intensity obtained for buffer containing 12 μM ThioT. The end of the lag phase was determined manually. Elongation rate was fitted to the central region of the exponential phase. Final fluorescence was determined at 10 h of incubation.

8.4.3 Dot blot

At various time points a volume of 5 μL sample was spotted onto Protran BA85 nitrocellulose blotting membrane. The membranes were blocked at 25 °C in phosphate-buffered saline containing 0.2% Tween20 (PBST XL) for 1 h and incubated for 1 h at 25 °C with primary rabbit polyclonal anti-oligomer antibody (A11), diluted 1:4000 in 100 mM Hepes pH 7.0 [27]. After incubation with secondary anti-rabbit-HRP-tagged antibody, diluted 1:5000 in phosphate-buffered saline containing 0.05% Tween20 (PBST) for 0.5 h at 25 °C, the membranes were visualized using the Immobilon™

Western chemiluminescent HRP substrate system.

8.4.4 Transmission electron microscopy (TEM)

A volume of 5 μL of Aβ was adsorbed to carbon-coated on 400-mesh copper grids for 1 min. The grids were washed in ultrapure water and stained with 1% (wt/vol) uranyl acetate. Samples were studied using a JEOL JEM-2100 microscope at an accelerating voltage of 200 kV or a JEOL JEM-1400 microscope at an accelerating voltage of 80 kV.

8.4.5 Atomic force microscopy (AFM)

AFM imaging was performed on a custom built instrument using Si_3N_4 tips with a spring constant of 0.5 N/m and a nominal tip radius of 10 nm. The measurements were made in tapping mode in air, with a tapping amplitude of less than 4 nm. The AFM scan settings were optimized to minimum force interaction with the sample. AFM samples were prepared by placing 5 μL of sample on freshly cleaved mica. After 4 min adsorption time, unbound Aβ was washed off with twice 100 μL ultrapure water and dried using a gentle N_2 stream. The images are represented in 3D after removal of height discontinuities between subsequent scan lines and compensation for piezo drift using SPIP software.

8.4.6 Far-UV circular dichroism (CD)

After 1.5 h incubation Aβ was diluted to 15 μM and placed in a quartz cuvette with an optical path of 3 mm and far-UV circular dichroism spectra were recorded in a Jasco J-715 spectrometer. The wavelength range was set from 260 to 190 nm with 0.2 nm resolution, 2.0 s response time, 2.0 nm bandwidth at a scanning speed of 50 nm min^{-1}. Data were collected as averages of eight scans. The spectra obtained were corrected by subtracting the spectrum obtained for buffer only.

8.4.7 Attenuated total reflection fourier-transform infrared spectroscopy (ATR FTIR)

Using a Bruker Tensor 27 infrared spectrophotometer equipped with a Bio-ATR II accessory, infrared spectra of aggregating Aβ (220 μM, 25 °C, in 50mM Tris buffer pH 7.4 containing 1mM EDTA) were recorded. The samples were applied to the FTIR sample holder and incubated for 1.5 h. Spectra were recorded in the range of 900 to 3500 cm^{-1} at a spectral resolution of 4 cm^{-1} at the beginning (time 0) and the end (time 1.5 h) of the experiment. Each measurement consisted of 120 accumulations. The spectrophotometer was continuously purged with dried air. The obtained spectra were corrected for atmospheric interference, baseline-subtracted and rescaled in the amide I area (1700 to 1600 cm^{-1}). Changes of secondary structure over 1.5 h incubation were analyzed by subtraction of the spectrum recorded at time 0.

8.4.8 *In silico* predictions

The statistical mechanics algorithm TANGO [51] was used to predict aggregation-prone regions in the Aβ peptide sequence [52]. TANGO provides an aggregation propensity (0-100%) per residue as output. An aggregating region is defined as a continuous stretch of residues with an individual TANGO score higher than 5% and a total score for the region higher than 50%. Total TANGO scores are calculated as the

sum of the individual residual TANGO scores for a given sequence. TANGO calculations were performed using http://tango.switchlab.org/ at a pH of 7.0, a temperature of 298.15 K and 0.02 M ionic strength without N- or C- terminal protection.

8.4.9 Molecular dynamics (MD) simulations

The NMR structure (protein data bank entry 1IYT) was used as starting structure of $A\beta_{42}$ and as a template to generate the other Aβ species studied here. All MD simulations were performed with GROMACS 4.5.3, using the OPLS/AA force field [53]. The LINCS algorithm [54] was used for bond-length constraining. The non-bonded pair list was updated every 10 fs. The simulation of each system was repeated at least 10 times, and then individually analyzed and their averaged properties here reported. Programs included in the GROMACS package, as well as some in-house scripts were used to perform the analysis of the trajectories. Molecular graphics images were produced using the UCSF Chimera package from the Resource for Biocomputing, Visualization, and Informatics at the University of California, San Francisco (supported by NIH P41 RR001081) [55].

8.4.10 Neuroblastoma cells and cytotoxicity

The human neuroblastoma cell line SH-SY5Y (ATCC number CRL-2266) was cultured in D-MEM:F-12 supplemented with 10% fetal bovine serum. The cells were incubated at 37 °C in a humidified 5% CO_2 atmosphere. Cytotoxicity assays were performed in 96-well plates after plating 25 000 cells per well in serum-deprived D-MEM:F-12. After pre-aggregation for 1.5 h Aβ was diluted in D-MEM:F-12 and added to the cells. After 24 h treatment, cell viability was analyzed using the Cell Titer Blue Cell Viability assay. After 4 h, color conversion was analyzed by measuring the fluorescence intensity of the samples at an excitation wavelength of 544 nm and an emission wavelength of 590 nm using a Fluostar OPTIMA fluorescence plate reader. Values are percent of cell viability ± SD, buffer signal was normalized to 100%.

8.4.11 Statistical analysis

Results from thioT fluorescence and cytotoxicity experiments were analyzed using two-tailed unpaired t-test for significance. Significance is indicated by ***$p<0.0001$, **$p<0.0005$, and *$p<0.005$. MD results were analyzed using two-way ANOVA with repeated measures to determine whether each group differs significantly from each other, and multivariate analysis to determine at which specific point the groups significantly differed. Bonferroni post-hoc analysis was applied. Significance is indicated by ##$p<0.005$. All properties determined by MD techniques are reported as the average property of 10 simulations ± SEM.

8.5 References

[1] Glenner G & Wong C (1984). Alzheimer's disease: initial report of the purification and characterization of a novel cerebrovascular amyloid protein. *Biochem. Biophys. Res. Commun.*, 120:885-890.

[2] Vigo-Pelfrey C, Lee D, Keim P, Lieberburg I, Schenk D (1993). Characterization of β-amyloid peptide from human cerebrospinal fluid. *J. Neurochem.*, 61:1965-1968.

[3] Wiltfang J, Esselmann H, Bibl M, Smirnov A, Otto M, Paul S, Schmidt B, Klafki H, Maler M, Dyrks T, Bienert M, Beyermann M, Rüther E, Kornhuber J (2002). Highly conserved and disease-specific patterns of carboxyterminally truncated Aβ peptides 1-37/38/39 in addition to 1-40/42 in Alzheimer's disease and in patients with chronic neuroinflammation. *J. Neurochem.*, 81:481-496.

[4] Gu Y, Misonou H, Sato T, Dohmae N, Takio K, Ihara Y (2001). Distinct intramembrane cleavage of the β-amyloid precursor protein family resembling γ-secretase-like cleavage of Notch. *J. Biol. Chem.*, 276:35235-35238.

[5] Sato T, Dohmae N, Qi Y, Kakuda N, Misonou H, Mitsumori R, Maruyama H, Koo E, Haass C, Takio K, Morishima-Kawashima M, Ishiura S, Ihara Y (2003). Potential link between amyloid β-protein 42 and C-terminal fragment γ 49-99 of β-Amyloid Precursor Protein. *J. Biol. Chem.*, 278:24294-24301.

[6] Bentahir M, Nyabi O, Verhamme J, Tolia A, Horré K, Wiltfang J, Esselmann H, De Strooper B (2006). Presenilin clinical mutations can affect γ-secretase activity by different mechanisms. *J. Neurochem.*, 96:732-742.

[7] Saito T, Suemoto T, Brouwers N, Sleegers K, Funamoto S, Mihira N, Matsuba Y, Yamada K, Nilsson P, Takano J, Nishimura M, Iwata N, Van Broeckhoven C, Ihara Y, Saido T (2011). Potent amyloidogenicity and pathogenicity of Aβ43. *Nat. Neurosci.*, 14:1023-1032.

[8] Takami M, Nagashima Y, Sano Y, Ishihara S, Morishima-Kawashima Y, Funamoto S, Ihara Y (2009). γ-Secretase: successive tripeptide and tetrapeptide release from the transmembrane domain of β-carboxyl terminal fragment. *J. Neurosci.*, 29:13042-13052.

[9] Jarrett J & Lansbury P (1993). Seeding "one-dimensional crystallization" of amyloid: a pathogenic mechanism in Alzheimer's disease and scrapie? *Cell*, 73:1055-1058.

[10] Bitan G, Kirkitadze M, Lomakin A, Vollers S, Benedek G, Teplow D (2003). Amyloid β-protein (Aβ) assembly: Aβ40 and Aβ42 oligomerize through distinct pathways. *Proc. Natl. Acad. Sci. USA*, 100:330-335.

[11] Benseny-Cases N, Cocera M, Cladera J (2007). Conversion of non-fibrillar β-sheet oligomers into amyloid fibrils in Alzheimer's disease amyloid peptide aggregation. *Biochem. Biophys. Res. Commun.*, 361:916-921.

[12] Weggen S, Eriksen J, Das P, Sagi S, Wang R, Pietrzik C, Findlay K, Smith T, Murphy M, Bulter T, Kang D, Marquez-Sterling N, Golde T, Koo E (2001). A subset of NSAIDs lower amyloidogenic Aβ42 independently of cyclooxygenase activity. *Nature*, 414:212-216.

[13] Eriksen J, Sagi S, Smith T, Weggen S, Das P, McLendon D, Ozols V, Jessing K, Zavitz K, Koo E, Golde T (2003). NSAIDs and enantiomers of flurbiprofen target γ-secretase and lower Aβ42 in vivo. *J. Clin. Invest.*, 112:440-449.

[14] Laino C (2009) In follow-up analysis of clinical trial, NSAIDs seem to preserve cognitive function in patients with healthy brains. *Neurol. Today*, 9:21-22.

[15] Oehlrich D, Berthelot D, Gijsen H (2011). γ-Secretase modulators as potential disease modifying anti-Alzheimer's drugs. *J. Med. Chem.*, 54:669-698.

[16] Imbimbo B & Giardina G (2011). γ-Secretase inhibitors and modulators for the treatment of Alzheimer's disease: disappointments and hopes. *Curr. Top. Med. Chem.*, 11:1555-1570.

[17] Lewczuk P, Esselmann H, Meyer M, Wollscheid V, Neumann M, Otto M, Maler J, Rüther E, Kornhuber J, Wiltfang J (2003). The amyloid-β (Aβ) peptide pattern in cerebrospinal fluid in Alzheimer's disease: evidence of a novel carboxyterminally elongated Aβ peptide. *Rapid Commun. Mass Spectrom.*, 17:1291-1296.

[18] Maddalena A, Papassotiropoulos A, Gonzalez-Agosti C, Signorell A, Hegi T, Pasch T, Nitsch R, Hock C (2004). Cerebrospinal fluid profile of amyloid β peptides in patients with Alzheimer's disease determined by protein biochip technology. *Neurodegenerative Dis.*, 1:231-235.

[19] Harper J & Lansbury P (1997). Models of amyloid seeding in Alzheimer's disease and scrapie: mechanistic truths and physiological consequences of the time-dependent solubility of amyloid proteins. *Annu. Rev. Biochem.*, 66:385-407.

[20] Biancalana M & Koide S (2010). Molecular mechanism of Thioflavin-T binding to amyloid fibrils. *Biochim. Biophys. Acta*, 1804:1405-1412.

[21] Stine W, Dahlgren K, Krafft G, LaDu M (1996). The nanometer-scale structure of amyloid-β visualized by atomic force microscopy. *J. Prot. Chem.*, 15:193-203.

[22] Röhrig U, Laio A, Tantalo N, Parrinello M, Petronzio R (2006). Stability and structure of oligomers of the Alzheimer β peptide Aβ16-22: from the dimer to the 32-mer. *Biophys. J.,* 91:3217-3229.
[23] Levine H III (1993). Thioflavine T interaction with synthetic Alzheimer's disease β-amyloid peptides: Detection of amyloid aggregation in solution. *Prot. Sci.,* 2:404-410.
[24] Lambert M, Barlow A, Chromy B, Edwards C, Freed R, Liosatos M, Morgan T, Rozovsky I, Trommer B, Viola K, Wals P, Zhang C, Finch C, Krafft G, Klein W (1998). Diffusible, nonfibrillar ligands derived from Aβ1-42 are potent central nervous system neurotoxins. *Proc. Natl. Acad. Sci. USA,* 95:6448-6453.
[25] Lesné S, Koh M, Kotilinek L, Kayed R, Glabe C, Yang A, Gallagher M, Ashe K (2006). A specific amyloid-β protein assembly in the brain impairs memory. *Nature,* 440:352-357.
[26] Ahmed M, Davis J, Aucoin D, Sato T, Ahuja S, Aimoto S, Elliott J, Van Nostrand W, Smith S (2010). Structural conversion of neurotoxic amyloid-β1-42 oligomers to fibrils. *Nat. Struct. Mol. Biol.,* 17:561-567.
[27] Kayed R, Head E, Thompson J, McIntire T, Milton S, Cotman C, Glabe C (2003). Common structure of soluble amyloid oligomers implies common mechanism of pathogenesis. *Science,* 300:486-489.
[28] Cerf E, Sarroukh R, Tamamizu S, Breydo L, Derclaye S, Dufrêne Y, Narayanaswami V, Goormaghtigh E, Ruysschaert J-M, Raussens V (2009). Antiparallel β-sheet: a signature structure of the oligomeric amyloid β-peptide. *Biochem. J.,* 421:415-423.
[29] Kabsch W & Sander C (1983). Dictionary of protein secondary structure: pattern recognition of hydrogen-bonded and geometrical features. *Biopolymers,* 22:2577-2637.
[30] Chávez-Gutiérrez L, Bammens L, Benilova I, Vandersteen A, Benurwar M, Borgers M, Lismont S, Zhou L, Van Cleynenbruegel S, Esselmann H, Wiltfang J, Serneels L, Karran E, Gijsen H, Schymkowitz J, Rousseau F, Broersen K, De Strooper B (2012). The mechanism of γ-secretase dysfunction in familial Alzheimer disease. *EMBO J.,* 31:2261-2274.
[31] Welander H, Franberg J, Graff C, Sundström E, Winblad B, Tjernberg L (2009). Aβ43 is more frequent than Aβ40 in amyloid plaque cores from Alzheimer disease brains. *J. Neurochem.,* 110:697-706.
[32] Bibl M, Mollenhauer B, Wolf S, Esselmann H, Lewczuk P, Kornhuber J, Wiltfang J (2007). Reduced CSF carboxyterminally truncated Aβ peptides in frontotemporal lobe degenerations. *J. Neural. Transm.,* 114:621-628.
[33] Mann D, Iwatsubo T, Ihara Y, Cairns N, Lantos P, Bogdanovic N, Lannfelt L, Winblad B, Maat-Schieman M, Rossor M (1996). Predominant deposition of amyloid-β42(43) in plaques in cases of Alzheimer's disease and hereditary cerebral hemorrhage associated with mutations in the amyloid precursor protein gene. *Am. J. Pathol.,* 148:1257-1266.
[34] Scheuner D, Eckman C, Jensen M, Song X, Citron M, Suzuki N, Bird T, Hardy J, Hutton M, Kukull W, Larson E, Levy-Lahad E, Viitanen M, Peskind E, Poorkaj P, Schellenberg G, Tanzi R, Wasco W, Lannfelt L, Selkoe D, Younkin S (1996). Secreted amyloid β-protein similar to that in the senile plaques of Alzheimer's disease is increased in vivo by the presenilin 1 and 2 and APP mutations linked to familial Alzheimer's disease. *Nature Med.,* 2:864-870.
[35] Citron M, Westaway D, Xia W, Carlson G, Diehl T, Levesque G, Johnson-Wood K, Lee M, Suebert P, Davis A, Kholodenko D, Motter R, Sherrington R, Perry B, Yao H, Strome R, Lieberburg I, Rommens J, Kim S, Schenk D, Fraser P, St George-Hyslop P, Selkoe D (1997) Mutant presenilins of Alzheimer's disease increase production of 42-residue amyloid β-protein in both transfected and transgenic mice. *Nature Med.,* 3:67-72.
[36] Younkin S (1998). The role of Aβ42 in Alzheimer's disease. *J. Physiol. Paris,* 92:289-292.
[37] Krishnan R, Goodman J, Mukhopadhyay S, Pacheco C, Lemke E, Deniz A, Lindquist S (2012). Conserved features of intermediates in amyloid assembly determine their benign or toxic states. *Proc. Natl. Acad. Sci. USA,* 109:11172-11177.
[38] Ladiwala A, Litt J, Kane R, Aucoin D, Smith S, Ranjan S, Davis J, Van Nostrand W, Tessier P (2012). Conformational differences between two amyloid β oligomers of similar size and dissimilar toxicity. *J. Biol. Chem.,* 287:24765-24773.
[39] Shen L, Ji H, Zhang H (2008). Why is the C-terminus of Aβ(1-42) more unfolded than that of Aβ(1-40)? Clues from hydrophobic interaction. *J. Phys. Chem. B.,* 112:3164-3167.
[40] Päiviö A, Nordling E, Kallberg Y, Thyberg J, Johansson J (2004). Stabilization of discordant helices in amyloid fibril-forming proteins. *Prot. Sci.,* 13:1251-1259.
[41] Nerelius C, Sandegren A, Sargsyan H, Raunak R, Leijonmarck H, Chatterjee U, Fisahn A, Imarisio S, Lomas D, Crowther D, Strömberg R, Johansson J (2009). α-Helix targeting reduces amyloid-β peptide toxicity. *Proc. Natl. Acad. Sci. USA,* 106:9191-9196.
[42] Ito M, Johansson J, Strömberg R, Nilsson L (2011). Unfolding of the amyloid β-peptide central helix: mechanistic insights from molecular dynamics simulations. *PLoS ONE,* 6:e17587.

[43] Wisniewski T & Sadowski M (2008). Preventing β-amyloid fibrillization and deposition: β-sheet breakers and pathological chaperone inhibitors. *BMC Neurosci.,* 3:9 Suppl 2:S5.
[44] Choi U, McCann J, Weninger K, Bowen M (2011). Beyond the random coil: stochastic conformational switching in intrinsically disordered proteins. *Structure,* 19:566-576.
[45] Borreguero J, Urbanc B, Lazo N, Buldyrev S, Teplow D, Stanley H (2005). Folding events in the 21-30 region of amyloid β-protein (Aβ) studied in silico. *Proc. Natl. Acad. Sci. USA,* 102:6015-6020.
[46] Lazo N, Grant M, Condron M, Rigby A, Teplow D (2005). On the nucleation of amyloid β-protein monomer folding. *Protein Sci.,* 14:1581-1596.
[47] Baumketner A, Bernstein S, Wyttenbach T, Lazo N, Teplow D, Bowers M, Shea J (2006) Structure of the 21-30 fragment of amyloid β-protein. *Prot. Sci.,* 15:1239-1247.
[48] Masman M, Eisel U, Csizmadia I, Penke B, Enriz R, Marrink S, Luiten P (2009). In silico study of full-length amyloid β 1-42 tri- and penta-oligomers in solution. *J. Phys. Chem. B.,* 113:11710-11719.
[49] Campioni S, Mannini B, Zampagni M, Pensalfini A, Parrini C,Evangelisti E, Relini A, Stefani M, Dobson C, Cecchi C, Chiti F (2010) A causative link between the structure of aberrant protein oligomers and their toxicity. *Nat. Chem. Biol.,* 6:140-147.
[50] Golde T, Ran Y, Felsenstein K (2012). Shifting a complex debate on γ-secretase cleavage and Alzheimer's disease. *EMBO J.,* 31:2237-2239.
[51] Fernandez-Escamilla A, Rousseau F, Schymkowitz J, Serrano L (2004). Prediction of sequence-dependent and mutational effects on the aggregation of peptides and proteins. *Nat. Biotechnol.,* 22:1302-1306.
[52] Kang J, Lemaire H, Unterbeck A, Salbaum J, Masters C, Grzeschik K, Multhaup G, Beyreuther K, Müller-Hill B (1987). The precursor of Alzheimer's disease amyloid A4 protein resembles a cell-surface receptor. *Nature,* 325:733-736.
[53] Jorgensen W & Tirado-Rives J (1988). The OPLS potential functions for proteins, energy minimizations for crystals of cyclic peptides and crambin. *J. Am. Chem. Soc.,* 110:1657-1666.
[54] Hess B, Bekker H, Berendsen H, Fraaije J (1997). LINCS: A linear constraint solver for molecular simulations. *J. Comput. Chem.,* 18:1463-1472.
[55] Pettersen E, Goddard T, Huang C, Couch G, Greenblatt D, Meng E, Ferrin T (2004). UCSF Chimera--a visualization system for exploratory research and analysis. *J. Comput. Chem.,* 25:1605-1612.

9

Concluding remarks on the work described and on the Alzheimer disease field.

The increasing number of Alzheimer disease patients as a result of the aging population, their need for care and the related economical consequences are one motive in the search for medication that stops disease progress, reverses symptoms and, ultimately, that leads to prevention of disease onset. The human burden, both for patients and for caregivers, and the social consequences are a second reason to fight Alzheimer disease. This thesis has focused on the complexicity of the total Aβ pool as insight thereof allows for better understanding of disease mechanisms and for the identification of potential drug targets or of crucial processes to intervene with. Aβ peptides are the main component of brain amyloid plaques and their release, as well as their aggregation behavior can be affected by mutations leading to early-onset Alzheimer disease. These observations led to the hypothesis that Aβ is the prime actor underlying Alzheimer disease. The results in this thesis describe how variability of the Aβ sequence can be generated and how it affects aggregation and toxicity.

9.1 Considerations when preparing Aβ for *in vitro* and cell experiments.

In the last decade a wide variety of transient Aβ species have been reported to be crucial in the aggregation pathway of Aβ while exerting different degrees of toxicity. Aggregation is a complex and highly dynamic process which is to a great extent influenced by environmental conditions such as ionic strength or pH as well as intrinsic Aβ peptide parameters including peptide length, sequence variations and truncations, as is underlined by the results reported in this thesis. However, reports describing the aggregation properties of these peptide variations vary greatly. As Aβ has been proven notoriously difficult to solubilize, resulting in large variations of the reported experimental conditions to investigate its aggregation, it is not inconceivable that a significant portion of the observed variation between the reported key Aβ species is the result of differences in the solubilization procedures or in environmental conditions used [1-5]. These variations deviate the attention from the 'real' problem.

We found that a variety of factors are critically important when preparing Aβ in solution for *in vitro* studies and we describe how to practically address these factors. For example, the preparation of a solution of predominantly monomeric Aβ virtually free of seeding species according to a standardized procedure serves as an important basis for understanding aggregation events. A seed is a nucleated species that, when added to a monomeric peptide solution, leads to a very rapid aggregation of that solution as it bypasses the rate-limiting nucleation step in the nucleation pathway [6],[7]. Non-standardized or uncontrolled seeding of solutions therefore may mask the aggregation properties of a monomeric peptide solution. Moreover the composition of Aβ samples needs to be compatible not only with the major biophysical techniques, but also with the more sensitive cell cultures and experiments involving primary neurons. We describe and validate a method yielding monomeric Aβ without seeds in a buffer containing none of the chemicals used to achieve seed-free sample preparation. The presence of these chemicals, HFIP and DMSO, were found to influence aggregation events and are found to be toxic in a biological context. Moreover, our protocol allows for the study of co-aggregation of different Aβ variants which which allows for the study of more complex mixtures of Aβ variants. Crucial to mimick and understand the coexistence of Aβ in the brain. Further experimental parameters such as choice of buffer, Aβ concentration and temperature remain variable, and also play a role in determining the aggregation characteristics of Aβ.

The buffer in which Aβ is dissolved is crucial in determining aggregation and toxicity characteristics of the peptide. Most commonly used biological buffers such as Tris, phosphate buffered saline and Hepes are suitable for many applications, both *in vitro* as well as in cell culture experiments. Alternatively, Aβ peptides may be directly solubilized into cell culture medium. High ionic strength and a pH close to the isoelectric point of the peptide (near pH 5.0) tend to increase the aggregation rate of Aβ [8],[9] as a result of charge screening. The choice of buffer is mainly determined by the limitations of the experimental set-up or the requirements of other biomolecules used in the experiment. For example, buffers may need to be free of compounds toxic for cells and compatible with most commonly used biophysical assays including NMR, CD or mass spectrometry [10]-[12].

Once Aβ is solubilized in the desired buffer, the concentration of Aβ needs to be carefully controlled as aggregation is a strongly concentration-dependent process [13].

Both the degree and rate of association are influenced by the protein concentration. Moreover, according to the monomer-addition aggregation model, formation of a nucleus only occurs above a critical concentration [14]. Further, the peptide concentration used for *in vitro* experiments is a highly debated issue in the field. Concentrations in the micromolar range are widely used and are often required for *in vitro* aggregation studies [6,15]. The major critique however is that these 'high' concentrations are far above concentrations as observed *in vivo* which are in the nanomolar range [16]. The nanomolar range is however not experimentally accessible for most biophysical techniques, e.g. FTIR and NMR require peptide concentrations of 50 to 200 μM. However, a recent study described how local effective intracellular Aβ concentrations may be much higher reaching concentrations in the low μM range [17,18]. The 'natural' time scale to develop Alzheimer disease is considered to be in the order of magnitude of decades. This time scale is not very conveniently followed experimentally. Therefore, the extrapolation to higher concentration is assumed to accelerate the aggregation process so that it is still comparable with the *in vivo* situation but within a practical time scale for a single experiment.

A further requirement to match the *in vivo* situation is that aggregation experiments should ideally be conducted at a temperature of 37 °C. This temperature requirement can usually be accommodated for with incubation, *in situ* recordings in temperature-controlled set-ups or cell culture experiments. Common on-the-bench preparation and further handling of the sample however cannot always be executed at 37 °C. A further problem when investigating the aggregation process of a fast aggregating peptide such as Aβ is that incubation at 37 °C results in rapid aggregation kinetics hindering the study of early aggregation intermediates [19]. Lowering the incubation temperature e.g. to 20 °C makes this study more manageable. Lowering temperature even further to 4 °C on the other hand resulted in delayed aggregation (data not published) which could be explained by the formation of off-pathway oligomeric intermediates that interfere with the study of aggregation processes.

Future research would greatly benefit from a consensus of solubilization procedures and experimental parameters to investigate Aβ aggregation and toxicity to allow for large-scale comparison of experimental data obtained in various laboratories to pinpoint important factors and as such simplify a greatly complicated field [20].

9.2 Contribution of distinct Aβ peptide regions to aggregation.

The Aβ pool in the brain comprises various peptide lengths, N-terminally truncated forms and post-translationally modified peptides [21,22]. The consequence of a high degree of Aβ variability on aggregation has been described as one of the primary aims of this thesis. The aggregation profiles of the heterogenous APP processing products such as N-truncated Aβ and various disease-related mutants of $A\beta_{42}$ were reported, while the possible contribution of Aβ peptide length to disease development was investigated in more detail.

A comprehensive study of various Aβ peptides allowed for an in-depth understanding of the aggregation determinants within the Aβ sequence. The Aβ sequence contains a first aggregation zone located in the central region (spanning residues 16 to 22) and a second zone located in the C-terminus (from residue 28 onwards) [23,24]. Based on our results using fluorescence spectroscopy, electron microscopy, immunohistochemistry and computational analysis using Aβ variants and mutants displaying stronger or

weaker aggregation propensities in these zones, we suggest that the zone located in the C-terminus of the Aβ peptide is the primary driving force for aggregation while the central region exerts a more 'regulatory' function in the aggregation process. While the C-terminus is responsible for rapid aggregation into randomly organized networks, as is the case for $A\beta_{42}$ and $A\beta_{43}$, the central region allows for a slower but more organized aggregation process, resulting in highly ordered fibrils upon shortening the peptide sequence from 42/43 to 40/38 residues. When the C-terminal aggregating zone is too strong and enforces very rapid aggregation, the regulating role of the central zone is overruled and less regular aggregates are formed.

Comparison of modified Aβ peptides with their unmodified counterparts allowed for the identification of the effects of the modification on the aggregation process. Modifications like biotinylation or fluorescent tagging are widely used in experimental approaches as they can be used for interaction studies or visualization of the Aβ peptides [25-27]. Our results indicate that the aggregation behavior of Aβ is almost certainly influenced by tagging the peptide. Following aggregation kinetics of the labeled peptide by thioT fluorescence, confirming fibril formation by TEM or AFM or performing structural analysis by FTIR can identify any discrepancy between the aggregation behavior of the unlabeled and labeled peptide. Even though rapid screening might not reveal significant differences in the behavior of the labeled peptide as compared to the unlabeled form, observations could still be influenced by the tag. Repeating the experiments with a different tag, or with the tag linked to another position of the peptide could serve as control experiments. Common mutations of APP are located in the central region of Aβ or near the secretase cleavage sites [28]. Many of these mutations affect the amount or the spectrum of released Aβ from APP while some - but not all - also influence the aggregating behavior of the resulting Aβ peptide. These Aβ mutants display an aggregating behavior that is very similar to that of the wild type peptide. This observation fits well with the previously described hypothesis that the aggregation of the peptides is driven by the C-terminal region, which is not affected in these mutants. The variance in elongation rate and fibril morphology observed for these mutants can be attributed to the alteration of the 'regulatory' capacities of the central region. Hence, it is likely that the early-onset FAD cases related to these mutations are primarily the result of altered APP processing, and are to a minor extent determined by the behavior of the resulting Aβ proteins. These observations are also important with regard to sporadic cases of Alzheimer disease: focussing on the release of Aβ peptides might be a more promising therapeutic approach than acting on the aggregation of Aβ. The role of the N-terminus (residues 1-15 approx.) in aggregation is less decisive than the rest of the sequence. The N-terminal region contributes to aggregation, but the exact determinants remain elusive [15]. Here, we investigated the role of the N-terminus by comparing the aggregation of the p3 peptides (residues 17-40/42) with that of the full-length Aβ peptides. The p3 peptides are released through the non-amyloidogenic APP processing pathway by α- and γ-secretase and are generally considered as 'safe' [29,30] although the peptides showed significant oligomerization and fibrillization in the assays described in this thesis.

9.3 *In vitro* Aβ aggregation studies should investigate complexes.

Although the spectrum of Aβ peptides in the brain is heterogeneous, most studies focus on one or two of the more common variants of Aβ, usually $A\beta_{40}$ or $A\beta_{42}$. It has

been reported that Aβ40 can affect the behavior of Aβ42 and *vice versa* [8,31-36]. The influence of both isoforms on each other's behavior has been used to emphasize the difference between both isoforms. However, little has been investigated on the extent of influence and on the mechanisms underlying it. Further, nothing is reported on a possible similar effect by other, less prevalent, Aβ isoforms. Evidence is accumulating that other Aβ isoforms are involved in Alzheimer disease progress [37,38]. It is thus of utmost importance for the understanding of disease mechanisms to study the behavior of Aβ in mixtures, so as to mimic the *in vivo* situation. Here, we used a multidisciplinary approach to unravel the degree and mechanisms of mutual influence of less studied Aβ isoforms. The results presented here emphasize that general detection of Aβ peptides other than Aβ40 and Aβ42 can provide useful insights in the mechanisms underlying Alzheimer disease.

Specific mutations in the γ-secretase complex or in APP result in an increased production of Aβ42 shifting the Aβ42:Aβ40 ratio roughly to 3:7, compared to 1:9 for unaffected subjects [39,40]. Our results indicate that a small concentration of Aβ42 in an otherwise Aβ40 dominated composition can have potentially beneficial effects on the aggregation process but that very small increases in the ratio make the mixture behave similar to Aβ42 in isolation despite the excess of Aβ40 present. These observations provide a possible explanation for the early-onset clinical picture seen in patients carrying such mutations. Further, our study of various APP mutations related to FAD shows that these mutations interfere with the cleavage of APP by β- and γ-secretase resulting, respectively, in an increased production of Aβ and a shifted spectrum of released Aβ isoforms. The increased release of Aβ is a known risk factor for Alzheimer disease [41,42], but we show here that mutations resulting in early-onset Alzheimer disease can also affect the release of Aβ38. Aβ peptide lengths other than the 40 and 42 amino acid forms had not been associated with FAD before and Aβ38 is generally considered as less aggregating. Altogether these data suggest that levels of Aβ isoforms other than 40 and 42 may inform on disease progress and might serve as biomarkers in the blood or CSF, which might bring new diagnostic opportunities. We show that Aβ38 is more aggregation prone than Aβ40, in contrast to the postulate that shorter Aβ peptides are less prone to aggregation. But more importantly, when added to Aβ40 or Aβ42, Aβ38 almost immediately induces aggregation of the resultin mixtures. Moreover, Aβ38 surprisingly converted Aβ40 into a cytotoxic species while exerting a cytoprotective effect on Aβ42. This finding again indicates the possibility of an important role for Aβ38. Molecular dynamic studies indicated that Aβ38 displays high molecular plasticity compared to Aβ40 and Aβ42. This peptide has the tendency to exhibit conformational fluctuations at short time-scales between structures that resemble Aβ40 and Aβ42/43 alternatively. To explain the aggregation and cytotoxic inducing effect of Aβ38 on Aβ40 it is possible that the flexibility of the Aβ38 molecules acts as a template for Aβ40 and by converting to Aβ42-like conformations drags Aβ40 towards an alternative aggregation pathway. On the other hand, the fluctuating behavior of Aβ38 could affect the conformation of Aβ42 to be less toxic. Further molecular dynamics studies of these peptides in each others' presence should elucidate these effects. Nevertheless, it is interesting to speculate to which extent an 'infectious' Aβ conformation may apply to Aβ-induced toxicity analogous to prion-like activity. The increase in aggregation kinetics observed for mixtures of Aβ38 and Aβ40 might result in a less organized and ordered aggregation, which is also suggested by the fibrillar

morphology. Maybe this less ordered aggregation goes through different intermediates and conformational states than the more organized variant, which could be a possible explanation for the induced toxicity observed. Similarly, $A\beta_{38}$ might temper $A\beta_{42}$ aggregation slightly and control the reaction to induce more organized association, and decrease toxicity. Seeding experiments can further analyze the effects of $A\beta_{38}$ on nucleation and aggregation of $A\beta_{40}$ and $A\beta_{42}$ while cell culture assays and primary neuron studies can further help to assess toxicity and to elucidate the pathways leading to toxicity.

The slight structural differences between various isoforms of Aβ that also exert different toxic effects, strongly suggest that conformation, and not size or a specific association, is related to toxicity [43-45]. Moreover, interaction of Aβ with the oligomer-recognizing A11 antibody mostly correlated with the outcome of the cell culture assays we performed and pre-incubation of the Aβ solution with the antibody abolished toxicity. On the other hand when analyzing the mixtures of Aβ, no correlation between A11 reactivity and toxicity was found and A11 reactivity seemed inversely correlated to thioT intensity. These observations suggest that the A11 antibody recognizes a common structural feature of oligomers albeit not exclusively. Being a polyclonal antibody it is plausible that this antibody recognizes epitopes other than the specific 'toxic' epitope of Aβ oligomers. Aβ solutions that rapidly oligomerize but contain only a small portion of toxic oligomers show no correlation between A11 reactivity and toxicity. Hence, the search for the toxic species might actually be the search for the toxic conformation. This toxic conformation might as well be a common trait between the various proteins related to conformational diseases. Similar to the prion protein where the cellular form has to convert into the prion form, oligomers in neurodegenerative diseases might have to undergo a conformational change to adopt the toxic conformation as additional step in the aggregation process.

The rather broad interpretation of toxicity in experimental set-ups might also explain the poor correlation with A11 reactivity. Depending on the assays used, toxicity can have a different meaning. When using cell culture assays, toxicity is assessed as cell viability. The advantages of the cell culture set-up - rapid read-outs, easy handling, many replications, rather low-budget and with few ethical issues - are balanced by the crude read-out, informing on survival or cell death without much nuance, or details of the mechanisms involved. Primary cultures which are more labour-intensive and less well-accepted from an ethical point-of-view than neuroblastoma cell cultures, can provide more detailed information on neuronal health and on the mechanisms underlying toxicity. Toxicity in studies involving primary neuronal cultures can be extended to provide detailed information on cell (mal)functioning including from an organelle perspective, synaptic activity, and activation of apoptotic pathways directly related to the type of hippocampal neuronal cells relevant to Alzheimer disease while neuroblastoma cells lack the machinery allowing activity measurements. When studying cognitive deficits in memory formation and memory loss, cultures are no longer suitable and animal behavior studies are necessary. *In vivo* studies need to be well-considered as they are time-consuming, have a less straight-forward read-out compared to biophysical or cell culture assays, are more expensive and need to be justified from an ethical point of view. In these studies, toxicity is assessed on a behavioral level, as a loss of memory e.g., and only in a second step dissection can inform on possible molecular events. To obtain a full understanding of the different aspects involved in

inducing cognitive deficits in Alzheimer disease it is necessary to combine the various disciplines and compare read-outs.

9.4 Therapeutic approach to Alzheimer disease: which way to go?

Current therapeutics can slow disease progress in the early stages of Alzheimer disease by improving neuronal communication and minimizing neuronal damage [45]. Various strategies aiming to halt or reverse disease progress, or even prevent occurrence are being examined [47]. The complex nature of Alzheimer disease on one hand brings many opportunities but on the other hand hinders intervention strategies. The lack of success with the ample therapeutic attempts made during the last decade requires re-consideration of the possible approaches.

A first possible scenario in the fight against Alzheimer disease aims to identify those at risk at an early pre-symptomatic stage and to prevent the development of the disease. Disease mechanisms are most probably activated many years before the first symptoms manifest themselves. Early diagnosis thus implies the need for biomarkers indicating changes in these mechanisms. The sporadic nature of Alzheimer disease complicates this approach, as it requires large-scale testing of the population, preferentially using blood or saliva over CSF samples. Taking into account that society is aging, prevalence of Alzheimer disease is increasing and that consensus on biomarkers for disease development has not been reached, prevention might not be the best strategy at this moment. Possible early biomarkers are related to the processing of APP and indicate (i) changes in the balance between the non-amyloidogenic and amyloidogenic pathway or (ii) changes in the spectrum of Aβ peptides, given the fact that these changes are rapidly and accurately reflected outside the brain. Other possible biomarkers could be those that indicate neuroinflammation or neuronal damage [48-50].

Early and accurate diagnosis is also important to cure Alzheimer disease as neuronal loss cannot be reversed. Currently, diagnosis is made by ruling out all other possible causes for the symptoms, it is not conclusive and often occurs at later disease stages. When looking for a cure, diagnostic tools need to be improved to allow fast and certain diagnosis. As neuron recovery is possible when exposure to a cytotoxic stimulus was limited in time rapid diagnosis can improve the success rate of attempts to a cure. It is also not clear yet what the point-of-no-return is for neuronal survival, that is at which point a damaged neuron undergoes definite apoptosis. Studies into such mechanisms may provide information to which extent it is possible to actually cure a neurodegenerative disease such as Alzheimer disease. When cytotoxicity cannot be prevented, the treatment has to be administered rapidly after first cytotoxic stimuli occurred and has to eliminate or reverse the cytotoxicity. Despite the extensive efforts made to understand Alzheimer disease, insights are currently insufficient to provide curative therapy.

A third action plan is the treatment of Alzheimer disease. Molecules that effectively reduce the brain damage responsible for the most important symptoms could significantly postpone disease development. Such compounds could be neuroprotective, act on tau, reduce oxidative damage, interfere with neuroinflammation [47,52,53] or be 'multi-target' compounds. In the sporadic cases of Alzheimer disease where the first symptoms are manifested at old age, this approach could bring symptomatic relief without acting on disease mechanisms and turn Alzheimer disease into a chronic

disorder. Although the costs related to treatment remain, the need for specialized care will reduce and the social burden of Alzheimer disease will improve. Effective Alzheimer therapeutics might interfere with the molecular mechanisms involved in APP processing and Aβ generation. However, blocking these processes has been proven ineffective [54]. Modulation of the enzymes involved to carefully manipulate the balance of the various processing steps is the latest attempt [54,55]. The problem however is the rather basic knowledge of the resulting peptide pool. The data presented in this thesis strongly indicate that modulation of Aβ release could be counter-effective and indicate that $A\beta_{38}$, generally considered as safe and focussed on in current drug development approaches, might be decisive in the onset of Alzheimer disease. The modulation of the Aβ release can benefit from in-depth characterization of the total Aβ spectrum in healthy and diseased individuals. Such therapy can be effective when restoring the 'natural' Aβ balance. Besides, brain deposits are to a lesser extent found in elderly without any sign of dementia [56]. This observation suggests that not the aggregation itself underlies neurodegeneration. Compounds reducing aggregation or circumventing, blocking or eliminating the toxic assemblies on the aggregation pathway might be another successful attempt. Further, such compounds might be useful in the fight against other conformational diseases as aggregation has a common structural basis [57].

9.5 Quo Vadis? Where do we go from here?

The major cause of Alzheimer disease remains elusive although factors such as Aβ and tau behaving aberrantly in disease cases have been identified. The problem resembles the 'chicken or the egg-paradigm': Is Aβ the true cause of the disease leading to cellular imbalances and tau hyperphosphorylation, does the cascade start from tau hyperphosphorylation or is there another event causing cellular distress affecting Aβ generation and/or tau phosphorylation?

The research presented in this thesis on the contribution of Aβ peptide variation on disease progress does not provide a complete insight into Alzheimer disease progress, but brings further insights into the molecular mechanisms underlying this disease and emphasizes the importance of understanding the behavior of the total Aβ pool. The extensive research conducted already has yielded detailed understanding of the basic mechanism in Alzheimer disease such as the pathways leading to Aβ production, and the aggregation characteristics of the predominant Aβ peptides. Intervention strategies based on this knowledge have not been very successful. Alzheimer disease has been identified as a multi-factorial disease in which other parameters such as neuroinflammation, oxidative stress, genetic factors and co-factors such as apolipoprotein E isoforms play a major role in determining its course [58-60]. Even though many studies are now actively seeking the contribution of individual parameters to disease progress, a consensus from this perspective has not been reached. It has been shown that non-steroidal anti-inflammatory drugs (NSAIDs) have some effect in inhibiting disease progress but are not completely capable of halting its development [61]. Also single anti-oxidant treatment has shown some, but only partial relief [62]. Alzheimer disease should therefore not be treated as a single-cause disease using single-target therapy but using a multi-target drug. More recently, experimental approaches have headed more towards cell-based studies investigating the cellular cascades following exposure to Aβ. The understanding of these cellular events might

provide an alternative way to intervene with the cascades inducing cytotoxicity or leading to neuronal loss. Further, exploration of the pathways leading to neuronal loss, and the biomarkers thereof, might enable early detection of neurodegeneration in Alzheimer disease.

9.6 References

[1] Lambert M, Barlow A, Chromy B, Edwards C, Freed R, Liosatos M, Morgan T, Rozovsky I, Trommer B, Viola K, Wals P, Zhang C, Finch C, Krafft G, Klein W (1998). Diffusible, nonfibrillar ligands derived from Aβ1-42 are potent central nervous system neurotoxins. *Proc. Natl. Acad. Sci. USA,* 95:6448-6453.

[2] Hoyer W, Antony T, Cherny D, Heim G, Jovin T, Subramaniam V (2002). Dependence of α-synuclein aggregate morphology on solution conditions. *J. Mol. Biol.*, 322:383-393.

[3] Bitan G, Kirkitadze M, Lomakin A, Vollers S, Benedek G, Teplow D (2003). Amyloid β-protein (Aβ) assembly: Aβ40 and Aβ42 oligomerize through distinct pathways. *Proc. Natl. Acad. Sci. USA,* 100:330-335.

[4] Hepler R, Grimm K, Nahas D, Breese R, Dodson E, Acton P, Keller P, Yeager M, Wang H, Shugrue P, Kinney G, Joyce J (2006). Solution state characterization of amyloid β-derived diffusible ligands. *Biochemistry*, 45:15157-15167.

[5] Lesné S, Koh M, Kotilinek L, Kayed R, Glabe C, Yang A (2006). A specific amyloid-β protein assembly in the brain impairs memory. *Nature*, 440:352-357.

[6] Jarrett J, Berger E, Lansbury P (1993). The carboxy terminus of the β amyloid protein is critical for the seeding of amyloid formation: implications for the pathogenesis of Alzheimer's disease. *Biochem.*, 32:4693-4697.

[7] Jarrett J & Lansbury P (1993). Seeding one-dimensional crystallization of amyloid: a pathogenic mechanism in Alzheimer's disease and scrapie? *Cell*, 73:1055-1058.

[8] Snyder S, Ladror U, Wade W, Wang G, Barrett L, Matayoshi E, Huffaker H, Krafft G, Holzman T (1994). Amyloid-β aggregation: selective inhibition of aggregation in mixtures of amyloid with different chain lengths. *Biophys. J.*, 67:1216-1228.

[9] Johansson A, Berglind-Dehlin F, Karlsson G, Edwards K, Gellerfors P, Lannfelt L (2006). Physiochemical characterization of the Alzheimer's disease-related peptides Aβ1-42 Arctic and Aβ1-42 wt. *FEBS. J.,* 273:2618-2630.

[10] Kelly S, Jess T, Price N (2005). How to study proteins by circular dichroism. *Biochim. Biophys. Acta*, 1751:119-139.

[11] Loo J & Kaddis C (2007). Direct characterization of protein complexes by electrospray ionization mass spectrometry and ion mobility analysis. In: K Downard (2007). *Mass spectrometry of Protein Interactions*. Hoboken: Wiley & Sons, ch 1.

[12] Muskett F (2011). Sample preparation, data collection and processing. In: G Roberts & L-Y Lian eds. (2011). *Protein NMR Spectroscopy: Practical techniques and applications*. Hoboken: Wiley & Sons, ch 1.

[13] Burdick D, Soreghan B, Kwon M, Kosmoski J, Knauer M, Henschen A, Yates J, Cotman C, Glabe C (1992). Assembly and aggregation properties of synthetic Alzheimer's A4/β amyloid peptide analogs. *J. Biol. Chem.*, 267:546-554.

[14] Harper J & Lansbury P (1997). Models of amyloid seeding in Alzheimer's disease and scrapie: Mechanistic truths and physiological consequences of the time-dependent solubility of amyloid proteins. *Annu. Rev. Biochem.*, 66:385-407.

[15] Bolognesi B, Kumita J, Barros T, Esbjorner E, Luheshi L, Crowther D, Wilson M, Dobson C, Favrin G, Yerbury J (2010). ANS binding reveals common features of cytotoxic amyloid species. *ACS Chem. Biol.*, 5:735-740.

[16] Seubert P, Vigo-Pelfrey C, Esch F, Lee M, Dovey H, Davis D, Sinha S, Schlossmacher M, Whaley J, Swindlehurst C, McCormack R, Wolfert R, Selkoe D, Lieberburg I, Schenk D (1992). Isolation and quantification of soluble Alzheimer's β-peptide from biological fluids. *Nature*, 359:325-327.

[17] Ellis R (2001). Macromolecular crowding: obvious but underappreciated. *Trends Biochem. Sci.*, 26:597-604.

[18] Hu X, Crick S, Bu G, Frieden C, Pappu R, Lee J-M (2009). Amyloid seeds formed by cellular uptake, concentration, and aggregation of the amyloid-β peptide. *Proc. Natl. Acad. Sci. USA*, 106:20324-20329.

[19] Kusumoto Y, Lomakin D, Teplow D, Benedek G (2005). Temperature-dependence of amyloid-protein fibrillization. *Proc. Natl. Acad. Sci. USA,* 95:12277-12282.

[20] Benilova I, Karan E, De Strooper B (2012). The toxic Aβ oligomer and Alzheimer's disease: an emperor in need of clothes. *Nat. Neurosci.*, 15:349-357.

[21] Iwatsubo T, Saido T, Mann D, Lee V, Trojanowski J (1996). Full-length amyloid-β(1-42(43)) and amino-terminally modified and truncated amyloid-β42(43) deposit in diffuse plaques. *Am. J. Pathol.*, 149:1823-1830.

[22] Wiltfang J, Esselmann H, Bibl M, Smirnov A, Otto M, Paul S, Schmidt B, Klafki H, Maler M, Dyrks T, Bienert M, Beyermann M, Rüther E, Kornhuber J (2002). Highly conserved and disease-specific patterns of carboxyterminally truncated Aβ peptides 1-37/38/39 in addition to 1-40/42 in Alzheimer's disease and in patients with chronic neuroinflammation. *J. Neurochem.*, 81:481-496.
[23] Balbach J, Petkova A, Oyler N, Antzutkin O, Gordon D, Meredith S, Tycko R (2002). Supramolecular structure in full-length Alzheimer's β-amyloid fibrils: evidence for a parallel β-sheet organization from solid-state nuclear magnetic resonance. *Biophys. J.*, 83:1205-1216.
[24] Fernandez-Escamilla A, Rousseau F, Schymkowitz J, Serrano L (2004). Prediction of sequence-dependent and mutational effects on the aggregation of peptides and proteins. *Nat. Biotechnol.*, 22:1302-1306.
[25] Leissring M, Lu A, Condron M, Teplow D, Stein R, Farris W, Selkoe D (2003). Kinetics of amyloid β-protein degradation determined by novel fluorescence- and fluorescence polarization-based assays. *J. Biol. Chem.*, 278:37314-37320.
[26] Nelson R, Sawaya M, Balbirnie M, Madsen A, Riekel C, Grothe R, Eisenberg D (2005). Structure of the cross-β spine of amyloid-like fibrils. *Nature*, 435:773-778.
[27] Zhao W, De Felice F, Fernandez S, Chen H, Lambert M, Quon M, Krafft G, Klein W (2008). Amyloid β oligomers induce impairment of neuronal insulin receptors. *FASEB J.*, 22:246-260.
[28] Cruts M & Van Broeckhoven C (1998). Molecular genetics of Alzheimer's disease. *Ann. Med.*, 30:560-565.
[29] Naslund J, Jensen M, Tjernberg L, Thyberg J, Terenius L, Nordstedt C (1994). The metabolic pathway generating p3, an Aβ-peptide fragment, is probably non-amyloidogenic. *Biochem. Biophys. Res. Commun.*, 204:780-787.
[30] Postina R (2012). Activation of α-secretase cleavage. *J. Neurochem.*, 120:46-54.
[31] Frost D, Gorman P, Yip C, Chakrabartty A (2003). Co-incorporation of Aβ40 and Aβ42 to form mixed pre-fibrillar aggregates. *Eur. J. Biochem.*, 270:654-663.
[32] Yoshiike Y, Chui D, Akagi T, Tanaki N, Takashima A (2003). Specific compositions of amyloid-β peptides as the determinant of toxic β-aggregation. *J. Biol. Chem.*, 278:23648-23655.
[33] Wang R, Wang B, He W, Zheng H (2006). Wild-type presenilin 1 protects against Alzheimer disease mutation-induced amyloid pathology. *J. Biol. Chem.*, 281:15330-15336.
[34] Kim J, Onstead L, Randle S, Price R, Smithson L, Zwizinski C, Dickson D, Golde T, McGowan E (2007). Aβ40 inhibits amyloid deposition in vivo. *J. Neurosci.*, 27:627-633.
[35] Yan Y & Wang C (2007). Aβ40 protects non-toxic Aβ42 monomer from aggregation. *J. Mol. Biol.*, 369:909-916.
[36] Jan A, Gokce O, Luthi-Carter R, Lashuel H (2008). The ratio of monomeric to aggregated forms of Aβ40 and Aβ42 is an important determinant of amyloid-beta aggregation, fibrillogenesis, and toxicity. *J. Biol. Chem.*, 283:28176-28189.
[37] Lewczuk P, Esselmann H, Otto M, Maler J, Henkel A, Henkel M, Eikenberg O, Antz C, Krause W-R, Reulbach U, Kornhuber J, Wiltfang J (2004). Neurochemical diagnosis of Alzheimer's dementia by CSF Aβ42, Aβ42/Aβ40 ratio and total tau. *Neurobiol. aging* 25:273-281.
[38] Maddalena A, Papassotiropoulos A, Gonzalez-Agosti C, Signorell A, Hegi T, Pasch T, Nitsch R, Hock C (2004). Cerebrospinal fluid profile of amyloid β peptides in patients with Alzheimer's disease determined by protein biochip technology. *Neurodegener. Dis.*, 1:231-235.
[39] Duff K, Eckman C, Zehr C, Yu X, Prada C, Perez-Tur J, Hutton M, Buee L, Harigaya Y, Yager D, Morgan D, Gordon M, Holcomb L, Refolo L, Zenk B, Hardy J, Younkin S (1996). Increased amyloid-β42(43) in brains of mice expressing mutant presenilin 1. *Nature*, 383:710-713.
[40] Scheuner D, Eckman C, Jensen M, Song X, Citron M, Suzuki N, Bird T, Hardy J, Hutton M, Kukull W, Larson E, Levy-Lahad E, Viitanen M, Peskind E, Poorkaj P, Schellenberg G, Tanzi R, Wasco W, Lannfelt L, Selkoe D, Younkin S (1996). Secreted amyloid β-protein similar to that in the senile plaques of Alzheimer's disease is increased in vivo by the presenilin 1 and 2 and APP mutations linked to familial Alzheimer's disease. *Nat. med.*, 2:864-870.
[41] Jervis G (1948). Early senile dementia in mongoloid idiocy. *Am. J. Psychiat.*, 105:102-106.
[42] Citron M, Oltersdorf T, Haass C, McConlongue L, Hung A, Seubert P, Vigo-Pelfrey C, Lieberburg I, Selkoe D (1992). Mutation of the β-amyloid precursor protein in familial Alzheimer's disease increases β-protein production. *Nature*, 360:672-674.
[43] Urbanc B, Cruz L, Yun S, Buldyrev S, Bitan G, Teplow D, Stanley H (2004). In silico study of amyloid β-protein folding and oligomerization. *Proc. Natl. Acad. Sci. USA*, 101:17345-17350.
[44] Yun S, Urbanc B, Cruz L, Bitan G, Teplow D, Stanley H (2007). Role of electrostatic interactions in amyloid β-protein (Aβ) oligomer formation: a discrete molecular dynamics study. *Biophys. J.*, 92:4064-4077.

[45] Ahmed M, Davis J, Aucoin D, Sato T, Ahuja S, Aimoto S, Elliott J, Van Nostrand W, Smith S (2010). Structural conversion of neurotoxic amyloid-β(1-42) oligomers to fibrils. *Nat. Struct. Mol. Biol.*, 17:561-567.
[46] Hartman S & Möbius H (2003). Tolerability of memantine in combination with cholinesterase inhibitors in dementia therapy. *Int. Clin. Psychopharm.*, 18:81-85.
[47] Rafii M & Aisen P (2009). Recent developments in Alzheimer's disease therapeutics. *BMC Med.*, 7:7.
[48] Fellgiebel A, Kojro E, Müller M, Scheurich A,Schmidt L, Fahrenholz F (2009). CSF APPsα and phosphorylated tau protein levels in mild cognitive impairment and dementia of Alzheimer's type. *J. Geriatr Psych Neur.*, 22:3-9.
[49] Shi M, Sui Y-T, Peskind E, Li G, Hwang H-J, Devic I, Ginghina C, Edgar J, Pan C, Goodlett D, Furay A, Gonzalez-Cuyar L, Zhang J (2011). Salivary tau species are potential biomarkers of Alzheiemer disease. *J. Alzheimers Dis.*, 27:299-305.
[50] Cooper-Knock J, Kirby J, Ferraiuolo L, Heath P, Rattray M, Shaw P (2012). Gene expression profiling in human neurodegenerative disease. *Nat. Rev. Neurol.*, 8:518-530.
[51] Kuperstein I, Broersen K, Benilova I, Rozenski J, Jonckheere W, Debulpaep M, Vandersteen A, Segers-Nolten I, van der Werf K, Subramaniam V, Braeken D, Callewaert G, Bartic C, D'Hooge R, Martins I, Rousseau F, Schymkowitz J, De Strooper B (2010). Neurotoxicity of Alzheimer's disease Aβ peptides is induced by small changes in the Aβ42 and Aβ40 ratio. *EMBO J.*, 29:3408-3420.
[52] Longo F & Massa S (2004). Neuroprotective strategies in Alzheimer's disease. *Neurotherapeutics*, 1:117-127.
[53] Solito E & Sastre M (2012). Microglia function in Alzheimer's disease. *Front. Pharmacol.*, 3:14.
[54] De Strooper B, Vassar R, Golde T (2010). The secretases: enzymes with therapeutic potential in Alzheimer disease. *Nat. Rev. Neurol.*, 6:99-107.
[55] Weggen S, Eriksen J, Das P, Sagi S, Wang R, Pietrzik C, Findlay K, Smith T, Murphy M, Bulter T, Kang D, Marquez-Sterling N, Golde T, Koo E (2001). A subset of NSAIDs lower amyloidogenic Aβ42 independently of cyclooxygenase activity. *Nature*, 414:212-216.
[56] Esiri M & Wilcock G (1986). Cerebral amyloid angiopathy in dementia and old age. *J. Neurol. Neurosur. PS.*, 49:1221-1226.
[57] Sunde M, Serpell L, Bartlam M, Fraser P, Pepys M, Blake C (1997). Common core structure of amyloid fibrils by synchrotron X-ray diffraction. *J. Mol. Biol.*, 273:729-739.
[58] Tamagno E (2003). Multiple signaling events in amyloid β-induced oxidative stress-dependent neuronal apoptosis. *Free Radical Bio. Med.*, 35:45-58.
[59] White J, Manelli A, Holmberg K, Van Eldik L, Lady M (2005). Differential effects of oligomeric and fibrillar amyloid-β 1-42 on astrocyte-mediated inflammation. *Neurobiol. dis.*, 18:459-465.
[60] Nimmrich V & Ebert U (2009). Is Alzheimer's disease a result of presynaptic failure? Synaptic dysfunctions induced by oligomeric β-amyloid. *Rev. Neuroscience.*, 20:1-12.
[61] Laino C (2009). In follow-up analysis of clinical trial, NSAIDs seem to preserve cognitive function in patients with healthy brains. *Neurol. Today*, 9:21-22.
[62] Gilgun-Sherki Y, Melamed E, Offen D (2003). Antioxidant treatment in Alzheimer's disease: current state. *J. Mol. Neurosci.*, 21:1-11.

Appendix

Following Aβ peptides were chemically synthesized.

$A\beta_{37}$	DAEFRHDSGYEVHHQKLVFFAEDVGSNKGAIIGLMVG
$A\beta_{38}$	DAEFRHDSGYEVHHQKLVFFAEDVGSNKGAIIGLMVGG
$A\beta_{40}$	DAEFRHDSGYEVHHQKLVFFAEDVGSNKGAIIGLMVGGVV
$A\beta_{42}$	DAEFRHDSGYEVHHQKLVFFAEDVGSNKGAIIGLMVGGVVIA
$A\beta_{43}$	DAEFRHDSGYEVHHQKLVFFAEDVGSNKGAIIGLMVGGVVIAT

$A\beta_{42}$

D7N	DAEFRHNSGYEVHHQKLVFFAEDVGSNKGAIIGLMVGGVVIA
A21G	DAEFRHDSGYEVHHQKLVFFGEDVGSNKGAIIGLMVGGVVIA
E22G	DAEFRHDSGYEVHHQKLVFFAGDVGSNKGAIIGLMVGGVVIA
E22K	DAEFRHDSGYEVHHQKLVFFAKDVGSNKGAIIGLMVGGVVIA
E22Q	DAEFRHDSGYEVHHQKLVFFAQDVGSNKGAIIGLMVGGVVIA
D23N	DAEFRHDSGYEVHHQKLVFFAENVGSNKGAIIGLMVGGVVIA

biotin-$A\beta_{40}$	biotin-DAEFRHDSGYEVHHQKLVFFAEDVGSNKGAIIGLMVGGVV
$A\beta_{40}$-K-biotin	DAEFRHDSGYEVHHQKLVFFAEDVGSNKGAIIGLMVGGVV-K-biotin
biotin-$A\beta_{42}$	biotin-DAEFRHDSGYEVHHQKLVFFAEDVGSNKGAIIGLMVGGVVIA
$A\beta_{42}$-K-biotin	DAEFRHDSGYEVHHQKLVFFAEDVGSNKGAIIGLMVGGVVIA-K-biotin

$p3_{17-40}$	LVFFAEDVGSNKGAIIGLMVGVV
$p3_{17-42}$	LVFFAEDVGSNKGAIIGLMVGVVIQ

Purity of the chemically synthesized Aβ peptides was confirmed by MALDI-TOF mass spectrometry and LC-MS (insets).

The mass-to-charge (*m/z*) spectra of all Aβ peptide variants display one or two major peaks that correspond to the single or double charged ion species derived from the full length monomeric peptide. Insets show the elution of the peptide from the column in a single, monomeric peak.

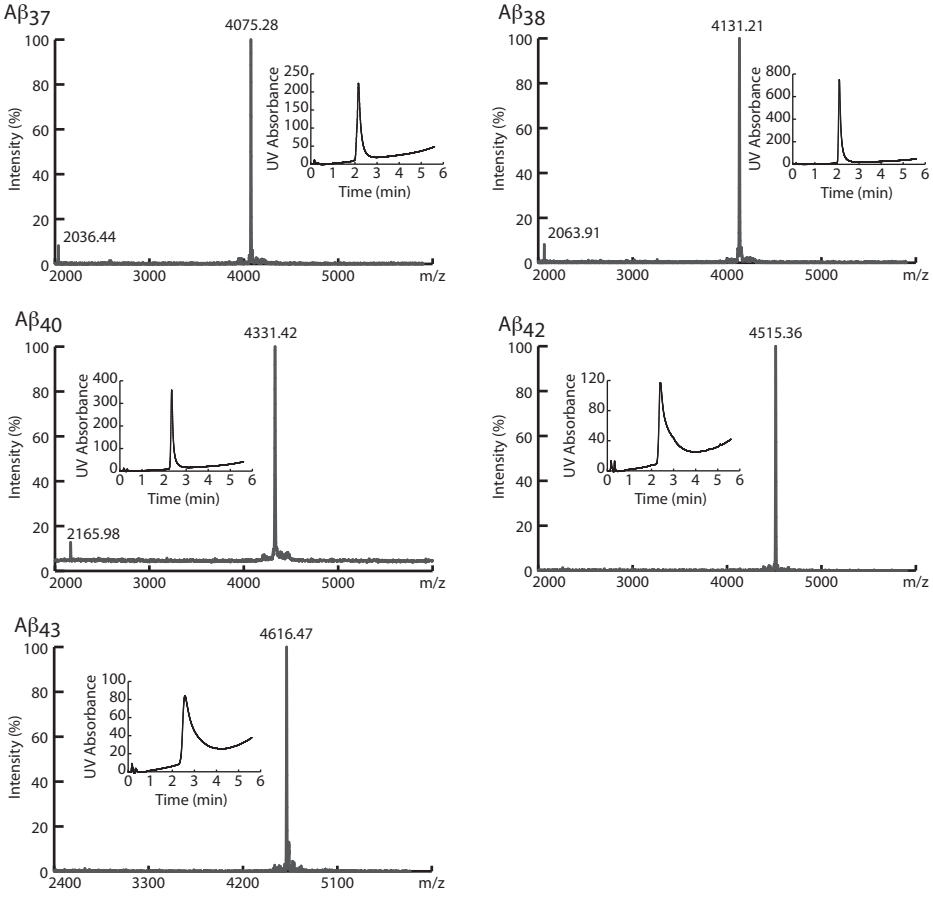

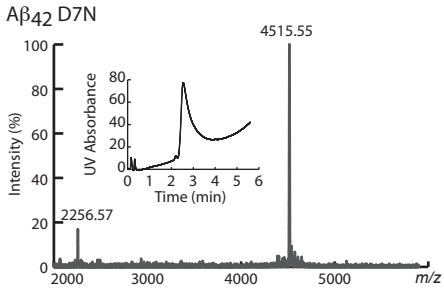
Aβ42 D7N
4515.55
2256.57
Intensity (%)
UV Absorbance
Time (min)
m/z

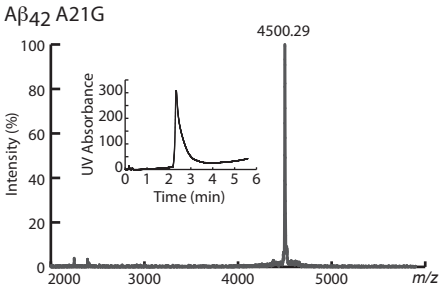
Aβ42 A21G
4500.29
Intensity (%)
UV Absorbance
Time (min)
m/z

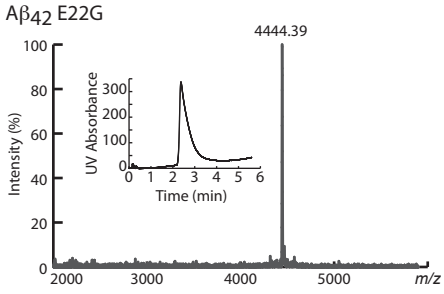
Aβ42 E22G
4444.39
Intensity (%)
UV Absorbance
Time (min)
m/z

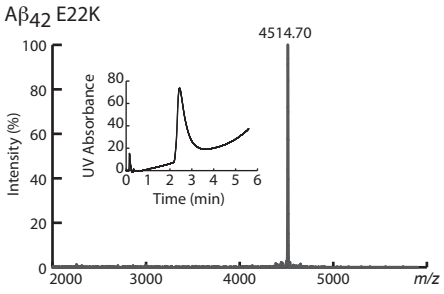
Aβ42 E22K
4514.70
Intensity (%)
UV Absorbance
Time (min)
m/z

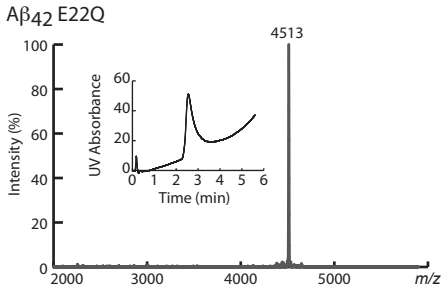
Aβ42 E22Q
4513
Intensity (%)
UV Absorbance
Time (min)
m/z

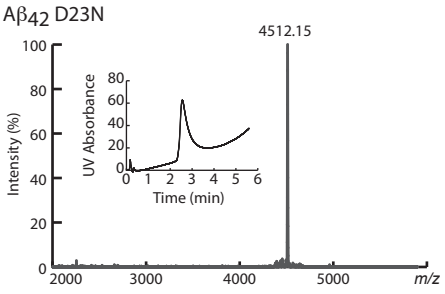
Aβ42 D23N
4512.15
Intensity (%)
UV Absorbance
Time (min)
m/z

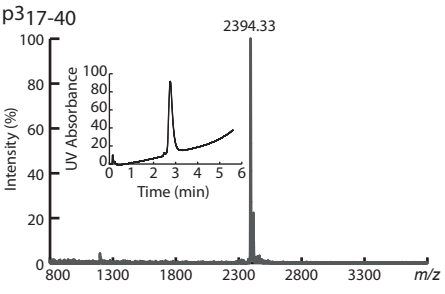
p317-40
2394.33
Intensity (%)
UV Absorbance
Time (min)
m/z

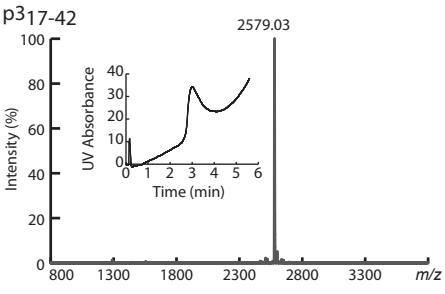
p317-42
2579.03
Intensity (%)
UV Absorbance
Time (min)
m/z

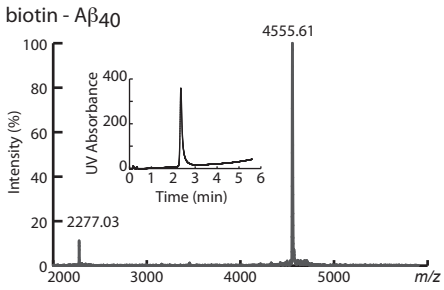
biotin - Aβ40
4555.61
2277.03
Intensity (%)
UV Absorbance
Time (min)
m/z

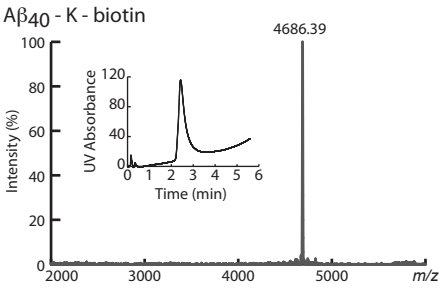
Aβ40 - K - biotin
4686.39
Intensity (%)
UV Absorbance
Time (min)
m/z

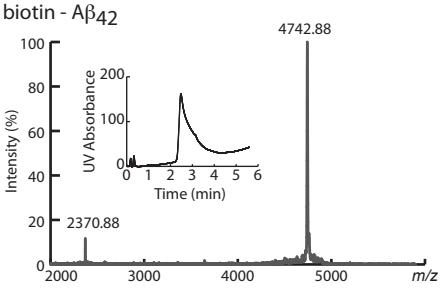
biotin - Aβ42
4742.88
2370.88
Intensity (%)
UV Absorbance
Time (min)
m/z

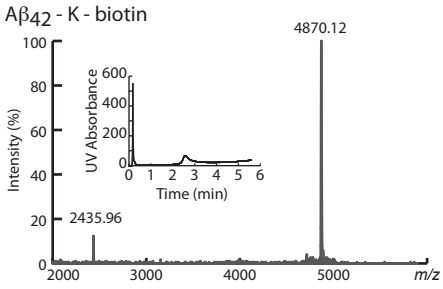
Aβ42 - K - biotin
4870.12
2435.96
Intensity (%)
UV Absorbance
Time (min)
m/z

B

Appendix

Aβ peptides show direct and non-preferential random interaction

Electron spray ionization-mass *m/z* spectrum (ESI-MS) of monomeric and dimeric Aβ prepared from a 1:1 $A\beta_{40}$:$A\beta_{42}$ ratio upon 100-fold dilution from DMSO in acetonitrile:water (1:1, v/v). The box denotes the spectral location of dimers. Spectral contributions by $A\beta_{40}$ or $A\beta_{42}$ are denoted by circles or squares respectively.

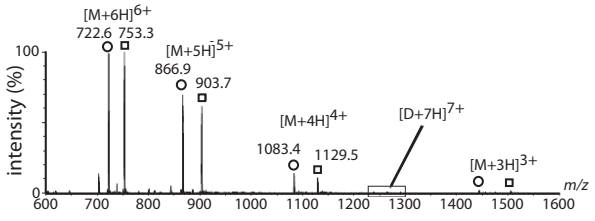

Magnification of the ESI-MS (*m/z*) dimer spectrum of $A\beta_{40}$ and $A\beta_{42}$. Spectral contributions by $A\beta_{40}$ or $A\beta_{42}$ are denoted by circles or squares respectively. Quantitation of ESI-MS data indicate that $A\beta_{40}$ and $A\beta_{42}$ interact to form dimers in a random manner.

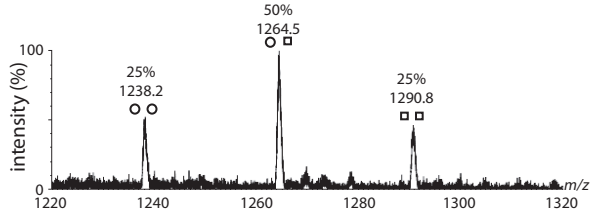

Dimer formation between Aβ42:Aβ40 ratios 1:9 and 3:7 is also random. Both heterdimers (Aβ40-Aβ42 *m/z* 1264.5) and homodimers (Aβ40-Aβ40 *m/z* 1238; Aβ42-Aβ42 *m/z* 1291) are detected.

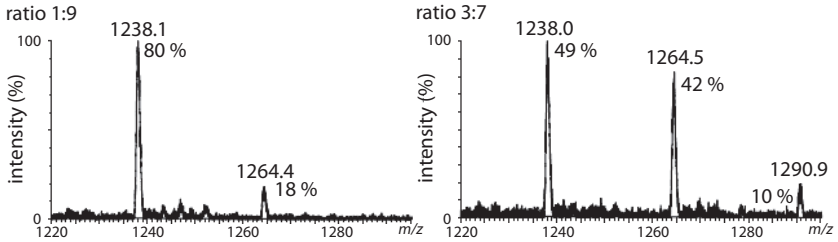

Deconvoluted electrospray ionization mass spectra of the various Aβ42:Aβ40 ratios at time 0 h.

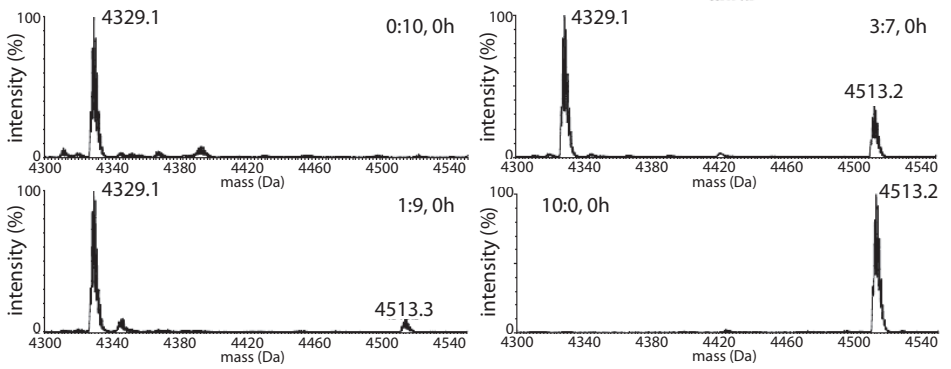

Deconvoluted ESI-MS spectra of mixtures of various Aβ lengths were recorded immediately after mixing and 100-fold dilution in acetonitrile:water containing 0.1% acetic acid. The intensity differences in the peaks corresponding to both Aβ peptides indicate that mixtures were not exactly composed of 50% of each peptide. The region of the spectrum where dimers are detected is boxed.

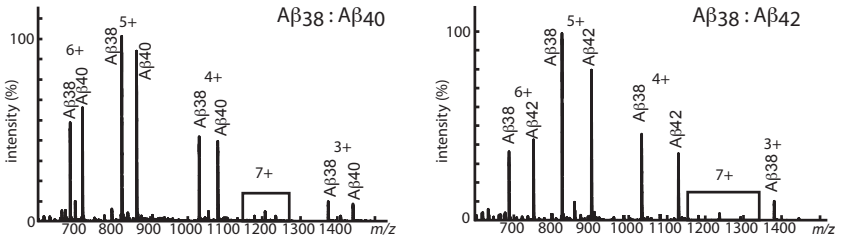

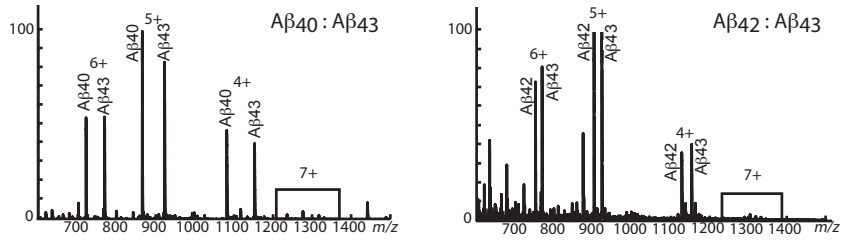

Magnification of the ESI-MS (*m/z*) dimer spectrum shows that a small population of mixed dimers is formed without any preference to form homo- or heterodimers.

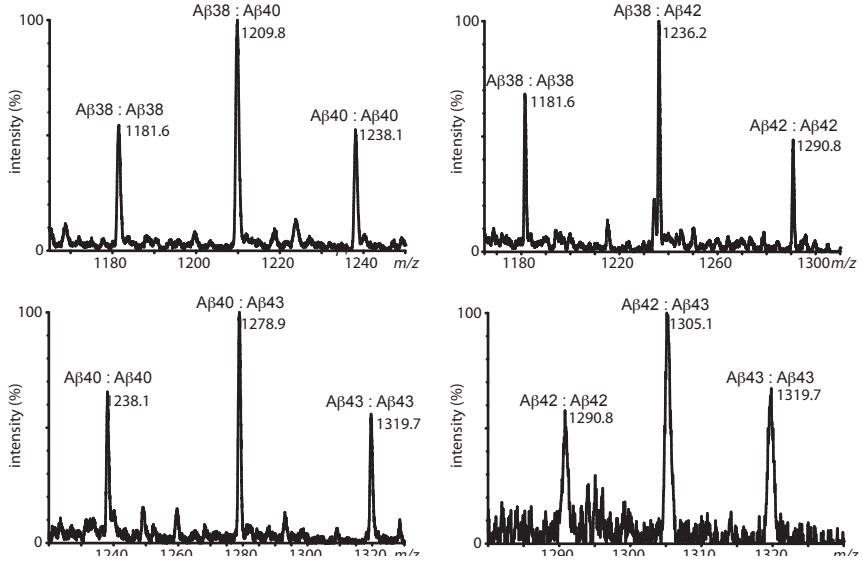

Summary

Proteins are the work horses of our body. Amongst other functions, they are part of the immune system, ensure transport of oxygen and are necessary for digestion amongst others. Each protein is adapted and optimized for its function. There are innumerable different proteins coupled to the myriads of biological processes. Some proteins require a specific three-dimensional conformation to execute their function while others remain unfolded. The nonnative interaction of proteins can cause their aggregation. When protein quality control systems cannot prevent these interactions, protein aggregates are formed. When proteins are trapped in such aggregates, they can no longer execute their function, which leads to diseases like cystic fibrosis. On the other hand protein aggregates can induce cellular damage causing disease, as occurs in Alzheimer disease.

Alzheimer disease is characterized by severe memory loss. The disease is mainly observed in elderly, but rare hereditary forms cause early-onset (before the age of 65) of Alzheimer disease. On a molecular level, neuronal loss, extracellular plaques of amyloid-β (Aβ) and intracellular tangles of tau characterize Alzheimer disease. The actual cause underlying Alzheimer disease has not been identified yet, but evidence is pointing to the aggregation of Aβ.

The Aβ protein is released from a larger protein in the brain. The enzymes that ensure this cleavage are a not very precise and introduce heterogeneity in the length of the released Aβ peptides. The Aβ peptide can vary in length between 33 and 49 amino acids. The 40 and 42 forms, $A\beta_{40}$ and $A\beta_{42}$, are the predominant peptides released. It is assumed that longer forms of Aβ are more aggregation-prone than the shorter variants. Mutations related to familial Alzheimer disease affect the enzymes releasing Aβ and cause a shift in the window of released Aβ peptides.

As Aβ40 and Aβ42 are the predominant forms, most research has focused on their behavior in the past. In this thesis the emphasis is on the influence of more expanded heterogeneity of Aβ on aggregation. First, the protocol enabling the dissolution of monomeric Aβ allowing for detailed characterization of aggregation is described. This procedure yields a solution which is compatible both with cell-culture studies as well as with the most common biophysical techniques. The second part of the thesis analyzed the aggregation of various Aβ lengths and disease-related mutations (Chapter 3) to gain insight into the mechanisms that underly aggregation. The effect of disease-related mutations on the release of Aβ seems to be more dominant than the influence on aggregation of the related Aβ mutants (Chapter 4). In the last part the emphasis is on the mutual influence of various Aβ forms. Therapeutic approaches might benefit from these insights as various Aβ forms co-exist in the brain. It has been reported before that Aβ40 and Aβ42 can alter the aggregation of the other form. The results presented here show that very small fluctuations of the amounts of Aβ42 determine the aggregation properties of the mixture, and the toxicity that it exerts on neurons (Chapter 5). The structural characterization of these mixtures indicates that it is not the final aggregates that are affected by the small fluctuations, but rather the smaller, toxic, oligomeric species formed during aggregation (Chapter 6). Detailed characterization of the mechanisms that release Aβ and the effect of disease-related mutations on these processes showed that not only levels of Aβ40 and Aβ42 are affected but that levels of Aβ38 are increased as well (Chapter 7). Although it is generally assumed that shorter Aβ lengths aggregate more slowly, and are less toxic, the data presented here show that Aβ38 aggregates more rapidly than Aβ40. Moreover, the minimally toxic Aβ38 affects a majority of Aβ40 and induces toxicity of the mixture while at the same time it can moderate toxicity of Aβ42 (Chapter 8).

Altogether the results in this thesis indicate that heterogeneity of Aβ is much more involved in Alzheimer disease than assumed before. Less frequent forms of the Aβpeptide are likely to be involved in progress of Alzheimer disease. This is an insight which might have far-reaching consequences for the development of therapeutics as current strategies primarily focus on Aβ40 and Aβ42 without much consideration of other Aβ forms.

Samenvatting

Eiwitten zijn de werkpaarden van ons lichaam. Zo maken ze onder andere deel uit van het immuunsysteem, staan in voor zuurstoftransport en nemen deel aan vertering. Elk eiwit is aangepast aan de specifieke functie die het uitvoert. In elk levend wezen moeten ontelbare processen uitgevoerd worden, en dus zijn er ook talloze eiwitten. Om hun specifieke functie uit te voeren moeten sommige eiwitten een specifieke structuur aannemen terwijl andere ongevouwen blijven. Wanneer eiwitten echter ongewenste interacties aangaan met andere eiwitten gaan ze samenklonteren. Wanneer de kwaliteitscontrole systemen van de cel de eiwitten niet kunnen beletten om te aggregeren, kunnen de eiwitten hun functie niet meer uitoefenen wat kan leiden tot ziektes zoals cystische fibrose. Bijkomend kunnen de geagreggeerde eiwitten schade aanrichten zoals gebeurt bij de ziekte van Alzheimer.

De ziekte van Alzheimer wordt gekarakteriseerd door geheugenverlies, en komt voornamelijk voor bij oudere personen. Sommige erfelijke vormen van de ziekte veroorzaken een vervroegd ziektepatroon (bij patienten jonger dan 65). Op moleculair niveau wordt de ziekte van Alzheimer gekenmerkt door verregaand verlies van neuronen, extracellulaire 'plaques' van amyloid-β (Aβ) eiwitten en intracellulaire 'tangles' van tau eiwitten. De eigenlijke oorzaak van de ziekte is nog niet achterhaald maar de meeste gegevens wijzen in de richting van Aβ.

Het Aβ eiwit wordt in de hersenen geknipt uit een groter eiwit. De enzymen die instaan voor deze vrijgave zijn niet heel nauwkeurig en introduceren variatie in de lengte van het Aβ wat wordt vrijgegeven. De lengte van Aβ kan varieren tussen 33 en 49 aminozuren, waarbij de 40 en 42 vormen de meest voorkomende zijn. Er wordt aangenomen dat de langere vormen van Aβ meer geneigd zijn tot aggregeren dan de kortere vormen. Mutaties die leiden tot de erfelijke vormen van de ziekte van Alzheimer beïnvloeden de enzymen die Aβ vrijgeven en veroorzaken een verschuiving van het

spectrum vrijgegeven Aβ.

Aangezien Aβ40 en Aβ42 de meest voorkomende vormen zijn, werden in het verleden vooral deze vormen bestudeerd. In deze thesis wordt echter de nadruk gelegd op de invloed van grotere variatie van de Aβ eiwitten op hun aggregatie. Eerst (hoofdstuk 2) wordt een algemene procedure beschreven voor het oplossen van Aβ op een manier die het mogelijk maakt om aggregatie vanaf de monomeren te kunnen volgen en in een formulering die geschikt is voor celcultuur studies, en de meeste biofysische technieken. Het volgende deel van de thesis beschrijft de aggregatie van verschillende lengtes en ziekte-gerelateerde mutanten (hoofdstuk 3) om inzicht te krijgen in de mechanismen die leiden tot aggregatie. De invloed van ziekte-gerelateerde mutaties op de vrijgave van Aβ lijkt een meer doorslaggevende rol te spelen in het vervroegd optreden van de ziekte van Alzheimer dan de aggregatie van de mutante Aβ eiwitten (hoofdstuk 4). Het derde deel van de thesis gaat na wat de invloed is die verschillende vormen van Aβ op elkaar uitoefenen. Deze invloed is zeer relevant voor het ontwikkelen van medicatie aangezien de verschillende vormen van Aβin de hersenen ook samen voorkomen. Dat Aβ40 en Aβ42 elkaar kunnen beïnvloeden was reeds geweten. Maar de resultaten hier tonen dat zeer kleine fluctuaties in de hoeveelheid Aβ42 bepalend zijn voor de aggregatie van het mengsel, en voor de schade die aangericht wordt aan neuronen (hoofdstuk 5). Structureel onderzoek van deze mengsels toont aan dat niet de uiteindelijke aggregaten verschillen, maar wel de kleinere toxische oligomere associaties die gevormd worden tijdens het aggregatie proces (hoofdstuk 6). Gedetailleerd onderzoek van de mechanismen die de Aβ vrijgave beïnvloeden in de ziekte-gerelateerde mutaties bracht aan het licht dat niet alleen Aβ40 en Aβ42 niveau's worden aangetast, maar dat ook de hoeveelheid Aβ38 stijgt (hoofdstuk 7). Hoewel algemeen wordt aangenomen dat kortere lengtes van Aβ veilig zijn (traag aggregeren, en weinig toxisch zijn), tonen de resultaten hier dat Aβ38 sneller aggregeert dan Aβ40. Daarenboven slaagt het weinig toxische Aβ38 er in om grote hoeveelheden Aβ40 zo te beïnvloeden dat ze toxisch worden terwijl het de toxiciteit van Aβ42 tempert (hoofdstuk 8).

De resultaten in deze thesis geven aan dat de grote variatie van Aβ een veel grotere rol speelt dan voorheen werd aangenomen. Minder frequent voorkomende vormen van Aβ zijn betrokken bij de ziekte van Alzheimer, en zijn veel minder onschuldig dan wordt gedacht. Dit inzicht is van primair belang voor de ontwikkeling van medicatie voor de ziekte van Alzheimer aangezien momenteel vooral wordt gefocust op Aβ40 en Aβ42, zonder rekening te houden met andere vormen.

Acknowledgments

Mijn naam staat dan wel op de kaft van dit boekje, in mijn eentje zou het er heel anders uitgezien hebben. Heel veel mensen hebben bijgedragen aan deze thesis - sommige op wetenschappelijk vlak, andere langs de persoonlijke kant. Op tv komen al deze mensen in de aftiteling, hier krijgen ze dit soort hoofdstukje.

Als Frederic Rousseau en Joost Schymkowitz niet in mij geloofd hadden, was er nooit een thesis geweest. Met het nodige enthousiasme op de juiste momenten, discussies over experimenten en resultaten maar zeker ook door mij de vrijheid te geven om te proberen en fouten te maken hebben jullie mij gemotiveerd en ongelofelijk veel geleerd. Het switch lab zou niet zijn wat het is zonder Hannah die de administratieve weg kent, experimenteel advies geeft, en het lab draaiend houdt. De switch-tijd is ook in grote mate bepaald door de fijne collega's die ook een beetje vrienden zijn geworden. Wim verdient hier een speciale vermelding voor al de tips en trucjes, hulp en de aflossing bij de experimenten waar we 12 uur lang aggregatie wilden volgen. Greet, Jacinte en Ola hebben ook specifiek bijgedragen door vaak te luisteren, raad te geven en op tijd en stond mee te vluchten naar Opinio om eens afstand te nemen.

Vinod Subramaniam heeft mij met open armen ontvangen in Twente en er op toegezien dat ik mij thuis voelde. Samen met Sylvia, Kim, Dirk Roelof en de andere collega's is dat zeker gelukt! De nieuwe omgeving was zeer stimulerend en het was heerlijk om een jaar bij jullie te mogen doorbrengen. Josey het is zeer boeiend om te zien hoe je groeit en evolueert. Het is een hele eer om dat van dichtbij te mogen volgen. Jou begeleiden heeft mij ook veel geleerd, sorry voor de fouten die ik zeer zeker heb gemaakt. Jesper hopelijk valt onze biologische aanpak met buikgevoel te modelleren in een logisch systeem. Ik wens jullie allebei heel veel succes!

Er zijn ergere dingen dan van half oktober tot half november in Granada verblijven. Quico heeft er zijn lab voor mij opengesteld en mij meer dan welkom laten voelen. Op wetenschappelijk vlak hebben Bertrand en ik gediscussieerd, nagedacht en geëxperimenteerd. Abeta heeft in elk geval niet al zijn geheimen prijs gegeven.

Het IWT, Boehringer Ingelheim en EMBO moeten hier ook vermeld worden omdat ze de nodige financiële steun hebben gegeven. Er is niet veel uitleg nodig om duidelijk te maken dat het er zonder hen helemaal anders had uitgezien.

Ellen het was zeer leuk dat je bij het team kwam. We hebben plezier gemaakt samen, ik heb veel van jou opgestoken en ik hoop dat het wederzijds was. Samen met Iryna heb ik vele uren gespendeerd bij imec waarbij we elkaar beter hebben leren kennen en we heel vaak bijna filosofische gesprekken hadden over onze projecten. Van Kris en alle andere mensen met wie ik in die vier jaar heb samengewerkt, heb ik telkens iets opgepikt. Het zijn er te veel om allemaal te vermelden maar ze betekenen evenveel.

Kerensa, iedereen die mijn doc van dichtbij heeft gevolgd (ik in de eerste plaats) beseft maar al te goed dat deze thesis in al haar schoonheid voor een groot deel ook jouw verdienste is geweest. Ik moest maar eens met de post-docs praten ... en mijn gevoel zei dat ik graag met jou wilde werken. Dus vroeg ik tijdens een lab-uitje in een niet-nader genoemd Indisch restaurant of er in jouw project plaats was voor een doctoraat-student. En de rest is geschiedenis. Ik ken heel weinig andere studenten die begeleid worden door iemand die zoveel kansen biedt en zo onzelfzuchtig is. Als buffer om mij de tijd te geven om resultaat te halen, maar ook vol vertrouwen dat de data er zouden komen in de tijd tussen inschrijven voor het congres en het maken van de poster. Jij hebt een grote rol gespeeld in wie ik in die vier jaar geworden ben, in het lab maar ook daarbuiten.

Het spreekt voor zich dat ik vooral gevormd ben door het thuisfront. Mama en papa die ons altijd hebben voorgehouden dat we alles kunnen, zolang we het maar willen. Maar ook dat we er voor 100 % voor moeten gaan en er hard voor moeten werken. Paulien en Tim waar we altijd mee kunnen ontspannen, en niet aan het werk denken ;-) Wannes, al die jaren de rots in de branding. Het is helemaal niet vanzelfsprekend dat ik een maand naar Granada kan, we met heel ons hebben en houden naar Enschede verkassen en ik mijn huishoudelijke taken compleet verwaarloos omdat ik een thesis moet schrijven. Ik zal het niet meer doen ... tot een nieuwe uitdaging ons pad kruist en het weer begint te kriebelen :-)

Publication list

Conference contributions (oral)

Vandersteen A, Jonckheere W, Rousseau F, Schymkowitz J, and Broersen K
"Amyloid β-peptide length strongly affects aggregation kinetics"
VIB Science Club - October 30, 2009 - Leuven, Belgium

Vandersteen A, Benilova I, Jonckheere W, Rousseau F, Schymkowitz J, and Broersen K
"Biophysical consideration of γ-secretase modulation as potential target for Alzheimer's disease"
8th EBSA European Biophysics Congress - August 23-27, 2011 - Budapest, Hungary

Conference contributions (poster)

Vandersteen A, Jonckheere W, Rousseau F, Schymkowitz J, and Broersen K
"Amyloid β-peptide length strongly affects aggregation kinetics"
* ICAD International Conference on Alzheimer's disease - July 11-16, 2009 - Vienna, Austria
* Annual Scientific P6/43 meeting - October 26, 2009 - Brussels, Belgium
"Amyloid-β 1-38 and 1-43: less abundant, but also less important toward AD progress?"
* Conférence J Monod "Protein misfolding and assembly in ageing and disease"- June 5-9, 2010 - Roscoff, France
"A biophysical (re)consideration of modulation of γ-secretase activity to produce shorter Aβ peptide lengths as potential target for AD?"
* 12th Annual Network conference of Alzheimer's Research UK - March 16-17, 2011 - Leeds, United Kingdom

Vandersteen A, Benilova I, Jonckheere W, De Baets G, Rozenski J, Eberle W, De Strooper B, Schymkowitz J, Rousseau F, Subramaniam V, and Broersen K
"Biophysical consideration of γ-secretase modulation as potential target for AD. Consequences of amyloid-β peptide length variation."
* Annual Dutch meeting on molecular and cellular biophysics - October 3-4, 2011 - Veldhoven, The Netherlands

PROCEEDING ARTICLE

Vandersteen A, Benilova I, Jonckheere W, Rousseau F, Schymkowitz J, and Broersen K (2011). Biophysical consideration of γ-secretase modulation as potential target for Alzheimer's disease. *European biophysics journal with biophysics letters*, 40:95-95.

JOURNAL ARTICLES

Kuperstein I, Broersen K, Benilova I, Rozenski J, Jonckheere W, Debulpaep M, Vandersteen A, Segers-Nolten I, Van Der Werf K, Subramaniam V, Braeken D, Callewaert G, Bartic C, D'Hooge R, Martins I, Rousseau F, Schymkowitz J, and De Strooper B (2010). Neurotoxicity of Alzheimer's disease Aβ peptides is induced by small changes in the $A\beta_{42}$ to $A\beta_{40}$ ratio. *EMBO J.*, 29:3408-3420.

Zhou L, Brouwers N, Benilova I, Vandersteen A, Mercken M, Van Laere K, Van Damme P, Demedts D, Van Leuven F, Sleegers K, Broersen K, Van Broeckhoven C, Vandenberghe R, and De Strooper B (2011). Amyloid precursor protein mutation E682K at the alternative β-secretase cleavage β'-site increases Aβ generation. *EMBO Mol. Med.*, 3:291-302.

Broersen K, Jonckheere W, Rozenski J, Vandersteen A, Pauwels K, Pastore A, Rousseau F, and Schymkowitz J (2011). A standardized and biocompatible preparation of aggregate-free amyloid-β peptide for biophysical and biological studies of Alzheimer disease. *PEDS protein engineering design & selection*, 24:743-750.

Pauwels K, Williams T, Morris K, Jonckheere W, Vandersteen A, Kelly G, Schymkowitz J, Rousseau F, Pastore A, Serpell L, and Broersen K (2011). Structural basis for increased toxicity of pathological $A\beta_{42}$:$A\beta_{40}$ ratios in Alzheimer disease. *J. Biol. Chem.*, 287:5650-5660.

Chávez-Gutiérrez L, Bammens L, Benilova I, Vandersteen A, Benurwar M, Borgers M, Lismont S, Zhou L, Van Cleynenbreugel S, Esselmann H, Wiltfang J, Serneels L, Karran E, Gijsen H, Schymkowitz J, Rousseau F, Broersen K, and De Strooper B (2012). The mechanism of γ-secretase dysfunction in familial Alzheimer disease. *EMBO*, 31:2261-2274.

Vandersteen A, Masman M, De Baets G, Jonckheere W, Van Der Werf K, Marrink S, Rozenski J, Benilova I, De Strooper B, Subramaniam V, Schymkowitz J, Rousseau F, and Broersen K (2012). Molecular plasticity regulates oligomerization and cytotoxicity of the multi-peptide length Aβ pool. *J. Biol. Chem.*, 287:36732-36743.

Vandersteen A, Hubin E, Sarroukh R, De Baets G, Schymkowitz J, Rousseau F, Subramaniam V, Raussens V, Wenschuh H, Wildemann D, and Broersen K (2012). A comparative analysis of the aggregation behavior of amyloid-β peptide variants. *Febs Lett.*, first published online October 24, 2012.

KATHOLIEKE UNIVERSITEIT LEUVEN

UNIVERSITEIT TWENTE.

Vrije Universiteit Brussel

VIB

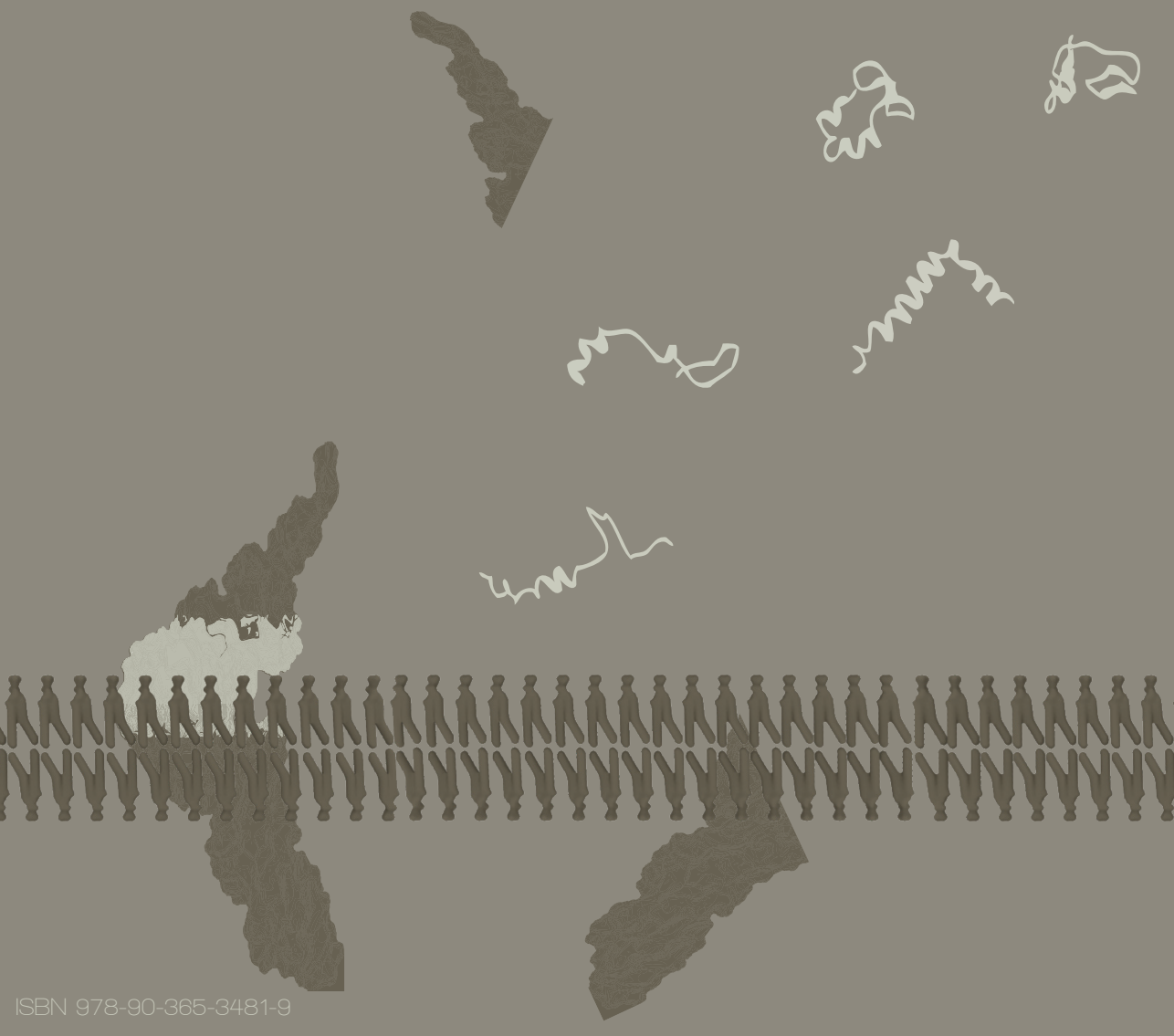

ISBN 978-90-365-3481-9